

**DEVELOPMENT OF A PREDICTION MODEL FOR SKID RESISTANCE OF
ASPHALT PAVEMENTS**

A Dissertation

by

ARASH REZAEI

Submitted to the Office of Graduate Studies of
Texas A&M University
in partial fulfillment of the requirements for the degree of

DOCTOR OF PHILOSOPHY

December 2010

Major Subject: Civil Engineering

Development of a Prediction Model for Skid Resistance of Asphalt Pavements

Copyright 2010 Arash Rezaei

**DEVELOPMENT OF A PREDICTION MODEL FOR SKID RESISTANCE OF
ASPHALT PAVEMENTS**

A Dissertation

by

ARASH REZAEI

Submitted to the Office of Graduate Studies of
Texas A&M University
in partial fulfillment of the requirements for the degree of

DOCTOR OF PHILOSOPHY

Approved by:

Chair of Committee,	Eyad A. Masad
Committee Members,	Dallas N. Little
	Amy Epps Martin
	Chris Mathewson
Head of Department,	John Niedzwecki

December 2010

Major Subject: Civil Engineering

ABSTRACT

Development of a Prediction Model for Skid Resistance of Asphalt Pavements.

(December 2010)

Arash Rezaei, B.S., Sharif University of Technology;

M.S., Sharif University of Technology

Chair of Advisory Committee: Dr. Eyad Masad

The skid resistance of asphalt pavement is a major characteristic that determines the driving safety on a road, especially under wet surface conditions. Skid resistance is primarily a function of the microtexture and macrotexture of a pavement surface. Microtexture is influenced by aggregate surface characteristics and is required to disrupt the continuity of surface water film and attain frictional resistance between the tire and the pavement surface. Macrotexture is affected mostly by mixture design or aggregate gradation and contributes to skid resistance by providing drainage paths of water that can be otherwise trapped between a tire and a pavement surface. The increase in macrotexture contributes to preventing hydroplaning and improving wet frictional resistance, particularly at high speeds. While much research has been conducted in the past to identify material factors that affect skid resistance, there is still a need to develop a model for predicting asphalt pavement skid resistance as a function of mixture characteristics and traffic level. The purpose of this study was to develop such a model based on extensive laboratory experiments and field measurements involving different mixture types and aggregate sources. The model incorporates functions that describe the resistance of aggregates to polishing and aggregate size distribution. The aggregate resistance to polishing was quantified by measuring aggregate texture using the Aggregate Imaging System (AIMS) before and after polishing in the Micro-Deval device. The analysis in this dissertation demonstrates how this model can be used to design mixtures and classify aggregates that provide desirable skid resistance levels.

DEDICATION

I dedicate this dissertation to my wonderful family, especially to my father and mother for instilling the importance of hard work and higher education.

ACKNOWLEDGEMENTS

It is a pleasure to thank those who made this dissertation possible. I am heartily thankful to my supervisor, Dr. Eyad Masad, whose encouragement, supervision, and support from the preliminary to the concluding level enabled me to develop an understanding of the subject. He continually and convincingly conveyed a spirit of adventure in regard to research and scholarship, and without his guidance and persistent help, this dissertation would not have been possible.

I would like to express the deepest appreciation to my committee members, Dr. Dallas N. Little, Dr. Amy Epps Martin, and Dr. Chris Mathewson, for their guidance and support throughout the course of this research.

I also would like to give special recognition to Mr. Arif Chowdhury, who is a research engineer at the Texas Transportation Institute. Without his corporation, I could not have gotten data.

My thanks and appreciation go to Mr. Tom Freeman and Mr. Pat Harris for patiently helping me with my work throughout the time it took me to complete my research.

Thanks also go to my friends and colleagues and the department faculty and staff for making my time at Texas A&M University a great experience. I also want to extend my gratitude to the Texas Department of Transportation, which provided the funding for my research study.

Finally, thanks to my mother and father for their encouragement.

TABLE OF CONTENTS

	Page
ABSTRACT.....	iii
DEDICATION.....	iv
ACKNOWLEDGEMENTS.....	v
LIST OF FIGURES.....	ix
LIST OF TABLES.....	xvi
CHAPTER	
I INTRODUCTION.....	1
Problem Statement.....	3
Objectives.....	3
Organization of the Study.....	4
II LITERATURE REVIEW.....	5
Introduction.....	5
Definition of Friction.....	5
Pavement Texture.....	8
Measurements Methods of Texture and Friction.....	12
Effect of Pavement Age and Weather on Skid Resistance.....	18
Age of the Surface.....	21
Seasonal and Daily Weather Variation.....	22
Aggregate Polishing Characteristics.....	24
Pre-Evaluation of Aggregate for Use in Asphalt Mixture.....	27
Predictive Models for Skid Resistance.....	29
International Friction Index (IFI).....	33
Wet Weather Accident Reduction Program (WWRP) in Texas.....	36
Summary.....	39
III MATERIALS AND LABORATORY TEST METHODS.....	42
Introduction.....	42
Aggregate Sources.....	42
Petrographic Analysis of Aggregates.....	45
Beckman Pit.....	46
Brownlee Pit.....	48
Brownwood Pit.....	51
Fordyce Pit.....	54
McKelligon Pit.....	55

CHAPTER	Page
Georgetown Pit	59
Testing of Aggregate Resistance to Polishing and Degradation.....	61
Los Angeles Abrasion and Impact Test.....	62
Magnesium Sulfate Soundness	63
British Pendulum Test	63
Micro-Deval Test.....	63
Aggregate Imaging System.....	65
Asphalt Mixture Types	66
Type C Mix Design	66
Type D Mix Design	67
Porous Friction Course	67
Asphalt Mixture Preparation.....	68
Slab-Polishing Methods.....	73
Testing of Mixture Resistance to Polishing.....	76
British Pendulum Skid Tester	77
Sand Patch Method	78
Dynamic Friction Tester	79
Circular Texture Meter	80
Laboratory Mixture Tests	81
Summary.....	84
 IV RESULTS AND DATA ANALYSIS	 85
Introduction.....	85
Aggregate Test Results	85
Mixture Test Results.....	91
Sand Patch Test.....	91
British Pendulum Test	96
CTMeter and DFT Tests	108
Aggregate Ranking Based on Laboratory Results.....	128
Summary.....	129
Sand Patch Test.....	130
British Pendulum Test	130
CTMeter and DFT Tests	131
 V A MODEL FOR ASPHALT MIX SURFACE FRICTION BASED ON LABORATORY RESULTS.....	 135
Introduction.....	135
Modeling Approach	136
Summary.....	146
 VI ANALYSIS OF SKID RESISTANCE OF ASPHALT PAVEMENT SECTIONS.....	 148

CHAPTER	Page
Introduction.....	148
Selection of the Field Sections and Data Mining.....	149
Analysis of the Collected Field Data	154
Traffic Load	158
Mix Design	160
Aggregate Type	163
Summary	177
 VII ANALYSIS OF FRICTION AND TEXTURE OF ASPHALT PAVEMENT	
SECTIONS	178
Introduction.....	178
Selection of the Field Sections.....	178
Analysis of Field Measurements.....	182
Summary	187
 VIII A MODEL FOR PREDICTING SKID NUMBER OF ASPHALT	
PAVEMENTS.....	189
Introduction.....	189
Development of the System for Predicting Skid Number	189
Sensitivity Analysis of Prediction System.....	196
Recommended System for Predicting Skid Number	200
Illustration of an Aggregate Classification System Based on	
Proposed Model	201
Skid Analysis of Asphalt Pavements (SAAP)	202
Summary	212
 IX CONCLUSIONS AND RECOMMENDATIONS.....	213
Conclusions.....	213
Recommendations.....	215
 REFERENCES	217
 APPENDIX A	241
 APPENDIX B.....	254
 APPENDIX C	259
 APPENDIX D.....	289
 VITA.....	296

LIST OF FIGURES

		Page
FIGURE 1	Schematic plot of hysteresis and adhesion.	7
FIGURE 2	Pavement wavelength and surface characteristics.....	10
FIGURE 3	Schematic plot of microtexture/macrotecture.	10
FIGURE 4	Schematic plot of the effect of microtexture/macrotecture on pavement friction.	12
FIGURE 5	Different data acquisition methods.....	17
FIGURE 6	Decrease of pavement skid resistance as a result of polishing under traffic loading.	22
FIGURE 7	Generalized pavement-polishing model.	23
FIGURE 8	Aggregate methods for providing pavement texture.....	27
FIGURE 9	Mineral composition related to skid resistance.	32
FIGURE 10	First aggregate classification chart.	37
FIGURE 11	Modified aggregate classification chart (second edition).....	38
FIGURE 12	Map of Texas showing aggregate quarries by county location.	43
FIGURE 13	Aggregate classification based on old aggregate classification system. ..	44
FIGURE 14	Micritic, low porosity limestone from the Beckman pit.....	47
FIGURE 15	Grainstone with coated fossil fragments from the Beckman pit.	47
FIGURE 16	Coarsely crystalline limestone with Moldic pores from the Beckman pit.	48
FIGURE 17	Glauconitic dolomite from the Brownlee pit.....	49
FIGURE 18	Calcite and dolomite-cemented sandstone from the Brownlee pit.....	50
FIGURE 19	Heavily weathered dolomite from the Brownlee pit.	51
FIGURE 20	Sandy dolomitic limestone from the Brownwood pit.	52
FIGURE 21	Calcite and dolomite-cemented sandstone from the Brownwood pit.	53

	Page
FIGURE 22 Carbonate-cemented sandstone with abundant heavy minerals.	53
FIGURE 23 Chalcedony replacement of fossils and moldic porosity of Fordyce pit aggregates.	54
FIGURE 24 Chalcedony matrix with moldic pores from the Fordyce pit.....	55
FIGURE 25 Sandy dolomite from the El Paso, McKelligon pit.....	56
FIGURE 26 Fine-grained limestone from the El Paso, McKelligon pit.....	57
FIGURE 27 Dolomite and siderite-cemented sandstone from the McKelligon pit.....	58
FIGURE 28 Cross-polarized light view of altered granite from the McKelligon pit.	59
FIGURE 29 Fine-grained limestone with chalcedony from the Georgetown pit.	60
FIGURE 30 Moldic pores in limestone from the Georgetown pit.	60
FIGURE 31 Micro-Deval apparatus.	64
FIGURE 32 Mechanism of aggregate and steel ball interaction in Micro-Deval apparatus.	64
FIGURE 33 Schematic view of the AIMS system.	66
FIGURE 34 Schematic layout of each slab.	69
FIGURE 35 Schematic of the mold used in slab compaction.	71
FIGURE 36 Slab-thickness measuring scale used to adjust slab thickness.....	71
FIGURE 37 Walk-behind roller compactor.....	72
FIGURE 38 Schematic view of MMLS3.	74
FIGURE 39 Polishing machine assembly.....	76
FIGURE 40 British pendulum device.....	78
FIGURE 41 Schematic of sand patch method.	79
FIGURE 42 Schematic of measuring pavement skid resistance by DFT.	80
FIGURE 43 CTMeter.	81

	Page
FIGURE 44	Type D mixes degraded after 5000 cycles. 83
FIGURE 45	Aggregate properties. 86
FIGURE 46	Aggregate texture before and after Micro-Deval and percent change. 88
FIGURE 47	Aggregate angularity before and after Micro-Deval and percent change..... 88
FIGURE 48	Aggregate texture as function of Micro-Deval time..... 90
FIGURE 49	Measured MTD by sand patch method for different aggregates before and after polishing. 92
FIGURE 50	Results of British pendulum test for Type C mixes. 96
FIGURE 51	Results of the British pendulum test for PFC mixes. 96
FIGURE 52	British pendulum values for El Paso aggregate vs. polishing cycles. 101
FIGURE 53	British pendulum values for Beckman aggregate vs. polishing cycles. . 101
FIGURE 54	British pendulum values for Brownwood aggregate vs. polishing cycles..... 102
FIGURE 55	British pendulum values for Brownlee aggregate vs. polishing cycles..... 102
FIGURE 56	British pendulum values for Fordyce aggregate vs. polishing cycles. ... 103
FIGURE 57	British pendulum values for the 50 percent Beckman–50 percent Brownlee vs. polishing cycles..... 103
FIGURE 58	British pendulum values for El Paso aggregate vs. polishing cycles in PFC mix. 104
FIGURE 59	British pendulum values for Brownlee aggregate vs. polishing cycles in PFC mix. 104
FIGURE 60	British pendulum values for Brownwood aggregate vs. polishing cycles in PFC mix. 105
FIGURE 61	British pendulum values for Beckman aggregate vs. polishing cycles in PFC mix. 105
FIGURE 62	Calculated IFI for different aggregates vs. polishing cycle..... 108

	Page
FIGURE 63 Coefficient of friction for different aggregates vs. polishing cycle at 20 km/h.	109
FIGURE 64 MPD for different aggregates vs. polishing cycle.	109
FIGURE 65 Calculated IFI values vs. polishing cycle and fitted line for PFC mixes.	117
FIGURE 66 Calculated IFI values vs. polishing cycle and fitted line for Type C mixes.	117
FIGURE 67 DF_{20} values vs. polishing cycle and fitted line for Type C mixes.	118
FIGURE 68 DF_{20} values vs. polishing cycle and fitted line for PFC mixes.	118
FIGURE 69 Terminal IFI values for different aggregate types.	120
FIGURE 70 Rate of IFI change for different aggregate types.	121
FIGURE 71 Initial IFI values for different aggregate types.	121
FIGURE 72 Terminal DF_{20} values for different aggregate types.	122
FIGURE 73 Rate of DF_{20} change for different aggregate types.	122
FIGURE 74 Initial DF_{20} values for different aggregate types.	123
FIGURE 75 Mean IFI values for different aggregate types.	129
FIGURE 76 Overview of the friction model.	135
FIGURE 77 Aggregate gradation and fitted line for Brownlee-Beckman Type C mix.	136
FIGURE 78 Aggregate gradation and fitted line for Fordyce aggregate Type C mix.	137
FIGURE 79 Aggregate gradation and fitted line for Brownwood aggregate Type C mix.	137
FIGURE 80 Aggregate gradation and fitted line for Brownlee aggregate Type C mix.	138
FIGURE 81 Aggregate gradation and fitted line for Beckman aggregate Type C mix.	138

	Page
FIGURE 82 Aggregate gradation and fitted line for El Paso aggregate Type C mix.	139
FIGURE 83 Aggregate gradation and fitted line for Brownwood aggregate PFC mix.	139
FIGURE 84 Aggregate gradation and fitted line for Beckman aggregate PFC mix.	140
FIGURE 85 Aggregate gradation and fitted line for Brownlee aggregate PFC mix.	140
FIGURE 86 Aggregate gradation and fitted line for El Paso aggregate PFC mix.	141
FIGURE 87 Predicted vs. measured terminal IFI values.	145
FIGURE 88 Predicted vs. measured initial IFI values.	145
FIGURE 89 Predicted vs. measured IFI rate of change.	146
FIGURE 90 Mixture types used in the selected road segments.	152
FIGURE 91 Data availability for the different TxDOT districts.	153
FIGURE 92 Coefficient of variation of measured skid resistance for different sections.	154
FIGURE 93 Measured SN values versus traffic level.	158
FIGURE 94 Median SN values versus traffic level.	159
FIGURE 95 Standard deviation of measured SN values versus traffic level.	159
FIGURE 96 Measured SN values for different mix types.	160
FIGURE 97 Median of measured SN values for different mix types.	161
FIGURE 98 Standard deviation of measured SN values for different mixes.	161
FIGURE 99 Standard deviation of the measured SN values for low TMF level.	162
FIGURE 100 Standard deviation of the measured SN values for medium and high TMF level.	163
FIGURE 101 Values of measured SN for different aggregate types.	164

	Page
FIGURE 102 Median of measured SN values for different aggregate and mix types.....	165
FIGURE 103 Median of measured SN values for Type C mix design.....	170
FIGURE 104 Median of measured SN values for PFC mix design.	173
FIGURE 105 Median of measured SN values for surface treatments grade 3.	175
FIGURE 106 Median of measured SN values for surface treatments grade 4.	176
FIGURE 107 Layout of the measurement section.....	181
FIGURE 108 Measured MPD values for different mix types.	183
FIGURE 109 Mean profile depth vs. measured skid number.....	184
FIGURE 110 Mean dynamic friction at 20 km/h for different aggregates.	185
FIGURE 111 Mean dynamic friction at 20 km/h for different aggregate types.	186
FIGURE 112 Dynamic friction at 20 km/h vs. measured skid number for different mix types.	187
FIGURE 113 TMF vs. number of polishing cycles.....	193
FIGURE 114 Measured skid number vs. calculated skid number using PIARC equation.	194
FIGURE 115 Measured skid number vs. calculated skid number using modified PIARC equation.....	195
FIGURE 116 Relationship between measured and calculated MPD values.	196
FIGURE 117 Terminal friction values for different aggregates and mix designs.....	198
FIGURE 118 Polishing rate for different aggregates.	199
FIGURE 119 IFI values as a function of TMF for sample 1.....	199
FIGURE 120 SN values as a function of TMF for sample 1.....	200
FIGURE 121 Initial window of the program.....	203
FIGURE 122 Aggregate gradation input window.	204

	Page
FIGURE 123 Manual aggregate gradation window.	204
FIGURE 124 AIMS texture data input window.	205
FIGURE 125 Texture data points selection window.	206
FIGURE 126 Two-point texture measurement input window.....	206
FIGURE 127 Three-point texture measurement input window.....	207
FIGURE 128 MPD value input window.....	208
FIGURE 129 Traffic data input window.	208
FIGURE 130 Analysis type window.	209
FIGURE 131 A sample plot of skid number over the service years.....	210
FIGURE 132 Classification value setting window.....	211
FIGURE 133 Classification sample.....	211

LIST OF TABLES

		Page
TABLE 1	Comparison between Different Skid Resistance and Texture Measuring Techniques.....	19
TABLE 2	Comparison of Different Polishing Techniques.....	30
TABLE 3	Aggregate Classification Table.....	39
TABLE 4	Aggregate Classification Based on New System.....	45
TABLE 5	Aggregates Analyzed in Petrographic Study.....	45
TABLE 6	Abbreviation Selected for Aggregates and Mix Types in This Study.....	68
TABLE 7	Average Air Void Content Measured for Each Slab.....	73
TABLE 8	Experimental Setup.....	82
TABLE 9	Aggregate Test Results.....	85
TABLE 10	Result of Shape Measurements by AIMS.....	87
TABLE 11	Regression Coefficient of Texture Model.....	89
TABLE 12	Regression Constants Based on Three Measuring Times.....	90
TABLE 13	Measured MTD by Use of Sand Patch Method for Different Mixes.....	92
TABLE 14	Levene Statistic to Check the Homogeneity of Variances.....	93
TABLE 15	Results of the ANOVA Analysis for the Effect of Aggregate Type.....	93
TABLE 16	Results of the ANOVA Analysis for the Effect of Mix Type.....	94
TABLE 17	Results of the ANOVA Analysis for the Effect of Polishing Cycles.....	94
TABLE 18	Significance Level for Different Aggregate Types in Type C Mix.....	95
TABLE 19	Significance Level for Different Aggregate Types in Type D Mix.....	95
TABLE 20	Significance Level for the Effect of Different Polishing Cycles on Mixtures with Different Aggregates.....	98

	Page
TABLE 21	Significance Level for the Mean BP Values for Different Loading Cycles 98
TABLE 22	Significance Level for the Mean BP Values for Different Mixture Type 99
TABLE 23	Regression Coefficients for Different Aggregate 100
TABLE 24	Pairwise Comparison of Different Aggregates in Type C Mix 107
TABLE 25	Significance Level (p-value) of the Mean DF_{20} Values for Different Aggregate Types in Type C Mix 112
TABLE 26	Significance Level of the Mean DF_{20} Values for Different Aggregate Types in PFC Mix 114
TABLE 27	Results of Comparing Calculated Values of IFI for Type C and PFC Mixes.....116
TABLE 28	Results of the T-test for Comparing IFI Mean Values in Type C and PFC Mixes..... 116
TABLE 29	Values of the Regression Parameters of Proposed Model for DF_{20} 119
TABLE 30	Values of the Regression Model Parameters for IFI..... 119
TABLE 31	Results of Regression Analysis on Type C Mix 124
TABLE 32	Results of Regression Analysis on PFC Mix 125
TABLE 33	R-Squared Values and Significant Level for Type C Mix..... 127
TABLE 34	Calculated Weibull Parameters for Different Mixes..... 142
TABLE 35	Correlation Coefficients for Different Aggregate Properties..... 143
TABLE 36	Different Parameter of the Friction Model Estimated by Regression Analysis..... 144
TABLE 37	Number of Road Sections in Each District 150
TABLE 38	Aggregate Sources Used in Pavement Sections..... 150
TABLE 39	Mixture Types Used in Road Segments..... 151
TABLE 40	Traffic Clusters in Terms of Traffic Multiplication Factor..... 155

	Page
TABLE 41	Summary of Skid Resistance Measurements 156
TABLE 42	Aggregate Ranking Based on Measured Skid Resistance for Surface Treatment Grade 3 in Low Traffic Level..... 166
TABLE 43	Aggregate Ranking Based on Measured Skid Resistance for Surface Treatment Grade 4 in Medium and Low Traffic Levels..... 167
TABLE 44	Aggregate Ranking Based on Measured Skid Resistance for Type C Mixture in High, Medium, and Low Traffic Levels 168
TABLE 45	Aggregate Ranking Based on Measured Skid Resistance for PFC Mixture in High, Medium, and Low Traffic Levels 168
TABLE 46	Field Sections Used in Measuring Friction and Texture..... 179
TABLE 47	Lane Distribution Factor 182
TABLE 48	Calculated Scale and Shape Factors for Different Mixes 191
TABLE 49	Selected Aggregates Based on Terminal Texture 197
TABLE 50	Selected Aggregates Based on Polishing Rate..... 197
TABLE 51	Skid Number Threshold Values after 5 Years of Service201
TABLE 52	Aggregate Classification for Different Roads..... 202

CHAPTER I

INTRODUCTION

In 2005, 6.1 million traffic crashes, 43,443 traffic fatalities, and approximately 2.7 million traffic-related injuries were reported by the National Highway Traffic Safety Administration (NHTSA) throughout the United States (1).

Nationwide studies show that between 15 to 18 percent of all crashes occur on wet pavements (2,3,4). According to the National Transportation Safety Board and the Federal Highway Administration (FHWA), approximately 13.5 percent of fatal accidents occur when pavements are wet (5,6). Several researchers indicated that there is a relationship between wet-weather accidents and pavement friction (7,8,9,10,11). During wet conditions, the water film covering the pavement acts as a lubricant and reduces the contact between the tire and the surface aggregate (12,13). Hence, wet-pavement surfaces exhibit lower friction levels than dry-pavement surfaces. In addition to the lubrication effect of water at high speeds, certain depths of water film without any facility to drain may result in hydroplaning, which is considered the primary cause of accidents in wet-weather conditions (12,14).

Current accident rates can be reduced greatly by implementing corrective measures in hazardous areas. Safety evaluation of the roads and analysis of the different factors affecting pavement friction are necessary for future safety improvements. Research studies have shown that an increase in average pavement friction from 0.40 to 0.55 would result in a 63 percent decrease in wet-pavement crashes (15,16). Research by Kamel and Gartshore also showed that by improving skid resistance, wet-weather crashes decreased by 71 percent on intersections and 54 percent on freeways (15,17). A study by the Organization for Economic Cooperation and Development (OECD) revealed that there was a linear relationship between the slipperiness of the pavement surface and crashes. Moreover, with an increase in slipperiness of the pavement surface, the rate of crashes increased (15,18).

This dissertation follows the style of *Transportation Research Record*.

Roe et al. reported that with an increase in pavement friction, the rate of crashes decreased (19). Wambold et al. reported a statistically significant relationship between wet-weather crashes and the skid numbers measured with a skid trailer (20). Other researchers also demonstrated the relationship between pavement skid resistance and the effect of pavement friction improvement on crash rates (21,22,23,24,25).

Pavement friction is primarily a function of the surface texture, which includes both microtexture and macrotexture. Pavement microtexture is defined as “a deviation of a pavement surface from a true planar surface with characteristic dimensions along the surface of less than 0.5 mm,” while the pavement macrotexture is defined as “a deviation of 0.5 mm - 50 mm” (26,27).

Microtexture is primarily an aggregate surface characteristic that provides a rough surface that disrupts the continuity of the water film and produces frictional resistance between the tire and pavement. Macrotexture is an overall asphalt mixture characteristic that provides surface drainage paths for water to drain quickly from the contact area between the tire and pavement. As a result, macrotexture helps to prevent hydroplaning and improve wet frictional resistance, particularly at high speeds (28,29,30). In addition to the physical characteristics of the pavement surface, several other factors that influence the level of skid resistance on the pavement surface are (5):

- age of the pavement surface,
- seasonal variation,
- traffic intensity, and
- road geometry.

While there is much research about increasing the life span of pavement materials, there is no direct specification for the selection and use of aggregate and mixture design to assure satisfactory frictional performance. In addition, current methods of evaluating aggregates for use in asphalt mixtures are mainly based on historical background of the aggregate performance (31,32).

The high correlation between pavement skid resistance and rate of crashes demands a comprehensive material selection and mixture design system. This study focuses on the analysis of the material characteristics including aggregate and mixture type that affect skid resistance. In addition, this study aims to develop a model for

predicting skid resistance as a function of mixture design, aggregate characteristics, and traffic level that can be used as a tool for maintenance purposes.

PROBLEM STATEMENT

Aggregate physical characteristics and asphalt mixture design are important factors that influence the skid resistance of asphalt pavements. There is a need for developing a model for predicting asphalt pavement skid resistance as a function of aggregates and asphalt mixture design, as well as traffic level. This model can be used to design and maintain asphalt pavements that exhibit safe levels of skid resistance. It can also be used to select the proper combination of aggregate source and mixture design that is needed to achieve the required skid resistance for a given traffic level.

OBJECTIVES

The objectives of this project are to (1) study the influence of aggregate properties and mix types on asphalt pavement skid resistance, and (2) develop a model for predicting asphalt pavement skid resistance. These objectives were achieved by measuring and analyzing frictional properties of laboratory-prepared specimens and asphalt pavement sections that included a wide range of aggregates and mix designs. This research study involved the following tasks:

- 1) Measure some characteristics of various aggregate sources.
- 2) Prepare laboratory specimens and measure their skid resistance, friction, and texture after different polishing intervals.
- 3) Develop a prediction model for skid resistance as a function of polishing cycles in the laboratory based on measurable aggregate characteristics and mix gradation.
- 4) Measure and analyze the skid resistance of many sections in the field with different mixture types and aggregate sources.

- 5) Measure the texture using the circular texture meter (CTMeter) and the friction using the dynamic friction tester (DFT) in the field.
- 6) Relate the laboratory and field results to develop a prediction model for skid resistance as a function of aggregate texture, aggregate gradation, and traffic level.
- 7) Demonstrate the use of the new model in estimating the skid resistance of asphalt pavement sections incorporating different aggregate sources and mixture types.

ORGANIZATION OF THE STUDY

Chapter II of this dissertation includes the results of the literature review, while Chapter III includes a description of the materials and equipment used in this study. Chapter IV presents the results and discussion of the laboratory experiments, Chapter IV discusses the findings of the laboratory phase of this study, and Chapter V documents the development of the prediction model of skid resistance based on laboratory measurements. Chapter VI describes the analysis of the skid resistance measurements in the field, which is followed by a presentation of the results of measuring asphalt pavement frictional properties in Chapter VII. The system for predicting asphalt pavement skid number as a function of aggregate properties and mixture design is presented in Chapter VIII. The last chapter, Chapter IX, includes the conclusions and recommendations of this study.

CHAPTER II

LITERATURE REVIEW

INTRODUCTION

This chapter summarizes research studies that have been carried out on the characterization of the frictional properties of the pavement surface. It also explains the friction mechanism, the factors affecting frictional properties of the pavement surface, and the contributions of asphalt pavement microtexture and macrotexture to asphalt pavement surface friction. Additionally, methods that are currently used to measure the skid resistance and indices that have been used to describe friction and skid resistance are discussed. This chapter also discusses the different aggregate characteristics that have been reported to influence skid resistance, and the test methods that are used to measure these characteristics.

DEFINITION OF FRICTION

Pavement surface friction is a measure of pavement riding safety and has a great role in reducing wet-pavement skid accidents (33,34,35). Friction force between the tire and the pavement surface is an essential part of the vehicle-pavement interaction. It provides the driver with the ability to accelerate, maneuver, corner, and stop safely (36).

Skid resistance is the friction force developed at the tire-pavement contact area (1). There are many factors contributing to the development of friction between tires and a pavement surface including the texture of the pavement surface, the vehicle speed, and the presence of water. Additionally, the characteristics of the construction materials, construction techniques, and weathering influence pavement texture (36). Wilson and Dunn addressed several factors that affect the frictional characteristics of a tire-pavement system. These factors can be categorized as (37):

- vehicle factors:

- vehicle speed,
- angle of the tire to the direction of the moving vehicle,
- the slip ratio,
- tire characteristics (structural type, hardness, and wear), and
- tire tread depth;
- pavement surface aggregate factors:
 - geological properties of the surfacing aggregate,
 - surface texture (microtexture and macrotexture), and
 - type of surfacing;
- load factors:
 - age of the surface,
 - the equivalent number of vehicle traffic loadings,
 - road geometry, and
 - traffic flow conditions;
- environmental factors:
 - temperature;
 - prior accumulation of rainfall, rainfall intensity, and duration, and
 - surface contamination.

Li and others stated that it is very difficult to develop comprehensive models to predict in-situ pavement friction because of the complicated nature of the tire-pavement interaction (34).

Moore, in an attempt to explain the friction phenomenon between the tire and the pavement, showed that frictional forces in rubber materials are comprised primarily of adhesive and hysteresis components, as shown in FIGURE 1 (38,39). During sliding on a wet pavement, a complex interplay between adhesion and hysteresis forces contributes to vehicle stopping distance.

Intermolecular binding or adherence at the surface level creates the adhesive component of friction. As the microasperities or surface irregularities of the two surfaces are exposed to each other, Van der Waals or dipole forces provide an attractive force, keeping the two asperities together and preventing further movement (36,40).

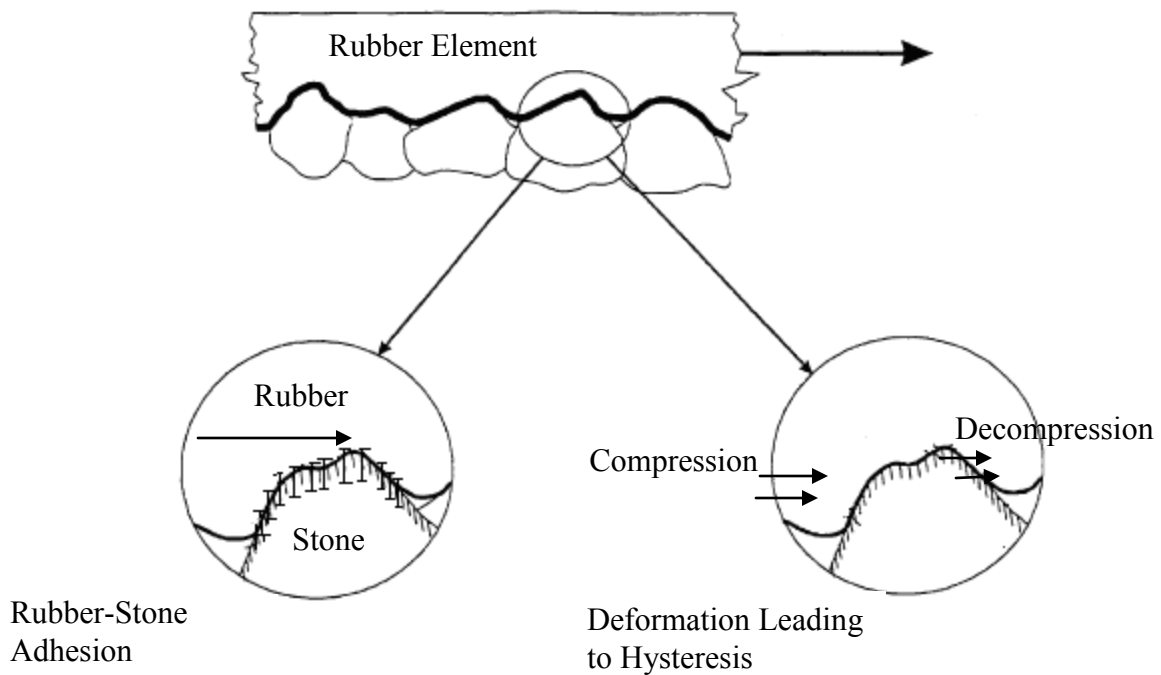


FIGURE 1 Schematic plot of hysteresis and adhesion (39).

The adhesion relates to the actual contact area between the tire and the pavement surface as well as the shear strength of the interface (39,41). The adhesion friction is dominant until critical slip occurs. Typically, at a driving speed on wet pavement, the adhesion accounts for two-thirds of the resistance force (42).

The hysteresis component of friction arises from the energy loss associated with the bulk deformation of rubber around the protuberance and depression of the pavement surface (43). It reflects the energy loss as the rubber is alternately compressed and expanded as it passes over the asperities of a rough surface pavement (39). Moreover, during a bulk deformation process, the friction force takes place at the interface of the moving objects. In this process, the tire drapes over, in, or around each macroasperity. After passing over the asperity, the rubber returns to its initial state but with a net loss of energy. This loss of energy contributes to the hysteresis part of friction (43).

Several researchers tried to relate the pavement texture and friction. Yandell emphasized the contribution of various texture scales to the hysteresis friction (44,45,46). Forster used linear regression analysis to show that the texture shape, defined also by an

average slope, explains friction satisfactorily (47). Roberts showed that the forces and the energy dissipation between the tire and the pavement surface depend on the material properties and the separation velocity (48). Kummer and Meyer reported that at high-speed sliding, the hysteresis component reaches a maximum value, while at relatively low speeds of sliding, adhesion is at a maximum value (36,49). Davis and others stated that there is a significant influence of mixture parameters on the ribbed tire skid resistance measurements and pavement texture as measured by a laser (3). Moreover, they stated that it is possible to predict some of the frictional properties of the surface mixes based on asphalt mix design properties (3).

In general, several studies reported that pavement texture influences skid resistance and friction. For example, Bond and others showed how differences in microtexture and macrotexture of pavement surfaces influence peak brake coefficients of a standard test tire (50,51). Leu and Henry demonstrated how skid resistance measurements on pavement surfaces are different based on their microtexture and macrotexture (52). Horne and Buhlmann, however, showed that surface friction measurements are poorly related to pavement texture measurements (51,53).

PAVEMENT TEXTURE

As travel safety and efficiency of road systems are of increasing importance to state agencies, friction measurements have become an essential part of pavement management systems (39). The friction-related properties of a pavement depend on its surface texture characteristics. These characteristics, as previously stated, are known as macrotexture and microtexture (49).

Macrotexture refers to the larger irregularities in the pavement surface (coarse-scale texture) that affect the hysteresis part of the friction. These larger irregularities are associated with voids between aggregate particles. The magnitude of this component depends on the size, shape, and distribution of coarse aggregates used in pavement construction, the nominal maximum size of aggregates, as well as the particular construction techniques used in the placement of the pavement surface layer (1,54).

Microtexture refers to irregularities in the surfaces of the aggregate particles (fine-scale texture) that are measured at the micron scale and are known to mainly be a function of aggregate particle mineralogy (1). These irregularities make the stone particles smooth or rough when touched. The magnitude of microtexture depends on initial roughness of the aggregate surface and the ability of the aggregate to retain this roughness against the polishing action of traffic and environmental factors (1,55). Microtexture affects mainly the adhesion part of the friction (1).

Several researchers tried to find quantitative measures to define microtexture and macrotexture and relate them to pavement friction. Moore defined three parameters for characterizing a surface texture: size, interspace or density, and shape (56). Taneerananon and Yandell showed that, compared with the two other parameters, the role of density or interspace is of minor importance in the water drainage mechanism (57). Kokkalis and Panagouli tried to explain surface texture by using fractals (58). They developed a model to relate surface depth and density to pavement friction.

According to the American Society for Testing and Materials (ASTM), pavement texture is divided into the two size classes of microtexture and macrotexture (ASTM E 867) (59). Surface asperities less than 0.5 mm (0.02 inch) in height are classified as microtexture, while asperities greater than 0.5 mm (0.02 inch) in size are considered as macrotexture (36). FIGURE 2 shows the different categories of pavement texture.

FIGURE 3 shows the schematic plot of the effect of micro/macrotexture on pavement friction. Adequate macrotexture is important for the quick dispersion of water accumulated on the surface of the pavement to prevent hydroplaning. Additionally, it aids in the development of the hysteresis component of friction that is related to energy loss as the tire deforms around macroasperities and consequently increases pavement friction (36,47,60). Macrotexture of the pavements could be estimated by simulating the percentage of contact points within the area of a tire footprint on the pavement surface (47). Bloem showed that an average texture depth of about 0.5 mm (0.02 inch) is required as the minimum to assure the desired depletion of water from the tire-pavement contact area (61).

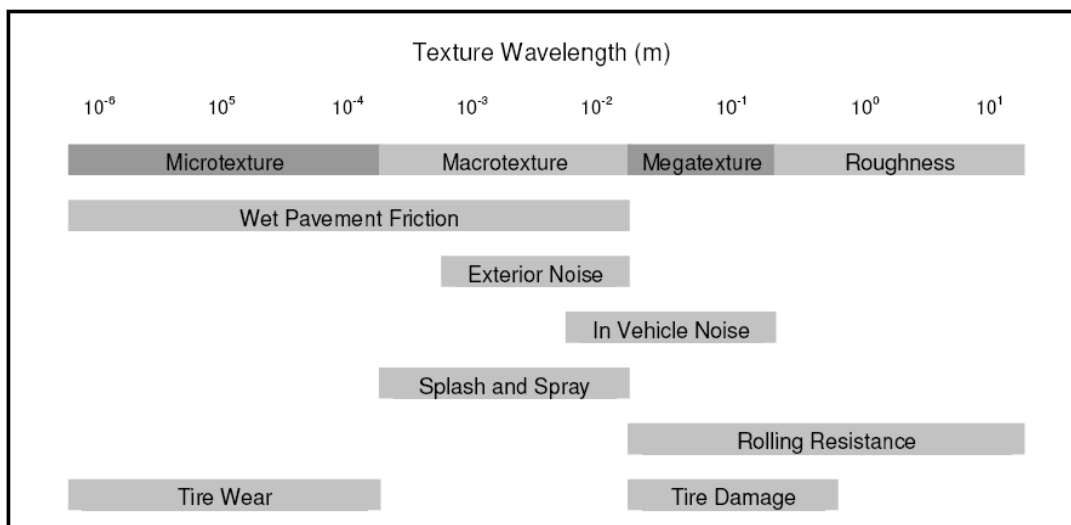


FIGURE 2 Pavement wavelength and surface characteristics (15).

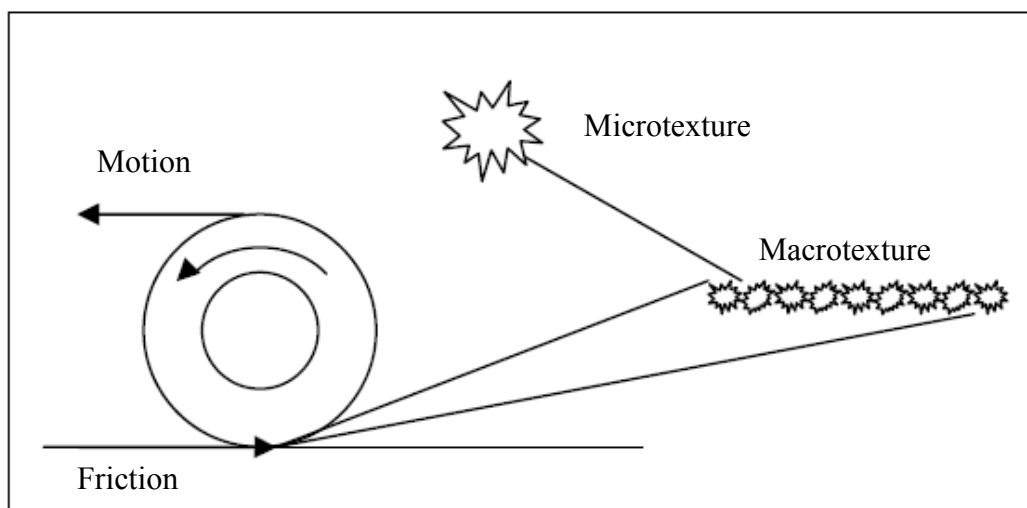


FIGURE 3 Schematic plot of microtexture/macrottexture (1).

Experiments conducted by Balmer showed that changes in surface textures from about 0.5 mm to over 3 mm (0.02 inch to 0.12 inch) resulted in a difference of 16 km/h (10 mph) in the speed for the initiation of hydroplaning (62,63).

Microtexture plays a significant role in the wet tire-pavement contact area. The size of microasperities plays a key role in overcoming the thin water film. Existence of microtexture is essential for squeezing the thin water film present in the contact area and generating friction forces (46). Moreover, the role of microtexture is to penetrate into the

thin water film present on the surface of the pavement so that the intimate tire-pavement contact is maintained (47). Drainage is controlled by the shape of microasperities (46,57,64). Savkooor also showed that drainage of the water film between the tire and the pavement is a function of amplitude and number of microasperities on a surface (46,65). Forster developed a parameter to account for microtexture (47). This parameter is a combination of average height and average spacing between microasperities. Horne stated that pavements with a good microtexture could delay hydroplaning (66,67). Pelloli based his research on five different types of surfaces found for which the amount of microtexture would affect the relationship between friction coefficient and the water depth accumulated on the surface (67,68). A study by Ong et al. showed that in the pavements comprised of coarse aggregates with high microtexture in the range of 0.2 mm to 0.5 mm, hydroplaning occurs at a 20 percent higher speed. This means that using materials with better microtexture reduces the chance of hydroplaning (67).

Moore reported a minimum water film thickness to be expelled by microasperities in the order of 5×10^{-3} mm (56). Bond and others stated the same order of magnitude from visual experiments conducted to monitor the water film between a tire and a smooth transparent plate (50).

Hogervorst stated that the change of skid resistance with vehicle speed depends on both microtexture and macrotexture (42). Microtexture defines the magnitude of skid resistance, and macrotexture controls the slope of skid resistance reduction as speed increases. Moreover, macrotexture affects the skid resistance of pavements at high speeds by reducing the friction-speed gradient and facilitating the drainage of water. Macrotexture has little effect on friction level at low speeds. Microtexture dominates and defines the level of friction at low speeds, as shown in FIGURE 4 (15,69,70). Researchers noted that both macrotexture and microtexture of pavement surface are influenced by the properties of the coarse aggregates exposed at the wearing course (36,47)

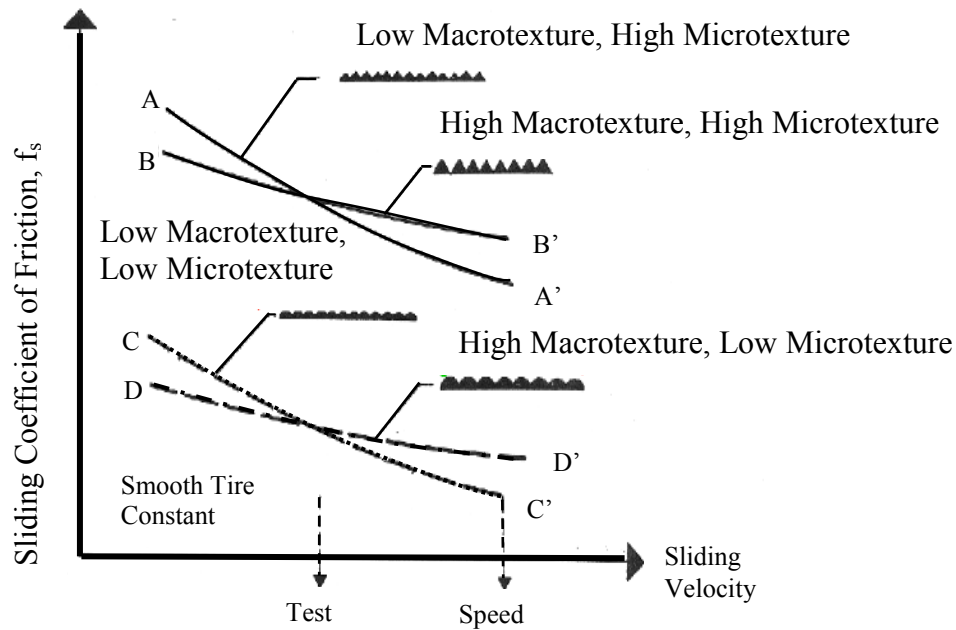


FIGURE 4 Schematic plot of the effect of microtexture/macrotexture on pavement friction (1).

MEASUREMENTS METHODS OF TEXTURE AND FRICTION

Field skid resistance is generally measured by the force generated when a locked tire slides along a pavement surface (71). These measurements should be precise, repeatable, and reproducible to reflect the real condition in the field (49). In general, pavement skid resistance is measured using a standard tire with the controlled wheel slip from 0 to 100 percent slip (ASTM E274, E303, E503, E556, E670, E707) (51,59).

There are four main types of skid resistance measuring approaches (72,73,74):

- locked wheel, where the force is measured while a 100 percent slip condition is produced;
 - sideways force, where the force is measured on a rotating wheel with a yaw angle of 20°;
 - fixed slip, where friction is measured for wheels that are constantly slipping;
- and

- variable slip, where devices are designed to measure at any desired slip, sweep through a predetermined set of values, or detect the maximum friction.

In each technique, the locked-wheel and variable-slip of tires and the relationship to the rolling, braking, or cornering friction coefficient is measured on wet-pavement surfaces (51).

Pavement friction testing with the locked wheel tester can be conducted with either a standard ribbed tire or a standard smooth tire (75). The most common method is the locked-wheel braking mode, which is specified by ASTM E274 (59). The concept of a skid trailer was introduced in the mid-1960s to improve the safety and efficiency of friction testing operations (39).

According to Saito et al., there are also some disadvantages associated with locked-wheel testers (76):

- Continuous measurement of skid resistance is not possible.
- Initial and operating costs of the test equipment are still high (49).
- Tests are conducted at only one speed so that speed dependency of skid resistance cannot be determined without repeated measurements on the same sections of road at different speeds.

Other types of measurement modes include the fixed slip, the variable slip, and the sideways force or cornering mode. In the slip mode (fixed or variable), the friction factor is a function of the slip of the test wheel while rolling over the pavement. The sideways mode uses a test wheel that moves at an angle to the direction of motion. The use of this test procedure is based upon the assumption that the critical situation for skid resistance occurs in cornering (76).

The above-mentioned methods are categorized as field modes. Other testing modes include portable and laboratory testers. The most common tester is the British pendulum tester (BPT), which is a dynamic pendulum impact-type tester and is specified in ASTM E303. The British pendulum tester (77) is one of the simplest and least-expensive instruments used in the measurement of friction characteristics of pavement surfaces. The BPT has the advantage of being easy to handle both in the laboratory and in the field. However, this method provides only a measure of a frictional property at a low speed (76). Although it is widely suggested that BPT measurements are largely governed

by the microtexture of the pavement surface, experience has shown that the macrotexture can also affect the measurements (35,78). Moreover, Fwa et al. and Liu et al. showed that the British pendulum measurements could be affected by the macrotexture of pavement surfaces, the aggregate gap width, or the number of gaps between aggregates (78,79). The BPT can also produce misleading results on coarse-textured test surfaces (75). Other researchers also pointed out that the BPT exhibited unreliable behavior when tested on coarse-textured surfaces (80,81,82). Won and Fu showed that the test results using a BPT were highly sensitive and resulted in a large variability (83). For the test results to be purely indicative, several factors need to be carefully controlled: the coupon curvature, the arrangement of aggregate particles on the coupon, the length of the contact path, and the slider load. All of these factors have significant effects on the results. The aggregates are further polished or conditioned during slider swing; consequently, the degree of polishing varies from aggregate type to aggregate type (83).

The DFT is a disc-rotating-type tester that measures the friction force between the surface and three rubber pads attached to the disc. The disc rotates horizontally at a linear speed of about 20 to 80 km/hr (12 to 50 mph) under a constant load. It touches the surface at different speeds, so the DFT can measure the skid resistance at any speed in this range (76). Studies by Saito et al. showed that there is a strong relationship between the coefficient of friction of the DFT and the British pendulum number (BPN) at each point for each measuring speed (76).

Measuring the pavement microtexture and macrotexture and relating these measurements to pavement skid resistance has been a major concern for pavement researchers (84,85,86). Macrotexture is generally measured using a volumetric technique. Essentially, this method consists of spreading a known volume of a material (sand, glass beads, or grease) on the pavement surface and measuring the resulting area. Dividing the initial volume by the area gives mean texture depth (MTD) (60,87). It has been reported that the sand patch method, Silly Putty method, and volumetric methods are burdensome to use in routine testing (55).

The outflow meter test (OFT) is another method to measure pavement macrotexture (88). The outflow meter measures relative drainage abilities of pavement surfaces. It can also be used to detect surface wear and predict correction measures (89).

The OFT is a transparent vertical cylinder that rests on a rubber annulus placed on the pavement. Then, the water is allowed to flow into the pavement, and the required time for passing between two marked levels in the transparent vertical cylinder is recorded. The recorded time indicates the ability of the pavement surface to drain water. This time is reported as the outflow time and can be related to pavement macrotexture (84).

As a result of significant advances in laser technology, computational power, and speed of small computers, several systems are now available to measure macrotexture at traffic speeds. The profiles produced by these devices can be used to compute various profile statistics such as the mean profile depth (MPD), the overall root mean square (RMS) of the profile height, and other parameters that reduce the profile to a single parameter (84). The mini-texture meter developed by British Transport and Road Research Laboratory (55), the Selcom laser system developed by researchers at the University of Texas at Arlington (55,90), and the noncontact high-speed optical scanning technique developed by the researchers at Pennsylvania State University (55,91) are examples of these systems. The first two of these devices use a laser beam to scan the pavement surface and, consequently, estimate pavement texture depth. The third device makes use of a strobe band of light with high infrared content to produce shadowgraphs. This equipment can collect data from a vehicle moving with traffic speed (55).

A device for measuring MPD called the CTMeter was introduced in 1998 (1,92). The CTMeter is a laser-based device for measuring the MPD of a pavement at a certain location. The CTMeter can be used in the laboratory as well as in the field. It uses a laser to measure the profile of a circle 11.2 inches (284 mm) in diameter or 35 inches (892 mm) in circumference (84). The profile is divided into eight segments of 4.4 inches (111.5 mm). The mean depth of each segment or arc of the circle is computed according to the standard practices of ASTM and the International Standard Organization (ISO) (84). Testing indicated that the CTMeter produced comparable results to the ASTM E965 sand patch test. Studies by Hanson and Prowell indicated that the CTMeter is more variable than the sand patch test (29).

There are several methods for measuring the microtexture (46). Schonfeld developed a method for the Ontario Transportation Department based on subjective assessment using photos taken from the pavement (93). He defined microtexture levels

from road stereo photography. Despite the fact that this method is a subjective and global method, the attributed levels were related to microasperity size and shape (46).

In a research study at Pennsylvania State University, it was found that there is a high correlation between the zero speed intercept of the friction-speed curve of the Penn State model and the RMS of the microtexture profile height. In addition, researchers found that the BPN values were highly correlated to this parameter. Therefore, the BPN values could be considered as the surrogate for microtexture measurements (94). In other studies, scanning electron microscope (SEM) imagery was used to capture images of the aggregate surface and measure aggregate microtexture and polishing action of traffic simulated in the laboratory by the British accelerated polishing test (95,96,97).

Direct measurements using optic or laser devices are gaining popularity because of their simplicity and ease of use. Forster used cameras to digitize and measure road profile images obtained from a projection device (47). He developed a parameter that combines measurements of the average height and average spacing of the microtexture asperities. Samuels used a laser sensor to record profiles directly (98). The laser system, with a measuring range of 6 mm and a spot size of around 0.1 to 0.2 mm, was not able to detect significant differences in microtexture between pavement surfaces (46). Yandell and Sawyer developed a device using the same measurement principle for in-situ use (45).

Improvements of measuring devices in recent years have made the measuring techniques faster and more reliable. New data acquisition techniques include interferometry, structured light, various 2D profiling methods, and the Scanning Laser Position Sensor (SLPS). FIGURE 5 shows a chart of topographic data acquisition techniques operating near the target scales that could be used on pavements (51).

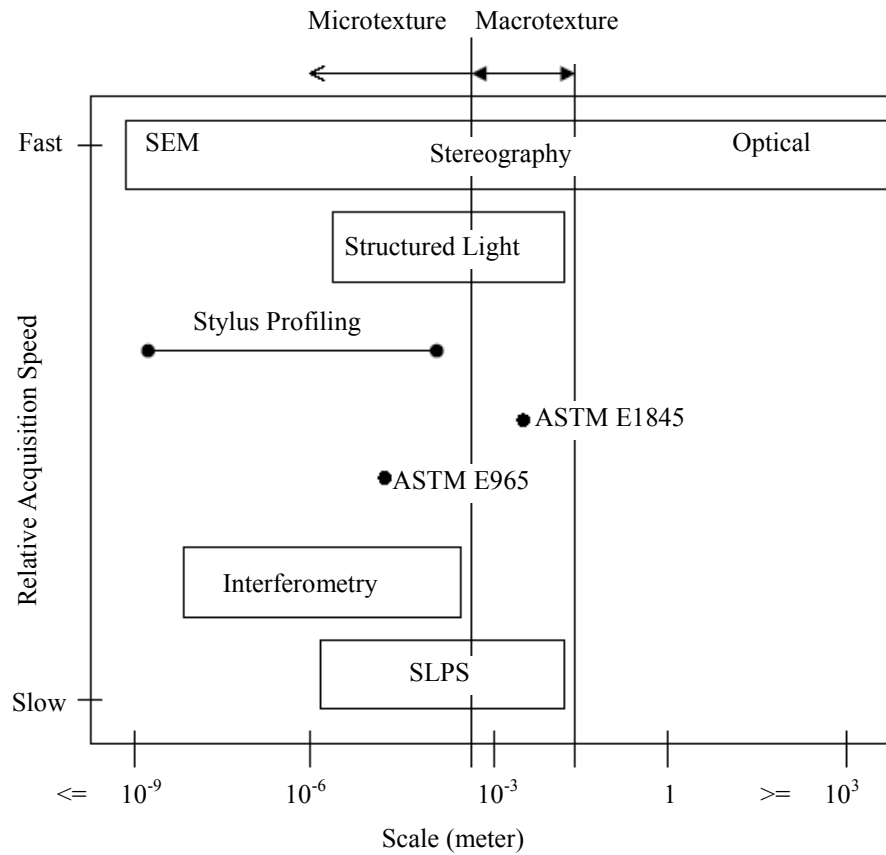


FIGURE 5 Different data acquisition methods (51).

Interferometry and the stylus profiling techniques are two different methods for measuring topographic data at scales that can be used for determining pavement texture (51).

Structured light and the SLPS are new methods of acquiring surface topography. These methods, however, have been proven to have limited functionality in measuring the surface asperities in the full range of different surfaces elevations. The SLPS was designed specifically for acquiring topographic data from pavement surfaces. This device is highly portable and can be easily utilized for in-situ measurement (51).

Stereo photography is a historical tool for the qualitatively visual inspection of surface features (93). Visual inspection requires special focusing tools and a pair of images (stereo pair), each taken at a specific distance perpendicular to the inspected surface. This technique can potentially be used to measure the topographic features of the surface, but the precision is obviously limited by the imagery equipment. Digital scanning systems and computer algorithms have recently been developed to analyze the pictures taken and generate the surface texture (51). TABLE 1 shows a summary comparison between different measuring devices and the advantages and disadvantages of each method (99).

The Aggregate Imaging System (AIMS) introduced by Masad et al. is one of the most recent methods, measuring the aggregate texture directly by use of a microscope and a digital image processing technique. This technique and the relationship of its results to asphalt pavement skid resistance will be discussed in the following chapter (100).

EFFECT OF PAVEMENT AGE AND WEATHER ON SKID RESISTANCE

Pavement skid properties or friction decreases over the life of the pavement due to an increase in accumulated traffic (35). Both microtexture and macrotexture change as a result of traffic loading. The rate of change in pavement texture depends on the aggregate type and mix design and traffic configuration.

TABLE 1 Comparison between Different Skid Resistance and Texture Measuring Techniques (99)

Device	About Device	Properties	Strengths	Weaknesses	Specs/used by
British Pendulum Tester	Pendulum arm swings over sample	Evaluates the amount of kinetic energy lost when a rubber slider attached to the pendulum arm is propelled over the test surface	Portable, very simple, widely used	Variable quality of results, cumbersome and sometimes ineffective calibration, pendulum only allows for a small area to be tested	ASTM E303
Michigan Laboratory Friction Tester	Rotating wheel	One wheel is brought to a speed of 40 mph and dropped onto the surface of the sample. Torque measurement is recorded before wheel stops.	Good measure of the tire/surface interaction, similar to towed friction trailer	Poor measurement of pavement Macrotexture, history of use on aggregate only	MDOT
Dynamic Friction Tester	Rotating sliders	Measures the coefficient of friction	Laboratory or field measurements of microtexture	N/A	ASTM E1911
North Carolina Variable Speed Friction Tester	Pendulum-type testing device	Pendulum with locked-wheel smooth rubber tire at its lower end	Can simulate different vehicle speeds	Uneven pavement surfaces in the field may provide inaccurate results.	ASTM E707
Pennsylvania Transportation Institute (PTI) Tester	Rubber slider	Rubber slider is propelled linearly along surface by falling weight	Tests in linear direction	Companion to Penn State reciprocating polisher, fallen into disuse	Formerly by PTI
Sand Patch	Sand spread over circular area to fill surface voids	Measures mean texture depth over covered area	Simple	Cumbersome, poor Repeatability, average depth only	ASTM E965

TABLE 1 Continued

Device	About Device	Properties	Strengths	Weaknesses	Specs/used by
Grease Patch	Grease spread over surface	Measures mean texture depth over covered area	Simple	Cumbersome, poor repeatability, average depth only, not widely used	NASA
Outflow Meter	Water flows from cylinder through surface voids	Estimates average texture	Simple, quick	For non-porous surfaces only	FHWA
Dromometer	Stylus traces surface	Lowers a tracing pin that creates a profile of the specimen surface	Can measure both microtexture and macrotexture	Can only be used on small areas of pavement	----
Surtronic 3+ Profilometer	Stylus traces profiles	Horiz. Res = 1 micrometer Vert. Res = 0.001 micrometer Traverse Length = 25.4 mm	Can read microtexture and macrotexture	Can only be used on small areas of pavement	----
Circular Track Meter	Laser based	Laser mounted on an arm that rotates on a circumference of 142 mm and measures the texture	Used with DFT, fast, portable, repeatable	Measures small area, relatively new	ASTM E2157

Moreover, weather-related factors also affect the surface microtexture and macrotexture properties of in-service pavements, and thus the pavement friction (12). The following subsections describe these factors that influence skid resistance.

Age of the Surface

Almost all new pavement surfaces have high texture and skid resistance. Aggregates used in road construction have to be resistant to crushing and abrasion to provide adequate skid resistance (42). Pavement texture, however, decreases over time because of the abrasive effects of traffic.

Traffic has a cumulative effect on a pavement; it wears the pavement surface and polishes the aggregate over time (12). The traffic wears and polishes the pavement surface to a value that may be less than that determined by the standard polished stone value (PSV) test in the laboratory (101). This polishing effect is caused by the horizontal forces applied by the vehicle tires on the pavement surface. The protruding aggregates are worn off and polished, and the surface microtexture and macrotexture reduce under these forces (36, 47, 102, 103, 104,). In addition, under the compacting effect of traffic, the protruding aggregates may be embedded in the pavement layer, which leads to a reduction in the depth of macrotexture. Accordingly, up to a 40 percent reduction in skid resistance as a result of pavement wear has been reported (105). Polishing of aggregates also relates to traffic intensity and classification. Furthermore, commercial vehicles contribute to most of the polishing (106). The geometries of the road gradients, curves, pedestrian crossings, roundabouts, and stop and give-way controlled intersections experience higher stresses, resulting in more polished surfaces. Polishing is related to traffic volumes, where high-volume areas require a better mixture design and construction (5).

The general trend for pavement skid resistance is such that pavement surfaces attain their peak skid resistance condition after a few weeks of traffic action because of wearing of the pavement surface. After that, skid resistance declines at a rapid rate at first as the exposed aggregate is worn, and some of its microtexture and macrotexture properties are lost as traffic loads polish the surface aggregates in the wheel paths. Then,

it declines more slowly and reaches an equilibrium state in which small deviations in skid resistance are experienced while traffic levels are constant and no structural deterioration is evident. This usually happens after 1 to 5 million passenger vehicles pass, or two years (3, 5, 76,107,108). FIGURE 6 shows the variation of pavement skid resistance versus pavement age.

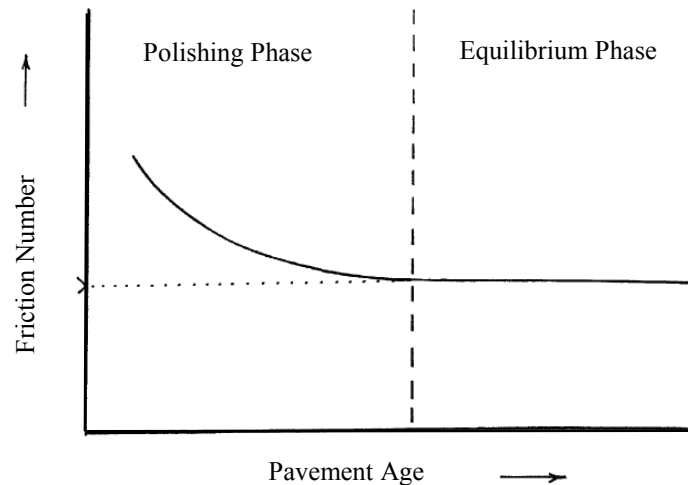


FIGURE 6 Decrease of pavement skid resistance as a result of polishing under traffic loading (109).

Seasonal and Daily Weather Variation

Weather-related factors (e.g., rainfall, air temperature, wind, etc.) are partially responsible for seasonal variations in the frictional properties of the tire-pavement interface (12). There are distinct seasonal patterns in skid resistance levels. Studies in the United Kingdom (81), U.S. (13,110), and New Zealand (111) showed a sinusoidal variation in skid resistance with seasonal change (37).

Generally, there is a decrease in pavement skid resistance from the seasonal changes of spring to fall (112). Summer months have the lowest levels of skid resistance caused by a decrease in precipitation. Dry weather in the summer allows the accumulation of fine particles and debris that accelerate polishing of the pavement surface. West and Ross showed that the size of grit affects the polishing rate of aggregates (113). The combination of polishing and particle accumulation, together with

contamination from vehicles, such as oil drippings and grease, results in a loss of microtexture and macrotexture during the summer months (37). A variation of approximately 30 percent of skid resistance has been observed between the minimum in the summer to the peak during the winter (112).

In winter, rainwater rinses the finer particles responsible for polishing and reacts with some aggregate surfaces. This results in a higher microtexture and macrotexture and, consequently, higher friction in the pavement surface (37). Some researchers also suggest that the water film covering the pavement for longer periods in winter acts as a lubricant and reduces the polishing effect of vehicles on the surface aggregate (37).

Day-to-day fluctuation of up to 15 pavement skid numbers has also been reported as a result of extreme changes in weather conditions (3,114). FIGURE 7 shows the generalized pavement-polishing model.

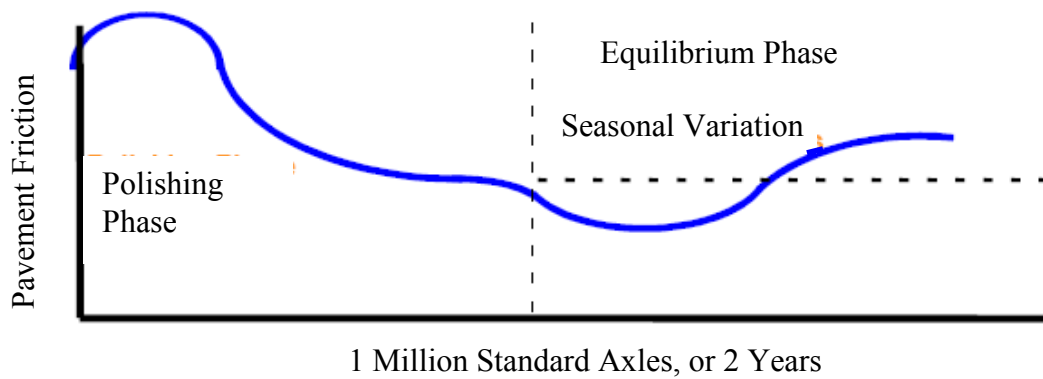


FIGURE 7 Generalized pavement-polishing model (5).

Temperature variation can also affect the frictional properties of pavement surfaces. Flintsch et al., through statistical analysis, showed that pavement temperature has a significant effect on the pavement frictional properties (12). In their studies, they found that for the finer wearing surface mixes, pavement friction tends to decrease with an increase in the pavement temperature at low speeds. At high speeds, the effect is reversed, and pavement friction tends to increase with an increase in pavement temperatures. The temperature-dependent friction versus speed models appears to be mix-dependent (12).

In another research study, Subhi and Farhad showed that both components of friction (hysteresis, adhesion) decrease with an increase in temperature (115).

AGGREGATE POLISHING CHARACTERISTICS

The ability of an aggregate to resist the polishing action of traffic has long been recognized as a highly important requirement for its use in pavement construction (61,116,117,118,119,120,121). Coarse aggregate characteristics (e.g., angularity and resistance to wear) are believed to have a significant role in providing adequate skid resistance in pavements. Generally, the desired pavement texture is attained and retained by use of hard, irregularly shaped coarse aggregate. Hard, polish-resistant coarse aggregate is essential to avoid reducing skid resistance of asphalt surfaces (61). The role of fine aggregate becomes significant only when used in relatively large quantities (122). Hogervorst showed that sharp, hard sand particles are highly desirable for enhancing the adhesion component of pavement friction (42).

Aggregates vary in their ability to maintain their microtexture against the polishing action of traffic. More specifically, aggregates polish or become smoother at different rates based upon their mineralogy (30,99). It is a common practice to assume that aggregates with lower Los Angeles (LA) abrasion loss, lower sulfate soundness loss, lower freeze-thaw (F-T) loss, lower absorption, and higher specific gravity have better resistance to polishing. Many researchers, however, believe that the LA abrasion test and other physical tests (e.g., freeze and thaw test) may not yield good predictions of polishing susceptibility, and reliability of predicting aggregate field polishing resistance using a single laboratory test is poor (30,113,123).

The petrographic examination is a valuable tool to understand the polishing process and to make recommendations for the use of aggregates (46,122). Generally, rocks containing igneous and metamorphic constituents are less susceptible to polishing than sedimentary rocks and could improve the overall frictional properties of the pavement surface (113).

Synthetic aggregates, e.g., slag or expanded lightweight aggregate (fabricated by heating natural clay), can also improve pavement frictional resistance (30,124,125).

Limestone, the most common type of aggregate used in road construction and the most susceptible aggregate type to polishing, produces the lowest skid resistance and is the main cause of slipperiness on pavements (120). Individual limestone deposits differ considerably in their resistance to polishing. For some types of carbonate aggregates (e.g., dolomite), polishing susceptibility has been found to decrease with an increase of clay content (31). Liang and Chyi found that as the calcite and dolomite contents increase, the polish susceptibility of aggregates decreases to a certain level. Further increases in the calcite and dolomite content results in an increase in polish susceptibility (126). The difference between polishing susceptibility in different aggregates can also be attributed to differences in the content of wear-resistant minerals, mainly silica (61). The siliceous particle content is considered to be equal to the insoluble residue after treatment in hydrochloric acid under standardized conditions. The resistance of limestone to polishing decreases as its purity increases (127). Bloem stated that the siliceous particle content should be at least 25 percent to have satisfactory polish resistance (61). Furthermore, the size of the siliceous particle is also important and affects polishing susceptibility. Quartz sandstone is considered excellent in frictional properties and exhibits higher wet-friction values because differential wear and dislodging of individual particles under traffic contribute to the desired surface texture (128,129). Furthermore, the quartz sandstone group is composed of hard quartz particles cemented together with a brittle silica binder. The resistance of these particles against abrasion is very satisfactory (61). These particles are exposed when the cement is worn away by traffic; therefore, this kind of aggregate has an excellent frictional performance, and its resistance to polishing is always high. As stated previously, the limestone and flint groups yield the lowest resistance. These types of aggregates have a simple fine cryptocrystalline structure and uniform hardness. Other groups, such as basalt, granite, and quartzite, have intermediate resistance against polishing. This intermediate resistance is related to the presence of altered feldspars and shattered grains of quartz and quartzite dislodging from a more resistant matrix. The basalt group, however, yields high resistance because of its softer mineral composition and the proportion and hardness of secondary minerals. In

indigenous rock groups, the petrologic characteristics that affect resistance to polishing are the variation in hardness between the minerals and the proportion of soft minerals. Finer-grained allotriomorphic igneous rocks have a tough, cohesive surface that will polish considerably. Rocks with cracks and fractures in the individual mineral grains have higher resistance because such grains are weak and dislodge from the matrix easily, whereas finer-grained rocks tend to polish more readily (5,61,130). Sand and gravel are usually comprised of wear-resistant particles and have desirable frictional properties (61).

FIGURE 8 shows four different methods by which aggregates provide texture to a pavement surface. The first aggregate is a very hard, angular aggregate composed of a single mineral type. This aggregate resists polishing action, but it will eventually become less textured and more polished. Furthermore, rocks consisting of minerals with nearly the same hardness wear uniformly and tend to have a high polishing susceptibility (5).

The second aggregate type results in nearly the same type of wear pattern as the first, but the crystals forming the particle are not well cemented together. The soft mineral wears away rapidly, exposing the hard grains to traffic and providing a harsh and more textured surface. Before polishing the asperities of these hard grains, the aggregate matrix has been worn out to such an extent that it can no longer hold the hard particles, allowing them to be dislodged so that new angular, harsh grains can be exposed (109,131). This continual renewal of the pavement surface is believed to maintain good skid resistance properties. The aggregates that have coarse, angular, and harder mineral grains uniformly scattered in a softer mineral matrix have higher skid resistance (58).

The third and fourth aggregate types wear in similar fashion. Both of these aggregates are composed of a hard mineral and a weak matrix. For the fourth type, the air voids act as the weak matrix. As the particles are polished, the weak matrix breaks down and releases the worn hard minerals exposed to traffic. This exposes fresh, unweathered surfaces that maintain their texture for extended periods of time and keep their frictional properties for a longer period (132).

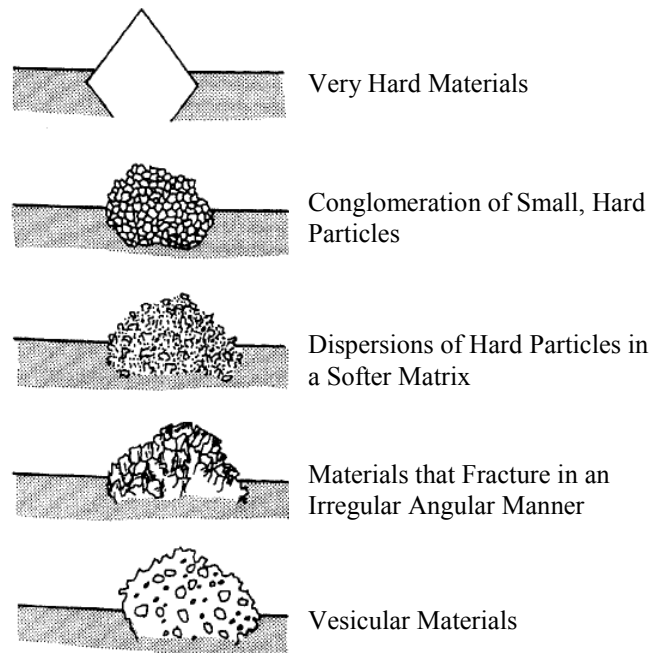


FIGURE 8 Aggregate methods for providing pavement texture (133).

PRE-EVALUATION OF AGGREGATE FOR USE IN ASPHALT MIXTURE

The resistance against polishing of an aggregate type is the key factor in providing skid resistance. The use of polish-resistant coarse aggregates or other aggregates with good frictional performance has always been considered a useful way to maintain friction above an acceptable level (58). The evaluation of the aggregates with respect to their polishing behavior can be achieved by using a laboratory test procedure (1).

Several researchers tried to develop laboratory test methods to pre-evaluate the aggregates and relate the properties of aggregates to skid resistance; however, there is little agreement among researchers in terms of the engineering properties that should be considered in an aggregate to provide adequate frictional resistance at various average daily traffic (ADT) levels.

Methods that are used for pre-evaluation of aggregates are mainly based upon using the British polish value (BPV). This test, however, is believed to measure only the microtexture of the pavement or the terminal polished value once the pavement reaches

its equilibrium skid resistance (134). Recent studies performed by Fwa et al. and Liu et al. showed that the BPN value is a function of many factors (e.g., magnitude and number of gaps between the aggregates' coupon curvature, the arrangement of aggregate particles in a coupon for heterogeneous materials such as gravel, the length of the contact path, and the slider load), and this test has a high variability (78,79,83).

Crouch et al. believed that current methods of pre-evaluating the aggregates for asphalt surface courses, such as the British pendulum and British polishing wheel, as well as chemical or mineralogical methods, are only able to classify well-performing aggregates (132,135). They used a modified version of the American Association of State Highways and Transportation Officials (AASHTO) standard device (AASHTO TP33) to measure the uncompacted voids in coarse aggregates that were subjected to various times in the LA abrasion test. Measuring the change in aggregate weight in the LA abrasion test for various times is an indication of the aggregates' abrasion and breakage rate. By this method, they were able to measure the angularity change indirectly. Although this method does evaluate how the aggregates change over time, it is still considered an indirect method, and it uses the LA abrasion test, which primarily breaks aggregates rather than abrading them (132).

Do and others used lasers to measure the surface profile of pavement sections to determine the microtexture and macrotexture of the pavement. These measurements were related to skid resistance (46,132). Gray and Renninger showed that polish susceptibility decreases as the presence of insoluble constituents such as silica increases (118). Tourenq and Fourmaintraux proposed a formula to calculate the PSV values of stones from their mineral hardness (96). Prowell et al. suggested Micro-Deval as a surrogate to determine an aggregate's resistance to weathering and abrasion instead of a sulfate soundness test (136). This Micro-Deval abrasion loss is also related to the change in macrotexture over time. Mahmoud recommended the use of Micro-Deval to polish aggregate and AIMS to measure loss of texture (137).

Polishing techniques are part of any aggregate classification system that evaluates the aggregate for use in the pavement surface. There have been several types of polishing equipment used in the past for polishing asphalt mixes, including:

- the Penn State Reciprocating Polishing Machine (ASTM E1393),
- the circular track polishing machine,
- the Michigan wear track, and
- the North Carolina State University (NCSU) Wear and Polishing Machine (ASTM E660).

Among the polishing techniques mentioned above, only the Michigan wear track is still being used; the others have been discontinued. The Michigan wear track polishes flat circular specimens, and the polishing action is simulated by three conical rubber rollers in the presence of water and grit (30,138). The National Center of Asphalt Technology (NCAT) has recently developed a new machine for polishing asphalt pavement slabs. In this machine, three rotating wheels move around a circle with the same diameter as the DFT and CTMeter devices, making it a suitable device for studying the effect of polishing with these devices (139). This machine is discussed in detail in the next chapter. TABLE 2 shows comparisons between different polishing devices.

PREDICTIVE MODELS FOR SKID RESISTANCE

Having a good model to predict friction change during the lifetime of a pavement would aid in predicting pavement performance and identifying the appropriate time for any treatment and rehabilitation measures.

TABLE 2 Comparison of Different Polishing Techniques (99)

Device	About Device	Properties	Strengths	Weaknesses	Specs/used by
British Polishing Wheel	Wheel for polishing away macrotexture	Curved aggregate specimens polished by a rotating wheel	Accelerated polishing for laboratory testing, bench sized	Coarse aggregate coupons only, does not affect macrotexture or mix properties	ASTM D 3319
Michigan Indoor Wear Track	Large circular track	Wheels centered around pivot point, move in circle around track	Close to real world	Track is very large and Cumbersome, time-consuming sample preparation, used for aggregates only	MDOT
NCSU Polishing Machine	Four wheels rotate around central pivot	Four pneumatic tires adjusted for camber and toe-out to provide scrubbing action for polishing	No need for water or grinding compounds, can polish aggregate or mixes	Polishes a relatively small area or few number of samples	ASTM E 660
NCAT Polishing Machine	Three wheels rotate around central pivot	Three pneumatic tires adjusted for camber and toe-out to provide scrubbing action for polishing	Sized to match DFT and CTMeter	New device developed by NCAT based on older devices	NCAT
Penn State Reciprocating Polishing Machine	Reciprocating pad	Reciprocates rubber pad under pressure against specimen surface while slurry of water and abrasive are fed to surface	Portable, can be used to polish aggregate or mix in laboratory or field	Polishes a relatively small area, oscillation obliterates directional polishing, fallen into disuse	ASTM E 1393

Because of the complex interaction between many factors affecting pavement skid resistance, developing such a model is not an easy task. Many researchers have tried to develop theoretical and empirical models to predict skid resistance. These models range from ones based on simple laboratory tests to complicated ones based on theoretical interaction between the tire and the pavement surface. These models are useful tools to predict pavement skid resistance over its life span.

Tire-pavement models are categorized into three different categories including (30):

- statistical-empirical, which is mainly based on collected road data with different characteristics and statistical analysis;
- fundamental, which is based on physical modeling of the pavement surface and tire; and
- hybrid, which is a combination of statistical and fundamental models.

Stephens and Goetz used the fineness modulus as a key factor to predict the skid resistance of an asphalt pavement (140). Dahir and others were the first to try relating aggregate characteristics to pavement skid resistance (141). In their research, they found some correlation between amount of acid insoluble particles and field skid performance, but not enough data to support a regression equation. They were the first to propose the use of the laboratory BPV as a surrogate for field terminal condition. They also considered the difference between the initial and terminal laboratory BPV as a measure of polishing characteristics of the aggregate (132). Henry and Dahir and Kamel and Musgrove then used the BPV of an aggregate sample as a parameter for the prediction of a pavement skid resistance (134,142). Henry and Dahir in other research found a relationship between BPV and microtexture (134). Moreover, they introduced the concept of percent-normalized gradient, which is a gradient of friction values measured below and above 60 km/hr speed and shows how strongly friction depends on the relative sliding speed. Moreover, this index incorporates both microtexture and macrotexture into the prediction of pavement skid resistance (15,134).

Mullen et al. studied the mineralogy of aggregates in relation to skid resistance. An optimum percentage of hard minerals distributed within a softer matrix was discovered, which allowed for the selection of materials that should perform well in the field (FIGURE 9) (143).

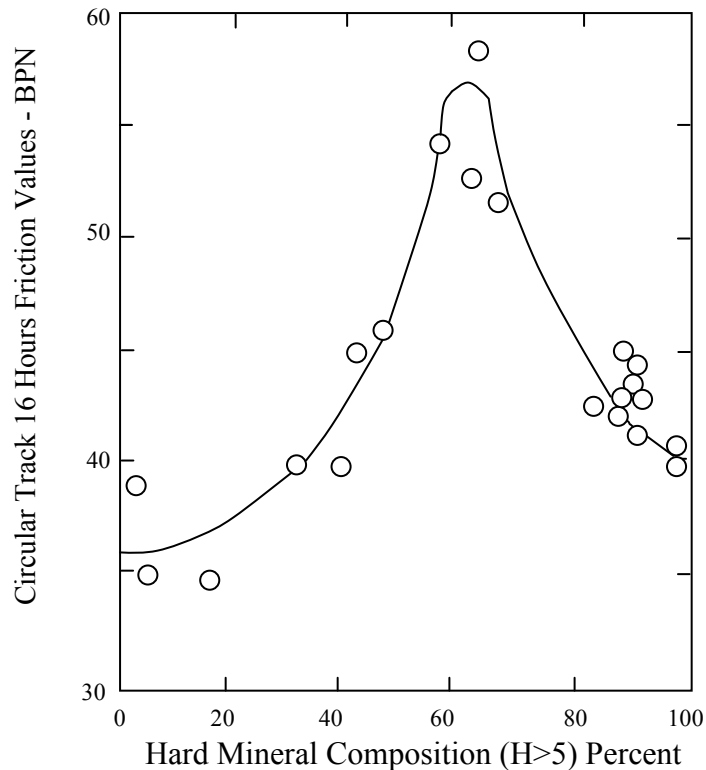


FIGURE 9 Mineral composition related to skid resistance (143).

Emery developed a pavement friction prediction model relating skid resistance to pavement age, accumulated traffic level, and mix properties including aggregate polish resistance, mixture volumetrics, and Marshall stability and flow. The field measurements showed a good agreement between measured and predicted values (144). Yandell et al. developed a complex physical model based on tire-pavement interaction (86). In their model, they considered the pavement surface and tread rubber properties as main factors affecting the skid number. Field verification showed a good agreement between predicted and measured values (86). Ergun et al. tried to relate pavement skid resistance and texture measurements by use of image analysis. They also showed there is a good agreement between measured and predicted skid values (60).

Stroup-Gardner and others found a good correlation between MPD and skid number. They also developed a model to predict skid number (145). Ahammed and Tighe found a close relationship between vehicle speed, surface texturing method, cumulative traffic volume, concrete compressive strength, and concrete pavement skid resistance and developed a model that was able to predict skid numbers for concrete pavements (146).

Luce et al. investigated the relationship between pavement friction and polishing susceptibility, mix gradation, and aggregate type. Based on measuring changes in the aggregate texture caused by abrasion in Micro-Deval, they proposed a method to relate pavement skid resistance to aggregate polishing resistance that was verified for nine different field test sections (132).

INTERNATIONAL FRICTION INDEX (IFI)

There are several measurement techniques throughout the world to assess pavement skid resistance. There are many indices explaining the skid resistance of a road including coefficient of friction, BPV, skid number, friction number, and IFI (30,85). How to harmonize different measurements of the skid resistance and make a unique base for comparing them is a concern. The IFI is a recent index that has been developed to harmonize friction and texture measurements by means of different test methods (20,26, 30,92, ,147,148,). This index was developed through collecting a wide range of friction data measured by several test methods on different pavement surfaces mainly in Spain and Belgium during an international Permanent International Association of Road Congresses (PIARC) study. In this study, a model originated by Penn State researchers was used. In this model, two important factors affecting pavement skid resistance were considered. The original model has the form of:

$$F_{\mu}(s) = F_0 \cdot e^{\frac{-s}{s^p}} \quad (1)$$

where:

S is slip speed,

F_{μ} is friction,

F_0 is a constant that relates to microtexture, and

S_p is a constant that relates to macrotexture (30,148).

During the international study done by PIARC, a curve relating slip speed was established for each pavement section. This so-called golden curve shows the friction experienced by a driver during emergency braking. Then, by using proper calibration factors, the equipment was able to predict the golden curve. It is worthwhile to know that the friction reported for each test section was at a speed of 60 km/h. The IFI is composed of two numbers—F60 and S_p —that are calculated as follows (30,148).

- Speed constant (S_p) parameter is calculated based on texture measurements:

$$S_p = a + b T_x \quad (2)$$

where “a” and “b” are calibration factors and different for each measuring device and T_x is a measure of pavement texture.

- The friction measurement at a slip speed FR(S) is then converted to a measurement at 60 km/h FR(60):

$$FR(60) = FR(S) \times e^{\left(\frac{S-60}{S_p}\right)} \quad (3)$$

- Finally, the F(60) is recalculated by the application of a speed adjusted friction value FR(60) and the following equation:

$$F60 = A + B FR(60) + C T_x \quad (4)$$

where “A,” “B,” and “C” are calibration constants for a selected friction device. These values have been standardized for each measuring device in ASTM E1960.

Two parameters used in the IFI calibrated model—wet friction at 60 km/h (F60) and the speed constant of wet pavement friction (S_p)—are indications of the average wet coefficient of friction experienced by a driver during a locked-wheel slide at a speed of 60 km/h and dependence of the wet-pavement friction on the sliding speed, respectively (30,111).

Based on ASTM E 1960, the calibration factors for the CTMeter are $a = 14.23$ $b = 89.72$ and for DFT are $A = 0.081$, $B = 0.732$. Based on these values, the IFI and S_p could be calculated as (59):

$$IFI = 0.081 + 0.732 DF_{20} e^{\frac{-40}{S_p}} \quad (5)$$

$$S_p = 14.2 + 89.7 MPD \quad (6)$$

where:

DF_{20} = wet friction number measured by DFT at the speed of 20 km/h,

MPD = MPD measured by CTMeter (mm).

These equations indicate that the effect of the wet friction coefficient at 20 km/h is more important than MPD. MPD is a parameter defined by ASTM E1845 as “the average of all of the mean segment depths of all of the segments of the profile,” where mean segment depth is “the average value of the profile depth of the two halves of a segment having a given base length,” and profile depth is “the difference between the amplitude measurements of pavement macrotexture and a horizontal line through the top of the highest peak within a given baseline.” This value could be easily read from a CTMeter (30,59).

The IFI values for the locked-wheel friction trailer using a smooth tire ($A = 0.04461$, $B = 0.92549$, and $C = 0.097589$) and rib tire ($A = -0.02283$, $B = 0.60682$, and $C = 0.097589$) at desired speeds are (30):

$$IFI = 0.045 + 0.925 \times 0.01 \times SN(64)S.e^{\frac{4}{S_p}} \quad \text{For Smooth Tire} \quad (7)$$

$$IFI = -0.023 + 0.607 \times 0.01 \times SN(64)R.e^{\frac{4}{S_p}} + 0.098 \times MPD \quad \text{For Rib Tire} \quad (8)$$

where $SN(64)S$ is the skid number measured at test speed of 64 km/h using a smooth or rib tire divided by 100.

Because the texture value is not measured during the friction measurement by trailer, using the previous equations for calculating the IFI requires two separate measurements by rib and smooth tire. Moreover, to determine the IFI, the two equations

for rib and smooth tire should be set equal; using another equation relating MPD and S_p values, the total unknowns reduce to one. Then, the IFI can be easily calculated (30).

WET WEATHER ACCIDENT REDUCTION PROGRAM (WWARP) IN TEXAS

In 1999, Texas Department of Transportation (TxDOT) implemented a statewide program to reduce skid-related accidents in the state of Texas. The objective of this program was to develop the most effective method to minimize wet-weather skidding accidents at a reasonable cost. This program uses all available resources such as accident data and analytical expertise, friction test devices, and local knowledge of roadway friction conditions to identify and correct sections of the roadway with a high number of skid accidents to ensure that the pavement has adequate and durable skid resistance throughout the design life of pavement (149).

Based on this program, the minimum acceptable friction level on the pavement surface is identified. TxDOT required that friction level be classified into three categories—low, moderate, and high—based on roadway attributes. The amount of rainfall (inches/year), traffic (average daily traffic), speed (mph), percent of trucks, vertical grade (percent), horizontal curve, driveway (per mile), cross slope (inches/ft), surface design life, and intersecting roadways are pavement attributes that define the required friction level.

The WWARP includes material testing and evaluation, pavement design and construction, and pavement management and rehabilitation practices to ensure that the pavement meets the acceptable friction level. Pavement design and construction, as part of this program, consists of evaluating the aggregate capability to provide adequate skid resistance properties.

Selecting the polish-resistant aggregate is a key factor to ensure adequate and durable pavement skid resistance. The Surface Aggregate Classification (SAC) system is one of the WWARP's outcomes that has experienced several changes since the inception of WWARP. The SAC system enables the mixture design engineer to select appropriate

aggregate type to be used in the pavement surface based upon pavement frictional requirements.

The first SAC was developed in 1999. In this SAC, the aggregates were classified into four groups based on their PSV and magnesium sulfate soundness test results, as shown in FIGURE 10. The following classification chart was used from October 1, 1999, to February 28, 2006.

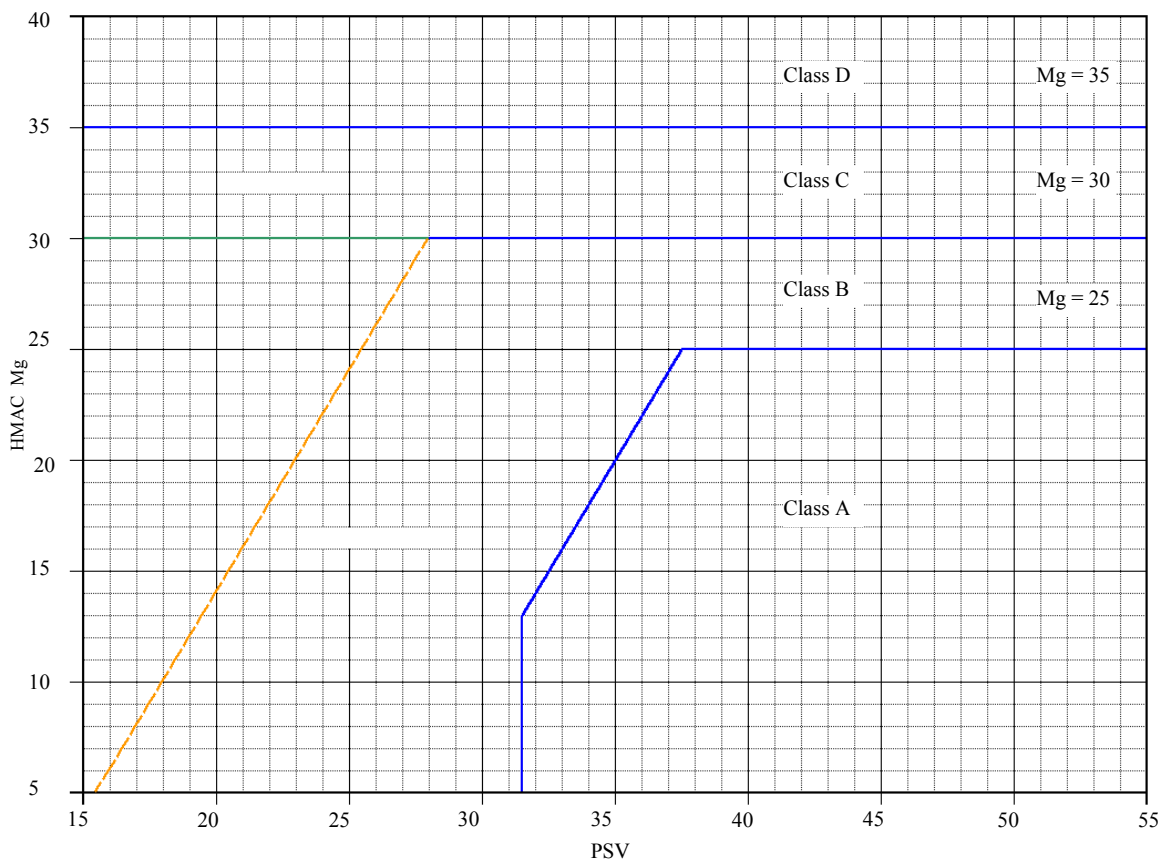


FIGURE 10 First aggregate classification chart.

The chart changed after February 28, 2006, and the inclined line between class B and class C was removed.

FIGURE 11 shows the second version of the SAC chart, which was used from March 2006 to December 2007. Based on this system:

- All bituminous coarse aggregates that had both an acid insoluble residue of 70 percent or greater and magnesium sulfate soundness loss of 25 percent or less were classified as class “A” sources.
- All aggregate sources that did not meet the criteria of a low carbonate source as defined above were classified based on a combination of their residual solid tire PSV and magnesium sulfate soundness weight loss. These materials were classified into groups (A, B, C, and D), as shown in FIGURE 11.

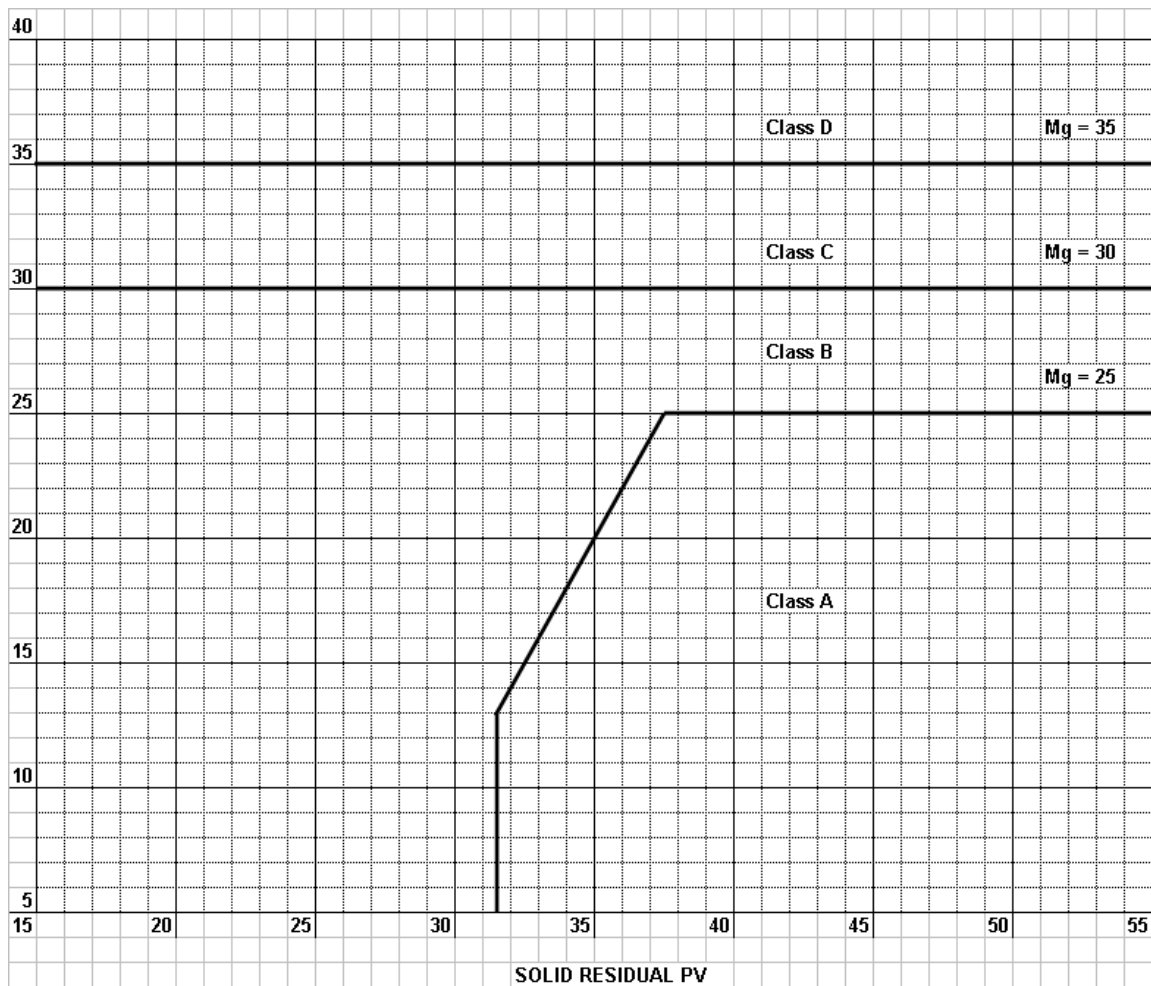


FIGURE 11 Modified aggregate classification chart (second edition).

In 2006, TxDOT contracted with the Texas Transportation Institute (TTI) to undertake a project to implement the AIMS in TxDOT operations. The research focused on measuring aggregate shape characteristics. Moreover, a new method was proposed in

the research to better test aggregate resistance to polishing. The proposed method was based on the magnesium sulfate soundness and texture results from AIMS. It proved to be more sensitive than the method that was being used by TxDOT. Furthermore, the new SAC system allowed the aggregates to be spread more evenly in four different categories (150).

TxDOT began a program called Aggregate Quality Monitoring Program (AQMP) in 1995 to provide the requirements and procedures for the Construction Division, Materials and Pavements Section (CST/M&P) to accept aggregate products that have demonstrated continuing quality and uniformity. In this program, TxDOT has revised the SAC system and released a new aggregate classification system. This system has been effective since December 2007. Based on the new system, the aggregates are classified according to TABLE 3 (151).

TABLE 3 Aggregate Classification Table

Property	Test Method	SAC A	SAC B	SAC C
Acid Insoluble Residue, % min	Tex-612-J	55		
5-Cycle Mg, % max	Tex-411-A	25	30	35
Crushed Faces, 2 or more, % min	Tex-460-A	85	85	85

SUMMARY

In this chapter, the importance of providing adequate levels of skid resistance was explained. Previous studies were reviewed, the results of which indicated that there is a strong relationship between wet-weather accidents and skid resistance of the pavement surface. Improving the pavement skid resistance was found to reduce the number of crashes in numerous research studies. This chapter also discussed the mechanism of friction between tire and pavement and the adhesion and hysteresis components of friction were explained.

Several research studies pointed out the pavement skid resistance is attributed to pavement microtexture and macrotexture. Macrotexture refers to the larger irregularities

on the pavement surface and associated with voids between aggregate particles and mainly affect the hysteresis part of the friction. The magnitude of this component depends on the size, shape, and distribution of coarse aggregates used in pavement construction. Microtexture refers to irregularities in the surfaces of the aggregate particles and is known to mainly be a function of aggregate particle mineralogy and affect the adhesion part of the friction.

Different methods for measuring pavement friction and texture were discussed in this chapter. Field skid resistance is generally measured by the force generated when a locked tire slides along a pavement surface. Other pavement texture and friction measuring techniques such as British pendulum, patch test, outflow meter, CTMeter, DFT, and recently developed imaging systems were also explained in this chapter.

Furthermore, the concept of IFI, which is used to harmonize different pavement friction measuring tools and express the pavement friction as a unique value measured by different equipment, was introduced.

Several research studies found that pavement friction decreases over time and reaches an equilibrium state in which the skid resistance remains almost constant. The polishing susceptibility of the aggregate was found to be one of the most important factors on the rate of decrease and terminal value of skid resistance. Many researchers tried to quantify polishing susceptibility of aggregates based on simple laboratory tests.

Petrographic examinations proved to give information about the polishing susceptibility. For example, the content of acid insoluble particles of an aggregate has the most influence on the polishing susceptibility. Some researchers concluded that limestone aggregate is more prone to polishing than granite. Several research studies, however, showed that other mechanical tests are also required to evaluate the aggregate resistance to polishing. Different test methods, such as the British pendulum test, LA abrasion test, and magnesium sulfate soundness test, were discussed in this chapter, and advantages and disadvantages of each one were explained.

The method currently used by the Texas Department of Transportation to evaluate the aggregate polishing susceptibility was also described. This method classifies aggregate based upon measuring the acid insoluble content, magnesium sulfate soundness weight loss, and percentage of aggregate with two or more crushed faces.

In order to plan for maintenance and rehabilitation of pavement surface, pavement friction prediction models are required. Different approaches to obtain such models were discussed in this chapter. The three main categories of predictive models discussed were (1) statistical-empirical, which is mainly based on collected road data with different characteristics and statistical analysis; (2) fundamental, which is based on physical modeling of the pavement surface and tire; and (3) hybrid, which is a combination of statistical and fundamental models. The literature search revealed that there are no models available to predict skid resistance based on material characteristics and traffic level. The following chapters present the experimental and analytical methods to develop such a model.

CHAPTER III

MATERIALS AND LABORATORY TEST METHODS

INTRODUCTION

This chapter presents the properties of aggregates and mixtures that were used in the laboratory experiments. These materials were selected to represent various aggregate sources and mixture designs used in the state of Texas. In addition, the chapter includes descriptions of the experimental methods that were used to measure the properties of aggregates and mixtures related to skid resistance.

AGGREGATE SOURCES

As mentioned previously, aggregate type and geological sources have a significant effect on the skid resistance of the pavement. Aggregates from five different sources in Texas were selected from:

- Beckman,
- Brownlee (partly composed of George town aggregate),
- Brownwood,
- Fordyce , and
- McKelligon (referred to as El Paso aggregate).

Because the frictional performance of the asphalt mixes is mainly governed by coarse aggregates, mineralogy of the coarse aggregate fractions was considered as the representations of the aggregate source. Because it is a common practice in Texas to blend soft limestone aggregates with a polish-resistant aggregate, another combination including 50 percent sandstone and 50 percent soft limestone was also tested. FIGURE 12 shows the geographical location of aggregate sources on a Texas map.

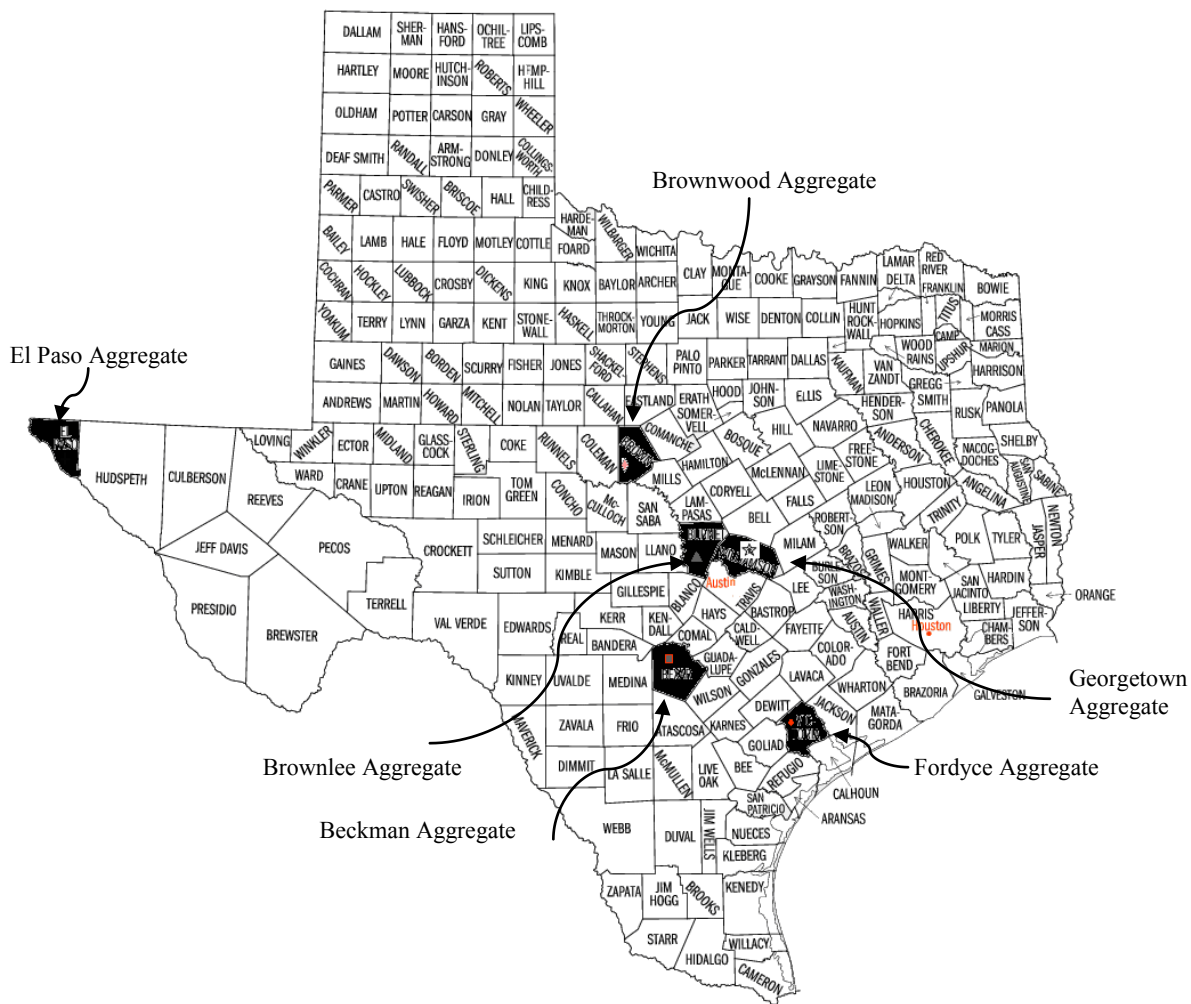


FIGURE 12 Map of Texas showing aggregate quarries by county location.

FIGURE 13 shows the aggregate classification based on the old system used in Texas. The classification of the aggregates used in this research has been show in this figure.

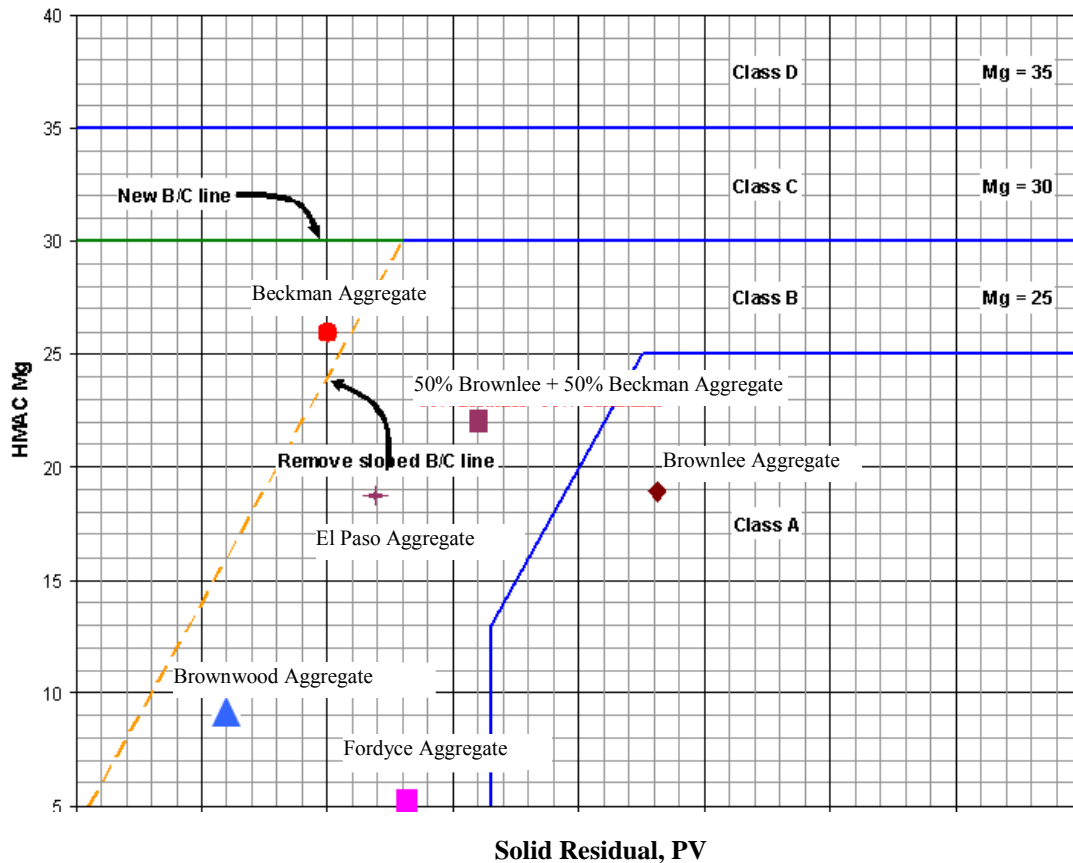


FIGURE 13 Aggregate classification based on old aggregate classification system.

Based on the two older versions of TxDOT SAC (FIGURE 13), Brownlee aggregate falls in class A, Beckman aggregate is classified as class C, and the remaining aggregates are classified as class B.

The new aggregate classification system in Texas uses TABLE 3, with aggregates classified as shown in TABLE 4. TABLE 4 shows that Fordyce aggregate, which was classified as B in a previous version of the SAC system, was promoted to class A, and Beckman aggregate is classified as SAC B in the new system. Other aggregates remain the same in both systems.

TABLE 4 Aggregate Classification Based on New System

Aggregate	Class
Brownlee	SAC A
El Paso	SAC B
Fordyce	SAC A
Brownwood	SAC B
Beckman	SAC B
50% Brownlee + 50% Beckman	NA

PETROGRAPHIC ANALYSIS OF AGGREGATES

To understand skid properties of the aggregates used in this study, thin sections of selected aggregates from six different Texas aggregate sources were analyzed (TABLE 5). The mineralogy and relative hardness (Mohs hardness scale) of each aggregate are listed as well. Different size fractions from each aggregate source were washed in distilled water to remove foreign matter and allow close inspection with a Meiji binocular microscope of select pieces of aggregate that were representative of the variations in each source. The aggregate pieces were selected for thin-section analysis based on color, angularity, density, and variations in surface texture.

TABLE 5 Aggregates Analyzed in Petrographic Study

Aggregate Source	Mineralogy	Mohs Hardness
Beckman pit	Calcite	3
Brownlee pit	Quartz, Feldspar, Dolomite, Calcite, Glauconite	7, 6, 3.5-4, 3, 2
Brownwood pit	Zircon, Quartz, Rutile, Feldspar, Dolomite, Calcite	7.5, 7, 6-6.5, 6, 3.5-4, 3
Fordyce pit	Quartz, Feldspar, Dolomite Siderite, Calcite	7, 6, 3.5-4, 3.5-4, 3
McKelligon pit	Quartz, Feldspar, Dolomite Siderite	7, 6, 3.5-4, 3.5-4
Georgetown pit	Quartz, Dolomite, Calcite	7, 3.5-4, 3

The aggregate pieces were then shipped to Texas Petrographic Services, Inc., in Houston to make thin sections. Each thin section was impregnated with blue-dyed epoxy (for easy pore delineation), and one-half of the section was stained with Alizarin Red-S to distinguish calcite and aragonite from dolomite. The calcite and aragonite were stained a red color, and dolomite remained unstained (152).

The thin sections were analyzed with a Zeiss Axioskop 40 petrographic microscope equipped with a rotating stage and a Pixelink digital camera. Photomicrographs were made of representative features for each aggregate fraction. The following sections explain the results of the observations and petrographic analysis performed on each aggregate type.

Beckman Pit

The Beckman pit is located near San Antonio, Texas. Samples from this site are characterized by a monomineralic composition (100 percent calcite). The texture varies from a low porosity fossiliferous grainstone to poorly cemented euhedral calcite with moldic porosity. FIGURE 14 illustrates a micritic limestone composed of 100 percent calcite. The red stain shows that the sample is composed of pure calcite. The darker areas are calcite mud (micrite), and the light areas are fossil fragments made of calcite. The grainstone in FIGURE 15 shows a low porosity limestone with abundant fossil fragments, which are composed entirely of calcite. This aggregate would normally have better skid resistance than the micrite shown in FIGURE 14, but it is monomineralic, which could decrease the skid resistance. However, this isn't always true because sometimes the monomineralic aggregates have a different hardness between the fabric and the matrix of the rock depending on whether the matrix weathered more than the fabric. If the fabric is more durable than the matrix, texture is created.

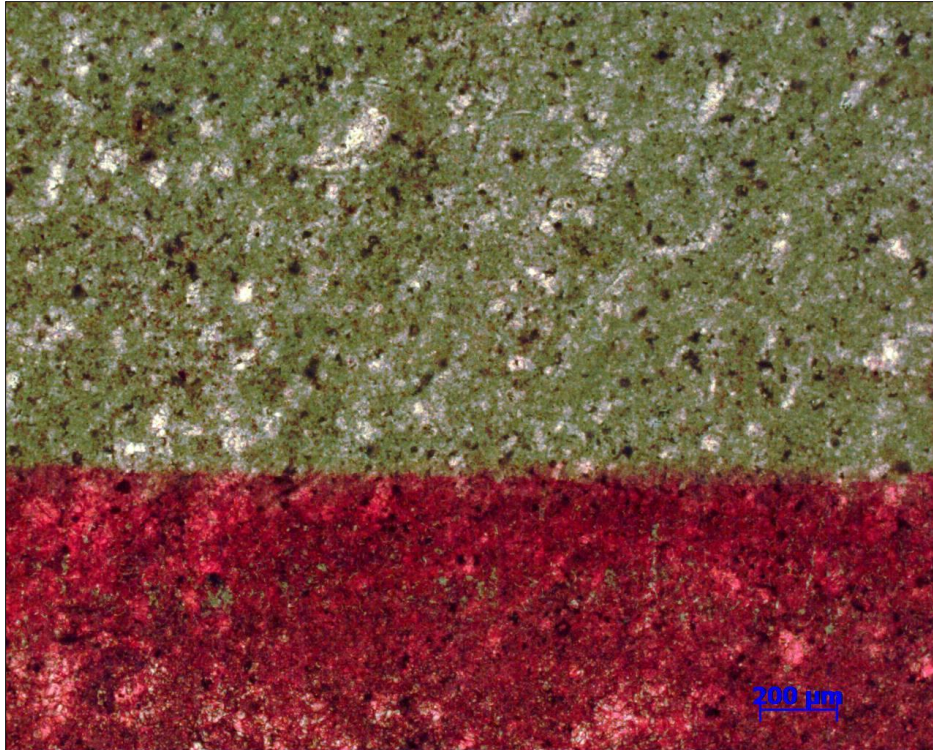


FIGURE 14 Micritic, low porosity limestone from the Beckman pit.

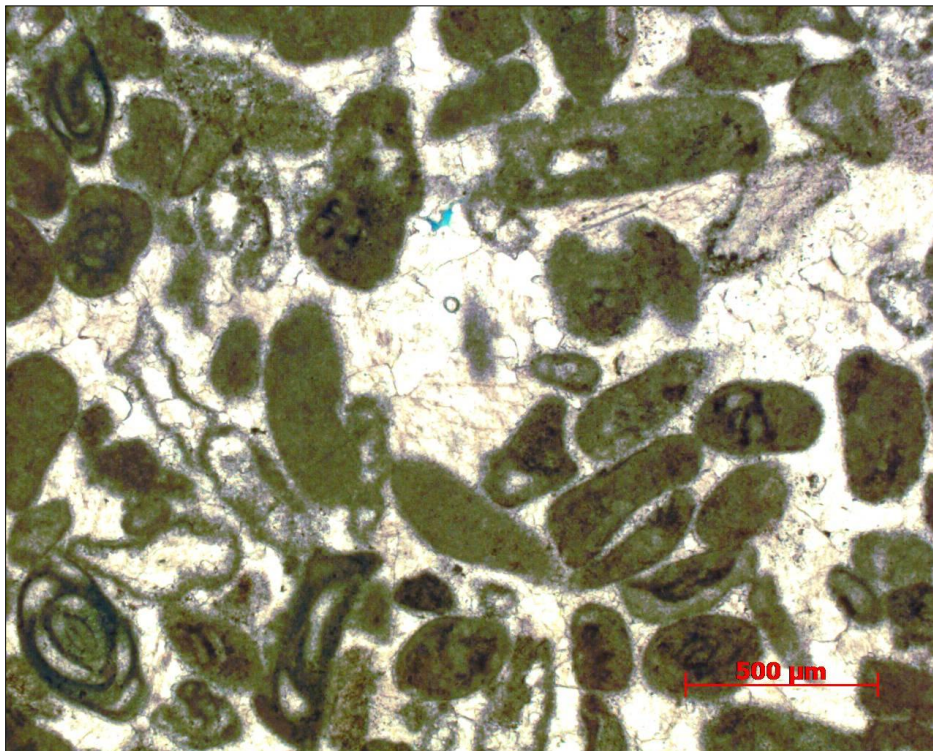


FIGURE 15 Grainstone with coated fossil fragments from the Beckman pit.

The limestone shown in FIGURE 16 has moldic (vuggy) porosity that increases its skid resistance. However, there is very little of this material in the aggregate sample collected. This aggregate would have a lower skid resistance because it is composed predominantly of only one mineral. Moreover, characterizing this aggregate can best be done by measuring the skid resistance of prepared samples of mixes containing this type of aggregate.

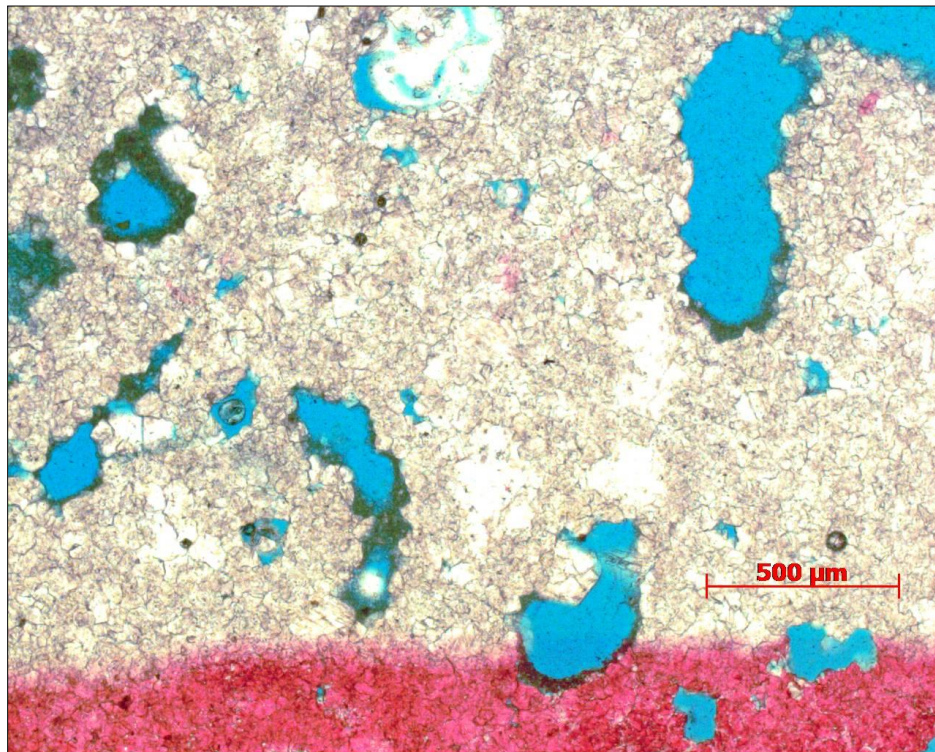


FIGURE 16 Coarsely crystalline limestone with Moldic pores from the Beckman pit.

Brownlee Pit

The Brownlee pit is a blend of sandstone and limestone. There are numerous rock types in this aggregate that include chert, glauconitic sandstone, limestone, sandy limestone, dolomite, and glauconitic dolomite. Some of the aggregate pieces are heavily weathered, and other pieces are unaltered rock. Examples include an altered glauconitic sandstone, as well as fresh to highly altered dolomite. FIGURE 17 shows an unaltered glauconitic dolomite. The unweathered glauconite grains are dark green, and the dolomite

crystals are white to gray. FIGURE 18 illustrates a calcite and dolomite-cemented sandstone. This rock should have good skid properties because it has constituents with different hardness, and there is very little porosity to weaken the rock. The sand grains are angular, which will contribute to improved skid properties.

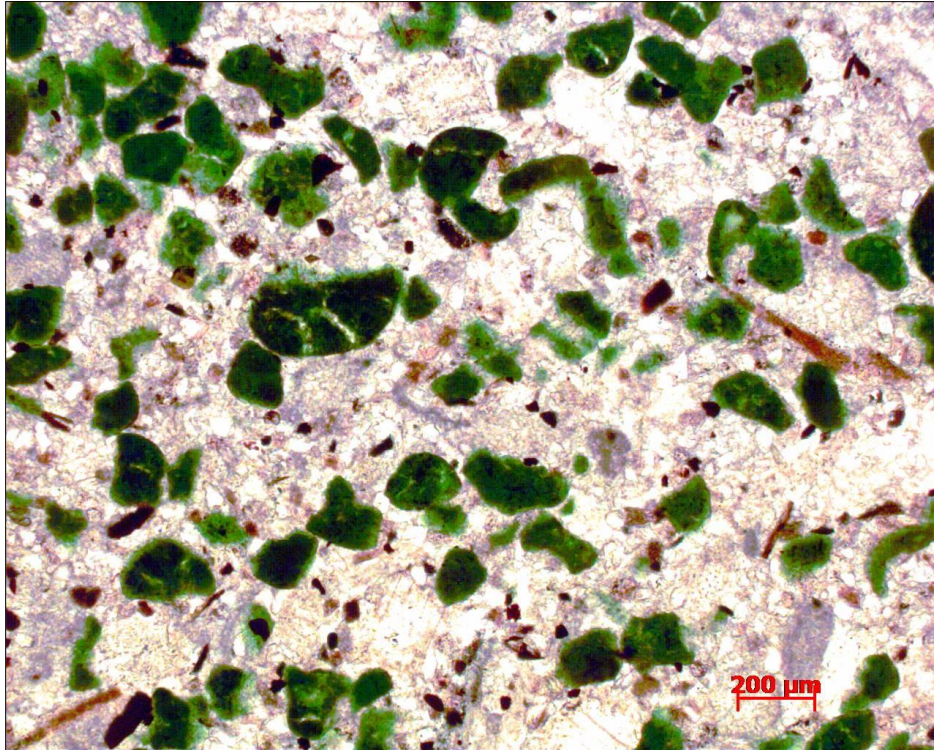


FIGURE 17 Glauconitic dolomite from the Brownlee pit.

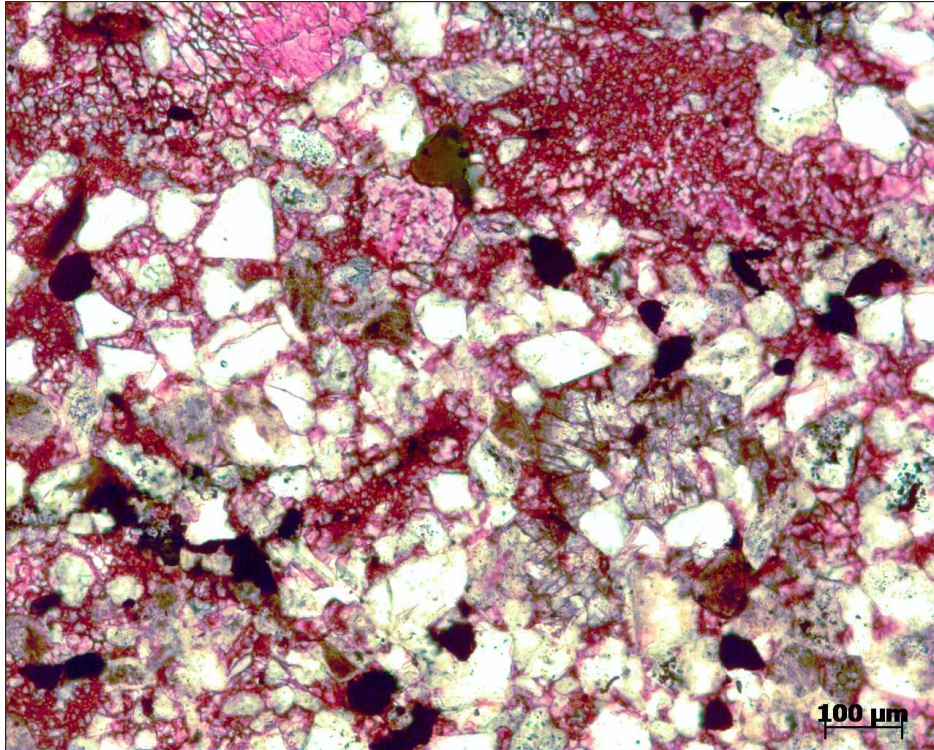


FIGURE 18 Calcite and dolomite-cemented sandstone from the Brownlee pit.

FIGURE 19 shows a heavily weathered dolomite. One can see abundant pore space (blue areas) between individual crystals in addition to many crystals being etched or partially dissolved. The mineralogy and texture of the Brownlee pit is very diverse. The skid properties of this aggregate will be highly dependent on relative percentages of fresh and heavily altered rock. The microtextural properties of the Brownlee pit are higher in the altered rock because of the continual rejuvenation of the aggregate surface because sand being plucked during wear. Moreover, this fresh rock may have better wear-resistance characteristics but may have less texture over time. Furthermore, a detailed laboratory study is needed to characterize the frictional properties of this rock.

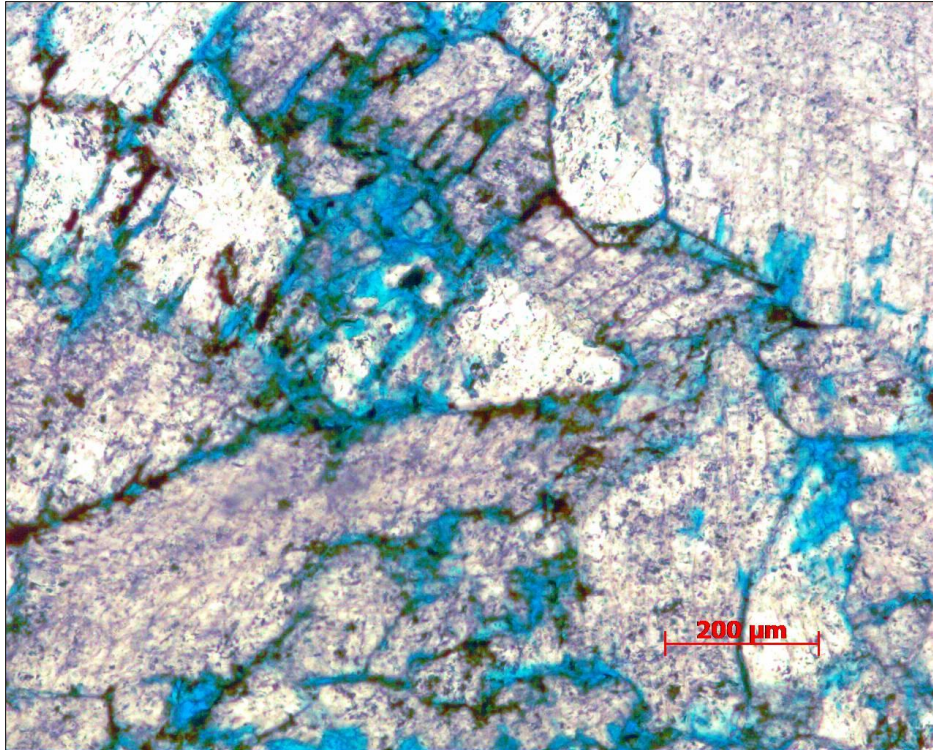


FIGURE 19 Heavily weathered dolomite from the Brownlee pit.

Brownwood Pit

The Brownwood pit is located near Brownwood, Texas. The aggregate from this location is predominantly limestone with variations in sand content. Most of the samples exhibit very little to no porosity and contain a variety of minerals. There was no evidence of heavily weathered aggregate in the Brownwood samples. FIGURE 20 illustrates a limestone with abundant dolomite and quartz sand clasts. The dolomite may be primary, or it may be a replacement of original aragonite filling voids in fossil fragments. Quartz grains are sub-rounded to angular white grains dispersed throughout the image along with calcite fossil fragments; micrite fills the intergranular volume. Although the properties give an indication of good skid resistance, other characteristics, such as skid insoluble material, are needed to estimate the amount of skid resistance particles in this aggregate type. Moreover, relying only on the result of a geological test on aggregate could be misleading.

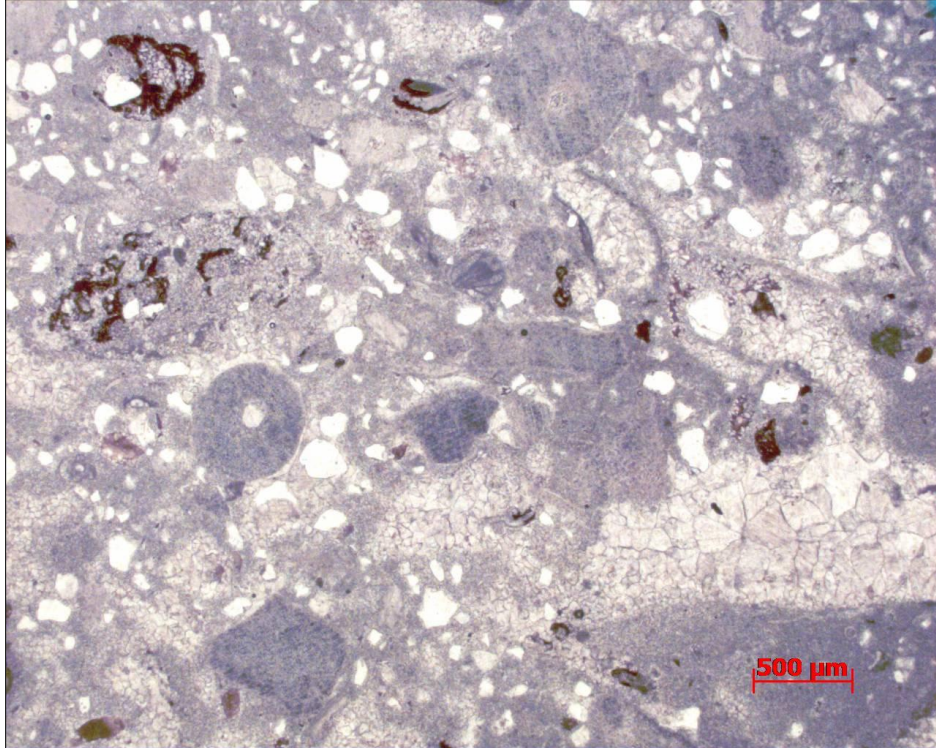


FIGURE 20 Sandy dolomitic limestone from the Brownwood pit.

The image in FIGURE 21 is sandstone with quartz and feldspar as the dominant constituents cemented by calcite (red) and lesser amounts of dolomite. This sample has a heterogeneous distribution of intergranular pore space. The angularity of the detrital grains and the carbonate cement should give this aggregate good skid properties. Heavy minerals (zircon, rutile) abound in the photomicrograph of the carbonate-cemented sandstone shown in FIGURE 22. The heavy minerals appear opaque and are concentrated in the lower half of the figure. There is no porosity visible in this image.

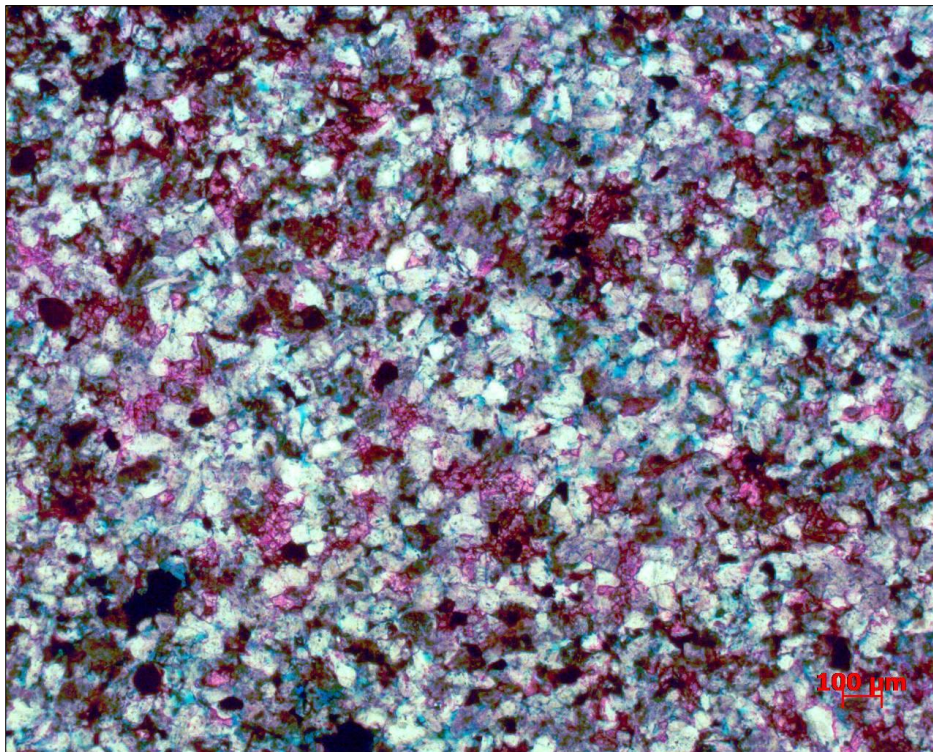


FIGURE 21 Calcite and dolomite-cemented sandstone from the Brownwood pit.

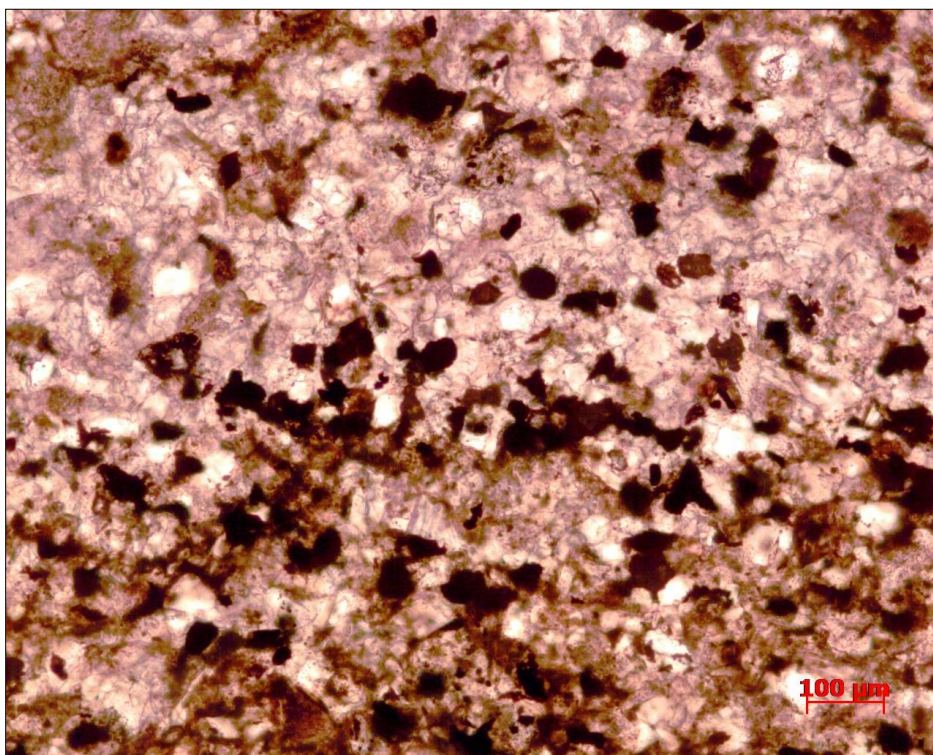


FIGURE 22 Carbonate-cemented sandstone with abundant heavy minerals.

Fordyce Pit

The Fordyce pit is near Victoria, Texas. Aggregates selected from the Fordyce pit samples show a diverse origin. Rock types range from a metamorphosed sandstone to sedimentary chert, fossiliferous limestone, silica-cemented sandstones, and dolomite. FIGURE 23 shows chalcedony replacing a fossil fragment (cigar-shaped object) as well as moldic pores derived from the dissolution of dolomite or calcite (blue). Calcite, dolomite, and siderite are preserved in the heavily silica-cemented region in the right half of the image. This aggregate should have good skid properties.

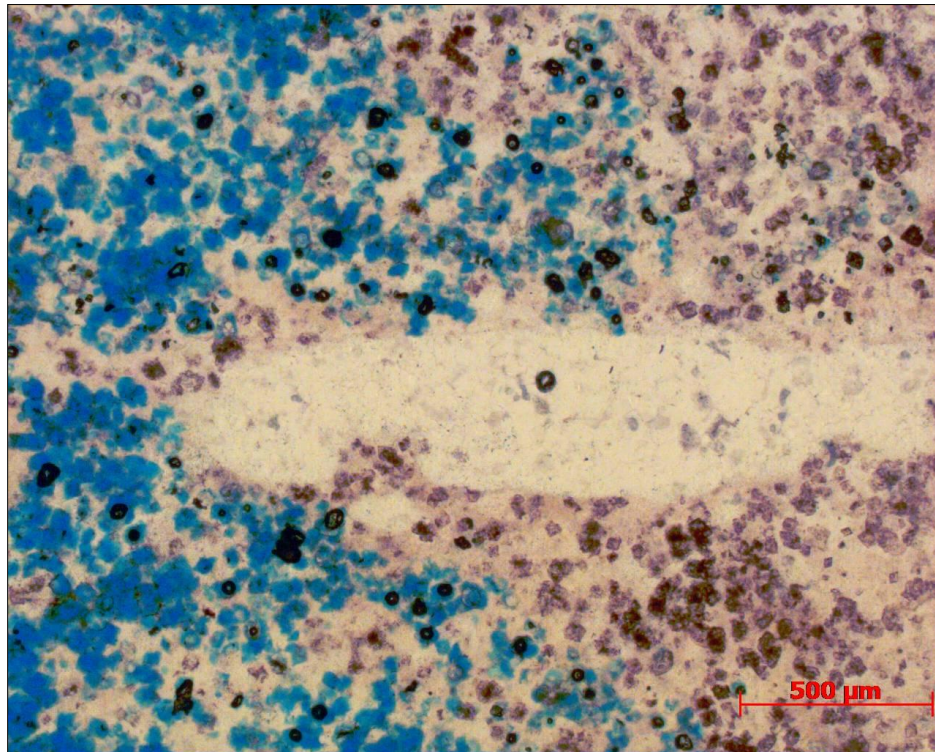


FIGURE 23 Chalcedony replacement of fossils and moldic porosity of Fordyce pit aggregates.

The aggregate depicted in FIGURE 24 is composed predominantly of chalcedony (microcrystalline quartz) with some rhombohedral calcite, dolomite, and siderite crystals preserved. There are some rhombohedral pores developed from the dissolution of dolomite or calcite that may give this aggregate good skid properties if the pores are large

enough. Overall, the different aggregate types found in this pit should provide good skid resistance for the pavement surface.

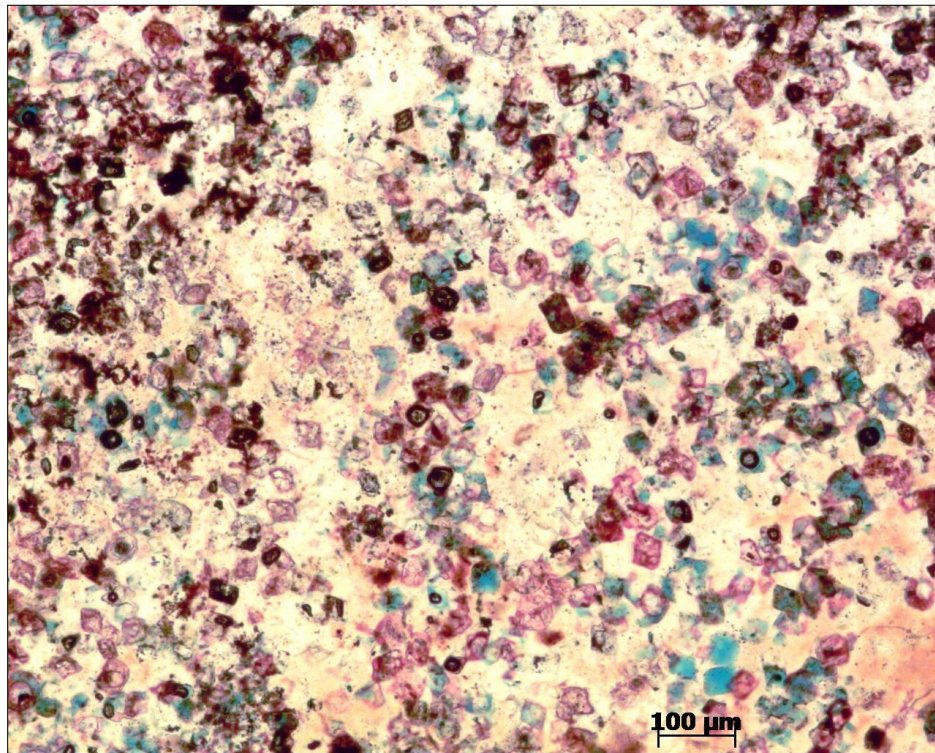


FIGURE 24 Chalcedony matrix with moldic pores from the Fordyce pit.

McKelligon Pit

The McKelligon pit is near El Paso, Texas. There is some highly weathered granite in the finer fractions (< 3/8 inch), but the aggregate is predominantly dolomite and sandy dolomite with minor fossiliferous limestone and sandstones with dolomite and siderite cement. This aggregate should have good skid properties, provided that fine-grained limestone be kept to a minimum.

The most dominant rock type in this pit is a sand-bearing dolomite, shown in FIGURE 25. The sand grains (white) are angular and composed of quartz, which will make a rough surface when the rock is polished, so this rock should give good skid properties. FIGURE 26 displays a very fine-grained limestone, composed of small calcite

crystals. This rock would not have good skid properties because of the small crystals all composed of the same mineral, which would generate a uniform polish.

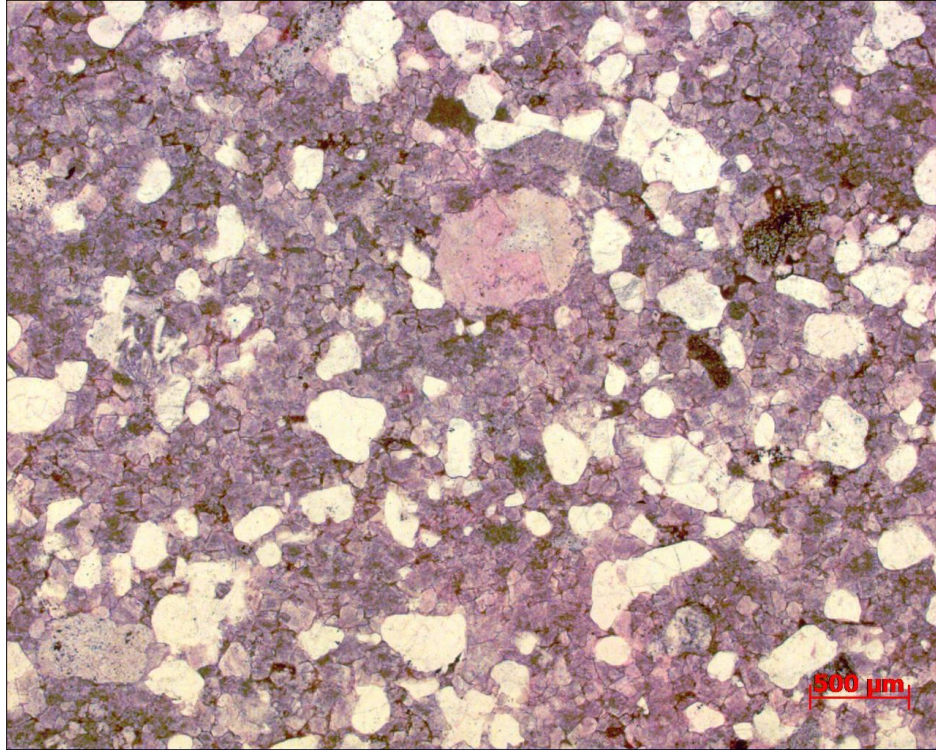


FIGURE 25 Sandy dolomite from the El Paso, McKelligon pit.



FIGURE 26 Fine-grained limestone from the El Paso, McKelligon pit.

The sandstone shown in FIGURE 27 is composed of quartz and feldspar detrital grains with dolomite dominating the intergranular volume. There is minor siderite (opaque-looking rhombs) and pore space (blue). There is also some quartz overgrowth cement present that would greatly increase the durability of the sample. This aggregate should have good skid properties.

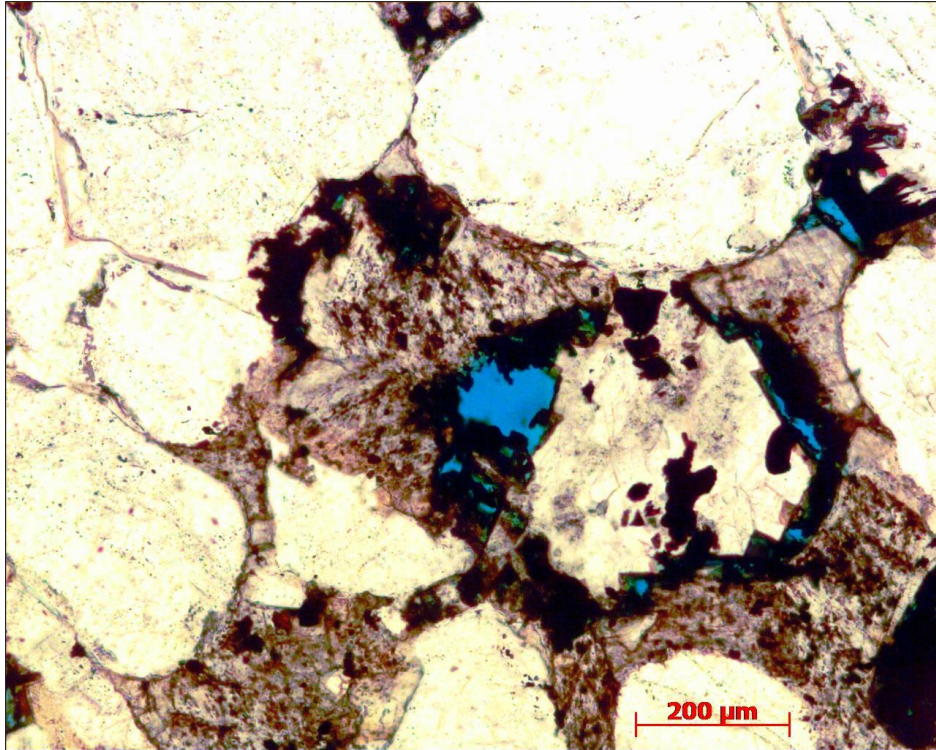


FIGURE 27 Dolomite and siderite-cemented sandstone from the McKelligon pit.

FIGURE 28 depicts one of only four granite samples. This piece is from a weathered rock because many of the grains are etched and are being chemically altered (as shown by the mottled texture of feldspar grain in the upper left corner of the image). Because of the sharp contacts and large grain sizes, and alteration of granite can be considered to have satisfactory skid resistance, but a more comprehensive field and laboratory study is required to classify this aggregate as a good skid resistant aggregate.

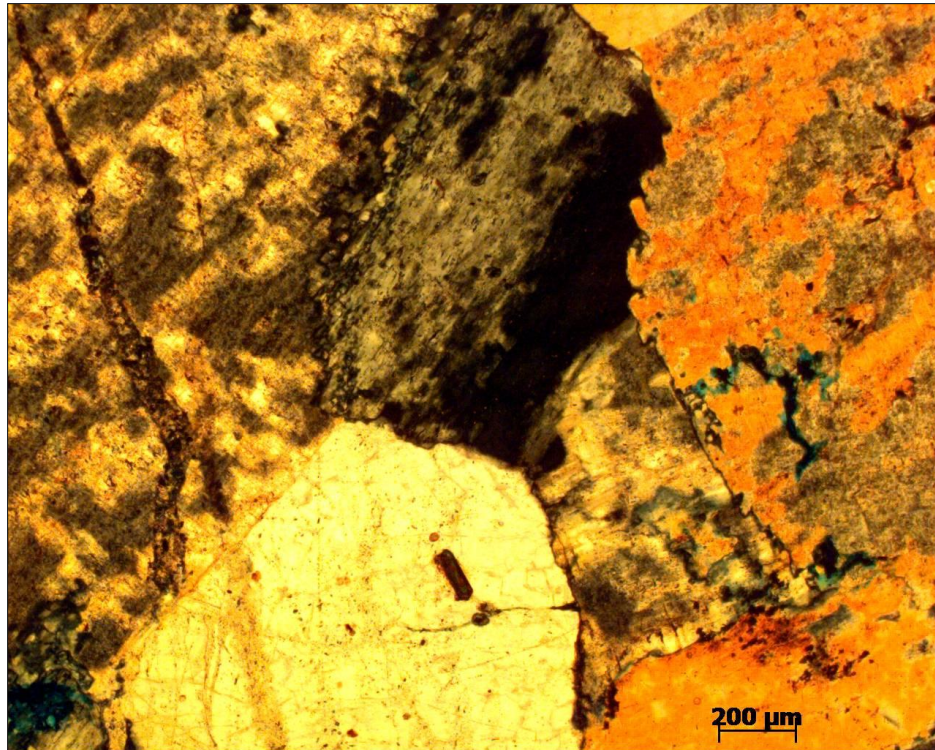


FIGURE 28 Cross-polarized light view of altered granite from the McKelligon pit.

Georgetown Pit

The Georgetown pit constitutes part of the aggregate called sandstone from Brownlee in this research. The aggregate samples from Georgetown are generally not very durable, but the poor durability can be an asset when it comes to skid performance. These aggregates will abrade rapidly and provide a continuously rough texture. FIGURE 29 displays an image of a fine-grained limestone with chalcedony (microcrystalline quartz) in the lower right side of image. This image was taken under cross-polarized light to accentuate subtle differences in crystallography. There is a large percentage of chalcedony and chert in these samples that will aid in skid resistance. Moldic pores (vesicles) also provide good skid resistance in rocks with lower durability (see FIGURE 30). The aggregate is extremely porous and poorly cemented, which will result in low durability, but it will generally increase the skid resistance.

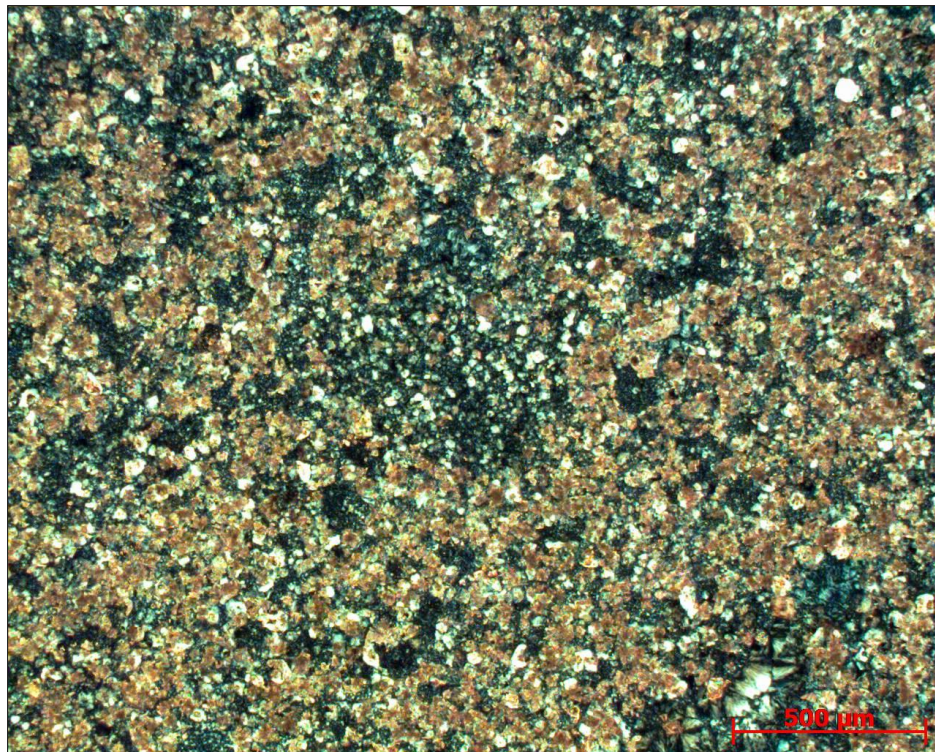


FIGURE 29 Fine-grained limestone with chalcedony from the Georgetown pit.

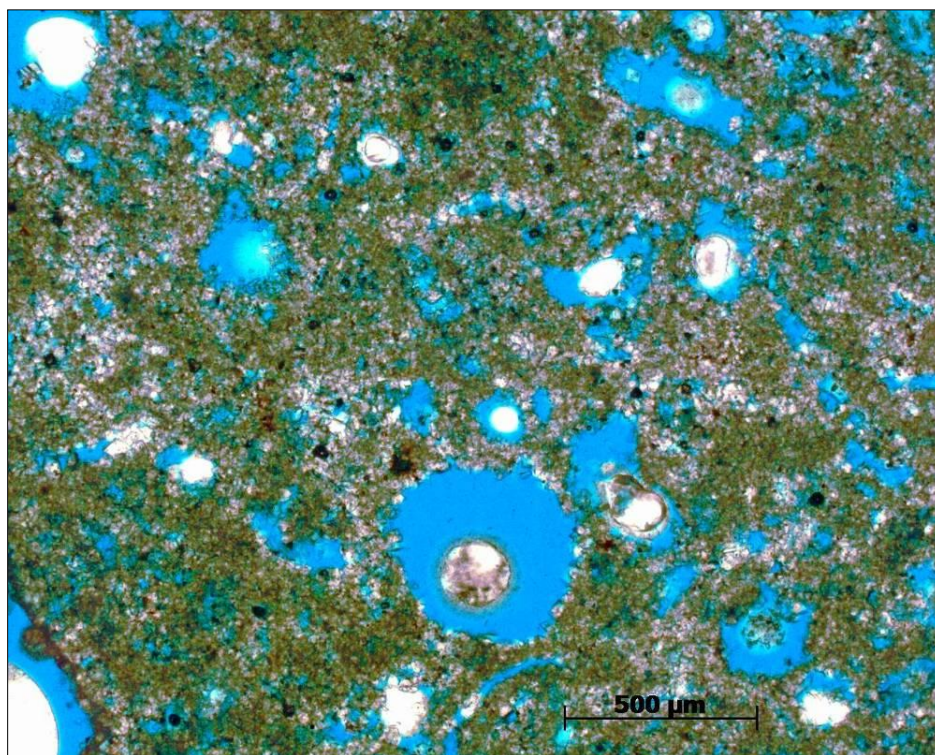


FIGURE 30 Moldic pores in limestone from the Georgetown pit.

In summary, all sources but one (Beckman aggregate) contained multiple mineral types and textures that have been shown to exhibit favorable skid properties. The quality depends on the percentage of good to poor aggregate present in a sample. Aggregate durability does not necessarily correlate with skid performance.

From a mineralogical point of view, El Paso, Brownwood, and Fordyce are predicted to have satisfactory skid properties. The combination of Georgetown and Brownlee, considered as Brownlee aggregate in this study, would have good skid properties. The worst aggregate would be from the Beckman pit.

The Beckman pit contained 100 percent calcite, which would result in the poorest skid resistance. The Brownlee pit contained a fair amount of weathered aggregates that not only could significantly reduce skid resistance but also might be able to maintain its skid properties as a result of the rejuvenation of the aggregate texture. The Georgetown pit sample has a lot of low durability aggregates, but the texture would help give it better skid properties. The El Paso (McKelligon pit) aggregates contained a fair percentage of weathered rocks, but weathering is not as detrimental for the El Paso aggregates because of the coarse grain size and variable mineralogy.

Although the petrographic analysis yields a good insight into mineral constituents, the results of petrographic analysis cannot be relied on as the only evaluation technique. Other mechanical and physical tests, e.g., soundness and Micro-Deval, are necessary to evaluate aggregate polishing susceptibility.

TESTING OF AGGREGATE RESISTANCE TO POLISHING AND DEGRADATION

As discussed previously, macrotexture and microtexture are two important factors providing skid resistance on the pavement surface. Macrotexture depends on the mixture characteristics and aggregate gradation, while microtexture depends mainly on the aggregate surface texture.

Microasperities on the surface of the aggregates provide surface microtexture, which plays a key role in providing skid resistance at lower speeds. The ability of an

aggregate type to maintain its rough texture against traffic loading is an important factor that has to be considered in a comprehensive aggregate classification system. There are several methods to evaluate the potential of an aggregate to resist polishing made by traffic loading. These methods can be classified into two major groups—the methods that measure the aggregate abrasion (loss of angularity and some breakage) during traffic loading and the methods that measure aggregate polishing (loss of texture). Furthermore, in these methods, change in one aggregate characteristic, e.g., magnesium sulfate soundness weight loss or BPV, is measured after special load application, and the changes are attributed to the aggregate polish or breakage resistance ability. These changes in aggregate properties are related to aggregate potential to resist polishing. Recent studies reveal that change in aggregate physical characteristics such as texture and angularity are good indicators of aggregate skid properties; hence, methods that are able to measure aggregate shape characteristics directly, such as AIMS, are preferable (132). In this study, several methods were applied to evaluate the aggregate polishing, abrasion, and breakage characteristics. These methods are discussed in this section.

Los Angeles Abrasion and Impact Test

The LA abrasion and impact test is an indication of aggregate degradation during transport and handling. It has been standardized under ASTM C535, AASHTO T 96, and Tex-410-A. In this test, the portion of aggregate retained on a sieve #12 is placed in a big rotating drum. This drum has some plates attached to its inner walls. A specified number of steel spheres are added to the drum, and it starts to rotate at 30 to 33 rpm for 500 revolutions. The material is then extracted and separated by use of a #12 sieve, and the proportion of the materials remaining on the sieve is weighed. The difference between this new weight and the original weight is compared to the original weight and reported as LA value or percent loss. The LA abrasion and impact test is believed to assess an aggregate resistance to breakage rather than abrasion as a result of wear (132,153).

Magnesium Sulfate Soundness

The magnesium sulfate soundness test is an indication of the durability of aggregates and is standardized under AASHTO T104 or Tex-411-A. The test involves submerging an aggregate sample in a solution of magnesium sulfate for a specified number of cycles (often five) and measuring the weight loss afterwards. According to the standard procedure for performing this test, the aggregate sample is dried and placed in the magnesium sulfate solution for 18 hr. Then, it is removed from the solution and dried again at oven temperature. This process is repeated five times; then, the loss of aggregate weight is reported.

British Pendulum Test

The British polish value is a measure of aggregate surface texture and shows the roughness of the aggregate surface. This test has been standardized under ASTM E3033-93 and Tex-438-A. The test was discussed in detail in Chapter II.

Micro-Deval Test

The Micro-Deval test is used to evaluate aggregate capability to resist abrasion in a wet environment. The test method originated in France in 1960 and was accepted as a European Union standard afterwards. The first use of this method was in Canada by the Ontario Ministry of Transportation, and it was adopted by AASHTO under the AASHTO T 327-05 test method entitled “Standard Test Method for Resistance of Coarse Aggregate to Degradation by Abrasion in the Micro-Deval Apparatus” (153). In this test, the durability and aggregate resistance to abrasion in the presence of water is evaluated. Moreover, this test evaluates how aggregates degrade when tumbled in a rotating steel container with steel balls in a wet environment (153,154). This test method has been adopted by TxDOT in the Tex-461-A standard procedure. In this test, a steel container is loaded with 5000 grams of steel balls and 1500 grams of an aggregate sample in the range of 4.75 mm to 16 mm and 2000 ml tap water. This material is subjected to 9600 to

12,000 revolutions, and the sample weight loss (weight of aggregate passing the #16 sieve size) is calculated and reported. FIGURE 31 shows the Micro-Deval apparatus, and FIGURE 32 shows the schematic mechanism of aggregate degradation.



FIGURE 31 Micro-Deval apparatus.



FIGURE 32 Mechanism of aggregate and steel ball interaction in Micro-Deval apparatus.

This test addresses aggregate resistance to abrasion better than other tests, such as the LA abrasion test, specifically in base and hot mix asphalt (HMA) materials where stone-to-stone interaction in a wet condition is more important. Moreover, the wet environment of the Micro-Deval is believed to simulate field conditions (155). Furthermore, recent studies show that this method is more repeatable and reproducible

than the other aggregate degradation tests, such as the magnesium sulfate soundness test and LA abrasion and breakage test (156).

Aggregate Imaging System

AIMS is an automated aggregate imaging system used to characterize aggregate shape characteristics. This system determines the angularity, shape, and texture of coarse aggregate as well as the shape and angularity of fine aggregates based on a scanning system and digital image processing. Masad et al. showed that there is no operator bias associated with this test method, and operator training for using this equipment is not complicated (157). In this system, coarse aggregates are placed on a tray with 7×8 grid points, and fine aggregates are spread uniformly on the tray with 20×20 grid points. Then, a digital camera with a predefined zoom level takes digital pictures of the aggregates. This system is also equipped with back-lighting and top-lighting units that can provide enough light intensity to capture a clear image of the aggregates. Three measures of aggregate shape properties are calculated based on these 2-D images taken from aggregates (132).

Texture is measured using AIMS by analyzing gray-scale images of the aggregate surface using the wavelet method. Moreover, the surface microasperities are visible from the variations in gray-level intensities that range from 0 to 255. A large variation in gray-level intensity indicates a rough surface texture, whereas a smaller variation in gray-level intensity shows a smooth surface. The wavelet transform analyzes the image as a two-dimensional signal of gray-scale intensities, and it gives a higher texture index for particles with rougher surfaces. Aggregate angularity, described as a deviation from a perfect circle, shows the irregularities on the aggregate surface on the macro level. Angularity is calculated using the gradient method and presented as an angularity index. Sphericity is another index that is extracted from digital images of aggregate samples. This index simply shows how close the aggregate is to a perfect sphere. The system is a result of a very comprehensive study at Texas A&M University, and all details and analysis procedures have been documented in Al-Rousan's Ph.D. dissertation (158). FIGURE 33 shows a schematic view of the AIMS system.

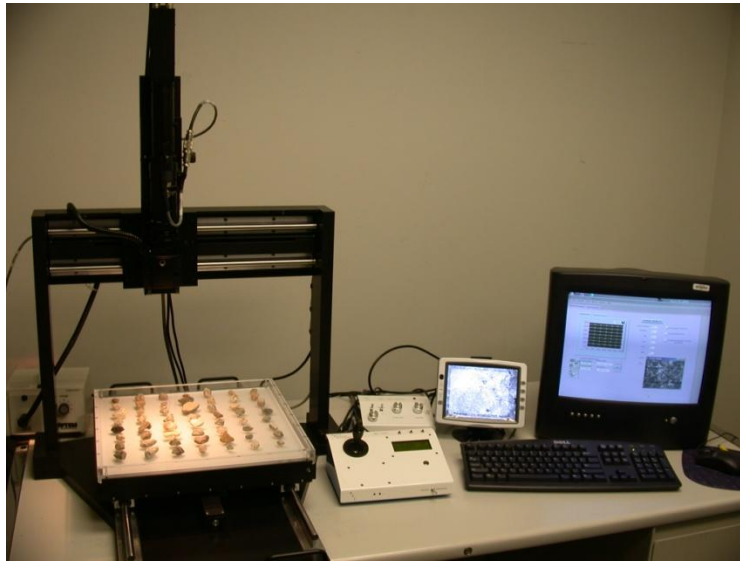


FIGURE 33 Schematic view of the AIMS system.

ASPHALT MIXTURE TYPES

During the laboratory part of the study, different asphalt mixture types containing different aggregate types were prepared and compacted into laboratory slabs and then tested. Three different mix designs were selected. These three mix designs are known to exhibit different frictional field performance and are common mix types used by TxDOT. During the sample preparation stage, laboratory-produced mixes were compacted into special metal molds and polished in a laboratory polisher to obtain the frictional resistance curve. Friction and texture measurements were performed intermittently after sample compaction and during polishing. The following sections describe each mix design.

Type C Mix Design

Type C mix design has a maximum aggregate size of 0.75 inch and consists of a minimum of 60 percent particles with two or more crushed faces. Moreover, this mix is used in asphalt layer thickness of 2 to 4 inches. Type C mix design is used as both an

intermediate and a wearing course in TxDOT projects. This mix is usually utilized on the highways and major arterials. In general, this mix has good performance against permanent deformation and also has good skid properties. Type C mix design has become the most common mixture design in TxDOT projects (159).

Type D Mix Design

Type D mix design is exclusively used for surface application and has a 0.5-inch maximum aggregate size. Moreover, this mixture gives smooth riding characteristics to the road and has good frictional properties. This mix is also used in overlay projects (159).

Porous Friction Course

Porous friction course (PFC) consists of an open-graded asphalt mixture containing a large proportion of one-sized coarse aggregates, typically from 0.375 to 0.5 inch in size, and a small percentage of fine aggregates. The large air content in the range of 20 ± 2 percent allows the water to pass through and drain quickly; therefore, this mixture has high skid resistance and reduces the chance of hydroplaning. Utilizing this mixture also improves visibility and reduces water splash and spray. PFC is usually laid over a stronger dense-graded asphalt mixture. Different kinds of additives are used (e.g., polymers, cellulose fibers, lime) to make PFC more durable in terms of resistance to moisture damage (159).

TABLE 6 lists the mixtures and aggregates used in this study, along with their selected abbreviations.

TABLE 6 Abbreviation Selected for Aggregates and Mix Types in This Study

Mixture Type Aggregate Type	Type C	PFC	Type D
Fordyce Aggregate	CFY		
Beckman Aggregate	C-BK	P-BK	D-BK
Brownwood Aggregate	C-BW	P-BW	
El Paso Aggregate	C-EP	P-EP	
Brownlee Aggregate	C-BL	P-BL	D-BL
50% Beckman + 50% Brownlee	C-BKBL		D-BKBL

ASPHALT MIXTURE PREPARATION

The mixture designs for each asphalt mixture were adopted based upon a mixture design that had been used in the field. In view of this, the mixture design for each mixture was collected by contacting TxDOT officials and consultant engineers who were responsible for the mixture design. Tables 53 to 64 in Appendix A illustrate the mix designs. For the mixes whose mix design was not available—Type D with 50 percent Beckman aggregate + 50 percent Brownlee aggregate, and Brownlee—a separate mixture design procedure according to TxDOT specification for Type D mix was performed. The optimum asphalt content was also estimated and used in preparation of test specimens.

The required amount of each aggregate type was collected from the producer, and the gradation of each of the individual types of aggregate was determined following the ASTM C 136 specification. The final gradation used in the production of the mixes was obtained by blending individual fractions in proportions specified in the mix design. The final blend did not differ from the target gradation by more than ± 5 percent for each sieve size during the blending of each bin. A modified PG 76-22s binder was used to prepare the laboratory mixtures. This binder grade is commonly used in Texas.

One slab from each mixture type was prepared and tested. Given that the minimum slab size required to measure the skid resistance by DFT and CTMeter is 17.75 inches by 17.75 inches, it was decided to prepare a 60-inch by 26-inch slab from

each mixture. This slab size provided three locations for measuring the skid resistance of the asphalt mixture surface. FIGURE 34 shows a schematic layout of the locations of the DFT and CTMeter measurements on the slab. Measurements were not taken close to the slab edge because of the unevenness caused during compaction.

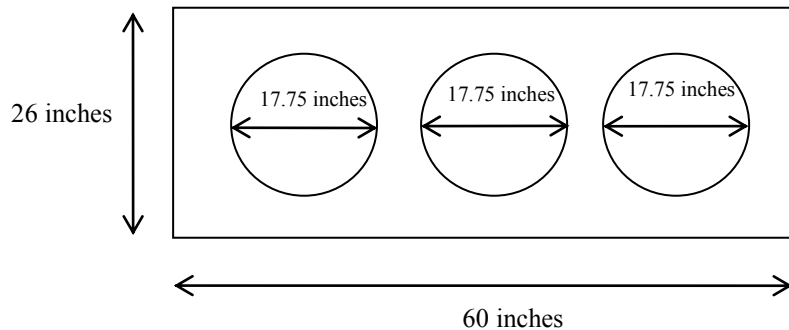


FIGURE 34 Schematic layout of each slab.

The experimental design for this study dealt with a large amount of materials. The amount of mix batch used for each slab was about 125 kg, with a total of about 1900 kg for all mixtures. About 100 kg of binder was used in preparing all mixes.

Aggregates for each mix were blended and split into seven 4-gal buckets for heating. The mix weight was calculated to produce a 2.5-inch-thick slab given the mold volume and bulk specific gravity (G_{mb}). The target percent air voids was 7 percent for Type C and Type D mixtures and 20 percent for the PFC mixture.

The 4-gal buckets containing aggregates were put into the oven one night before compaction at the mixing temperature. The asphalt binder was also split into small cans to achieve uniform heating. The small cans of the PG 76-22 asphalt type were also heated to their mixing temperature. The heated aggregate was weighed, and the optimum asphalt content was added to it and placed in the mixer for Type C and Type D mixtures. For the PFC mixtures, a 15-sec dry-mixing time was applied to the aggregate and fiber blend prior to adding asphalt to have a consistent mix. The mixing was performed in a 4-gal bucket-type laboratory mixer. In both cases, mixing continued to assure a consistent mix with a uniform asphalt film thickness around each particle. During the mixing time, a

long spatula was used to aid the mixing process and scratch off any fines and asphalt from the side of the container. This process helped to obtain a uniform mix with minimum segregation and a minimum number of uncoated aggregates (139). After mixing, the mix samples were placed into an oven in separate batches, and the mixes were conditioned for 2 hr at the compaction temperature (145°C or 293°F) according to the AASHTO R30 (2002) specification.

A specially developed laboratory compaction procedure was adopted to prepare the specimens in this study. Because the large size of the slabs limits the use of conventional compaction methods (e.g., kneading compactor), it was decided to use a walk-behind roller compactor. This equipment has been successfully utilized in the field and is fast. A metal mold was fabricated to confine the mix during the compaction. This mold consists of five metal pieces bolted together and forms a frame to confine the mixture. In this form, a 66-inch \times 33-inch baseplate is underlying two 2.36-inch \times 2.36-inch L-shape sections forming the walls. Two ramp-shape metal pieces were also fabricated and mounted at both ends of the frame to facilitate moving of the walk-behind roller compactor up to the frame. FIGURE 35 shows the schematic of the mold used to confine the mixture during compaction.

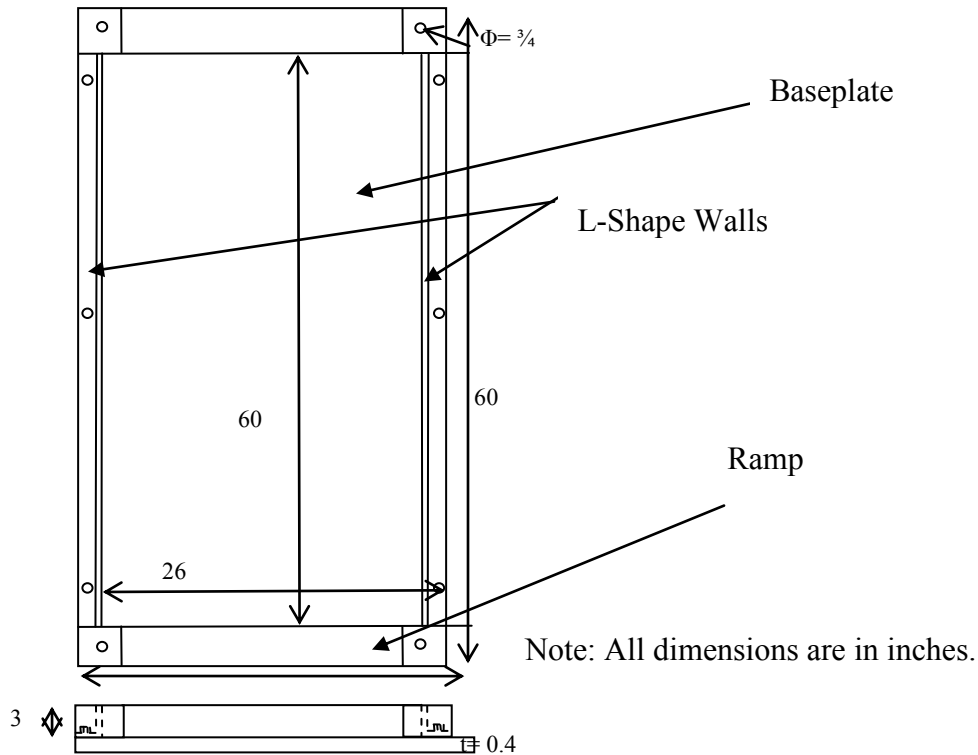


FIGURE 35 Schematic of the mold used in slab compaction.

It is difficult to measure the air void content directly by using a nuclear gauge because the metallic baseplate interrupts any direct measurement and results in incorrect measurements. Therefore, a scale was built to control the thickness of the slab as an indirect measure of air void (see FIGURE 36). Consequent measurements showed that this method was successful in controlling the compaction effort to obtain the desired air voids.

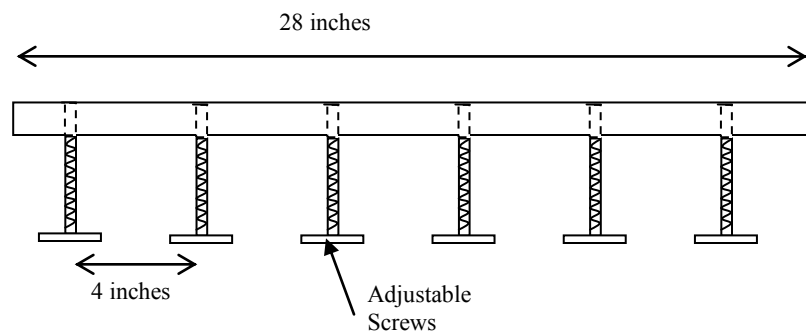


FIGURE 36 Slab-thickness measuring scale used to adjust slab thickness.

After mixing, the mixture was transported to the compacting area by a cart in the metal buckets and spread inside the frame, being uniformly distributed and flattened by a 30-inch rake. This process was done quickly and carefully to provide a smooth surface with minimum segregation and temperature loss (139). The mixture was then compacted by using the vibratory roller compactor (Ingersoll-Rand SX-170H). According to factory specifications, this compactor has a 595-lb operating weight and a 60.4-inch-long and 22-inch-wide drum size. Based on the manufacturer's recommendation, this compactor was used to compact the layers up to 9 inches in thickness. FIGURE 37 shows a picture of this compactor.



FIGURE 37 Walk-behind roller compactor.

During compaction, the slab thickness was measured periodically to assure the correct slab thickness. Rolling was continued until a regular surface was obtained at the required thickness. The typical rolling process took about 20-25 min. The slab was then left for 1 day to cool down and become ready for polishing and further measurement.

As previously mentioned, the target air voids of Type C, Type D, and PFC mixes were 7, 7, and 20 percent, respectively. To investigate the uniformity of compaction throughout the slab, six cores with 6-inch diameters were taken from each slab after

measuring terminal skid resistance. ASTM D 2726 (saturated surface-dry technique for dense-graded mixes) and D6752 (CoreLok apparatus for PFC mixes) test methods were used to determine the bulk specific gravity (G_{mb}). The air void content for each sample was calculated based on this G_{mb} and previously measured G_{mm} . TABLE 7 shows the results of the average air voids for each slab, with an average air void content of 7.9, 9.9, and 21 percent for Type C, Type D, and PFC, respectively.

TABLE 7 Average Air Void Content Measured for Each Slab

Aggregate Type	Mix Type	Average Air Void Content (%)
Brownlee	Type C	8.9
Brownwood		7.7
Beckman		7.1
El Paso		7.8
Fordyce		7.8
50% Brownlee + 50% Beckman		8.0
Brownlee	PFC	23.0
Brownwood		18.8
Beckman		24.0
El Paso		18.0
Brownlee	Type D	9.0
Beckman		10.8
50% Brownlee + 50% Beckman		9.8

SLAB-POLISHING METHODS

Several methods for polishing the slabs were investigated. It was desired to select a method that has the ability to polish large-scale asphalt mixture specimens and with good control on number of polishing cycles.

The first polishing method that was evaluated was the one-third scale Model Mobile Load Simulator (MMLS3). MMLS3 is an accelerated pavement testing system. Load frequency, tire pressure, temperature, and speed can be adjusted with this equipment (*160*). The MMLS3 consists of four rotating axles equipped with a 300 mm (11.8-inch) diameter pneumatic tire. The load level on each tire can vary between 2.1 kN to 2.7 kN by adjusting the suspension system. The tire pressure can be raised up to 800 kPa. This equipment is able to apply up to 7200 loads per second (*161*). FIGURE 38

shows a picture of the MMLS3. Slabs were compacted and placed under the MMLS3 for polishing. After several attempts, the use of MMLS3 for polishing was discontinued because of the following issues:

- The rate of polishing was very slow, and even after 200,000 cycles, the surface was not polished significantly.
- In each turn, only one strip with a 3-inch width is polished, and to make a measurement with the DFT and CTMeter, at least six polished strips were needed side by side. Therefore, the polishing process was time consuming.
- A significant amount of rutting was observed that was believed to adversely affect the friction measurements by the DFT and CTMeter.

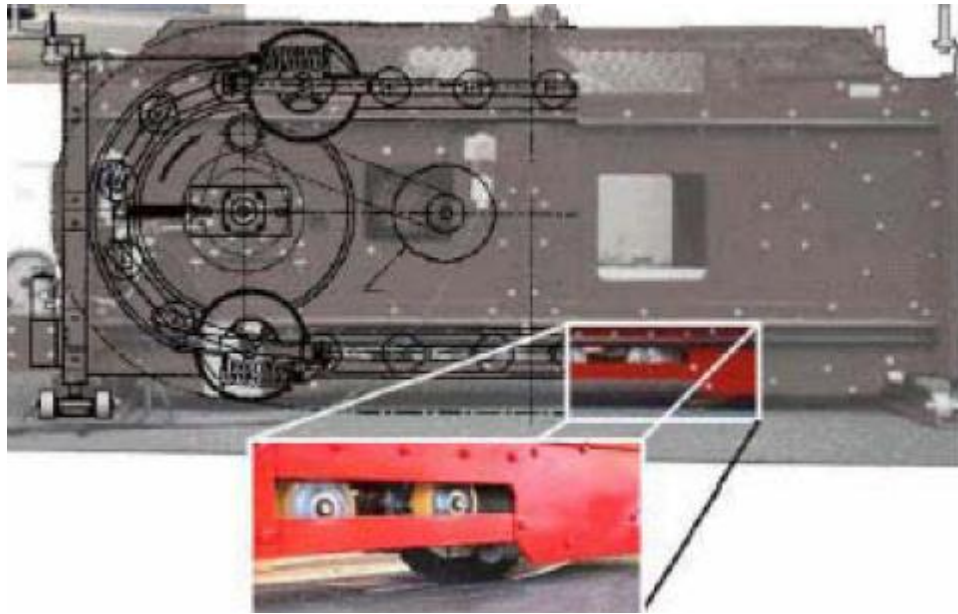


FIGURE 38 Schematic view of MMLS3 (162).

In the second method, a polishing test machine already evaluated by NCAT was used. The results of the study by Vollar and Hanson showed that this machine had satisfactory performance and could simulate field conditions (139). This machine has three 8-inch \times 3-inch caster wheels attached to a turntable. These three wheels spin on an 11.188-inch-diameter path; therefore, it is possible to measure the polished area by the DFT and CTMeter. It is believed that this configuration polishes the surface of the slabs similar to the action of traffic on a pavement. To guide the wheels in an 11.188-inch

circular track, the wheels are equipped with ball bearings that use a mounted fixture, maintaining the wheels on the track during the polishing time. The applied load on the wheels is variable and can be adjusted by adding or subtracting circular iron plates on the turning table. The turntable is hinged to the motor shaft by use of a square shaft and can easily move up and down; hence, this system facilitates adjusting the applied load to the wheels. FIGURE 39 shows the polishing machine assembly. This system is turned by a 0.5-hp electrical motor through a gearbox. The motor is equipped with a Baldor motor speed controller that facilitates changing the rotation speed. There is also a counter system provided to control the number of revolutions by use of an Omega digital counter and laser light pick-up. Moreover, this system can turn off the motor by reaching a preset value for number of revolutions. The turntable was put in a cage for safety. There is also a water spray system included in this polisher. The spraying system consists of three 0.25-inch PVC pipes on each side of the cage that can wash away the abraded material from the surface and allow polishing of the slab. An electric cut-off valve attached to the water spray system is synchronized with the Omega counter that cuts off the water after reaching the desired revolutions (139). The original machine was designed with the slabs inserted into the protecting cage, but in this study, the square rod linking the turntable and motor was modified so that it was possible to place the polisher on the slab and polish it.



FIGURE 39 Polishing machine assembly.

TESTING OF MIXTURE RESISTANCE TO POLISHING

There is no standard test procedure for measuring pavement friction during mix design; however, four different tests have been widely used to evaluate mixture skid properties such as macrotexture and microtexture. These tests include the British pendulum skid tester (ASTM D3319-00 and E303-93 [re-approved 2003]), a volumetric technique—sand patch test—(ASTM E965), the dynamic friction tester for measuring pavement surface friction (E1911-98), and the circular texture meter for measuring pavement macrotexture (ASTM E2157-01) (59). The following sections give a brief review of these methods (139).

British Pendulum Skid Tester

The British pendulum skid tester is probably the most widespread equipment in the world to measure skid resistance. BPT was invented by Percy Sigler in the 1940s and modified by UK Transport Laboratory in the 1960s (163). The skid tester is comprised of “a pendulum with tubular arm that rotates about a spindle attached to a vertical column. At the end of the tubular arm a head of constant mass is fitted with a rubber slider” (163). This test utilizes low-speed testing equipment to measure the frictional properties of the test material by swinging a pendulum with a specific normal load and standard rubber pad. The test results are reported as a number (British pendulum number) that is a measure of kinetic energy loss when the rubber slider is dragged on the surface, and that number is an indirect measure of pavement microtexture. This equipment can be used to measure the change in material skid characteristics as described in ASTM D 3319-00. The rubber slider has two different sizes for testing aggregate samples and pavement surface. The small rubber slider has a 1.5-inch width used for measuring aggregate properties. The large rubber slider, with a 3-inch width, is used for measuring pavement surface skid resistance. FIGURE 40 shows a picture of the British pendulum device (163).



FIGURE 40 British pendulum device.

Sand Patch Method

This is a simple test to measure the pavement macrotexture. The test is undertaken on any dry surface by spreading a known quantity of sand or any particulate fine-grain materials with uniform gradation, e.g., glass beads on the surface. The material is then evenly distributed over a circular area to bring it flush with the highest aggregate peaks. The diameter of this circle is measured in four different angles evenly spaced and averaged. By knowing the test material volume and diameter of the circle, the MTD can easily be calculated. FIGURE 41 shows the sand patch test being performed on an asphalt slab.



FIGURE 41 Schematic of sand patch method.

Dynamic Friction Tester

The DFT as described by ASTM E 1911 consists of three rubber sliders and a motor that reaches to 100 km/h tangential speed. The rubber sliders are attached to a 350 mm circular disk by spring-like supports that facilitate the bounce back of the rubber sliders from the pavement surface. The test is started while the rotating disk is suspended over the pavement and driven by a motor to a particular tangential speed. The disk is then lowered, and the motor is disengaged. In the meantime, water is sprayed on the rubber and pavement interface through surrounding pipes to simulate wet-weather friction. By measuring the traction force in each rubber slider by use of transducers and considering the vertical pressure that is reasonably close to the contact pressure of vehicles, the coefficient of friction of the surface is determined. The DFT can measure a continuous spectrum of dynamic coefficient of friction of pavement surfaces over the range of 0 to 80 km/h with good reproducibility (139,164). In addition, the DFT measurement at

20 km/h is an indication of the microtexture and is being used as a replacement of the BPN (15). FIGURE 42 shows a picture of the DFT.



FIGURE 42 Schematic of measuring pavement skid resistance by DFT.

Circular Texture Meter

The most current technology for measuring pavement macrotexture is the CTMeter described in ASTM E2157. In this device, a charged couple device (CCD) laser displacement sensor mounted on an arm 80 mm above the surface rotates around in a circle with a 142 mm radius. A motor at a tangential velocity of 6 mm/min drives the arm. The CCD laser takes 1024 samples of the pavement surface in one round with 0.87 mm spacing. The data are converted to digital format and stored in the memory of a laptop. To calculate the MPD, the data are divided into eight equal 111.5 mm arcs. The calculated MPD for each segment is averaged and presented as MPD for the test surface. The individual MPD values for each segment are also available for further investigation (165). FIGURE 43 shows a picture of a CTMeter.



FIGURE 43 CTMeter (29).

LABORATORY MIXTURE TESTS

Thirteen different slabs were prepared and polished by the polishing machine. The measurements were done after predefined polishing cycles. The polishing cycles continued to 100,000 cycles for dense mixes and 200,000 cycles for PFC mixtures. TABLE 8 presents the different slabs and polishing cycles for the designed mixtures.

TABLE 8 Experimental Setup

Mixture Type	Aggregate Type	Polishing Cycles
Type C	Beckman	
	Brownwood	
	Brownlee	Before Polishing, 5000, 10,000,
	El Paso	20,000, 35,000, 50,000, 75,000,
	Fordyce	100,000 cycles, Completely Polished
	50% Beckman + 50% Brownlee	
PFC	Beckman	
	Brownwood	Before Polishing, 5000, 10,000,
	Brownlee	20,000, 35,000, 50,000, 75,000,
	El Paso	100,000, 150,000, 200,000 cycles, Completely Polished
Type D	Beckman	Before Polishing, 5000, 10,000,
	Brownlee	20,000, 35,000, 50,000, 75,000,
	50% Beckman + 50% Brownlee	100,000 cycles, Completely Polished

According to TABLE 8, each slab was prepared and tested the day after compaction. The sand patch test, British pendulum test, DFT, and CTMeter were conducted on each slab before the slab was subjected to any polishing. Then, the polisher was placed on top of a slab and polishing started.

All Type D mixes degraded after 5000 polishing cycles and showed signs of raveling (see FIGURE 44). Because of raveling occurring in these mixes, it was decided to discontinue polishing these mixes, and they were dropped from the experimental design program.



FIGURE 44 Type D mixes degraded after 5000 cycles.

After application of the specified number of wheel passes on Type C and PFC mixtures, the specimen was removed and tested for texture and friction using CTMeter and DFT according to ASTM E 1911 and ASTM E 2157, respectively. Two measurements with DFT and six readings with CTMeter were taken from each polished strip. Because the limited width of the polished area restricted performing the sand patch and the British pendulum test, it was decided to continue performing the British pendulum test using a 1.5-inch rubber slider rather than a 3-inch rubber slider and to remove the sand patch test from the experimental program. This test was only used to measure the macrotexture of slabs before polishing and after reaching the terminal condition. After testing, the polisher was properly positioned on top of the slab such that the polishing was performed in the same path and polishing continued to the next level. This continued to 100,000 polishing cycles for dense-graded mixes and to 200,000 polishing cycles for PFC.

To achieve an entirely polished surface, the slabs were polished by a floor polisher. This machine included a rotating plate driven by a 175-rpm electrical motor. A #150 sandpaper mesh was used along with the floor polisher to polish the slabs to their terminal condition.

SUMMARY

As presented in this chapter, the aggregates used in the preparation of the asphalt mixtures were selected to represent different sources and exhibit a wide range of properties. Similarly, the mixtures were designed to represent those that are used in the State of Texas.

Petrographic examination was carried out to study the mineralogy of each aggregate type by preparing thin sections of each aggregate sample. Petrographic examination provided some preliminary speculations about the frictional performance of each aggregate, where aggregates with high calcite content (aggregates A and C) were assumed to have bad to moderate frictional properties and aggregates with high contents of insoluble materials (aggregates B and D) were assumed to have satisfactory frictional properties.

Several tests, such as the British pendulum test, LA abrasion test, magnesium sulfate soundness test, acid insoluble particle test, Micro-Deval test, and AIMS texture and angularity measurements before and after Micro-Deval, were performed on aggregates to evaluate aggregate resistance to polishing. The details of each test method were explained in the chapter.

Two dense-graded mix designs, i.e., Type D and Type C, and one open-graded mix design, i.e., PFC, were tested to study the effect of mix type on pavement friction. Different methods were tried to polish the slabs but the one that was found to be appropriate was NCAT polisher which contains a turn table and three caster wheels that rotate on each slab and polish it. Polishing of PFC continued up to 200,000 cycles and 100,000 for dense graded mixes. Several test methods including, British pendulum, sand patch test, CTMeter, and DFT were used to measure pavement texture and friction during polishing. Next chapter explains the results of each test method.

CHAPTER IV

RESULTS AND DATA ANALYSIS

INTRODUCTION

This chapter contains the results of the different laboratory measurements performed on the aggregates and mixes. The aggregate tests included the LA abrasion test, magnesium sulfate soundness test, British pendulum test, Micro-Deval test, acid insolubility value, and AIMS texture and angularity before and after Micro-Deval. The mixture tests included the sand patch, British pendulum, DFT, and CTMeter. Statistical analysis was conducted to determine the relationship between aggregate properties and mixture friction and texture.

AGGREGATE TEST RESULTS

As mentioned previously, aggregate properties such as gradation, size of particle, texture, shape, porosity, toughness, abrasion resistance, mineralogy, and petrography affect the pavement skid resistance (137). A complete set of measurements for evaluating different aggregate characteristics were performed, and the results are tabulated in TABLE 9.

TABLE 9 Aggregate Test Results

Test Procedure	Brownlee	Brownwood	El Paso	Beckman	Fordyce	Beckman + Brownlee
LA % Wt. Loss	24	25	30	33	19	28.5
Mg Soundness	19	9	19	26	4	22.5
Polish Value	38	21	24	25	28	31.5
Micro-Deval % Wt. Loss	16.2	11.2	14	24	2.1	20.1
Coarse Aggregate Acid Insolubility	58	1	10	1	80	29.5

It has been a common practice in Texas to mix aggregates with different performance levels to obtain a better-performing blend of aggregate. In this study, the aggregates from the Beckman quarry showed unsatisfactory field performance with respect to polishing combined with aggregates from the Brownlee quarry on a 50/50 proportion basis. The aggregate characteristic for this mix is believed to be the average of two values for Brownlee and Beckman. FIGURE 45 illustrates the different aggregate characteristics.

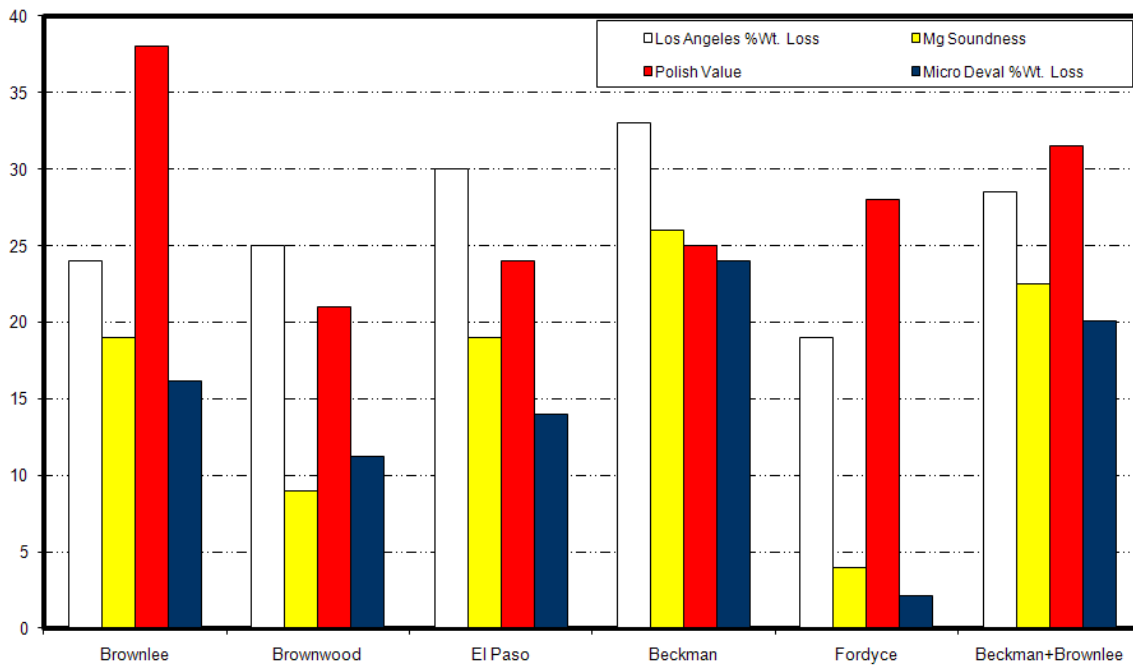


FIGURE 45 Aggregate properties (151,166).

FIGURE 45 shows that the Brownlee aggregate has the highest polish value. The Beckman aggregate has the highest weight loss in the Micro-Deval, magnesium sulfate soundness, and LA abrasion tests. Aggregate shape characteristics were also measured, and results are tabulated in TABLE 10.

TABLE 10 Result of Shape Measurements by AIMS

Test Procedure	Brownlee	Brownwood	El Paso	Beckman	Fordyce	Beckman + Brownlee (average)
Texture before Micro-Deval	265	193	269.3	80	142	172.5
Texture after Micro-Deval	222	95	192.6	36	108	129
Angularity before Micro-Deval	2868	2323	2865.6	2195	3959	2531.5
Angularity after Micro-Deval	1883	1730	2126.5	1671	2787	1777

Figures 46 and 47 show the change in texture and angularity before and after Micro-Deval. Figures 134 to 141 in Appendix B show the texture distribution for each aggregate type measured by AIMS.

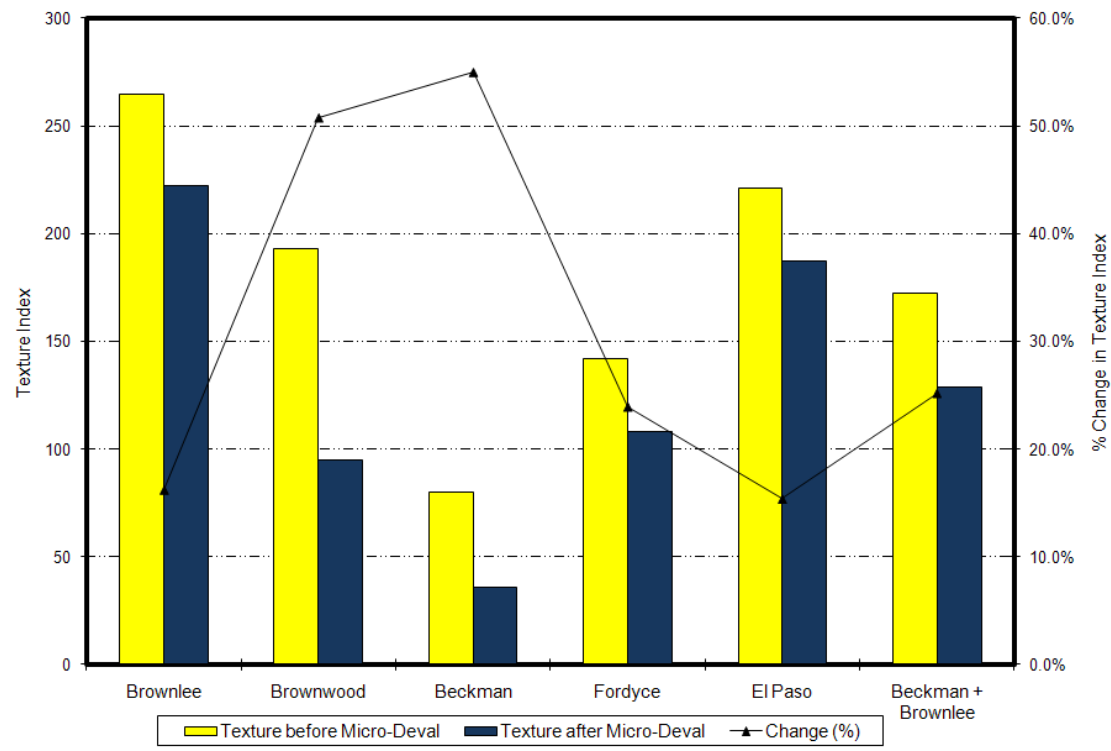


FIGURE 46 Aggregate texture before and after Micro-Deval and percent change.

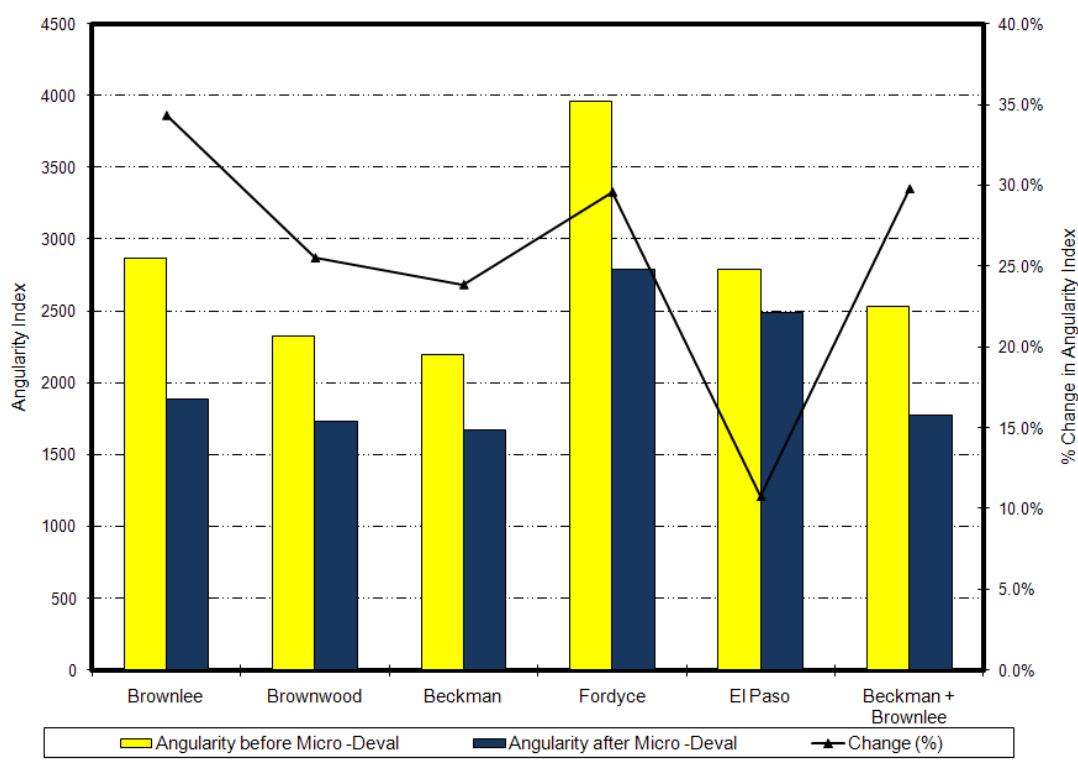


FIGURE 47 Aggregate angularity before and after Micro-Deval and percent change.

Figures 46 and 47 show that the El Paso aggregate and Brownlee aggregate had the highest texture before and after Micro-Deval. The Brownlee aggregate experienced the lowest drop in texture. The Beckman aggregate had the lowest texture before and after Micro-Deval, and the highest change in texture occurred in this aggregate type.

Luce performed a more detailed study to model the texture change in different aggregate types (132). In his study, he evaluated the aggregates' resistance to abrasion and polishing using the method originally developed by Mahmoud (137). In this method, the Micro-Deval test and the AIMS are used to estimate the aggregate polish resistance. Aggregates are subjected to 15, 30, 45, 60, 75, 90, 105, and 180 min of abrasion time in the Micro-Deval machine, according to Tex-461-A. Aggregates are scanned after polishing using AIMS to determine the change in aggregate shape properties over time and at their terminal condition (132). Mahmoud proposed the following equation to describe texture as a function of polishing time (137):

$$AIMSTexture = a + b \cdot \exp(-c \cdot t) \quad (9)$$

In this equation, a , b , and c are regression constants, while t is the time in the Micro-Deval (132). The regression constants can be determined using non-linear regression analysis. TABLE 11 shows the values of the regression constants for the different aggregate types.

TABLE 11 Regression Coefficient of Texture Model (132)

Parameter	Sandstone	Hard Limestone	Soft Limestone	Gravel	Granite
A	167.90	83.531	39.125	99.813	178.689
B	70.56	119.931	37.463	14.288	39.021
C	0.00788	0.020	0.025	1.600	0.013

Luce showed that texture and angularity of the aggregates decrease as the time in the Micro-Deval increases. Furthermore, he found that sandstone aggregate can maintain its original texture, and the curve is almost flat for this type of aggregate (132). FIGURE 48 shows the texture change for different aggregates versus polishing time in Micro-Deval.

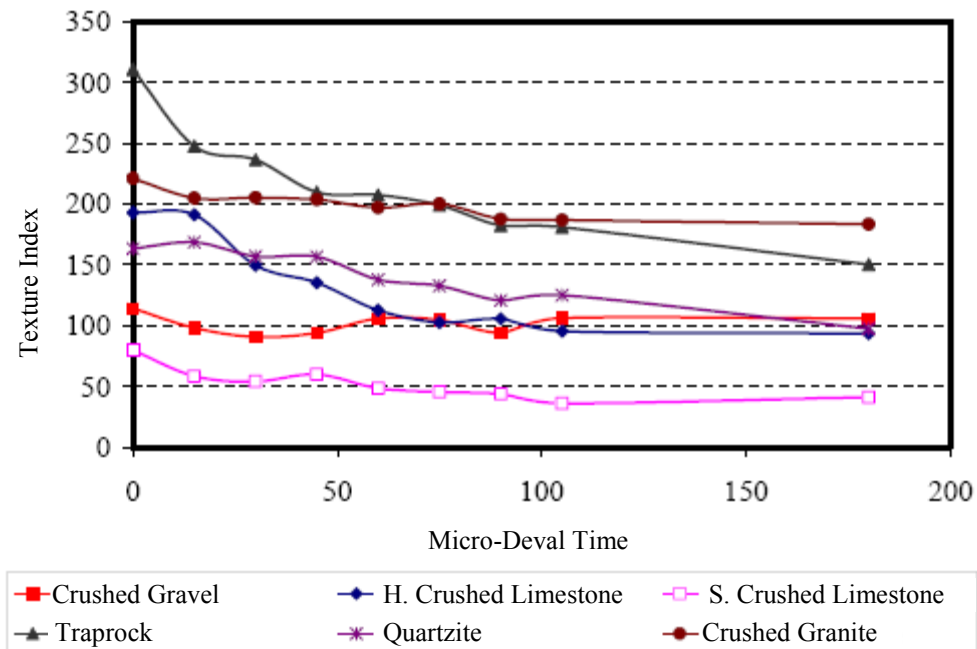


FIGURE 48 Aggregate texture as function of Micro-Deval time (150).

Further analysis by Masad et al. revealed that the loss of texture curve could be obtained by using only three different polishing intervals in Micro-Deval polishing (0, 105, and 180 min) instead of nine different times (150). The regression constants fitted, using three time intervals, are shown in TABLE 12.

TABLE 12 Regression Constants Based on Three Measuring Times (150)

Parameter	Brownlee	Brownwood	Beckman	Fordyce	El Paso
A	166.7	93.6	39.13	105.67	189.1
B	99.43	99.15	37.46	36.33	72.704
C	0.00553	0.04087	0.02505	0.02617	0.023

MIXTURE TEST RESULTS

This section presents the results of the sand patch, British pendulum, DFT, and CTMeter measurements for pavement texture and friction. It is followed by an analysis of the effect of each aggregate type on frictional properties of asphalt mixtures.

Sand Patch Test

The sand patch test was performed on the slabs at six locations, before polishing and after final polishing (terminal condition). FIGURE 49 shows the MTD for different mixes before and after polishing. This test was not performed on the slabs fabricated with PFC mixes because the glass beads used to measure the MTD penetrated into PFC voids.

FIGURE 49 and TABLE 13 show that the average MTD for Type C mixes was about 23 percent greater than it was for Type D mixes. A smaller MTD value indicates a smoother surface. The smaller nominal aggregate size used in Type D provided a smoother pavement with less macrotexture. Except for Brownlee and Brownwood aggregates, all mixes lost their macrotexture as a result of the abrasion effect of the polishing machine. It could be seen that the macrotexture of mixes containing Brownwood aggregate slightly increased after polishing.

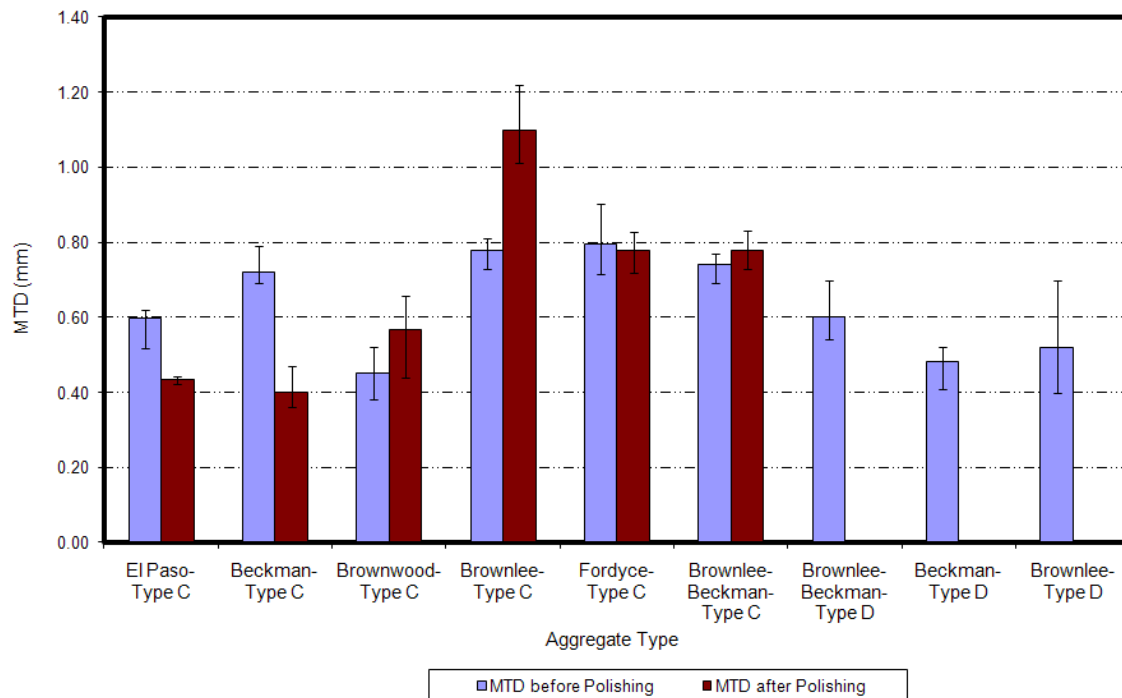


FIGURE 49 Measured MTD by sand patch method for different aggregates before and after polishing.

TABLE 13 Measured MTD by Use of Sand Patch Method for Different Mixes

Aggregate Type	Mix Type	MTD	
		Before Polishing	After Polishing
El Paso	Type C	0.60	0.43
Beckman		0.72	0.40
Brownwood		0.45	0.57
Brownlee		0.78	1.10
Fordyce		0.79	0.78
Brownlee-Beckman		0.74	0.78
Brownlee-Beckman	Type D	0.60	-
Beckman		0.48	-
Brownlee		0.52	-

To study the effect of aggregate type, mixture type, and polishing on the measured macrotexture of each slab using the sand patch method, a one-way analysis of variance (ANOVA) was performed.

The one-way ANOVA was used to test the equality of two population means for statistical significance. This analysis is done by partitioning the total variance into two components; one component is calculated based on random error, and the other one is determined based on the difference between two means. The second component is then tested for statistical significance. The F-distribution is used to investigate the significance of this component. If the test indicates significance, the null hypothesis that there is no significant difference between different groups of data is rejected, and the alternative hypothesis that the groups of data are different is accepted.

An important step in the ANOVA is verifying the validity of assumptions used in this analysis. One assumption of ANOVA is that the variances of different groups are equivalent. The Levene test is a standard approach to test homogeneity of variances. The Levene statistic in TABLE 14 rejects the null hypothesis that the group variances are equal. ANOVA, however, is robust to this violation when the groups are of equal or near-equal size and can still be used.

TABLE 14 Levene Statistic to Check the Homogeneity of Variances

Levene Statistic	df1	df2	Sig.
5.864	5	83	.000

TABLE 15 shows the results of the ANOVA analysis for the effect of aggregate type. The significance of the F-test in the ANOVA analysis is less than 0.001. Thus, the hypothesis that the average macrottexture values for different aggregates are equal is rejected. Therefore, mixtures with different aggregate types have different macrottexture. The results of the ANOVA analysis for different mix types are also tabulated in TABLE 16.

TABLE 15 Results of the ANOVA Analysis for the Effect of Aggregate Type

Sum of Squares		df	Mean Square	F	Sig.
Between Groups	1.774	5	.355	24.766	.000
Within Groups	1.189	83	.014		
Total	2.963	88			

TABLE 16 Results of the ANOVA Analysis for the Effect of Mix Type

	Sum of Squares	df	Mean Square	F	Sig.
Between Groups	.003	1	.003	.099	.753
Within Groups	2.960	87	.034		
Total	2.963	88			

The significance of the F-test in ANOVA is 0.753. This suggests that the null hypothesis that the macrotexture for Type C and Type D are equal cannot be rejected. These results show there is no significant difference between Type C and Type D mixes. The results of the F-test in TABLE 17 indicate that the difference between macrotexture before and after polishing is also not significant.

TABLE 17 Results of the ANOVA Analysis for the Effect of Polishing Cycles

	Sum of Squares	df	Mean Square	F	Sig.
Between Groups	.012	1	.012	.350	.555
Within Groups	2.951	87	.034		
Total	2.963	88			

The results of this analysis indicate that the sand patch does not detect the difference between macrotexture before and after polishing. The ANOVA shows the equality or inequality of the means between different groups. To learn more about the structure of the differences, other statistical methods are required. A pairwise comparison was performed for both Type C and Type D mixtures to find the source of the difference within each group. Tables 18 and 19 display the results for Type C and Type D mixes, respectively. The numbers in the third column show the mean difference between measured values of macrotexture for two different aggregates. A small asterisk next to the number denotes that the mean difference is significant at a 0.05 level.

In almost all cases, Brownlee aggregate had higher macrotexture. Beckman aggregate produced the lowest macrotexture. The higher macrotexture of Brownlee aggregate can be attributed to the continuous removal of the softer matrix and the dislodging of the hard particles during polishing that leads to a higher texture after polishing.

TABLE 18 Significance Level for Different Aggregate Types in Type C Mix

(I) Aggregate Type	(J) Aggregate Type	Mean Difference (I-J)	Std. Error	Sig.	95% Confidence Interval	
					Lower Bound	Upper Bound
Brownlee	Brownwood	.4189(*)	.06390	.000	.1963	.6415
	Beckman	.3343(*)	.07783	.006	.0740	.5945
	El Paso	.4114(*)	.06295	.000	.1902	.6326
	Fordyce	.1431	.05986	.407	-.0751	.3613
Brownwoo	Brownlee-Beckman	.2373(*)	.06395	.032	.0146	.4600
	Brownlee	-.4189(*)	.06390	.000	-.6415	-.1963
	Beckman	-.0847	.05993	.949	-.2954	.1261
	El Paso	-.0075	.03870	1.000	-.1346	.1196
Beckman	Fordyce	-.2758(*)	.03342	.000	-.3882	-.1635
	Brownlee-Beckman	-.1817(*)	.04030	.003	-.3139	-.0495
	Brownlee	-.3343(*)	.07783	.006	-.5945	-.0740
	Brownwood	.0847	.05993	.949	-.1261	.2954
El Paso	El Paso	.0772	.05891	.972	-.1321	.2864
	Fordyce	-.1912	.05559	.080	-.3977	.0154
	Brownlee-Beckman	-.0970	.05998	.872	-.3078	.1138
	Brownlee	-.4114(*)	.06295	.000	-.6326	-.1902
Fordyce	Brownwood	.0075	.03870	1.000	-.1196	.1346
	Beckman	-.0772	.05891	.972	-.2864	.1321
	Fordyce	-.2683(*)	.03157	.000	-.3737	-.1629
	Brownlee-Beckman	-.1742(*)	.03878	.003	-.3015	-.0468
Brownlee- Beckman	Brownlee	-.1431	.05986	.407	-.3613	.0751
	Brownwood	.2758(*)	.03342	.000	.1635	.3882
	Beckman	.1912	.05559	.080	-.0154	.3977
	El Paso	.2683(*)	.03157	.000	.1629	.3737
Brownlee- Beckman	Brownlee-Beckman	.0942	.03352	.159	-.0185	.2069
	Brownlee	-.2373(*)	.06395	.032	-.4600	-.0146
	Brownwood	.1817(*)	.04030	.003	.0495	.3139
	Beckman	.0970	.05998	.872	-.1138	.3078
Brownlee- Beckman	El Paso	.1742(*)	.03878	.003	.0468	.3015
	Fordyce	-.0942	.03352	.159	-.2069	.0185

* The mean difference is significant at the 0.05 level.

TABLE 19 Significance Level for Different Aggregate Types in Type D Mix

(I) Aggregate Type	(J) Aggregate Type	Mean Difference (I-J)	Std. Error	Sig.	95% Confidence Interval	
					Lower Bound	Upper Bound
Brownlee	Beckman	.2933(*)	.04685	.002	.1402	.4464
	Brownlee-Beckman	.0417	.05254	.833	-.1145	.1978
Beckman	Brownlee	-.2933(*)	.04685	.002	-.4464	-.1402
	Brownlee-Beckman	-.2517(*)	.03119	.000	-.3466	-.1567
Brownlee- Beckman	Brownlee	-.0417	.05254	.833	-.1978	.1145
	Beckman	.2517(*)	.03119	.000	.1567	.3466

* The mean difference is significant at the 0.05 level.

British Pendulum Test

The British pendulum test was performed three times in each of the three locations on the slabs. Figures 50 and 51 show the BP values for different mixes.

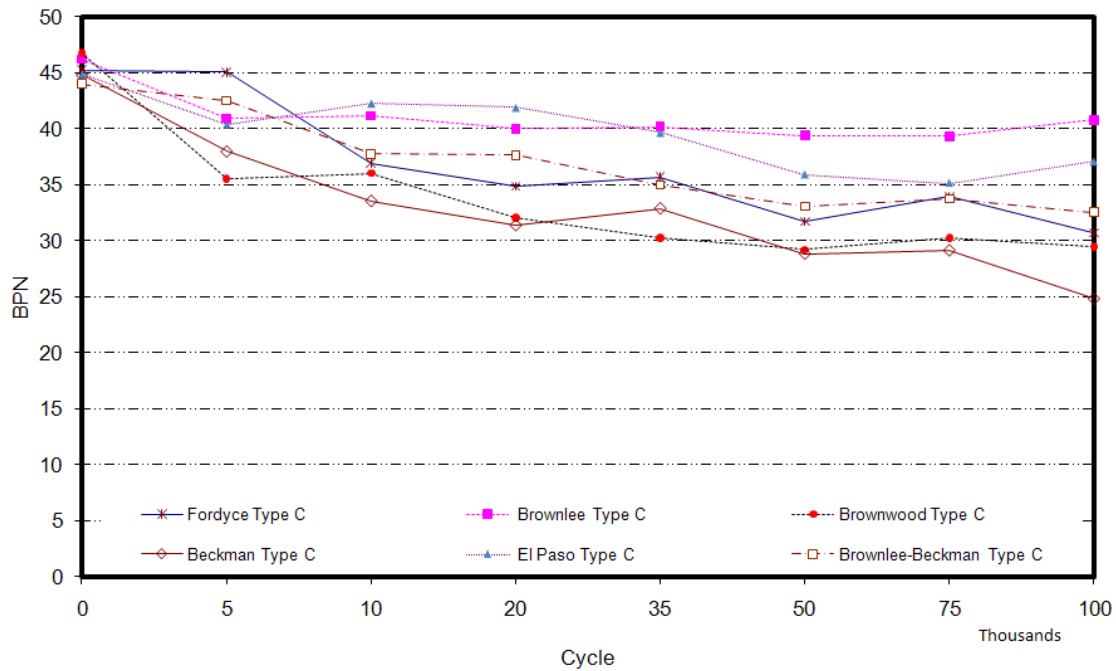


FIGURE 50 Results of British pendulum test for Type C mixes.

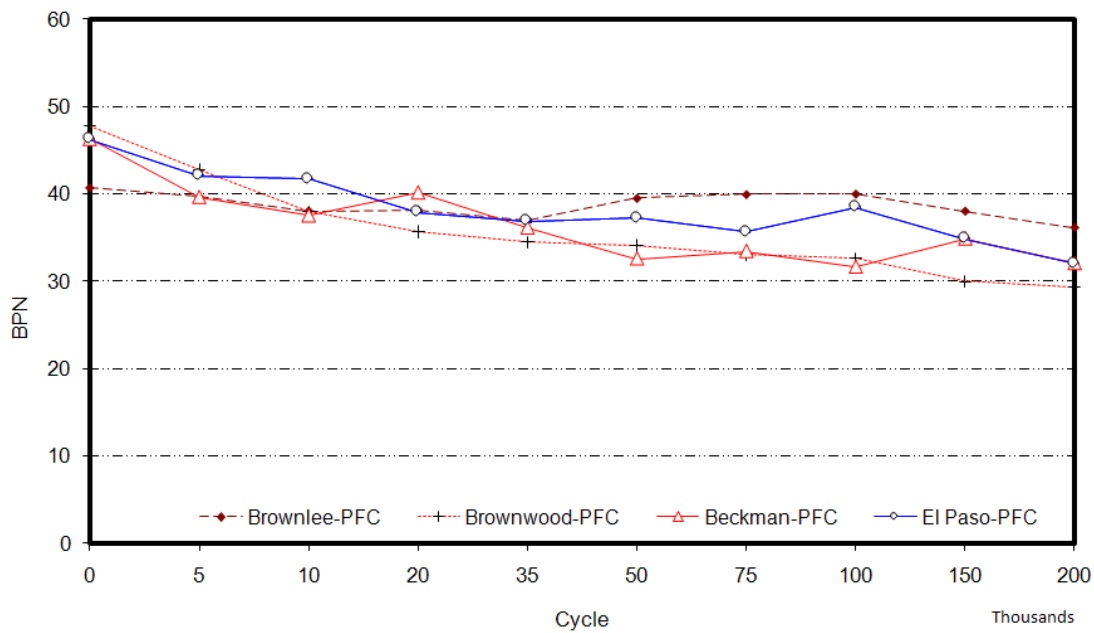


FIGURE 51 Results of the British pendulum test for PFC mixes.

As a general trend, it is clear that the BP value decreases as the number of polishing cycles increases. The rate of decrease in the British pendulum value is dependent on the aggregate type. TABLE 20 summarizes the results of the ANOVA at a 95 percent confidence level for different aggregates. The results show that there is a significant difference between the mean BP values for each aggregate type in each polishing cycle. Moreover, it indicates the polisher has the ability to decrease the surface skid resistance in terms of BP value and can obviously polish the surface.

TABLE 21 shows the mean BP values at different numbers of polishing cycles. In almost all cases—except sandstone—the p-value is very small, which supports the idea that there is a significant difference between measured BP values in different aggregates at a 95 percent confidence level. Further analysis presented subsequently, however, reveals that this difference is only due to Brownlee aggregate, and there is no significant difference between other aggregates.

Another ANOVA was done to examine the effect of mixture type on frictional characteristics of asphalt pavements (see TABLE 22). The results indicate that there is no statistical difference between the skid resistance of Type C and PFC mixes containing Brownlee aggregate. Furthermore, this aggregate has the same frictional performance in Type C and PFC mixes in both low and high numbers of polishing cycles. This is a result of continuous renewal of the aggregate surface exposed to a rubber slider. Moreover, Brownlee aggregate consists of hard particles in a softer matrix. Wearing the softer matrix off the aggregate allows the new hard particles to be exposed to traffic and will help this mix maintain its frictional properties. The PFC and Type C mixes containing Brownwood aggregate have statistically equal BP values in low-polishing cycles; however, when the polishing cycles increase, the PFC can maintain its skid properties relatively better than Type C mixes, and the BP value is higher. The difference between the BP value of Type C and PFC mixes containing Beckman aggregate is always significant. Moreover, PFC mixes containing Beckman aggregate always have a higher BP value than Type C mixes. The difference between skid properties of the mixes containing El Paso aggregate does not follow a clear trend. The PFC mixes containing this kind of aggregate are likely to have a higher BP value in low-polishing cycles, and

the results of the analysis do not show a significant difference between PFC and Type C mixes in high-polishing cycles.

TABLE 20 Significance Level for the Effect of Different Polishing Cycles on Mixtures with Different Aggregates

Aggregate Type	Mix Type	Polishing Cycle (thousands)									
		0	5	10	20	35	50	75	100	150	200
El Paso Beckman Brownwood Brownlee Fordyce Brownlee-Beckman	Type C	0.039	0.009	0.002	0	0	0	0	0	NA	NA
Brownlee El Paso Brownwood Beckman	PFC	0	0.001	0	0	0.054	0	0	0	0	0

TABLE 21 Significance Level for the Mean BP Values for Different Loading Cycles

Aggregate Type	Mix Type	Sig.
El Paso	Type C	0.0001
Beckman		0
Brownwood		0
Brownlee		0.0581
Fordyce		0
Brownlee-Beckman		0
Brownlee	PFC	0
El Paso		0
Brownwood		0
Beckman		0

TABLE 22 Significance Level for the Mean BP Values for Different Mixture Type

Aggregate Type	Mix Type	Cycle (thousands)							
		0	5	10	20	35	50	75	100
El Paso	Type C								
	PFC	0.30*	0.027	0.630	0.015	0.105	0.346	0.354	0.448
Beckman	Type C								
	PFC	0.000	0.005	0.024	0.00	0.003	0.000	0.002	0.006
Brownwood	Type C								
	PFC	0.148	0.11	0.36	0.001	0.014	0.005	0.001	0.006
Brownlee	Type C								
	PFC	0.001	0.281	0.067	0.168	0.107	0.964	0.796	0.715

* Highlighted numbers show the difference is not statistically significant.

To have a better understanding of the variation of the BP values for different mixes, the equation suggested by Mahmoud (Equation 9) was fitted to the data substituting texture with British pendulum value and time with polishing cycles in terms of 1000 cycles (137).

Figures 52 to 61 show the data and the fitted lines for different mixes. The results show that this equation could fit the data very well. TABLE 23 shows the values of the regression coefficients for different mixes after removing the outliers that were deemed unlikely based on mean and standard deviation of the data and fitting the function to the data by the least square method.

TABLE 23 Regression Coefficients for Different Aggregate

Aggregate Type	Mix Type	A	B	C
El Paso	Type C	35	9	0.026
Beckman		29	16	0.091
Brownwood		30	16	0.140
Brownlee		39	3	0.027
Fordyce		32	14	0.064
Brownlee-Beckman		33	11	0.053
Brownlee	PFC	37	3	0.052
El Paso		35	11	0.042
Brownwood		32	15	0.070
Beckman		33	11	0.050

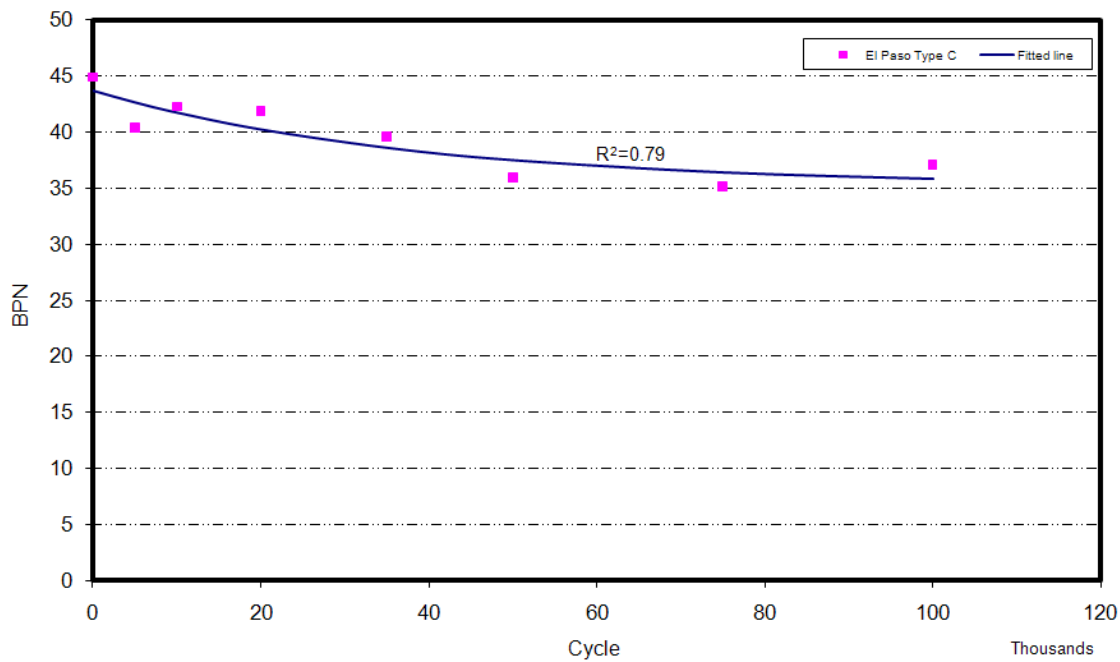


FIGURE 52 British pendulum values for El Paso aggregate vs. polishing cycles.

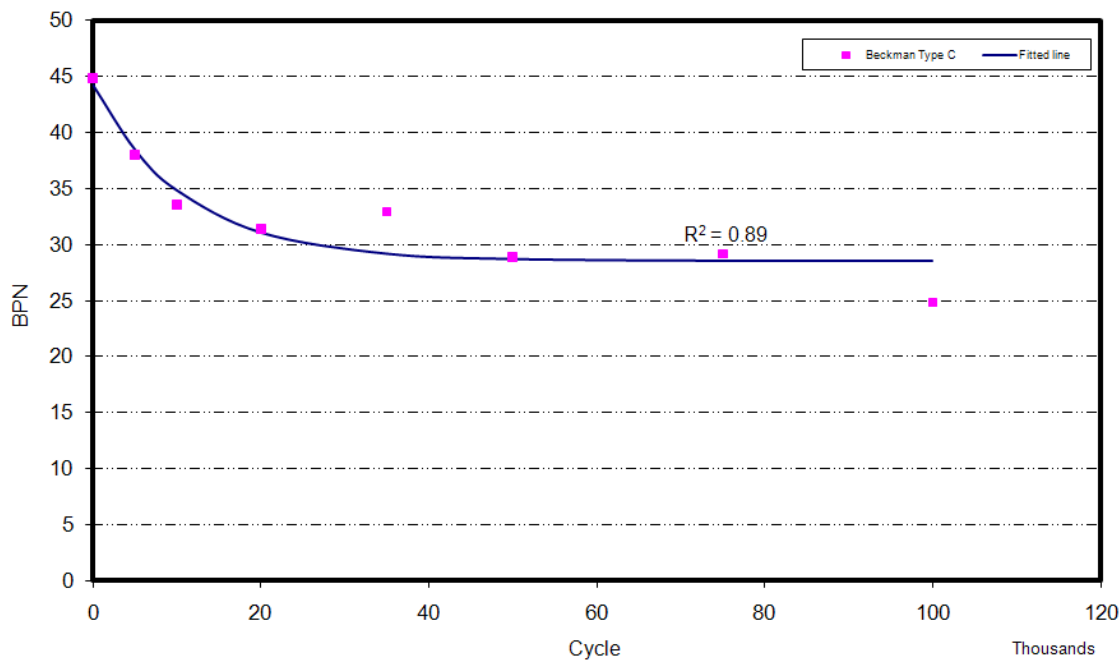


FIGURE 53 British pendulum values for Beckman aggregate vs. polishing cycles.

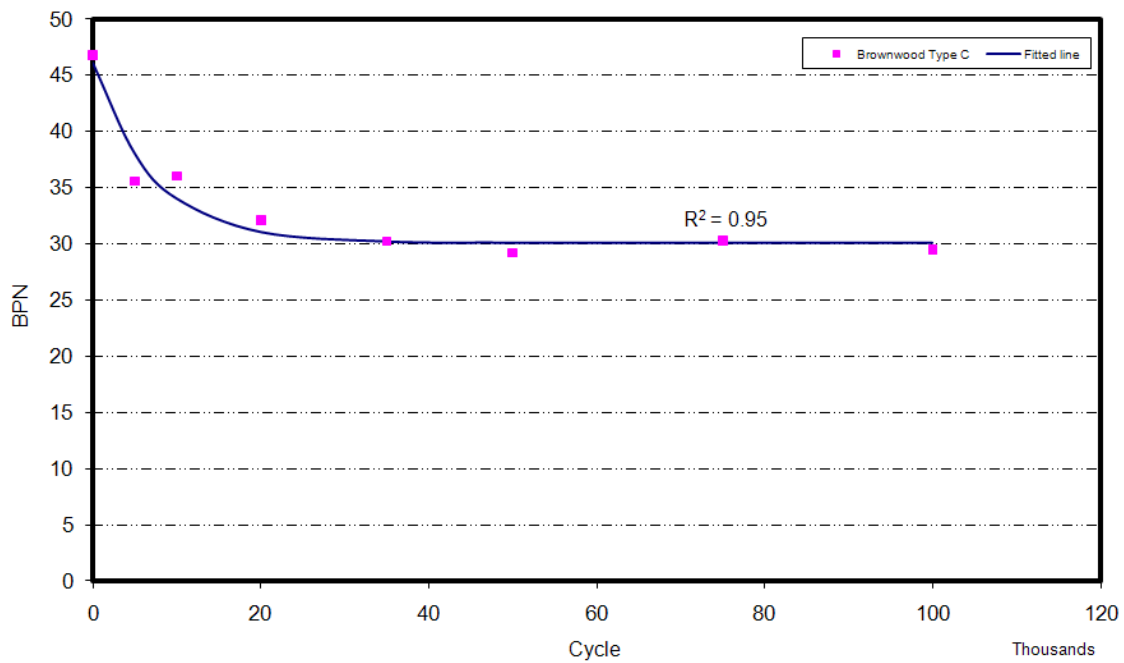


FIGURE 54 British pendulum values for Brownwood aggregate vs. polishing cycles.

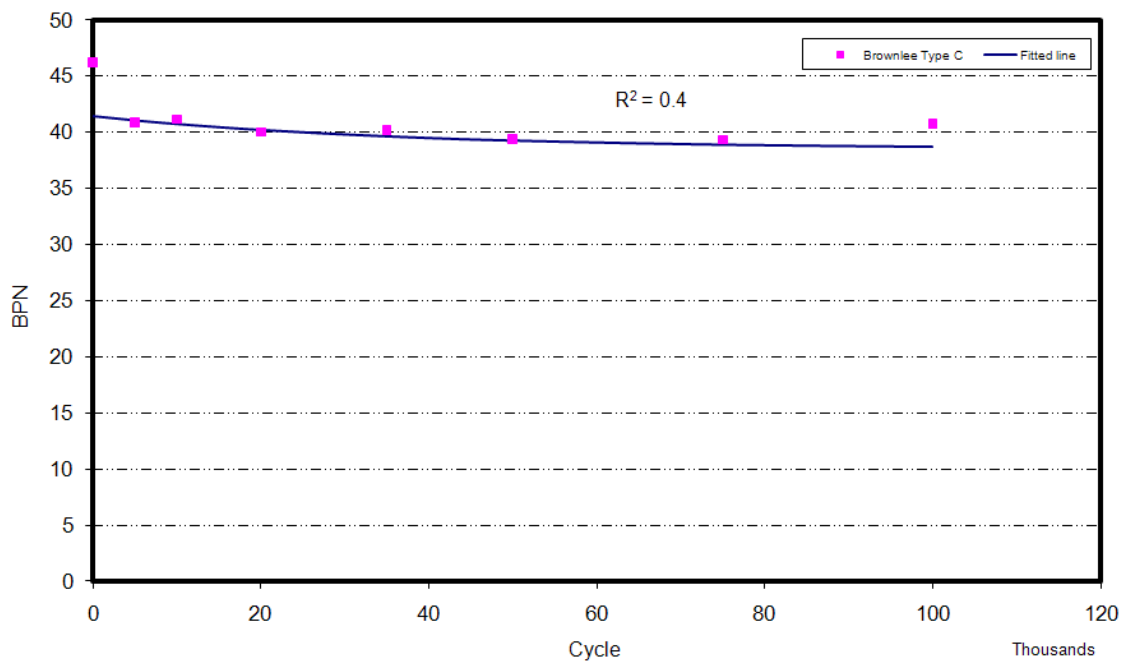


FIGURE 55 British pendulum values for Brownlee aggregate vs. polishing cycles.

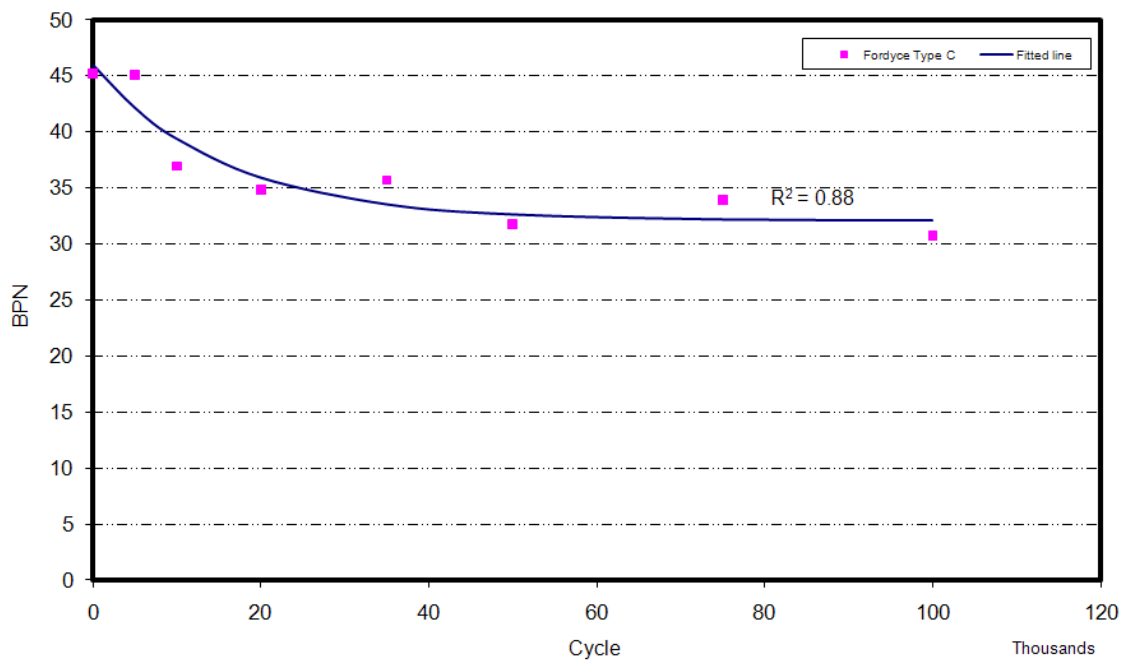


FIGURE 56 British pendulum values for Fordyce aggregate vs. polishing cycles.

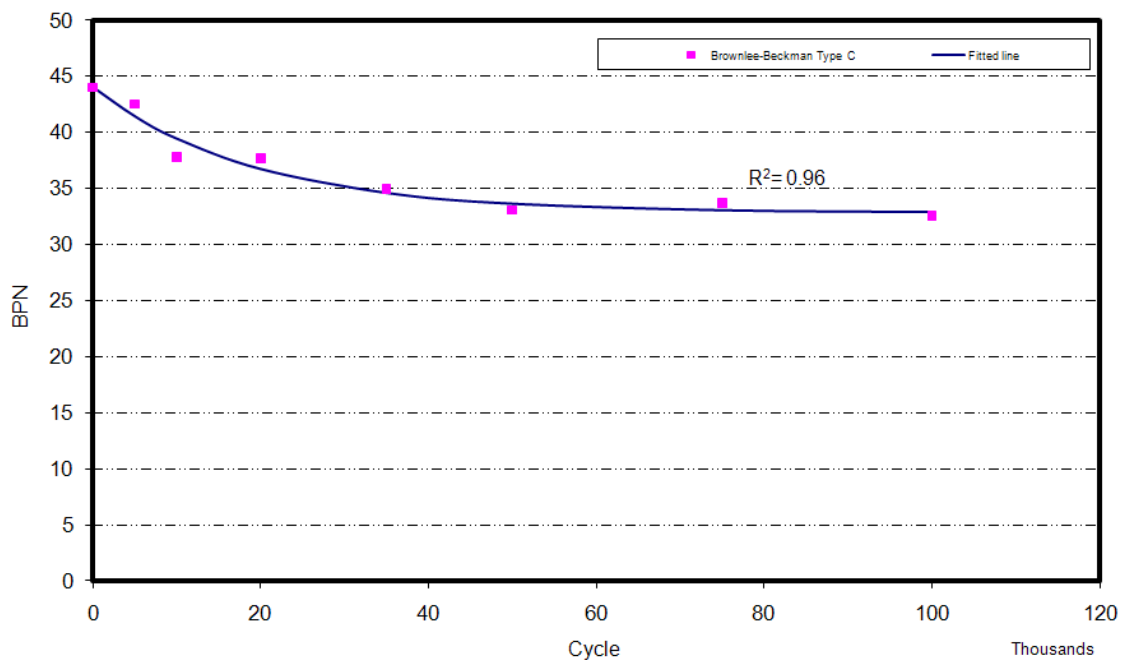


FIGURE 57 British pendulum values for the 50 percent Beckman–50 percent Brownlee vs. polishing cycles.

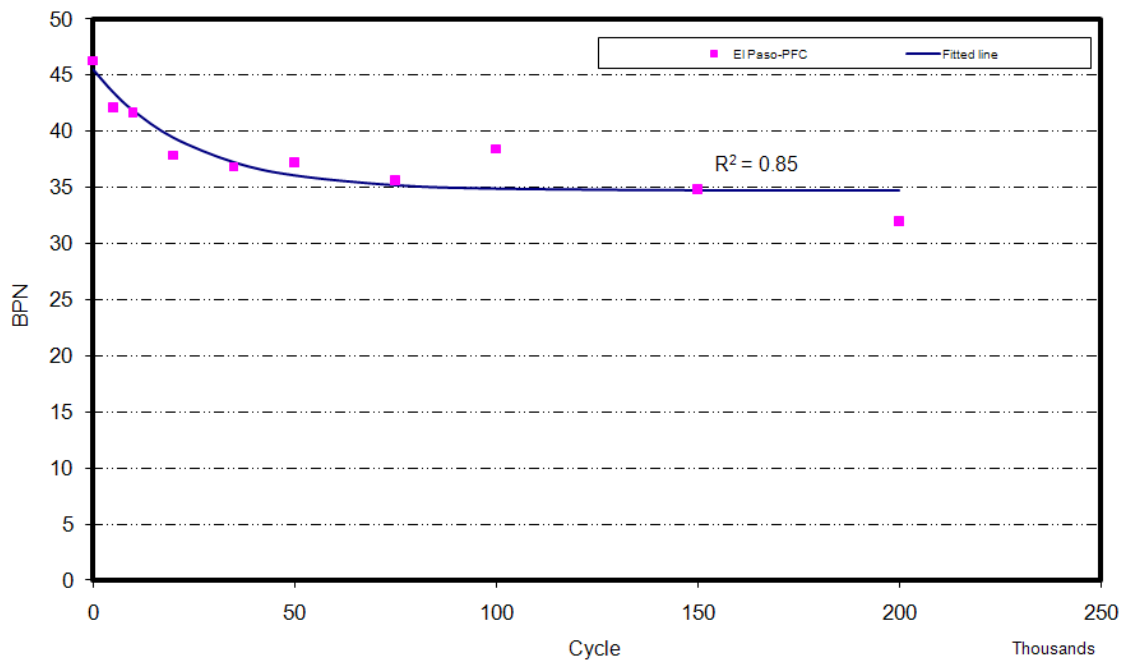


FIGURE 58 British pendulum values for El Paso aggregate vs. polishing cycles in PFC mix.

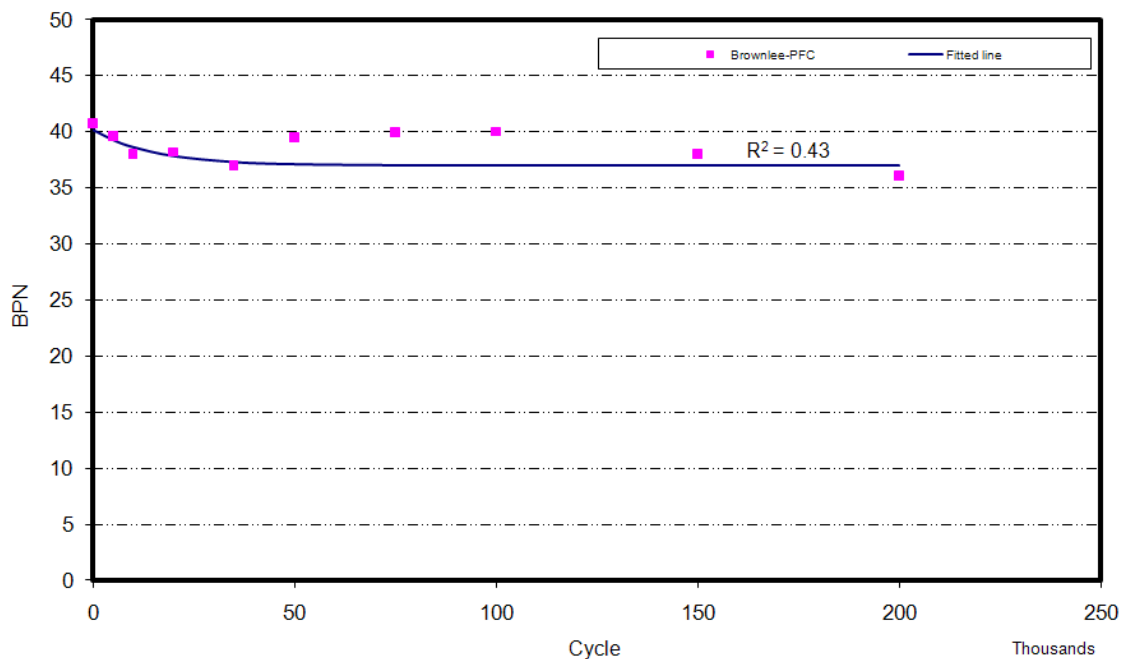


FIGURE 59 British pendulum values for Brownlee aggregate vs. polishing cycles in PFC mix.

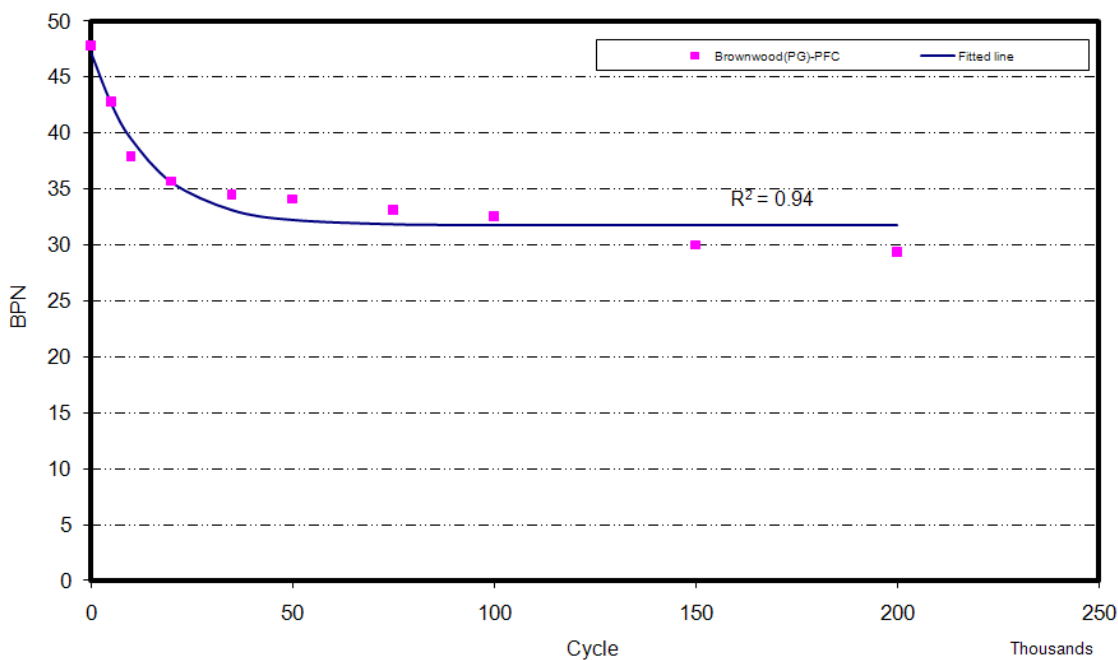


FIGURE 60 British pendulum values for Brownwood aggregate vs. polishing cycles in PFC mix.

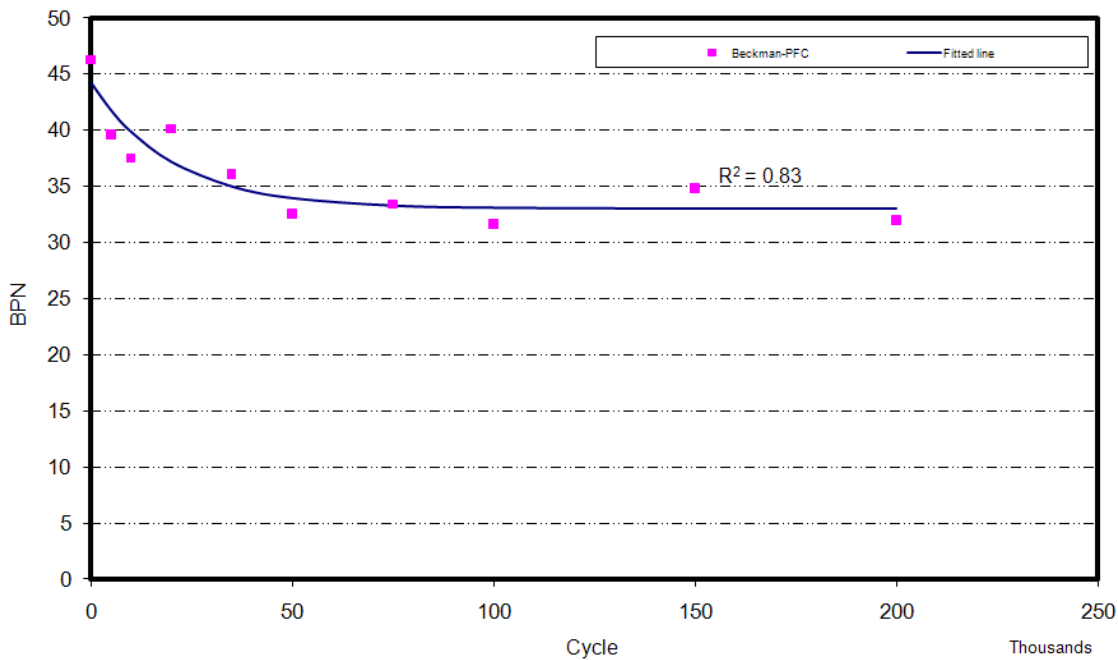


FIGURE 61 British pendulum values for Beckman aggregate vs. polishing cycles in PFC mix.

Figures 55 and 59 show that the change of BP values versus polishing cycle for Brownlee aggregate is very small. The same results were reported by Luce (132). This aggregate has the lowest change in BP values as a function of polishing cycles, and the highest terminal value compared to other aggregates. Moreover, this small change in BP value with polishing cycles in Brownlee aggregate texture contributes to its high skid resistance. El Paso aggregate has the second-lowest rate of decrease in BP value against polishing cycles and is polish-resistant. Mixing Beckman aggregate with Brownlee aggregate shows promising results because this mixture has the third-lowest rate of BP value change versus polishing cycles. Brownwood and Beckman aggregates as shown in Figures 60 and 61 have the highest rate of BP value loss versus polishing cycle and does not have a high terminal BP value. BP values for Brownlee aggregate in the PFC mixture are almost constant, which is similar to the BP values for Type C mixes.

The results of the ANOVA tabulated in TABLE 24 show the comparison between measured BP values for each pair of aggregates. The numbers in the third column illustrate the mean difference between BP values of corresponding aggregates. An asterisk next to a number indicates that the difference is significant at the 0.05 level. TABLE 24 does not show a statistical difference between each pair except for very high values (i.e., Brownlee aggregate). This indicates the limitation of British pendulum to detect the difference between frictional performances of aggregates with known differences in frictional characteristics.

TABLE 24 Pairwise Comparison of Different Aggregates in Type C Mix

(I) Aggregate Type	(J) Aggregate Type	Mean Difference (I-J)	Std. Error	Sig.
El Paso	Beckman	6.70875(*)	1.42299	.000
	Brownwood	5.92500(*)	1.43491	.003
	Brownlee	-1.35375	.94971	.928
	Fordyce	2.86958	1.31902	.418
	Beckman-Brownlee	2.61208	1.12609	.315
Beckman	El Paso	-6.70875(*)	1.42299	.000
	Brownwood	-.78375	1.72790	1.000
	Brownlee	-8.06250(*)	1.35226	.000
	Fordyce	-3.83917	1.63294	.296
	Beckman-Brownlee	-4.09667	1.48147	.120
Brownwood	El Paso	-5.92500(*)	1.43491	.003
	Beckman	.78375	1.72790	1.000
	Brownlee	-7.27875(*)	1.36480	.000
	Fordyce	-3.05542	1.64334	.660
	Beckman-Brownlee	-3.31292	1.49293	.387
Brownlee	El Paso	1.35375	.94971	.928
	Beckman	8.06250(*)	1.35226	.000
	Brownwood	7.27875(*)	1.36480	.000
	Fordyce	4.22333(*)	1.24239	.025
	Beckman-Brownlee	3.96583(*)	1.03528	.006
Fordyce	El Paso	-2.86958	1.31902	.418
	Beckman	3.83917	1.63294	.296
	Brownwood	3.05542	1.64334	.660
	Brownlee	-4.22333(*)	1.24239	.025
	Beckman-Brownlee	-.25750	1.38191	1.000
Beckman-Brownlee	El Paso	-2.61208	1.12609	.315
	Beckman	4.09667	1.48147	.120
	Brownwood	3.31292	1.49293	.387
	Brownlee	-3.96583(*)	1.03528	.006
	Fordyce	.25750	1.38191	1.000

* The mean difference is significant at the 0.05 level.

CTMeter and DFT Tests

As previously stated, the frictional properties of each mix were measured by CTMeter and DFT periodically during polishing. Using Equations 5 and 6 presented in the previous chapter, IFI components were calculated. The measured friction at 20 km/h (DF_{20}) was also reported as a good representation of the microtexture change against polishing. Figures 62 through 64 show the results of the IFI, DF_{20} , and MPD values.

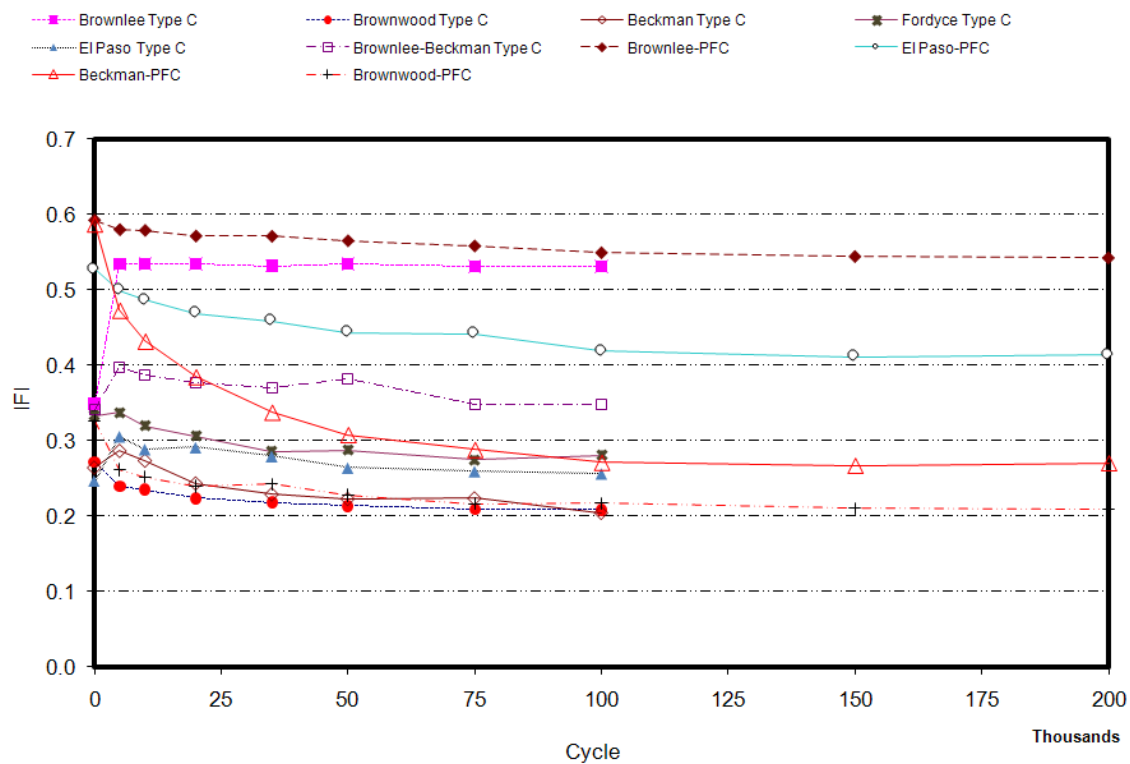


FIGURE 62 Calculated IFI for different aggregates vs. polishing cycle.

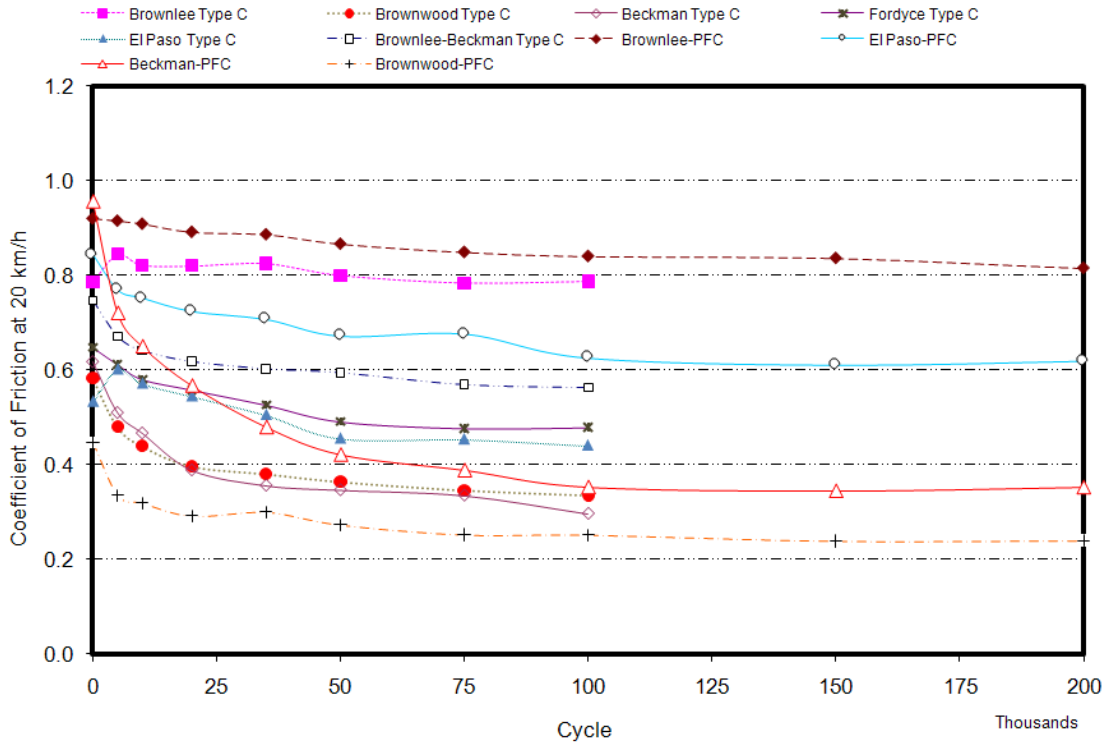


FIGURE 63 Coefficient of friction for different aggregates vs. polishing cycle at 20 km/h.

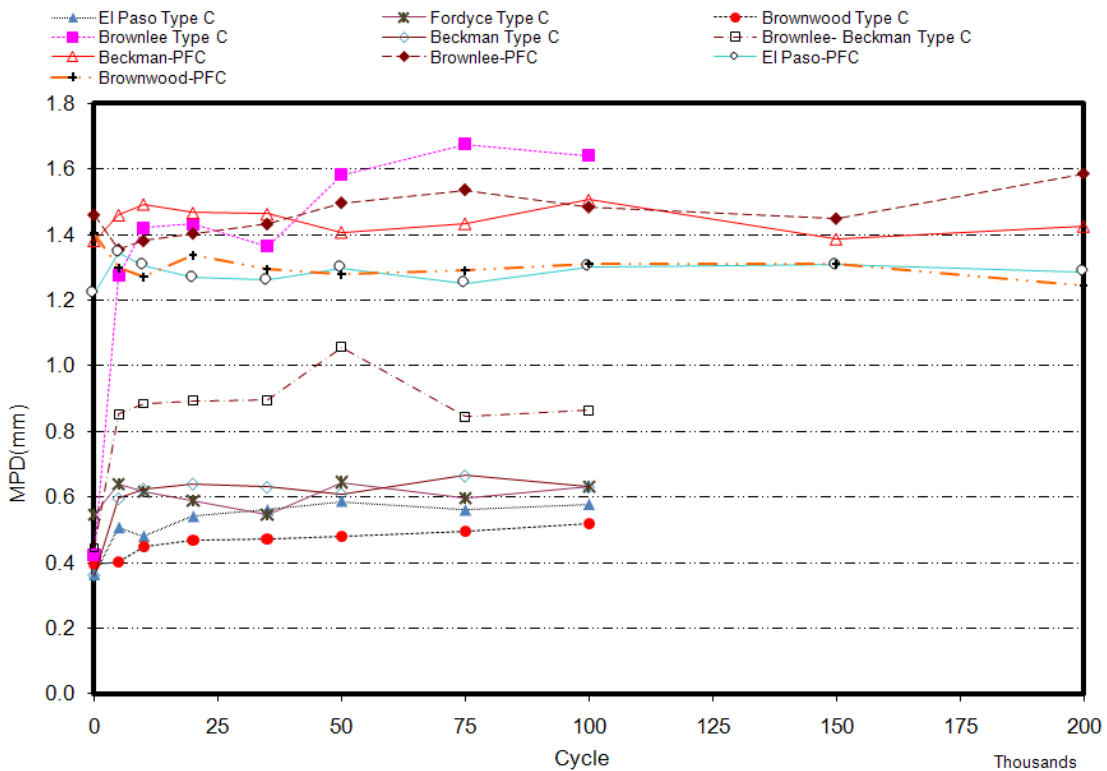


FIGURE 64 MPD for different aggregates vs. polishing cycle.

It is evident from FIGURE 63 that the coefficient of friction decreases with polishing cycle. In addition, some aggregates, such as the Beckman aggregate, show a rapid change in their measured coefficient of friction, while others, such as the Brownlee aggregate, remain almost constant during the polishing. It is clear that after a particular number of polishing cycles, each mix reaches a terminal condition in which no other changes occur afterwards. The rate of change and the terminal value of DF_{20} can be an indication of an aggregate's susceptibility to polishing and was investigated in this study.

The MPD values of different mixes displayed in Figure 64 vary in terms of number of polishing cycles and do not show a clear trend. Small changes in MPD could be related to aggregate abrasion during polishing or experimental error. For some types of aggregates (Brownlee aggregate), aggregate raveling related to moisture susceptibility was noticed.

Figure 62 shows the calculated IFI based on Equations 5 and 6. The IFI decreases as the polishing cycle increases. Moreover, the variation of microtexture— DF_{20} —has a more important role in the variation of IFI than macrotexture does. Therefore, the variation of DF_{20} and IFI are consistent and follow the same trend. An ANOVA was performed to study the effect of polishing cycles, speed, and aggregate type on measured values of DF_{20} for different mixes at different speeds and polishing cycles. The results are tabulated in Tables 25 and 26.

TABLE 25 Significance Level (p-value) of the Mean DF₂₀ Values for Different Aggregate Types in Type C Mix

Mix Type	Aggregate	Before Polish				5000		10,000		20,000	
		Speed	Polishing	Speed Effect	Aggregate Type	Speed Effect	Aggregate Type	Speed Effect	Aggregate Type	Speed Effect	Aggregate Type
Type C	Brownlee-Beckman	20	0.00	0.00	0.00	0.00	0.00	0.00	0.00	0.00	0.00
		40	0.00		0.00		0.00		0.00		0.00
		60	0.00		0.00		0.00		0.00		0.00
		80	0.00		0.00		0.00		0.00		0.00
	El Paso	20	0.00	0.00	0.00	0.00	0.00	0.00	0.00	0.00	0.00
		40	0.00		0.00		0.00		0.00		0.00
		60	0.00		0.00		0.00		0.00		0.00
		80	0.00		0.00		0.00		0.00		0.00
	Fordyce	20	0.00	0.00	0.00	0.00	0.00	0.00	0.00	0.00	0.00
		40	0.00		0.00		0.00		0.00		0.00
		60	0.00		0.00		0.00		0.00		0.00
		80	0.00		0.00		0.00		0.00		0.00
	Brownwood	20	0.00	0.00	0.00	0.00	0.00	0.00	0.00	0.00	0.00
		40	0.00		0.00		0.00		0.00		0.00
		60	0.00		0.00		0.00		0.00		0.00
		80	0.00		0.00		0.00		0.00		0.00
	Brownlee	20	0.00	0.00	0.00	0.00	0.00	0.00	0.00	0.00	0.00
		40	0.00		0.00		0.00		0.00		0.00
		60	0.00		0.00		0.00		0.00		0.00
		80	0.00		0.00		0.00		0.00		0.00
	Beckman	20	0.00	0.00	0.00	0.00	0.00	0.00	0.00	0.00	0.00
		40	0.00		0.00		0.00		0.00		0.00
		60	0.00		0.00		0.00		0.00		0.00
		80	0.00		0.00		0.00		0.00		0.00

TABLE 25 Continued

Mix Type	Aggregate	35,000		50,000		75,000		100,000	
		Speed Effect	Aggregate Type	Speed Effect	Aggregate Type	Speed Effect	Aggregate Type	Speed Effect	Aggregate Type
Type C	Brownlee-Beckman	0.00	0.00	0.00	0.00	0.00	0.00	0.00	0.00
			0.00		0.00		0.00		0.00
			0.00		0.00		0.00		0.00
			0.00		0.00		0.00		0.00
	El Paso	0.00	0.00	0.00	0.00	0.00	0.00	0.00	0.00
			0.00		0.00		0.00		0.00
			0.00		0.00		0.00		0.00
			0.00		0.00		0.00		0.00
	Fordyce	0.00	0.00	0.00	0.00	0.00	0.00	0.00	0.00
			0.00		0.00		2.53		0.00
			0.00		0.00		0.00		0.00
			0.00		0.00		0.03		0.00
	Brownwood	0.00	0.00	0.00	0.00	0.00	0.02	0.00	0.00
			0.00		0.00		0.00		0.00
			0.00		0.00		0.00		0.00
			0.00		0.00		0.00		0.00
	Brownlee	0.00	0.00	0.00	0.00	0.00	0.00	0.07	0.00
			0.00		0.00		0.00		0.00
			0.00		0.00		0.00		0.00
			0.00		0.00		0.00		0.00
	Beckman	0.00	0.00	0.00	0.00	0.00	0.00	0.00	0.00
			0.00		0.00		0.00		0.00
			0.00		0.00		0.00		0.00
			0.00		0.00		0.00		0.00

TABLE 26 Significance Level of the Mean DF₂₀ Values for Different Aggregate Types in PFC Mix

Mix Type	Aggregate	Speed	Before Polish		5000		10,000		20,000		
			Polishing	Speed Effect	Aggregate Type	Speed Effect	Aggregate Type	Speed Effect	Aggregate Type	Speed Effect	Aggregate Type
PFC	El Paso	20	0.00	0.00	0.00	0.00	0.00	0.00	0.00	0.00	0.00
		40	0.00		0.00		0.00		0.00		0.00
		60	0.00		0.00		0.00		0.00		0.00
		80	0.00		0.00		0.00		0.00		0.00
	Brownwood	20	0.00	0.00	0.00	0.00	0.00	0.00	0.00	0.11	0.00
		40	0.00		0.00		0.00		0.00		0.00
		60	0.00		0.00		0.00		0.00		0.00
		80	0.00		0.00		0.00		0.00		0.00
	Brownlee	20	0.20*	0.00	0.00	0.03	0.00	0.00	0.00	0.09	0.00
		40	0.29		0.00		0.00		0.00		0.00
		60	0.29		0.00		0.00		0.00		0.00
		80	0.38		0.00		0.00		0.00		0.00
	Beckman	20	0.00	0.00	0.00	0.00	0.00	0.00	0.00	0.00	0.00
		40	0.00		0.00		0.00		0.00		0.00
		60	0.00		0.00		0.00		0.00		0.00
		80	0.00		0.00		0.00		0.00		0.00

* Highlighted numbers show the difference is not statistically significant.

TABLE 26 Continued

Mix Type	Aggregate	35,000		50,000		75,000		100,000		150,000		200,000		
		Speed Effect	Aggregate Type	Speed Effect	Aggregate Type	Speed Effect	Aggregate Type	Speed Effect	Aggregate Type	Speed Effect	Aggregate Type	Speed Effect	Aggregate Type	
PFC	El Paso	0.00	0.00	0.00	0.00	0.00	0.00	0.00	0.00	0.00	0.00	0.00	0.00	
			0.00		0.00		0.00		0.00		0.00		0.00	
			0.00		0.00		0.00		0.00		0.00		0.00	
			0.00		0.00		0.00		0.00		0.00		0.00	
	Brownwood	0.03	0.00	0.06*	0.00	0.00	0.01	0.00	0.53	0.00	0.27	0.00	0.58	0.00
			0.00		0.00		0.00		0.00		0.00		0.00	
			0.00		0.00		0.00		0.00		0.00		0.00	
			0.00		0.00		0.00		0.00		0.00		0.00	
	Brownlee	0.02	0.00	0.00	0.00	0.00	0.00	0.00	0.06	0.00	0.00	0.00	0.00	0.00
			0.00		0.00		0.00		0.00		0.00		0.00	
			0.00		0.00		0.00		0.00		0.00		0.00	
			0.00		0.00		0.00		0.00		0.00		0.00	
	Beckman	0.00	0.00	0.00	0.00	0.00	0.58	0.00	0.01	0.00	0.45	0.00	0.37	0.00
			0.00		0.00		0.00		0.00		0.00		0.00	
			0.00		0.00		0.00		0.00		0.00		0.00	
			0.00		0.00		0.00		0.00		0.00		0.00	

* Highlighted numbers show the difference is not statistically significant.

The numbers in Tables 25 and 26 show the significance of the equality of means for each variable (e.g., aggregate type, speed, mix type) evaluated by the ANOVA. The statistical difference between the compared entities is significant when the p-value is less than 0.05.

The results in Table 25 show that the difference between the measured dynamic friction values for different aggregates in Type C mixes are significant at a 95 percent level of confidence. In this mix type, the measured values at different speeds for each polishing cycle are significantly different. The trends show that dynamic friction decreases as the speed increases in Type C mixes. The results also show that the difference between the measured values of friction in different polishing cycles is significant. These results confirm that the selected equipment is capable of polishing the surface that leads to a decrease in measured DF_{20} value as the number of polishing cycles increases.

TABLE 26 also indicates that the mean DF_{20} values for different aggregates in a PFC mix are not significant, and that the null hypothesis can be rejected. This indicates that aggregate type is a significant factor affecting frictional properties.

The results in Table 26 show that the significance level of the mean difference of the measured DF_{20} values for different speeds is significant in most cases except for El Paso aggregate. This means, in most cases, that there is no evidence for changing the friction at different speeds. The results also show that for all cases except for the Brownlee aggregate, the difference between measured DF_{20} in different polishing cycles is significant. Moreover, there is not a significant difference between the measured DF_{20} values for the Brownlee aggregate during polishing. Furthermore, owed to its petrographic nature, continuous polishing of this sandstone aggregate does not change its frictional properties.

Based on the measured values of dynamic friction at 20 km/h and MPD measured by CTMeter, the IFI was calculated for each mix and plotted against polishing cycles.

The ANOVA was performed by SPSS[®] software to study the effect of aggregate and mix type on the calculated IFI. The results tabulated in Tables 27 and 28 support the hypothesis that there is a significant difference between the calculated IFI in Type C and

PFC mixes. This result indicates that the PFC mixture has a higher IFI value and, consequently, can provide better skid resistance.

TABLE 27 Results of Comparing Calculated Values of IFI for Type C and PFC Mixes

Mix Type	N	Mean	Std. Deviation	Std. Error Mean
Type C	132	.3190	.09861	.00858
PFC	105	.4058	.13285	.01296

TABLE 28 Results of the T-test for Comparing IFI Mean Values in Type C and PFC Mixes

T-Value	df	Sig. (2-Tailed)	Mean Difference	Std. Error Difference	95% Confidence Interval of the Difference	
					Lower	Upper
-5.581	186.669	.000	-.0868	.01555	-.11745	-.05610

An equation with the same form as the one proposed by Mahmoud (Equation 9) was fitted to the data (137). Figures 65 through 68 show the measured DF_{20} and IFI values and the fitted curves for different mixes. The results show that this equation could fit the data substituting texture with IFI or DF_{20} values and time with polishing cycles in terms of 1000 cycles.

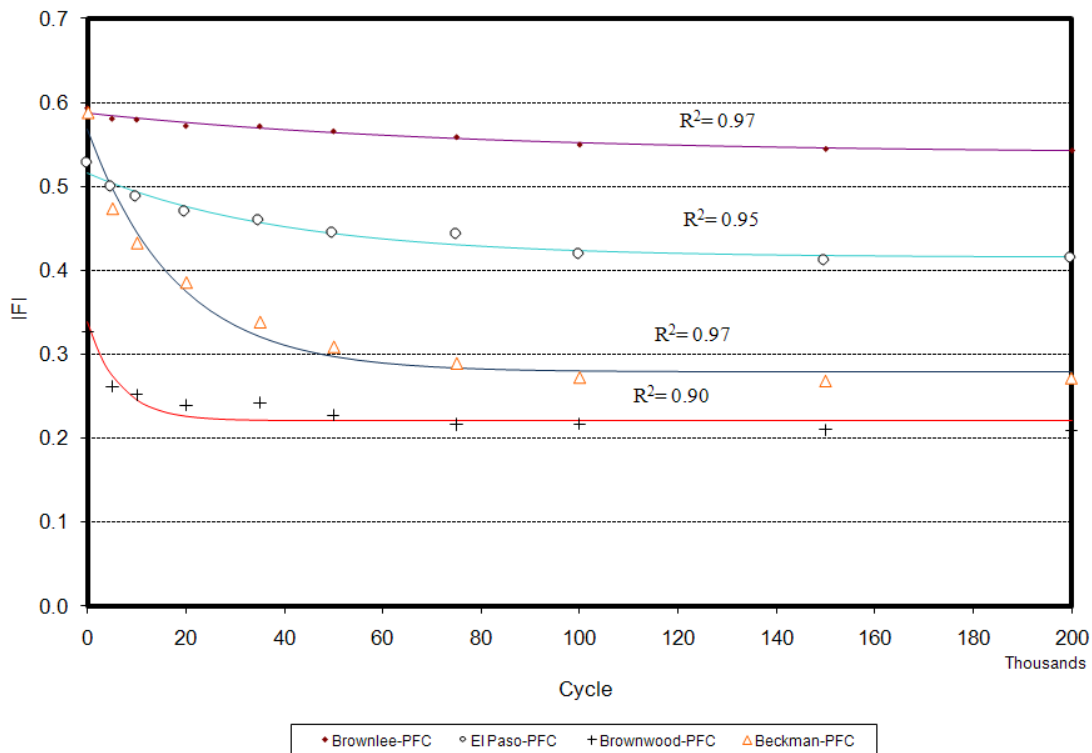


FIGURE 65 Calculated IFI values vs. polishing cycle and fitted line for PFC mixes.

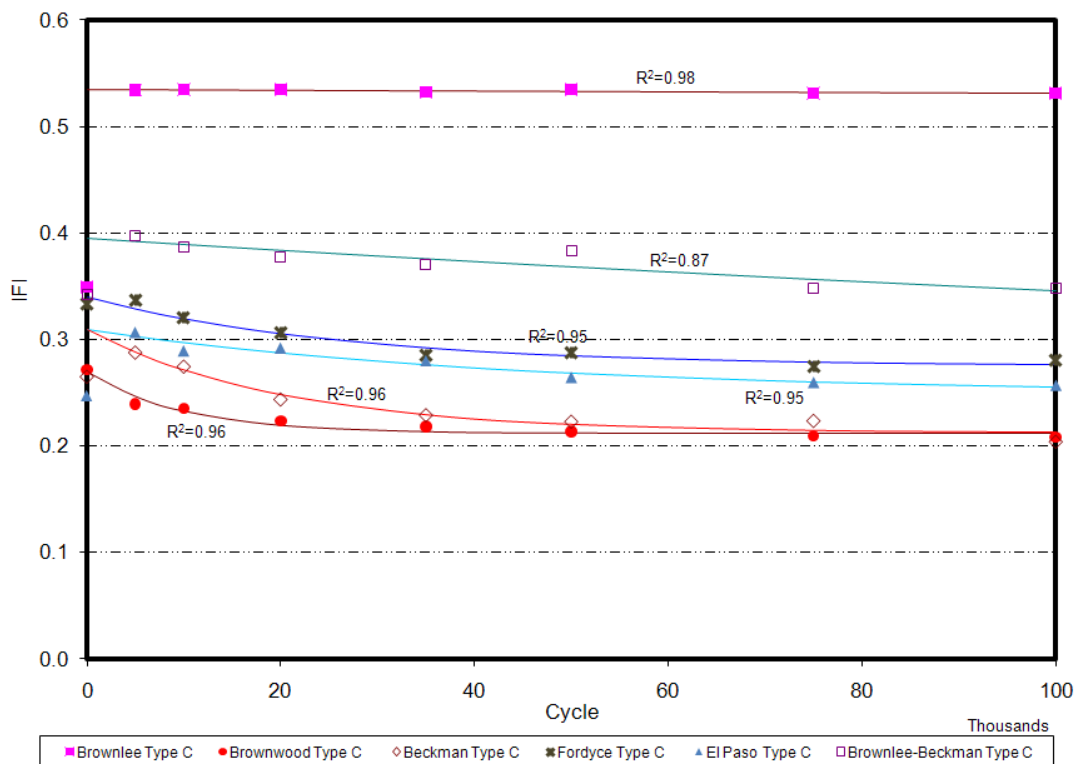


FIGURE 66 Calculated IFI values vs. polishing cycle and fitted line for Type C mixes.

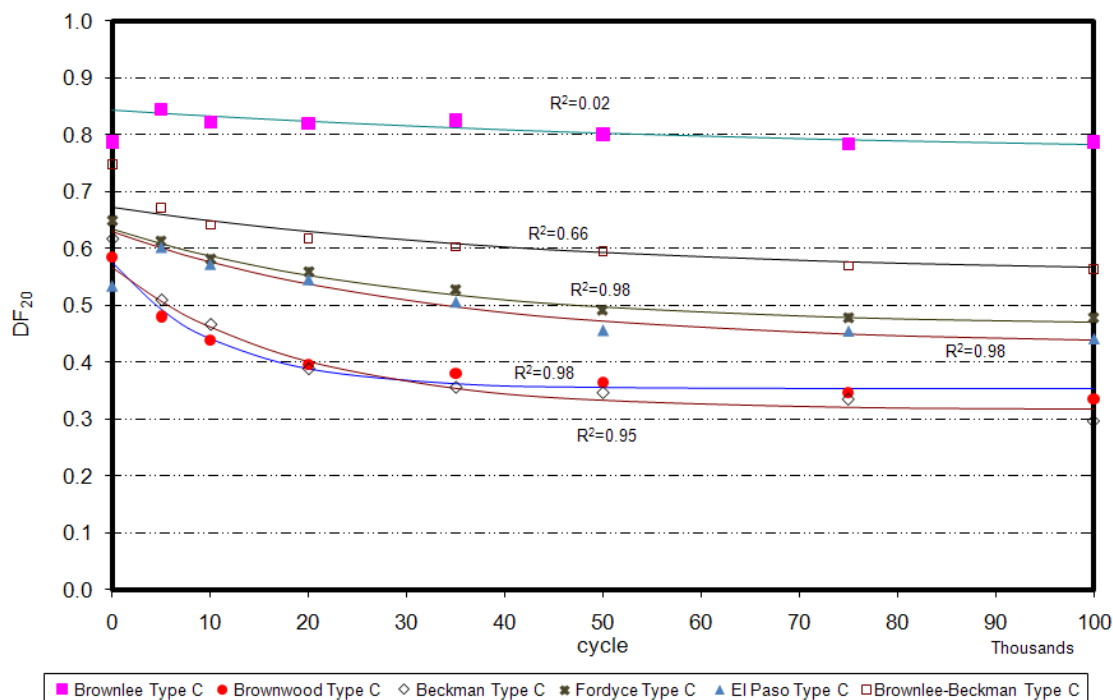


FIGURE 67 DF₂₀ values vs. polishing cycle and fitted line for Type C mixes.

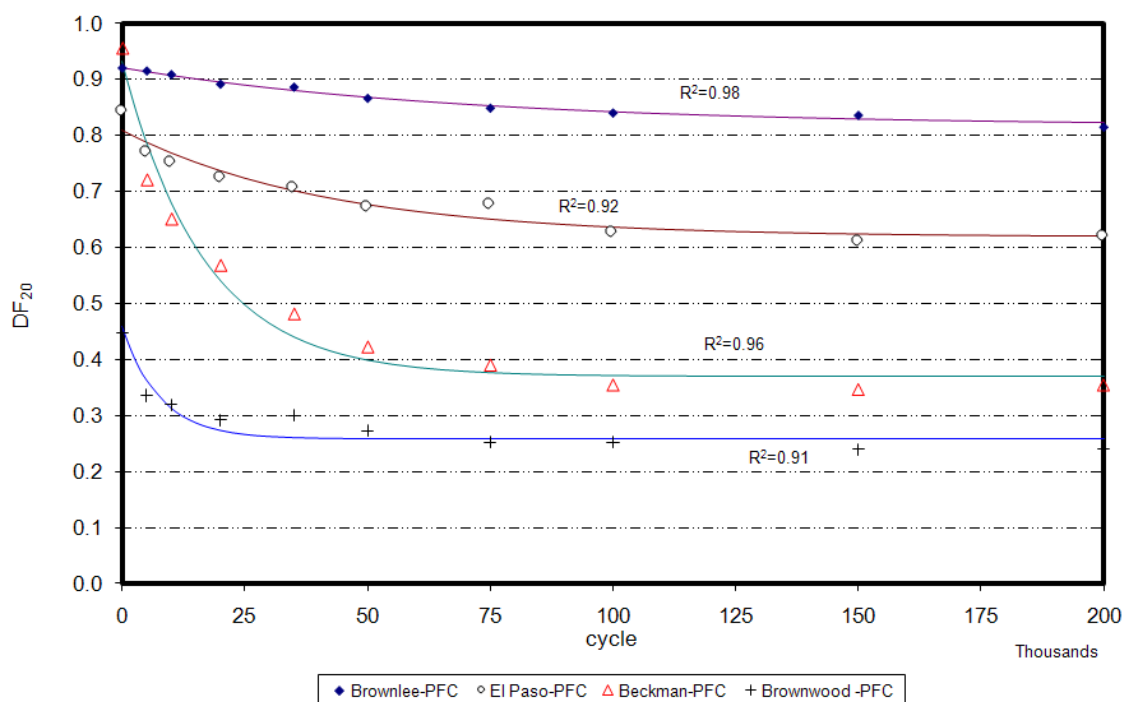


FIGURE 68 DF₂₀ values vs. polishing cycle and fitted line for PFC mixes.

The model parameters were found by the least sum of square errors (SSE) method. In this method, it is assumed that the minimum SSE would result in the model that best fits the measured data. Tables 29 and 30 show the magnitude of the regression coefficients for the DF_{20} and IFI.

TABLE 29 Values of the Regression Parameters of Proposed Model for DF_{20}

Mix Type	Aggregate Type	a	b	c
Type C	Brownlee	0.764	0.079	0.014
	Brownwood	0.354	0.223	0.093
	Beckman	0.317	0.251	0.054
	Fordyce	0.465	0.171	0.033
	El Paso	0.430	0.201	0.031
	Brownlee-Beckman	0.555	0.119	0.022
PFC	Brownlee	0.817	0.105	0.014
	El Paso	0.619	0.192	0.024
	Beckman	0.370	0.562	0.059
	Brownwood	0.258	0.201	0.129

TABLE 30 Values of the Regression Model Parameters for IFI

Mix Type	Aggregate Type	a	b	c
Type C	Brownlee	0.474	0.061	0.001
	Brownwood	0.212	0.058	0.102
	Beckman	0.213	0.097	0.050
	Fordyce	0.275	0.065	0.038
	El Paso	0.250	0.060	0.023
	Brownlee-Beckman	0.225	0.170	0.003
PFC	Brownlee	0.539	0.048	0.013
	El Paso	0.416	0.101	0.025
	Beckman	0.279	0.288	0.055
	Brownwood	0.221	0.117	0.155

The polishing rate (corresponding to the “c” parameter) is an important factor for the evaluation of pavement frictional properties. The lower the “c” value, the more resistant the specimen is to polishing. The other important parameter of the model is the “a” value, equivalent to the terminal friction value for either DF_{20} or IFI. A high “a” value corresponds to high pavement terminal friction and indicates a pavement that could better maintain its frictional properties.

Figures 69 through 74 depict the values shown in Tables 29 and 30 and indicate that the variation of both IFI and DF_{20} are consistent. In both cases, the Brownlee aggregate has the highest terminal and initial values, and the Beckman and Brownwood aggregates have the lowest values. Figures 69 through 74 also indicate that normally PFC mixes have higher IFI terminal and initial values than Type C mixes do. The rate of IFI change in Beckman and Brownwood aggregates is greater than for other types of aggregates, which shows that limestone aggregates are not able to maintain their initial frictional properties against polishing action.

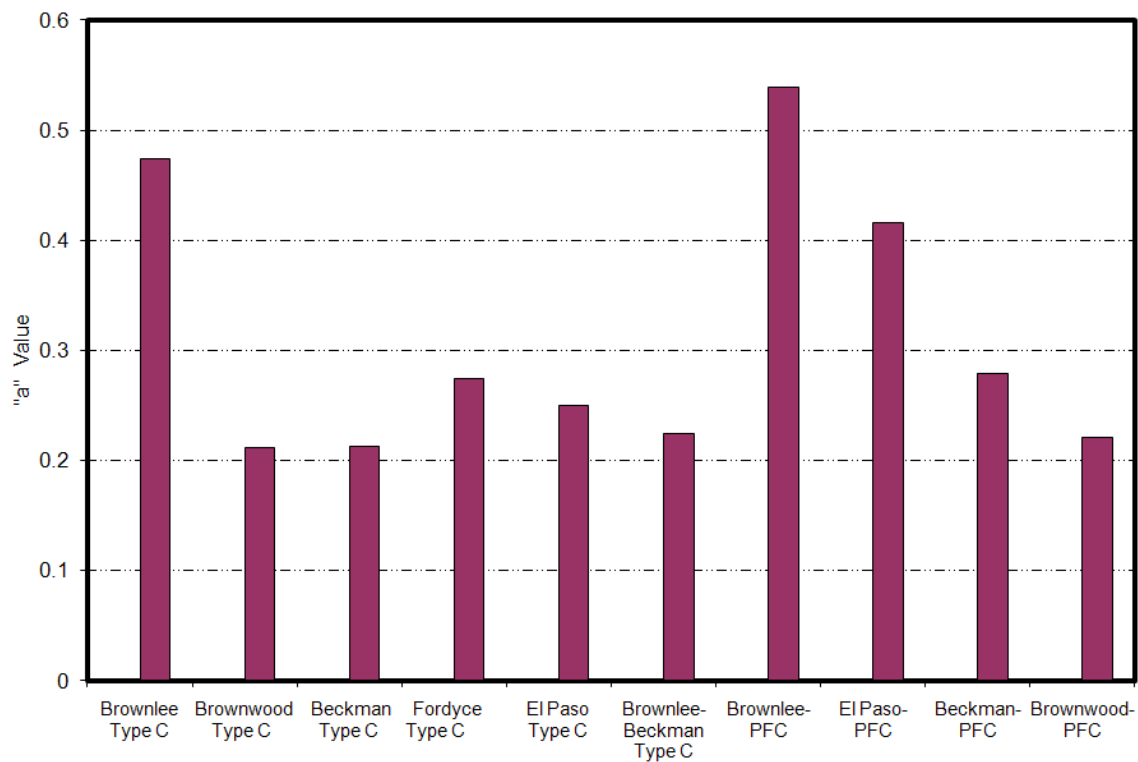


FIGURE 69 Terminal IFI values for different aggregate types.

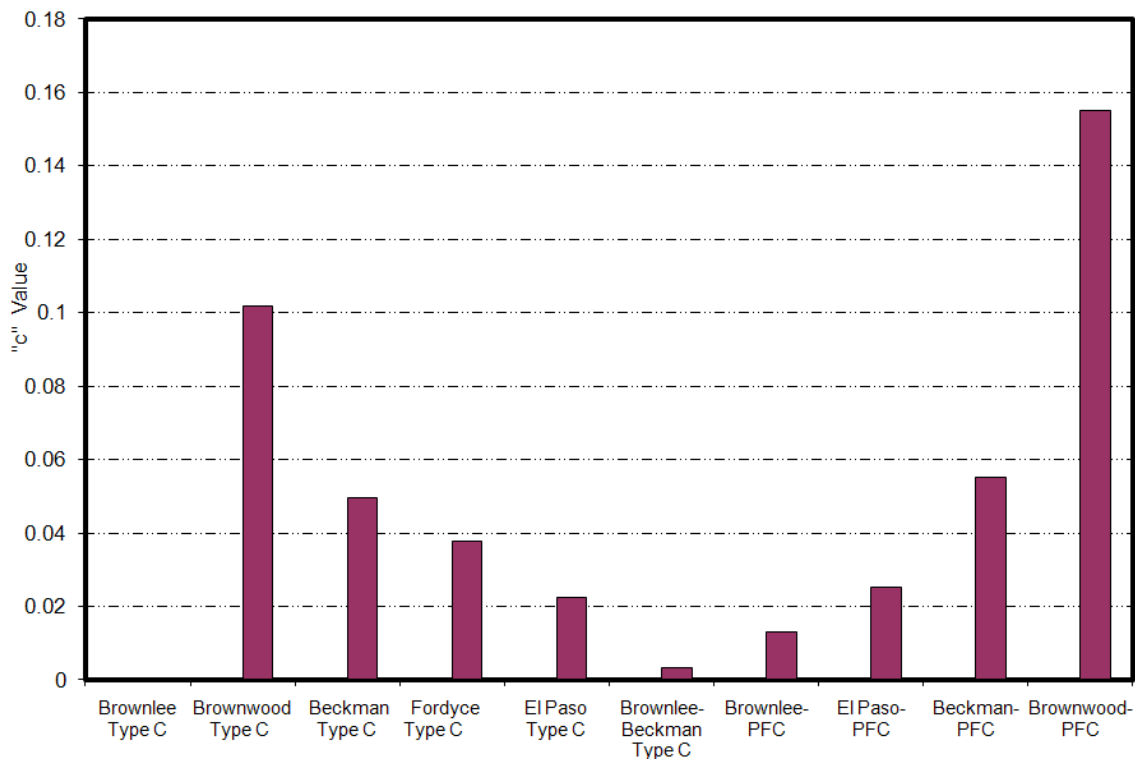


FIGURE 70 Rate of IFI change for different aggregate types.

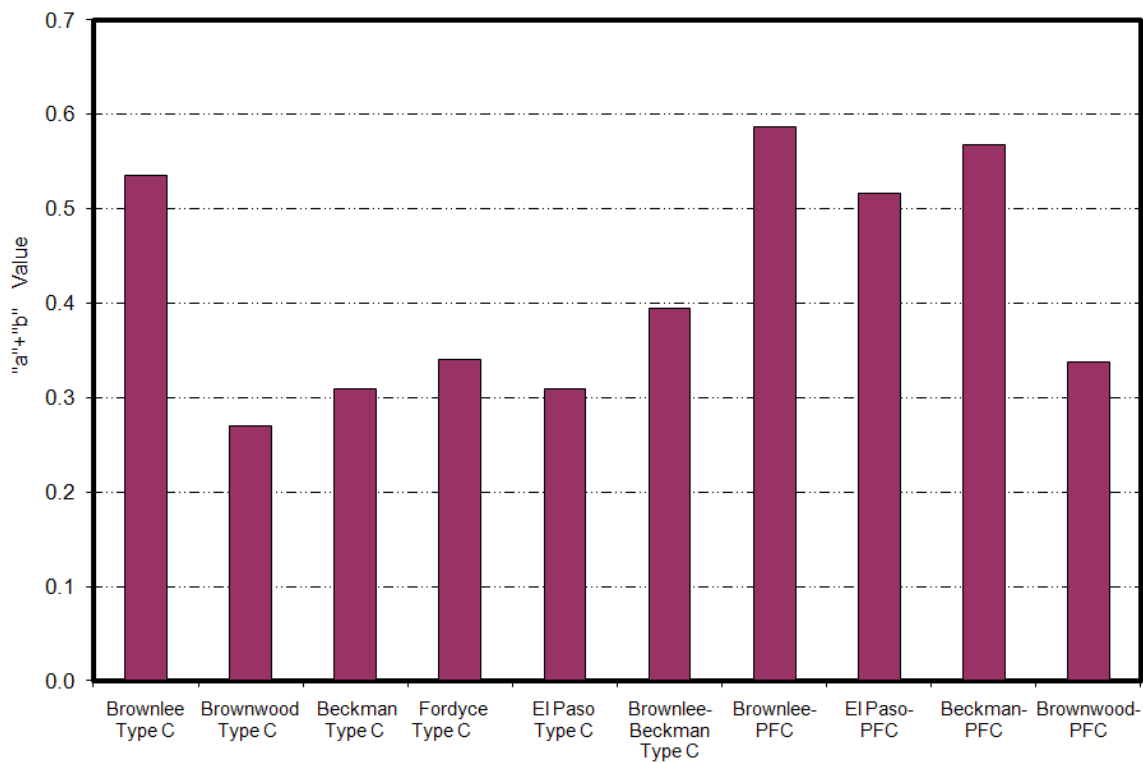


FIGURE 71 Initial IFI values for different aggregate types.

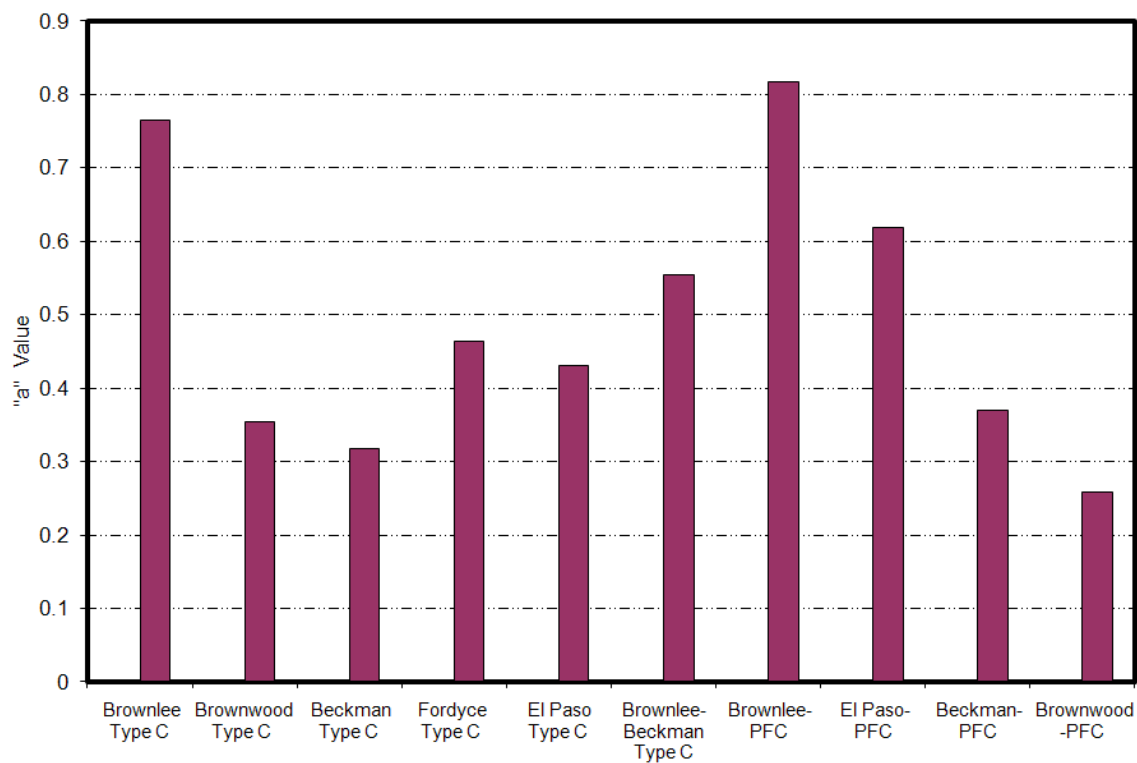


FIGURE 72 Terminal DF_{20} values for different aggregate types.

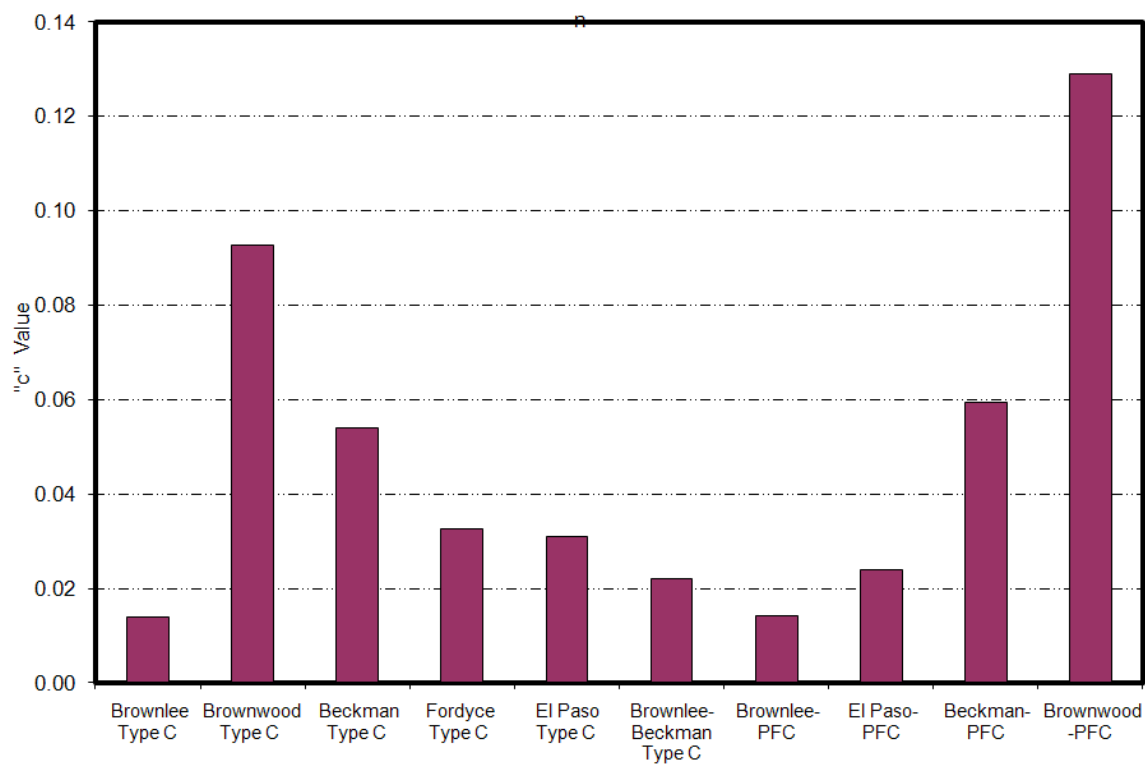


FIGURE 73 Rate of DF_{20} change for different aggregate types.

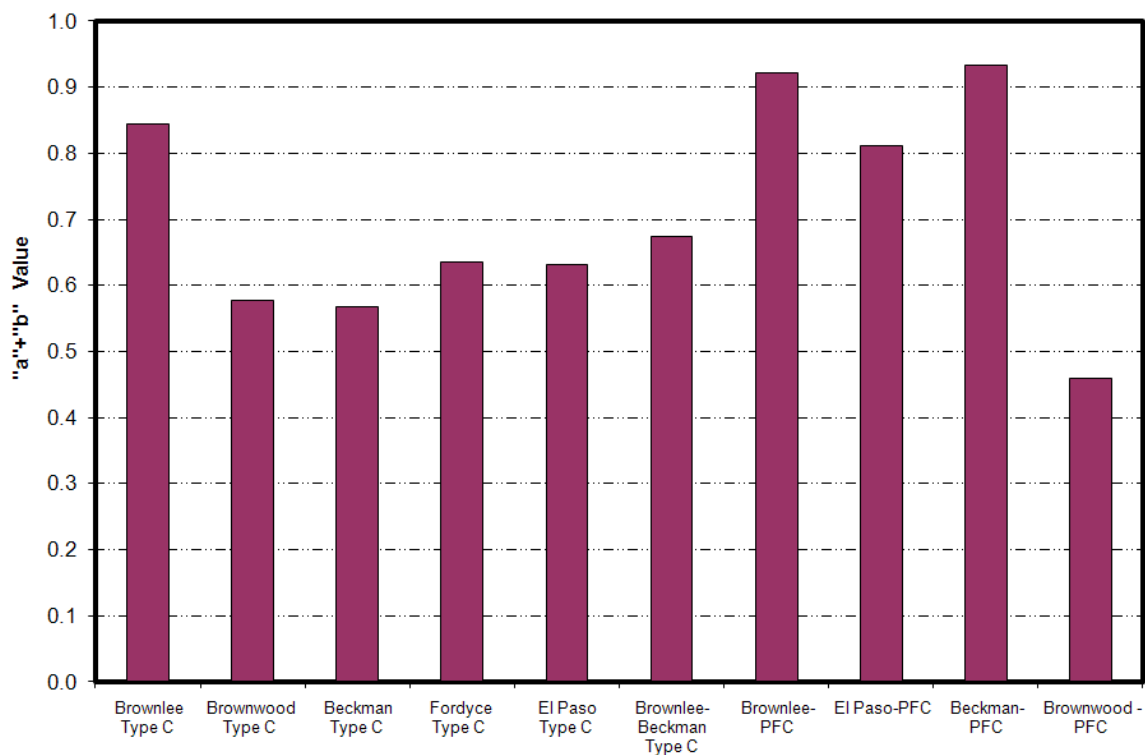


FIGURE 74 Initial DF_{20} values for different aggregate types.

In subsequent sections, the influence of different aggregate properties on the frictional properties of different mixes is discussed. Two parameters of the proposed model, the polishing rate (“c” value) and the terminal friction value IFI (“a” value), were selected as a measure of surface frictional properties. These two values were used to compare the influence of the aggregate properties on the skid resistance characteristics. A statistical correlation analysis was performed to evaluate the correlation between these two parameters and other aggregate properties.

In this analysis, two important statistical parameters were estimated, i.e., coefficient of correlation (R-value) and significance of correlation (p-value). The former is an indication of a linear relationship among variables, and the latter is determined from the hypothesis testing that the chosen independent variable is significant. A low p-value below the significance level— $\alpha=0.05$ was used in this study—indicates that the chosen variable is important in explaining the behavior of the dependent variable. Furthermore, this parameter shows if there is any significant statistical correlation between parameters.

Hence, different aggregate characteristics discussed in previous chapters were considered as the main aggregate characteristics affecting the frictional characteristics. To explain the effect of each aggregate's properties, a linear regression analysis was done, and the significance of the regression coefficients was studied. Tables 31 and 32 summarize the regression coefficients and the results of the statistical test on the significance of the regression parameters for Type C and PFC mixes.

TABLE 31 Results of Regression Analysis on Type C Mix

Mixture Frictional Characteristics	Aggregate Properties									
	LA % Wt Loss		Mg. Soundness		Polish Stone Value		MD % Wt. Loss		Acid Insolubility	
	R ²	p-value	R ²	p-value	R ²	p-value	R ²	p-value	R ²	p-value
DF ₂₀ Change	0.01	0.45	0.09	0.28	0.67	0.02	0.01	0.45	0.43	0.08
DF ₂₀ Terminal	0.14	0.23	0.01	0.43	0.90	0.00	0.00	0.50	0.38	0.09
IFI Change	0.00	0.45	0.09	0.28	0.68	0.02	0.05	0.33	0.27	0.14
IFI Terminal	0.16	0.22	0.01	0.43	0.70	0.02	0.01	0.44	0.35	0.11

Mixture Frictional Characteristics	Aggregate Properties							
	Texture Change BMD and AMD		Angularity Change BMD and AMD		Texture AMD		Angularity AMD	
	R ²	p-value	R ²	p-value	R ²	p-value	R ²	p-value
DF ₂₀ Change	0.73	0.01	0.35	0.11	0.38	0.10	0.10	0.27
DF ₂₀ Terminal	0.69	0.02	0.84	0.01	0.62	0.03	0.00	0.46
IFI Change	0.64	0.03	0.32	0.12	0.37	0.10	0.02	0.39
IFI Terminal	0.44	0.08	0.64	0.03	0.53	0.05	0.01	0.43

Note: BMD = Before Micro-Deval; AMD = After Micro-Deval.

TABLE 32 Results of Regression Analysis on PFC Mix

Mixture Frictional Characteristics	Aggregate Properties									
	LA % Wt Loss		Mg. Soundness		Polish Stone Value		MD % Wt. Loss		Acid Insolubility	
	R ²	p-value	R ²	p-value	R ²	p-value	R ²	p-value	R ²	p-value
DF ₂₀ Change	0.05	0.39	0.43	0.17	0.55	0.13	0.07	0.32	0.63	0.10
DF ₂₀ Terminal	0.05	0.39	0.09	0.35	0.81	0.05	0.00	0.48	0.96	0.01
IFI Change	0.09	0.35	0.53	0.13	0.51	0.14	0.13	0.32	0.54	0.13
IFI Terminal	0.09	0.35	0.08	0.36	0.83	0.04	0.00	0.48	0.97	0.01

Mixture Frictional Characteristics	Aggregate Properties							
	Texture Change BMD and AMD		Angularity Change BMD and AMD		Texture AMD		Angularity AMD	
	R ²	p-value	R ²	p-value	R ²	p-value	R ²	p-value
DF ₂₀ Change	0.61	0.11	0.10	0.34	0.42	0.18	0.35	0.20
DF ₂₀ Terminal	0.91	0.02	0.39	0.19	0.77	0.06	0.32	0.22
IFI Change	0.50	0.15	0.08	0.36	0.32	0.22	0.28	0.24
IFI Terminal	0.91	0.02	0.42	0.18	0.77	0.06	0.30	0.23

Tables 31 and 32 show a variety of aggregate properties assumed to have some effects on the measured friction of different surfaces. These properties include:

- LA abrasion weight loss,
- magnesium soundness test value,
- polish stone value,
- Micro-Deval weight loss,
- coarse aggregate acid insolubility,
- terminal texture measured by AIMS after Micro-Deval,
- terminal angularity measured by AIMS after Micro-Deval,
- change in texture before and after Micro-Deval measured by AIMS, and
- change in angularity before and after Micro-Deval measured by AIMS.

These tables show that the LA abrasion value could explain less than 20 percent variation in DF₂₀ and IFI change, and the coefficient of regression is not significant at the 95 percent confidence level. Therefore, the LA abrasion weight loss does not seem to be a significant factor in pavement skid resistance analysis. The same result could be

concluded for magnesium sulfate soundness value, Micro-Deval weight loss, and terminal angularity after Micro-Deval. Moreover, R-squared values for both Type C and PFC mixes are very low, and the p-value is higher than 0.05. The coarse aggregate acid insolubility value is likely to be an important factor in both IFI and DF_{20} terminal values and rate of change, although the R-squared values are not high in Type C mixes. The low R-squared value might be a result of data outliers. Further analysis was performed to investigate the effect of the coarse aggregate insolubility value without considering outliers. The results are discussed subsequently.

The results of the analysis show that British pendulum is a significant factor at a 95 percent confidence level. The R-square values are about 0.6 for rate of change in both Type C and PFC mixes and 0.8 for terminal values. This indicates that the BP value affects more on terminal IFI and DF_{20} values. Moreover, the results of the analysis show that the IFI and DF_{20} terminal values increase and IFI and DF_{20} rates of change decrease when the British pendulum value increases.

Change in texture before and after Micro-Deval and the texture after Micro-Deval are significant factors in terminal DF_{20} and IFI values and rates of change. Moreover, change in texture before and after Micro-Deval accounts for 73 and 64 percent change in DF_{20} and IFI variation, respectively, and is significant in Type C mixes. Texture change before and after Micro-Deval accounts for a 91 percent change in DF_{20} and IFI terminal values and is significant in PFC mixes. It is evident that the texture change has more influence on DF_{20} than IFI. This, in part, can be justified by the contribution of macrotexture in calculating the IFI value that makes the IFI change less dependent on microtexture than DF_{20} . Measured texture after Micro-Deval defines 62 and 53 percent change in DF_{20} and IFI terminal values, respectively, and is statistically significant in Type C mixes. In PFC mixes, the terminal texture value after the Micro-Deval test is responsible for 77 percent change in DF_{20} and IFI terminal values and is significant. As a general trend, an increase in terminal texture will result in an increase in DF_{20} and IFI terminal values and a decrease in DF_{20} and IFI rates of change. The same effect could be seen in texture change before and after Micro-Deval. Increase in texture change before and after Micro-Deval decreases the terminal value of DF_{20} and IFI and increases their rates of change.

Change in angularity before and after Micro-Deval affects the terminal DF_{20} and IFI values. When the angularity change before and after Micro-Deval increases, the terminal IFI and DF_{20} values increase.

Because the Brownlee aggregate had very high microtexture that might affect the results of the analysis, the mixes containing Brownlee aggregate were removed from the database and another analysis was performed. TABLE 33 summarizes the estimated R-squared values and significance level of considered parameters in the analysis.

TABLE 33 R-Squared Values and Significant Level for Type C Mix

Mixture Frictional Characteristics	Aggregate properties					
	LA % Wt Loss		Mg. Soundness		MD % Wt. Loss	
	R ²	p-value	R ²	p-value	R ²	p-value
IFI Change	0.05	0.36	0.19	0.23	0.04	0.37
IFI Terminal	0.36	0.14	0.31	0.16	0.59	0.06

Mixture Frictional Characteristics	Aggregate properties					
	Acid Insolubility		Texture Change BMD and AMD		Angularity AMD	
	R ²	p-value	R ²	p-value	R ²	p-value
IFI Change	0.17	0.24	0.55	0.08	0.06	0.34
IFI Terminal	0.83	0.02	0.59	0.06	0.97	0.00

This analysis revealed that LA weight loss and magnesium soundness values are not statistically significant in predicting the DF_{20} and IFI terminal values and rates of change. However, the coarse aggregate insolubility value is a significant factor on the terminal IFI value and could explain the 83 percent change in IFI. This analysis further showed that angularity after Micro-Deval is also a statistically significant factor on explaining the IFI terminal values. Moreover, the terminal IFI value increases when angularity after Micro-Deval increases. Similarly, an increase in coarse aggregate acid insoluble value increases terminal IFI value.

AGGREGATE RANKING BASED ON LABORATORY RESULTS

Selection of an aggregate type based on its frictional properties is an important step toward constructing a safe pavement with adequate skid resistance. A ranking system according to frictional properties will assist the selection of the most appropriate aggregate. The frictional properties of each aggregate type could be assessed by using a friction-polish cycle curve. An ANOVA was done to study the effect of mix type and aggregate on the measured F60. It was demonstrated that the difference between the measured IFI values of Type C and PFC mixes is significant. Moreover, any aggregate classification system that tends to classify aggregates should consider the mix type as an important factor.

FIGURE 75 shows the terminal IFI values of different aggregates for different mixes. The Brownlee aggregate had superior frictional performance in both Type C and PFC mixes. The results of the ANOVA in the previous section showed that there is a significant difference between measured IFI values of the Brownlee aggregate and those of other aggregates. This result is in agreement with the result of the TxDOT aggregate classification that considers Brownlee aggregate in class A. The next aggregate in the list is the El Paso aggregate that has been used in PFC mixes. This aggregate, however, does not have high terminal friction in Type C mixes. The El Paso aggregate in the PFC mix also had significant differences with all other aggregates and was the third in the list.

Mixing 50 percent Brownlee aggregate with 50 percent Beckman aggregate gives the blend superior frictional properties. Although the blend is classified as class B based on the current classification system, the frictional properties of the blend are significantly better than the Fordyce aggregate and the El Paso aggregate in Type C mixes.

The Beckman aggregate shows relatively good frictional properties in PFC mixes. This aggregate has a high amount of carbonate material that abraded quickly from the surface of the aggregate, filled the pores of PFC mixture in the laboratory experiment, and improved the skid resistance of the mix. This effect, however, could lead to a decrease in permeability.

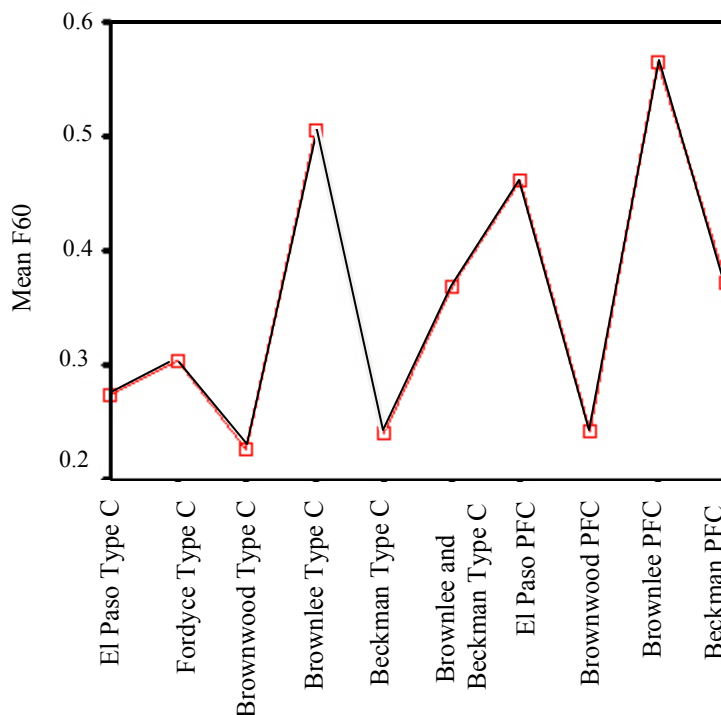


FIGURE 75 Mean IFI values for different aggregate types.

Although the Fordyce aggregate is the next in the group and has slightly better frictional properties than the El Paso aggregate, the difference is not statistically significant. The El Paso aggregate showed better frictional characteristics than Beckman and Brownwood aggregates.

Using the Brownwood aggregate in the PFC mix gives the mix slightly better frictional performance than in the Type C. No significant differences were observed in frictional properties of the Beckman and Brownwood aggregates.

SUMMARY

Several asphalt mix slabs were prepared and compacted in the laboratory, and their frictional properties were measured using the sand patch method, British pendulum test, dynamic friction test, and circular texture meter. The results of each test are summarized in this section.

Sand Patch Test

The sand patch test was performed on Type C and Type D mixes only. Comparing the mean MTD values of these two mixes before polishing showed that the average MTD values of Type C mixes were greater than those of Type D mixes. This is attributed to the larger maximum aggregate size in the Type C mix.

Although it seemed as if the MTD values of almost all mixes (except for sandstone) after polishing were less than the MTD values before polishing, statistical analysis did not show any significant differences between MTD values before and after polishing. Hence, it was concluded that the sand patch test was not able to detect changes in macrotexture due to polishing with the selected polishing device. The results showed that mixes with different aggregates had different MTD values. Thus, a pairwise comparison analysis was performed among mixtures with different aggregates to find the differences between MTD values of different aggregate types. The results showed that Brownlee aggregate had the highest MTD values among all aggregates, and both Beckman and Brownwood aggregates produced the lowest MTD values.

British Pendulum Test

The British pendulum test was performed on three different locations on each slab, and three measurements were conducted on each location. The TxDOT test requires using a 3-inch slider in the BP. However, it was not feasible to use this size because of the limited polished area resulting from the polishing machine used in this study. As a result, a 1.5-inch-wide rubber slider was used in all BP measurements.

The results indicated that BP values decreased with an increase in polishing cycles for all mixtures except mixtures containing Brownlee aggregate. For Brownlee aggregate, the BP values remained almost constant.

The BP values of PFC mixes were generally higher than those for Type C mixes. In addition, the frictional characteristics of some aggregates varied depending on the mix in which the aggregate was used. For example, the PFC and Type C mixes with Brownwood aggregate had similar BP values at a low number of polishing cycles.

However, the PFC mixes with Brownwood aggregate had higher BP values than corresponding Type C mixes at a high number of polishing cycles.

An analysis was performed to compare the results of measured BP values for each aggregate type. The results of the comparison among same mixtures with different aggregate types did not reveal any significant differences. Consequently, it was concluded that the British pendulum test was not able to detect the difference between frictional performances of aggregates with known differences in frictional characteristics.

CTMeter and DFT Tests

The CTMeter and DFT tests were performed at three different locations on each slab. The DFT was performed twice in each location, while the CTMeter was conducted six times at each location. No particular trend was observed for MPD values from the CTMeter of different mixes in terms of number of polishing cycles.

The result of dynamic friction testing at 20 km/h (DF_{20}) is an indication of microtexture (15). Therefore, this measure is a good indication of the aggregate contribution to pavement skid properties. A plot of measured dynamic friction in terms of polishing cycles showed that DF_{20} decreased as polishing cycles increased. The DF_{20} curves leveled off and reached a terminal value after a certain number of polishing cycles.

Statistical analysis was performed to evaluate the effect of several variables (i.e., aggregate type, mix type, polishing cycles, and speed) on the measured dynamic friction. The results showed that aggregate type affected the magnitude of dynamic friction in both Type C and PFC mixes. The results also showed that there was a significant difference in the measured friction at different numbers of polishing cycles for Type C mixes. In contrast, the magnitude of dynamic friction in PFC mixes did not have a significant difference between polishing cycles. The results also revealed that the PFC mix had a higher friction value than the Type C mix.

The equation proposed by Mahmoud (see Equation 9) was fitted to the calculated F60 values. The rate of change and terminal value of friction were estimated from this equation. Comparing the rate of change and terminal values for different aggregates

revealed that in all cases, the Brownlee aggregate had the highest terminal values and lowest rate of change in both Type C and PFC mixes. In contrast, mixes containing Beckman and Brownwood aggregates had the lowest terminal values and highest rates of change. This indicated that Beckman and Brownwood aggregates failed to preserve their frictional performance during load application. A combination of Brownlee and Beckman aggregates, however, performed satisfactorily and had a high terminal value and low rate of change compared to the Beckman aggregate. Fordyce and El Paso aggregates were almost the same and had fair frictional properties.

The dependency of terminal value and rate of change of DF_{20} and IFI on different aggregate characteristics was analyzed. The aggregate characteristics included in the analysis were LA impact and abrasion percent weight loss, magnesium soundness percent weight loss, British pendulum value, Micro-Deval percent weight loss, coarse aggregate acid insolubility, texture measurements after Micro-Deval by AIMS, angularity measurements after Micro-Deval by AIMS, change in texture before and after Micro-Deval, and change in angularity before and after Micro-Deval. The coefficient of determination (R-square) and the statistical significance were evaluated to study if the considered variable is important and at what percent it could define the variability of DF_{20} and IFI.

The results indicated that the LA impact and abrasion percent weight loss, magnesium soundness percent weight loss, Micro-Deval percent weight loss, angularity measurements after Micro-Deval by AIMS, and change in angularity before and after Micro-Deval were not significant factors in determining DF_{20} and IFI rates of change and terminal values.

The BP value, texture measured using AIMS after Micro-Deval, and change in texture before and after Micro-Deval were proved to be significant factors in explaining the rates of change and terminal values of DF_{20} and IFI. Furthermore, the rates of change of DF_{20} and IFI decreased as the BP value and texture after Micro-Deval increased. In addition, the terminal value of DF_{20} and IFI increased as the BP value and texture after Micro-Deval increased. The rate of change in texture before and after Micro-Deval affected the rates of change and terminal values of DF_{20} and IFI. The results showed that the rates of change in DF_{20} and IFI decreased and the terminal values increased as the rate

of change in texture before and after Micro-Deval decreased. The coarse aggregate acid insolubility test showed a significant effect on rates of change and terminal values of DF_{20} and IFI only when Brownlee aggregate was removed from the comparison. In such a case, the terminal DF_{20} and IFI increased as the acid insolubility test value increased. A change in angularity before and after Micro-Deval affected the terminal DF_{20} and IFI values. When the angularity change before and after Micro-Deval increased, the terminal IFI and DF_{20} values increased.

In summary, the results of the research indicated that it is possible to control and predict frictional properties of the pavement by selecting the aggregate type and HMA mix type. A new laboratory testing methodology to evaluate the key parameters in frictional characteristics of a flexible pavement was developed. These two key parameters were defined to be the rate of change in friction and terminal value for friction. These two values could be used as a basis for further comparisons between frictional performance of different aggregate types.

During this study, a complete set of experiments was performed to evaluate the aggregate properties by all current testing methods. The results of this research confirmed the findings of the previous research about the superior performance of the Brownlee aggregate. The results also showed the polishing susceptibility of Beckman and Brownwood aggregates.

The influence of aggregate type on asphalt concrete skid properties was investigated through preparing and testing laboratory slabs. The results of the analysis confirmed the strong relationship between mix frictional properties and aggregate properties. The main aggregate properties affecting the mix skid resistance were recognized to be British pendulum value, texture change before and after Micro-Deval measured by AIMS, terminal texture after Micro-Deval measured by AIMS, and coarse aggregate acid insolubility value.

Based on the findings, a model that is able to predict initial IFI, terminal IFI, and rate of polishing was developed using the parameters in the texture model developed by Mahmoud (see Equation 9). This model confirmed the benefits of texture measurements by AIMS, and it will help to predict mix friction based on gradation and aggregate resistance to polishing. Furthermore, this model facilitates selecting the appropriate

aggregate type for the desired mixture friction, and it could be used to classify aggregates based on their frictional properties. The next chapter explains the steps taken to develop the pavement prediction model.

CHAPTER V
A MODEL FOR ASPHALT MIX SURFACE FRICTION BASED ON
LABORATORY RESULTS

INTRODUCTION

This chapter presents a new model that expresses the IFI as a function of aggregate resistance to polishing and mix gradation. The concept of the model, as shown in FIGURE 76, incorporates aggregate shape characteristics measured by AIMS, mix design gradation, and polishing cycles in an equation that gives the IFI.

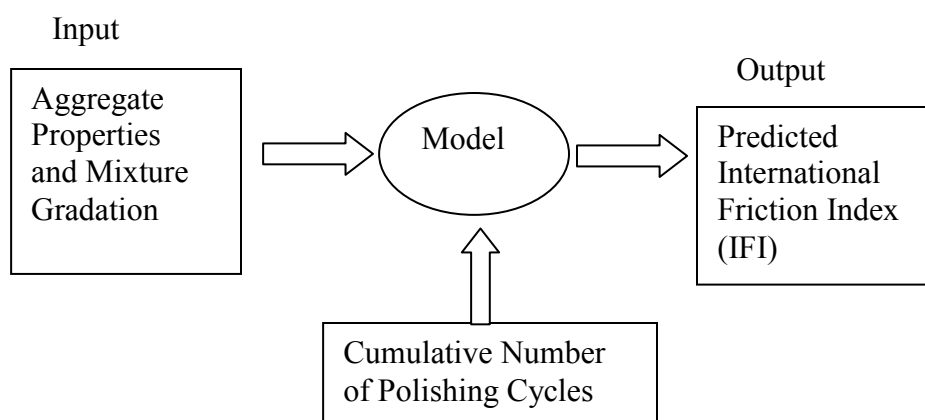


FIGURE 76 Overview of the friction model.

The friction model shown in FIGURE 76 consists of a set of equations that can predict IFI value at any given polishing cycle. Moreover, this model should predict three important parameters—initial IFI level (“a” + “b”), rate of change in IFI “c,” and terminal IFI value “a.”

MODELING APPROACH

The previous chapter showed that mixture type in terms of aggregate gradation has a significant effect on IFI parameters. To consider the aggregate gradation as a parameter in the friction model, a cumulative two-parameter Weibull distribution was used to fit the standard aggregate size distribution data (cumulative percent passing size). The cumulative two-parameter Weibull distribution has the form of:

$$F(x; k, \lambda) = 1 - e^{-\left(\frac{x}{\lambda}\right)^k} \quad (10)$$

where x is the variable (aggregate size in millimeter), and k and λ are model parameters known as shape and scale parameters, respectively. Figures 77 through 86 show the aggregate gradation and fitted line for different mixes.

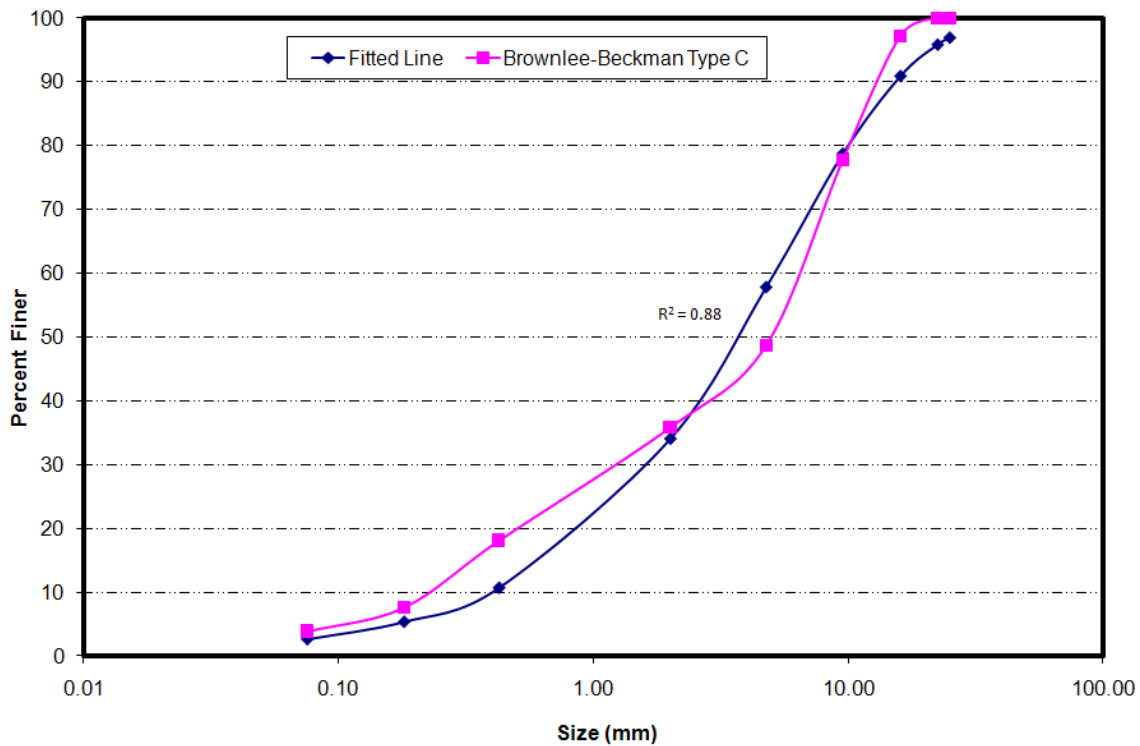


FIGURE 77 Aggregate gradation and fitted line for Brownlee-Beckman Type C mix.

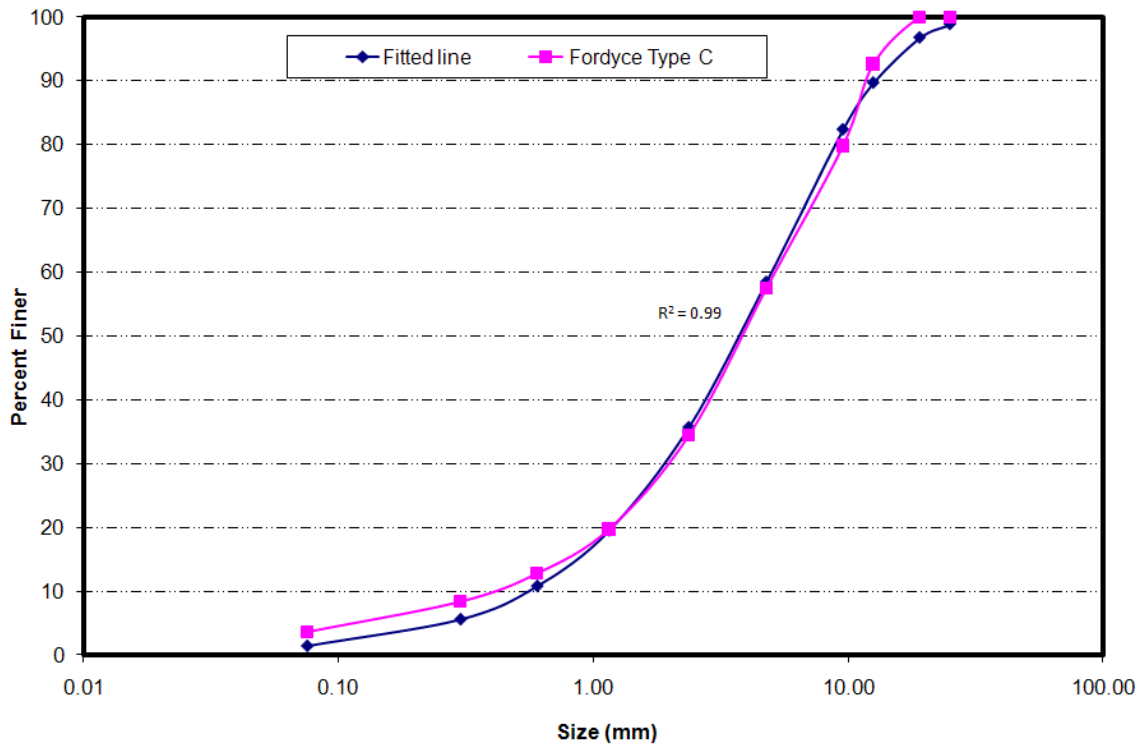


FIGURE 78 Aggregate gradation and fitted line for Fordyce aggregate Type C mix.

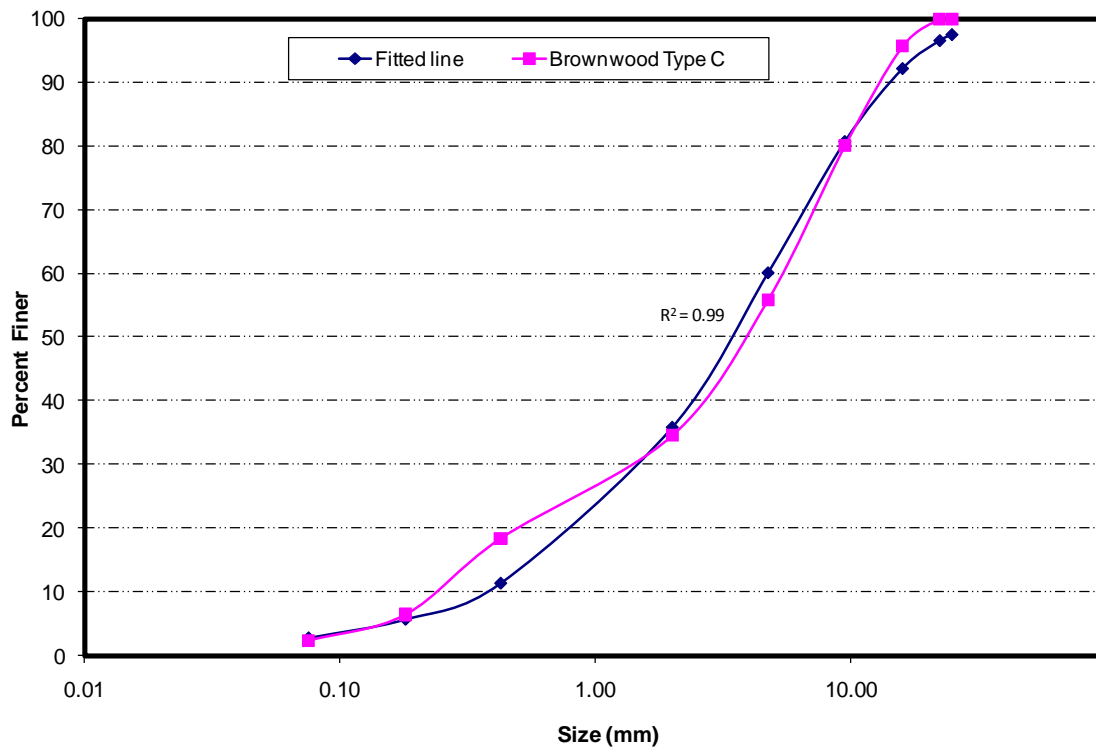


FIGURE 79 Aggregate gradation and fitted line for Brownwood aggregate Type C mix.

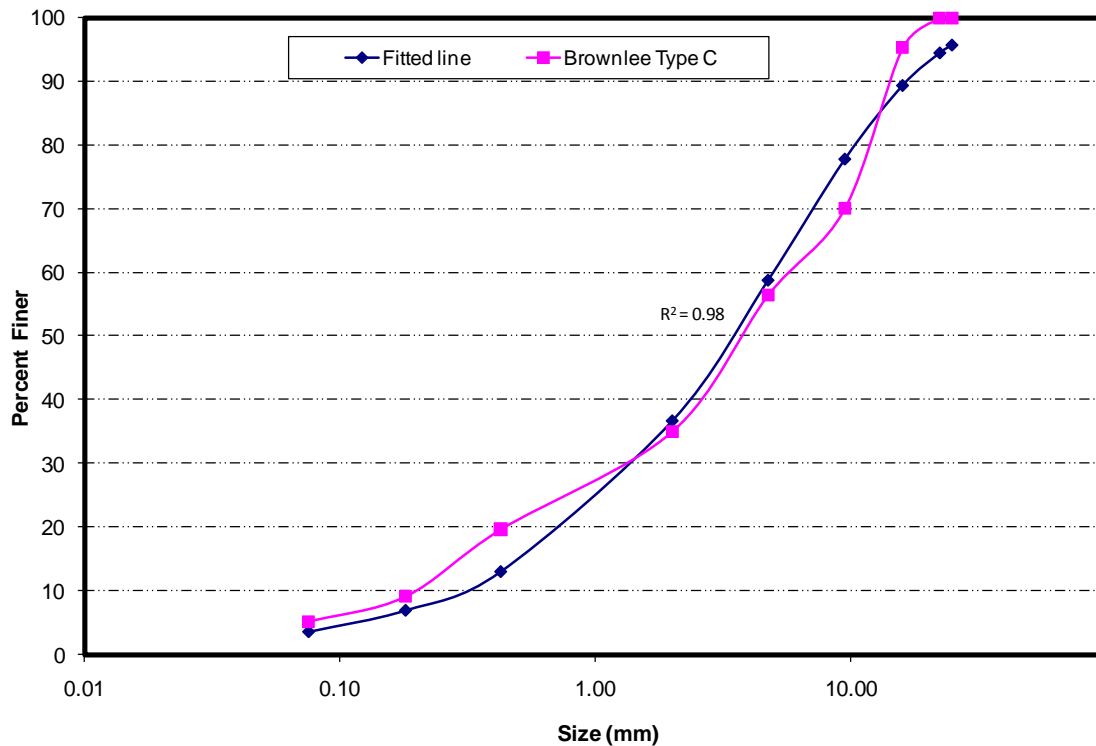


FIGURE 80 Aggregate gradation and fitted line for Brownlee aggregate Type C mix.

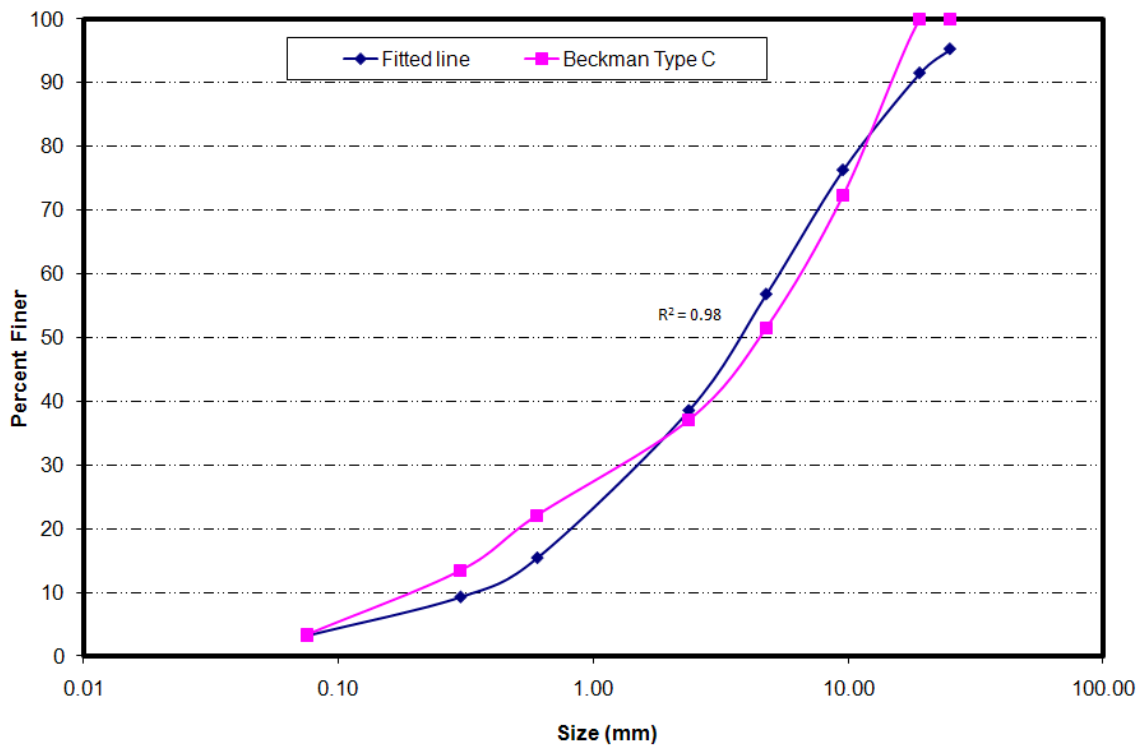


FIGURE 81 Aggregate gradation and fitted line for Beckman aggregate Type C mix.

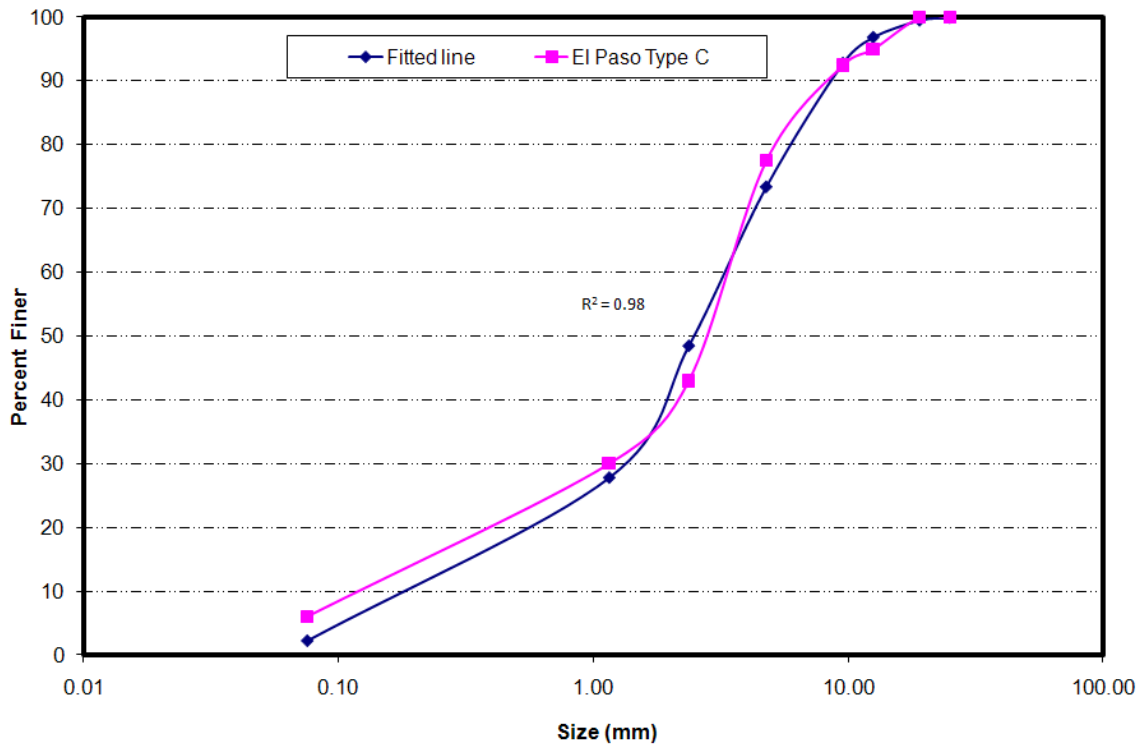


FIGURE 82 Aggregate gradation and fitted line for El Paso aggregate Type C mix.

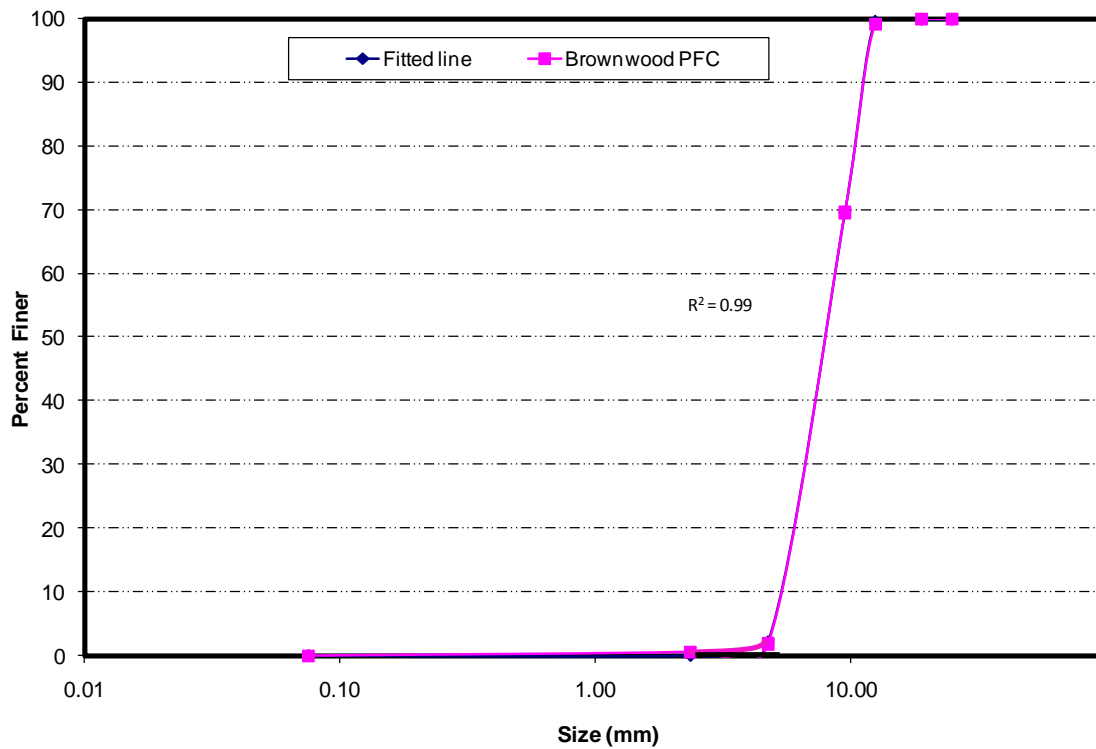


FIGURE 83 Aggregate gradation and fitted line for Brownwood aggregate PFC mix.

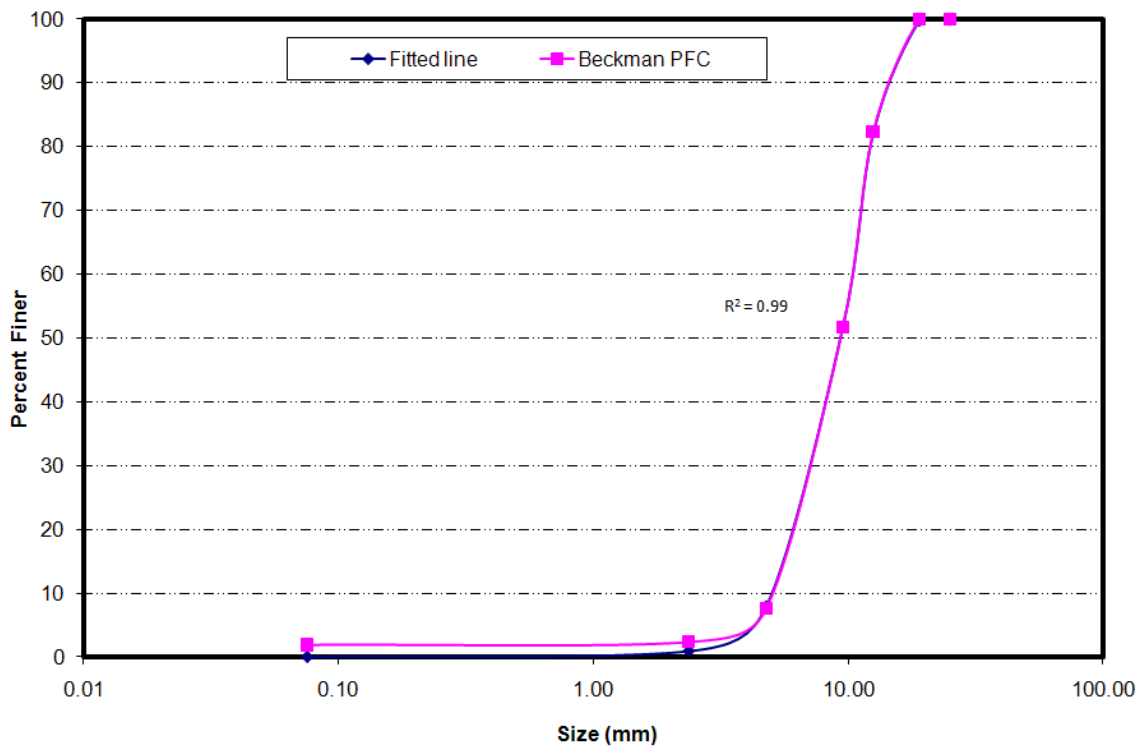


FIGURE 84 Aggregate gradation and fitted line for Beckman aggregate PFC mix.

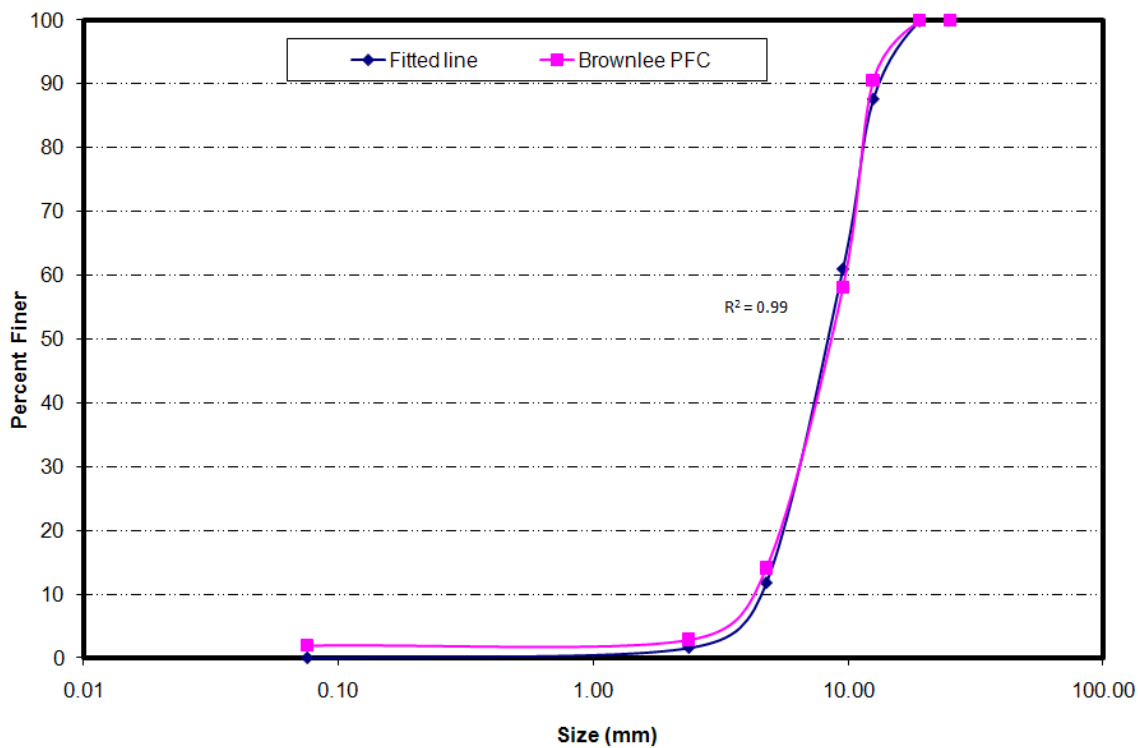


FIGURE 85 Aggregate gradation and fitted line for Brownlee aggregate PFC mix.

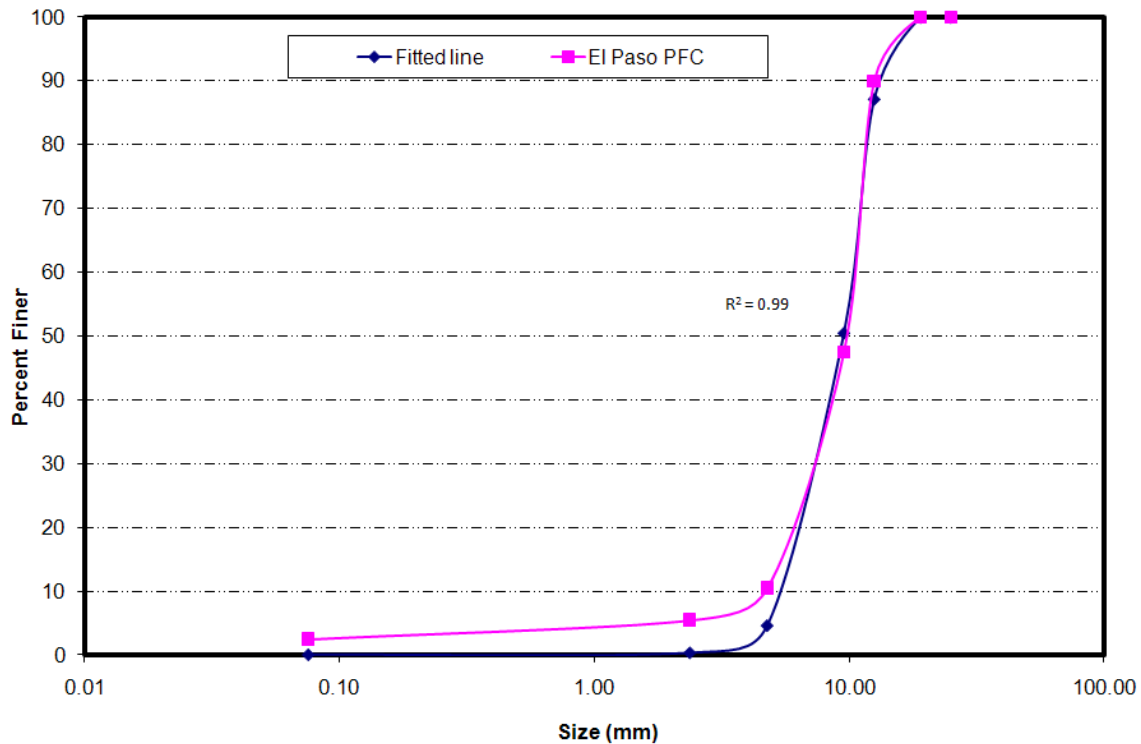


FIGURE 86 Aggregate gradation and fitted line for El Paso aggregate PFC mix.

TABLE 34 summarizes the calculated k and λ value for each mix. These parameters have been calculated using the SSE method.

TABLE 34 Calculated Weibull Parameters for Different Mixes

Aggregate Type	Mix Type	λ	κ
Brownlee-Beckman	Type C	5.653	0.843
Fordyce		5.419	0.983
Brownwood		5.245	0.842
Brownlee		5.554	0.764
Beckman		5.942	0.777
El Paso		3.495	0.863
Brownwood	PFC	9.213	5.755
Beckman		10.503	3.150
Brownlee		9.698	2.909
El Paso		10.399	3.908

The results of the previous chapter showed that AIMS texture indices have a high correlation with rate of change and terminal values of IFI, and this value could be potentially used in any model explaining the IFI. Selecting other aggregate properties that can be used in the model should be based on a statistical analysis. This analysis will show the minimum number of independent variables that can be used in the model. Any correlation between the independent variables will decrease the reliability of the model. TABLE 35 shows the cross-correlation between different parameters considered to be significant in the model. This table shows that the “a” (terminal value), “c” (rate of change), and “a” + “b” (initial value) parameters of the aggregate texture model have high correlation with polish value, texture after Micro-Deval, texture change before and after Micro-Deval, and coarse aggregate acid insolubility. This analysis shows that developing a model that includes parameters of the aggregate texture model proposed by Mahmoud (137) along with aggregate gradation parameters could satisfactorily explain the variation of IFI for different mixtures without any redundancy and cross-correlation.

TABLE 35 Correlation Coefficients for Different Aggregate Properties

Parameter	(1)	(2)	(3)	(4)	(5)	(6)	(7)	(8)	(9)	(10)	(11)	(12)
(1)		85.5%	-27.2%	82.4%	-77.4%	-77.4%	-62.5%	-19.2%	-63.7%	-16.0%	-27.4%	-4.3%
(2)	85.5%		24.4%	95.4%	-48.0%	12.6%	-14.3%	1.1%	-68.1%	-7.4%	-14.7%	-47.9%
(3)	-27.2%	24.4%		14.9%	62.3%	62.3%	90.0%	61.4%	2.8%	42.6%	44.3%	-91.0%
(4)	82.4%	95.4%	14.9%		-62.2%	32.8%	-15.9%	-16.5%	-84.6%	-27.5%	-22.9%	-29.9%
(5)	-77.4%	-48.0%	62.3%	-62.2%		-80.7%	72.9%	44.4%	77.9%	39.9%	27.7%	-48.6%
(6)	-77.4%	12.6%	62.3%	32.8%	-80.7%		-72.6%	-82.1%	-49.4%	-77.8%	-61.6%	73.9%
(7)	-62.5%	-14.3%	90.0%	-15.9%	72.9%	-72.6%		52.5%	15.3%	34.3%	47.0%	-65.1%
(8)	-19.2%	1.1%	61.4%	-16.5%	44.4%	-82.1%	52.5%		16.6%	96.8%	92.3%	-67.3%
(9)	-63.7%	-68.1%	2.8%	-84.6%	77.9%	-49.4%	15.3%	16.6%		27.6%	2.1%	-1.2%
(10)	-16.0%	-7.4%	42.6%	-27.5%	39.9%	-77.8%	34.3%	96.8%	27.6%		88.9%	-53.2%
(11)	-27.4%	-14.7%	44.3%	-22.9%	27.7%	-61.6%	47.0%	92.3%	2.1%	88.9%		-42.1%
(12)	-4.3%	-47.9%	-91.0%	-29.9%	-48.6%	73.9%	-65.1%	-67.3%	-1.2%	-53.2%	-42.1%	

(1) LA weight loss (percent)

(2) magnesium weight loss (percent)

(3) polish stone value

(4) Micro-Deval weight loss (percent)

(5) coarse aggregate acid insolubility

(6) change in texture before and after Micro-Deval

(7) change in angularity before and after Micro-Deval

(8) texture after Micro-Deval

(9) angularity after Micro-Deval

(10) terminal texture for aggregates (a_{agg} value)

(11) initial texture for aggregates ($a_{agg} + b_{agg}$)

(12) rate of texture change for aggregates (c_{agg} value)

A nonlinear regression analysis was performed to determine the coefficients for model parameters. TABLE 36 shows parameter estimates for the model.

TABLE 36 Different Parameter of the Friction Model Estimated by Regression Analysis

Parameter	Model	R ²
Terminal IFI (a_{mix})	$18.422 + \lambda$	0.96
Initial IFI ($a_{mix} + b_{mix}$)	$0.4984 \ln \left(5.656 \times 10^{-4} (a_{agg} + b_{agg}) + 5.846 \times 10^{-2} \lambda - 4.985 \times 10^{-2} k \right) + 0.8619$	0.82
IFI Rate of Change (c_{mix})	$0.765 \cdot e^{\left(\frac{-7.29710^{-2}}{c_{agg}} \right)}$	0.90

where:

AMD = aggregate texture after Micro-Deval,

$a_{agg} + b_{agg}$ = aggregate initial texture using texture model,

c_{agg} = aggregate texture rate of change using texture model,

k-value = Weibull distribution shape factor, and

λ -value = Weibull distribution scale factor.

The developed model for the terminal IFI value is significant at the 95 percent confidence level. This model consists of the aggregate terminal texture value measured after Micro-Deval and λ -value related to mix gradation. It was noted that this model has a high R-square and can account for 96 percent of the variation in terminal IFI.

FIGURE 87 shows the predicted terminal IFI values versus measured terminal IFI values. Based on this model, a higher texture after Micro-Deval will result in a higher terminal value for IFI. Likewise, the mixes with high λ -values—primarily PFC mixes—will have higher terminal IFI values.

TABLE 36 also shows that the initial IFI value depends on the aggregate initial texture value ($a_{agg} + b_{agg}$), which is calculated by fitting a model to a texture and corresponding gradation parameters k-value and λ -value. The model is significant overall and has a high R-square of 0.82. FIGURE 88 depicts the measured and predicted initial IFI values.

The rate of IFI change in TABLE 36 is only dependent upon the rate of texture change in the corresponding aggregate. The model is significant, and the R-square is 0.91. FIGURE 89 shows the predicted and measured rate of IFI change (“c” value).

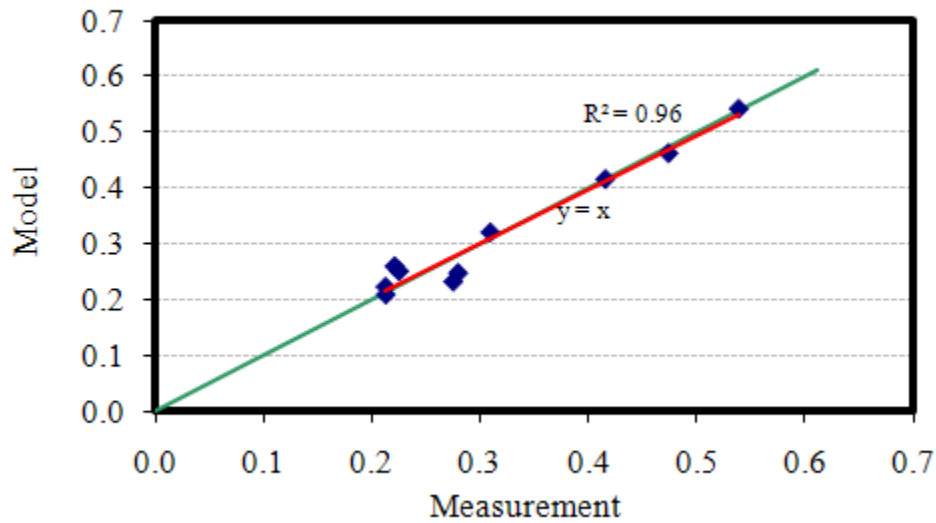


FIGURE 87 Predicted vs. measured terminal IFI values.

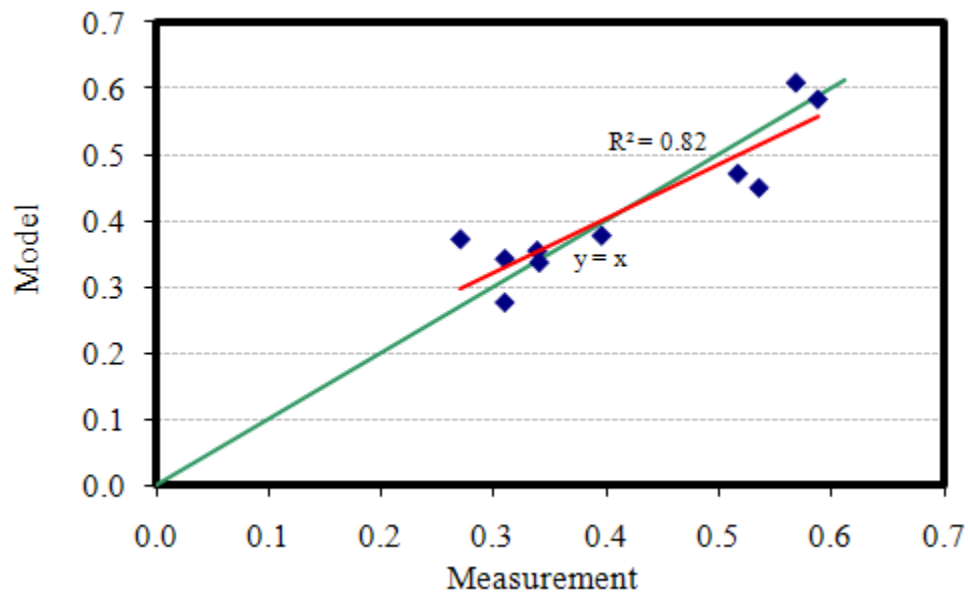


FIGURE 88 Predicted vs. measured initial IFI values.

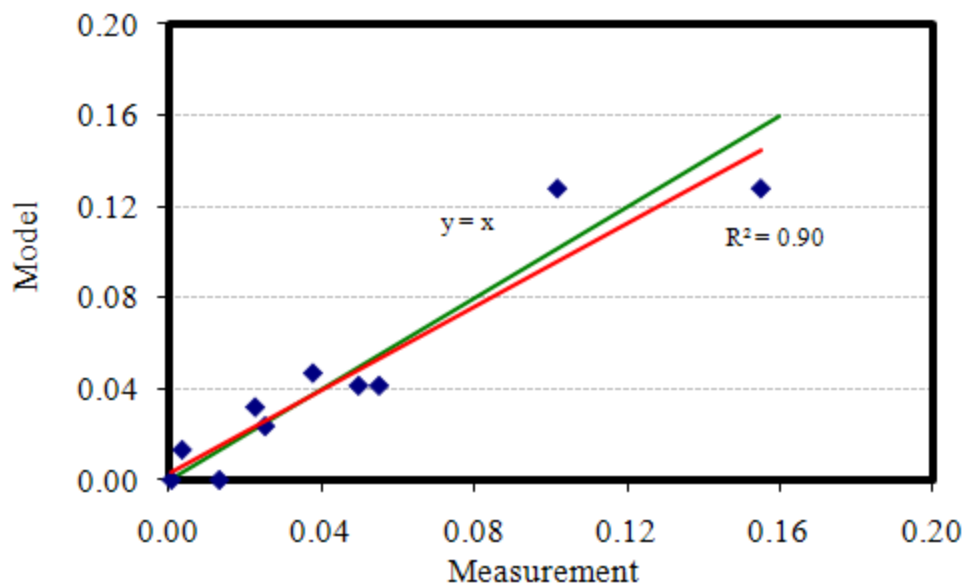


FIGURE 89 Predicted vs. measured IFI rate of change.

The R-square value for each parameter is reasonably high and could be used in the IFI model (Equation 9). Equation 9 could also be rewritten as Equation 11 to include all three parameters discussed above:

$$IFI = (a_{mix} + b_{mix}) \cdot e^{-c_{mix} \cdot n} - a_{mix} \cdot e^{-c_{mix} \cdot N} + a_{mix} \quad (11)$$

where N = polishing cycle in thousands of repetitions.

SUMMARY

The details of the approach to develop the laboratory pavement friction model were described in this chapter. The coefficients of the model previously proposed by Mahmoud (see Equation 9) were used to describe the change in aggregate texture. The two-parameter Weibull cumulative distribution function was used to fit the gradation curves.

Nonlinear regression analysis was performed to express the coefficients of the IFI model as functions of the coefficients of the Weibull cumulative distribution and the coefficients of the aggregate texture model consequently, a model for prediction of IFI as

a function of polishing cycles, mix gradation parameters, and aggregate texture characteristics was developed. Subsequent analysis showed that the developed model does a good job in predicting the rate of change, initial, and terminal values of IFI. The following chapters of this dissertation describe the extension of this model to describe the IFI and Skid Number based on field measurements.

CHAPTER VI

ANALYSIS OF SKID RESISTANCE OF ASPHALT PAVEMENT SECTIONS

INTRODUCTION

The objective of the field measurement phase of this study was to correlate laboratory measurements of the asphalt-mix friction and aggregate resistance to polishing to field skid-resistance measurements. This objective was achieved by developing and completing a comprehensive experiment of measuring skid resistance of field test sections incorporating different surface mixes.

Skid resistance is typically measured using the friction trailer, which is towed at a constant speed over the tested pavement. When the test is initiated, water is sprayed ahead of the tire so the wet pavement friction can be tested. The wheel is fully locked, and the resulting torque is recorded. Based on the measured torque (converted to a horizontal force) and dynamic vertical load on the test wheel, the wet coefficient of friction between the test tire and the pavement surface is calculated. The skid number (SN) is then reported as the coefficient of friction multiplied by 100 (15). The same speed should be maintained before the test and when the wheel is locked. The friction trailer is typically equipped with two types of tires: a rib tire on the right side, according to ASTM E501, and a smooth tire on the left side, according to ASTM E524 (59). Following the recommendation of the ASTM E-274 specification, the test speed (48, 64, or 80 km/h; 30, 40, or 50 mph) and type of tire (R for rib tire and S for smooth tire) should be cited when the skid number is reported (59). For example, SN(64)S indicates that the test was performed at a speed of 64 km/h (40 mph) with the smooth type of tire (SN40S is used if speed is reported in miles per hour). The friction trailer used by TxDOT is equipped with smooth tires and travels at a speed of 80 km/h (50 mph).

Extensive work was conducted in this project to create a database of sections with different friction characteristics. The initial selection of sections was intended to include the mixes and aggregates that were already tested in the laboratory phase of this research

study and to include sections for which the skid performance was available. The experimental design was revised several times to agree on a sound and inclusive experimental design. Moreover, the availability of skid data, availability of traffic data, variety of aggregate lithologies, variety of mix types, and availability of construction and maintenance records were the main factors considered in the selection of sections. The experimental design was then finalized and implemented in the field measurement phase of this project.

Intensive work was performed to collect all the data required in the experimental design. A huge amount of data was studied to choose and extract the most reliable data. Several meetings with TxDOT research groups were held to decide on the desired sections. Because the skid data and construction records of each project are kept in two different databases, a comparative study was done to select the sections with a wide range of construction history and a long record of skid data. Any discrepancies between the data and field observations were thoroughly investigated. TxDOT district offices were contacted to confirm the data integrity and accuracy. Many meetings and conference calls were held with data providers to obtain details about the data collection (e.g., the exact location of the tested field section, date and time, etc.). Afterward, the data were analyzed using statistical analysis methods.

SELECTION OF THE FIELD SECTIONS AND DATA MINING

After all the data was reviewed, 65 roads including 1527 Pavement Management Information System (PMIS) sections that cover a wide range of skid performance were identified. Each PMIS section is a particular stretch of roadway with predefined boundaries defined by reference markers. These sections are distributed across nine TxDOT districts.

TABLE 37 shows the number of sections in each district. The majority of PMIS sections are located within the Corpus Christi, Brownwood, San Antonio, and Yoakum Districts. These 1527 PMIS sections contain 4068 data records including different aggregate types and different mix types in different years. TABLE 38 shows 21 different

aggregate sources in Texas that were used in these sections. These aggregates were classified in different categories according to the TxDOT SAC system.

TABLE 37 Number of Road Sections in Each District

District	Number of Sections
Beaumont	12
Brownwood	285
Bryan	6
Corpus Christi	862
El Paso	46
Houston	116
Lubbock	24
San Antonio	182
Yoakum	148
Total	1527

TABLE 38 Aggregate Sources Used in Pavement Sections

No.	Aggregate	Material Type	TxDOT Classification
1	A	Crushed Siliceous Gravel	SAC A
2	B	Crushed Limestone-Dolomite	SAC B
3	C	Crushed Limestone-Dolomite	SAC B
4	D	Crushed Granite	SAC A
5	E	Crushed Limestone-Dolomite	SAC B
6	F	Crushed Limestone-Dolomite	SAC B
7	G	Crushed Limestone-Dolomite	SAC B
8	H	Sandstone	SAC A
9	I	Crushed Siliceous & Limestone Gravel	SAC A
10	J	Crushed Limestone Rock Asphalt	SAC B
11	K	Crushed Limestone-Dolomite	SAC B
12	L	Lightweight Aggregate	SAC A
13	M	Crushed Limestone-Dolomite	SAC B
14	N	Crushed Limestone-Dolomite	SAC B
15	O	Crushed Traprock	SAC A
16	P	Crushed Traprock	SAC A
17	Q	Crushed Limestone	SAC B
18	R	50 Percent Aggregate H + 50 Percent Aggregate K	SAC B
19	S	Crushed Rhyolite	SAC A
20	T	Crushed Granite	SAC A
21	U	Crushed Limestone	SAC B

Four different mixture designs were used in the selected PMIS sections. These four mixture designs were surface treatment with grade 4 (GR-4) aggregate, surface treatment with grade 3 (GR-3) aggregate, PFC, and Type C mixture design. TABLE 39 shows the number of roads within each mixture group (PFC and Type C are combined in the last column). FIGURE 90 shows the number of road segments with the specified mixture design. Although it is desirable to have a full record of the skid data for several years, some data were missing for some sections. FIGURE 91 shows the data coverage for each district.

TABLE 39 Mixture Types Used in Road Segments

District	Surface Treatment GR-4	Surface Treatment GR-3	Hot Mix Asphalt Concrete (PFC and Type C Mixes)
Beaumont	1		
Brownwood	17	12	
Bryan			1
Corpus Christi	33		2
El Paso			7
Houston	3		5
Lubbock			4
San Antonio	7		14
Yoakum		1	1
Total	61	13	34

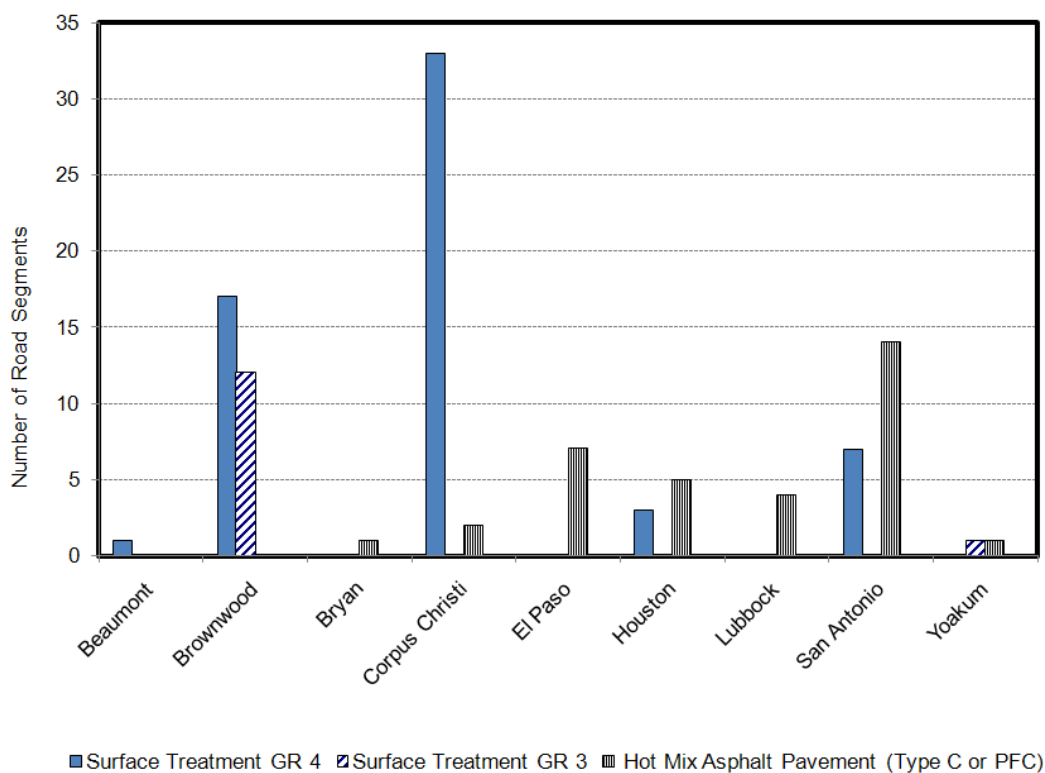


FIGURE 90 Mixture types used in the selected road segments.

To have a better understanding of the data variation, plots were produced that show the variation of the skid number versus PMIS section for each road segment. These graphs were the basis for the next step of the data analysis. It was found that road segments had a wide range of variation in the measured skid resistance. This variation can be caused by different factors such as aggregate type, mix type, traffic, environmental conditions, etc. The effects of different factors in the variation of the skid resistance are discussed subsequently.

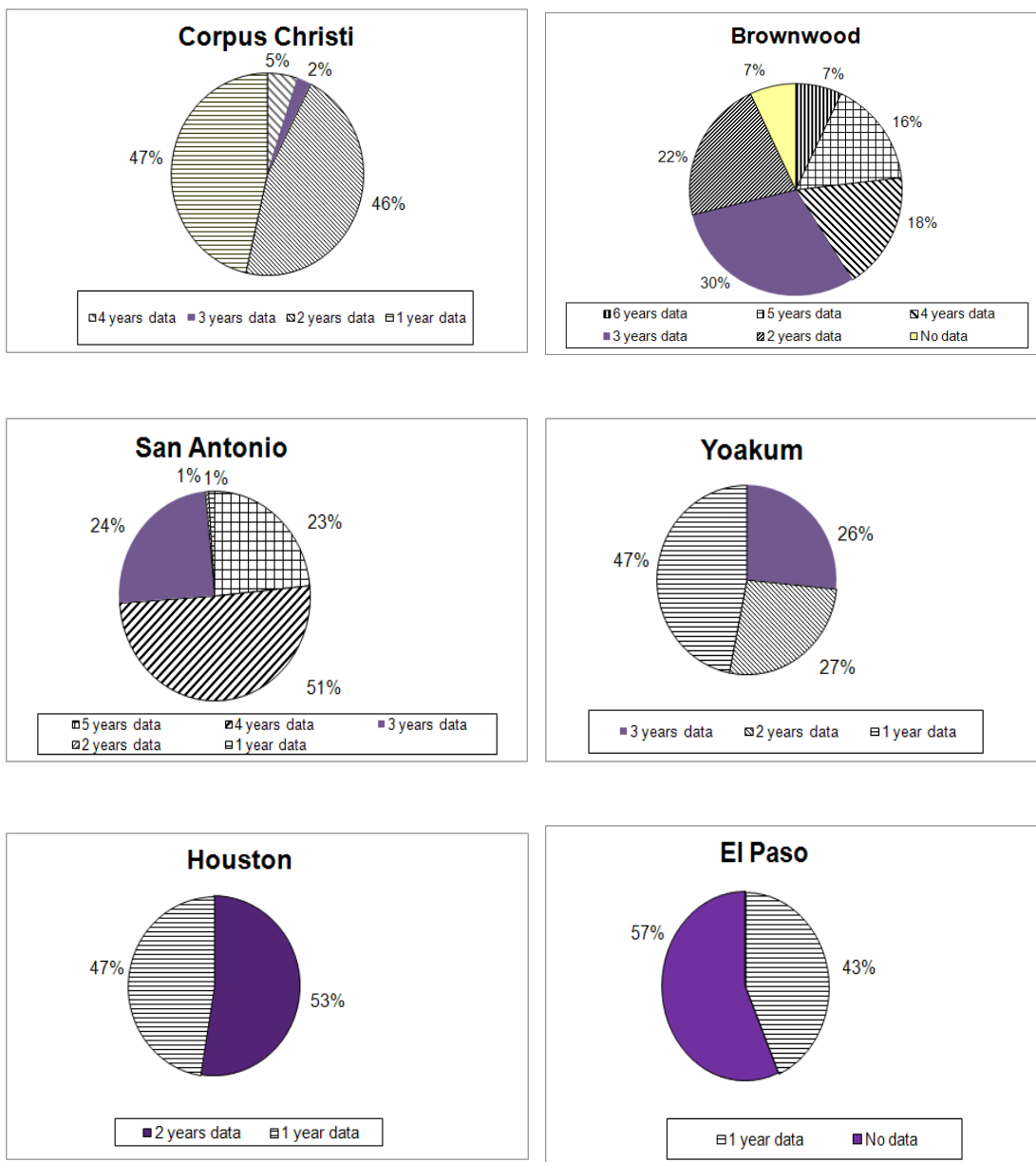


FIGURE 91 Data availability for the different TxDOT districts.

ANALYSIS OF THE COLLECTED FIELD DATA

Careful evaluation of the variation of the skid number reveals that the data have high variability. FIGURE 92 shows the coefficient of variation of the measured skid resistance for different road segments for each year. For example, in 2005, about 30 percent of the data have a coefficient of variation between 30 to 40 percent.

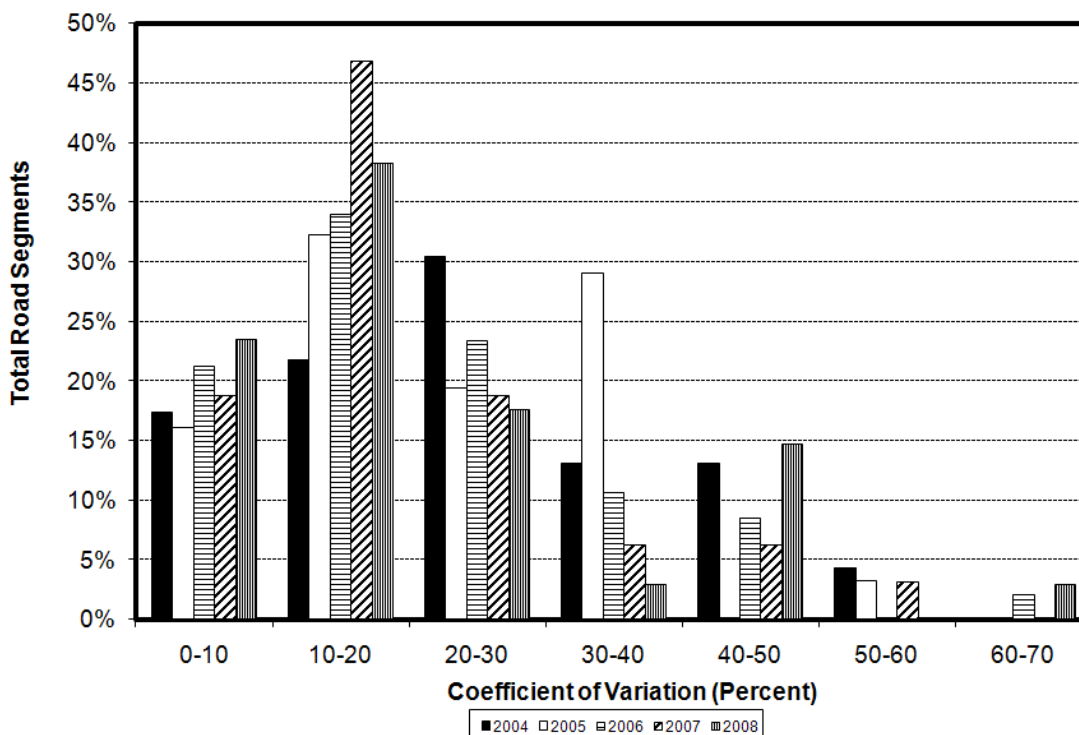


FIGURE 92 Coefficient of variation of measured skid resistance for different sections.

Because of the high variability of the data, analysis should consider the separate effects of different factors influencing skid resistance in order to be conclusive. In this section, the effects of different factors on the measured skid resistance are analyzed and discussed after making the following simplifications:

- As long as gradation remained the same, regardless of asphalt type, the surface treatment was assumed to be identical; e.g., surface treatment grade 4 was a combination of size 4 aggregates with AC-15P, AC-20-5TR, AC 20XP, and CRS-2P asphalt types. Furthermore, only two types of surface treatments

were considered in the analysis, and the effect of binder type on frictional characteristics was not considered.

- In order to compare different road categories in different service years, a parameter called the traffic multiplication factor (TMF) was defined. As shown in Equation 12, TMF is the multiplication of the annual average daily traffic (AADT) and number of years in service.

$$TMF = \frac{AADT \times YEARS \text{ IN SERVICE}}{1000} \quad (12)$$

This factor reflects the effect of both years in service and AADT for the most critical lane in the highway, i.e., the outer lane.

In order to study the variation of measured skid numbers as a function of traffic, it was decided to identify homogeneous subgroups of pavement sections in which the variation of skid number as a function of traffic is more consistent. A cluster analysis algorithm included in the SPSS statistical software package known as the two-step cluster method was implemented for this purpose. In this algorithm, the number of groups is established so that within-group variation is minimized and between-group variation is maximized. All the data in the database were classified in terms of their TMF for further analysis. The SPSS manual contains additional information about the details of this clustering analysis. TABLE 40 shows the TMF range for each cluster. A summary of the records based on the TMF class, aggregate type, and mix type is tabulated in TABLE 41.

TABLE 40 Traffic Clusters in Terms of Traffic Multiplication Factor

Level	Traffic Multiplication Factor
Low	0-5499
Medium	5500-13,499
High	13,500-24,999
Very High	25,000-40,000

TABLE 41 Summary of Skid Resistance Measurements

TMF Cluster	Mixture Design	Aggregate Type	N	Mean	Median	Min.	Max.	Std. Dev.
0-5500	Type C	Aggregate R	30	30.87	31.50	21	42	6.96
		Aggregate I	25	37.36	38.00	24	43	3.47
		Aggregate K	374	28.22	32.00	5	52	11.35
		Aggregate M	9	29.11	33.00	15	41	9.29
	PFC	Aggregate R	16	35.88	37.00	31	40	3.01
		Aggregate F	550	33.16	34.00	8	47	4.13
		Aggregate I	163	33.64	34.00	13	41	2.79
		Aggregate H	6	42.50	45.50	25	53	9.52
		Aggregate K	19	47.00	48.00	33	61	7.81
		Aggregate L	197	55.66	62.00	6	80	17.32
		Aggregate M	30	36.50	35.50	20	51	8.79
		Aggregate N	474	30.88	30.00	13	54	6.74
	Surface Treatment GR-4	Aggregate B	26	40.42	40.00	38	42	1.17
		Aggregate H	1	24.00	24.00	24	24	.
		Aggregate J	13	51.92	53.00	31	61	10.03
		Aggregate K	198	27.95	28.00	13	74	7.77
		Aggregate L	8	54.38	54.00	27	78	18.84
		Aggregate M	172	41.47	33.00	12	77	17.88
		Aggregate N	51	36.22	34.00	16	56	7.97
		Aggregate O	452	32.18	33.00	6	68	14.64
Aggregate P		46	29.17	28.00	16	65	8.42	
Aggregate Q	55	30.05	29.00	12	53	8.84		

TABLE 41 Continued

TMF Cluster	Mixture Design	Producer Name	N	Mean	Median	Min.	Max.	Std. Dev.
5500-13,500	Type C	Aggregate R	114	26.82	25.50	14	55	6.54
		Aggregate F	12	22.17	22.00	17	27	3.19
		Aggregate I	37	32.46	35.00	21	39	5.32
		Aggregate K	127	13.28	12.00	7	45	5.00
	PFC	Aggregate R	16	34.50	34.50	30	38	2.42
		Aggregate F	126	31.92	31.00	27	38	2.61
		Aggregate I	185	30.78	29.00	9	42	4.92
		Aggregate M	46	29.37	30.50	14	33	4.52
	Surface Treatment GR-3	Aggregate L	9	39.89	27.00	14	73	25.00
		Aggregate H	1	25.00	25.00	25	25	.
		Aggregate J	2	61.50	61.50	61	62	0.71
		Aggregate K	58	26.76	29.00	11	42	8.00
		Aggregate M	60	31.17	27.50	12	71	12.52
		Aggregate N	5	30.20	32.00	24	36	5.02
Aggregate O		95	24.53	27.00	6	36	8.35	
13,500-25,000	Type C	Aggregate R	62	22.53	21.50	14	38	4.57
		Aggregate K	2	17.00	17.00	15	19	2.83
	PFC	Aggregate R	16	29.94	30.50	26	32	2.08
		Aggregate I	72	24.78	24.50	13	36	2.96
		Aggregate M	19	28.32	28.00	26	35	2.36
	Surface Treatment GR-4	Aggregate K	12	14.33	14.00	11	20	2.64
		Aggregate M	9	23.33	23.00	11	34	7.66
		Aggregate Q	3	18.33	17.00	17	21	2.31
	25,000-40,000	Type C	Aggregate R	32	18.34	18.50	12	27
PFC		Aggregate R	16	29.94	29.50	26	36	2.54
Surface Treatment GR-4		Aggregate K	10	18.10	14.00	11	59	14.43

Traffic Load

FIGURE 93 shows the values of different skid numbers in terms of traffic level. Although the values of SN have high variability, a decreasing trend of SN values as a function of traffic level is identifiable. Because of high standard-error-of-mean values, a plot of median values was produced to extract the possible trend of SN values (see FIGURE 94). A clear trend shows that the SN value decreases when the traffic level increases. FIGURE 95 shows the standard deviation of measured SN values versus traffic level. Moreover, the mixes with very high or high traffic level have lower variability compared to mixes at the low traffic level.

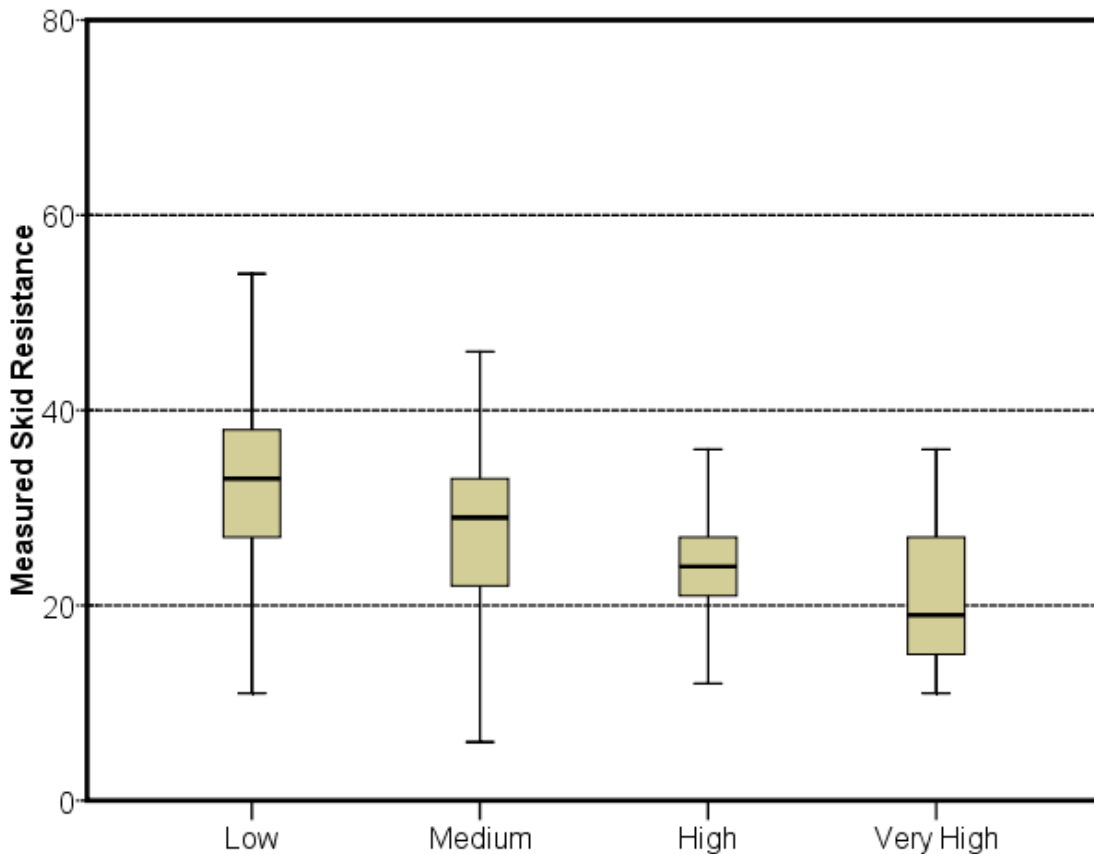


FIGURE 93 Measured SN values versus traffic level.

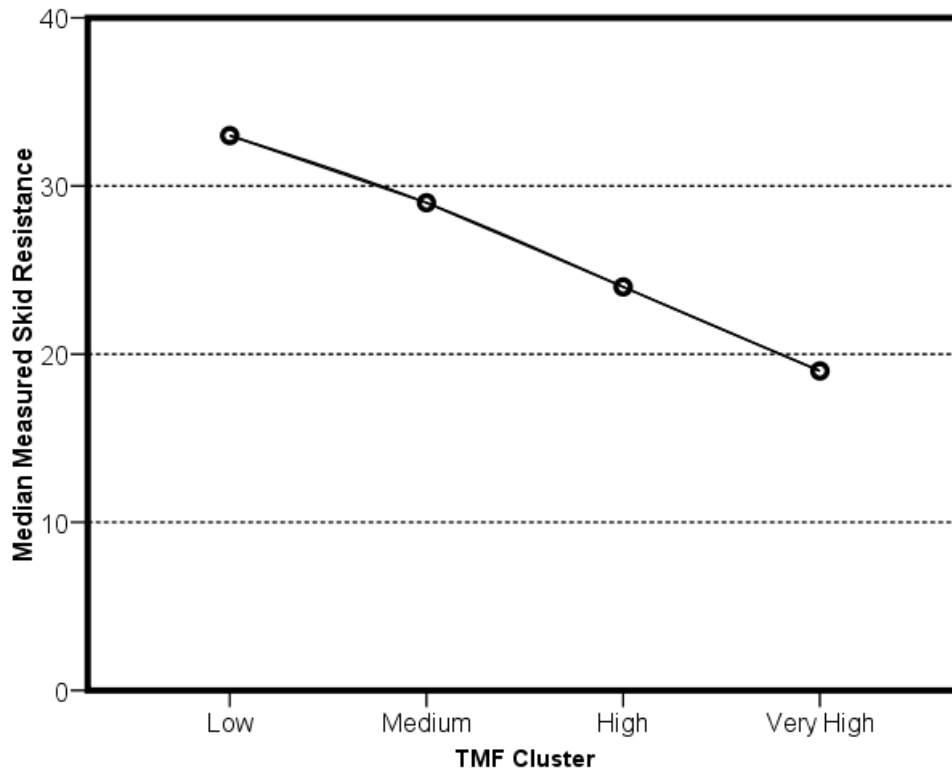


FIGURE 94 Median SN values versus traffic level.

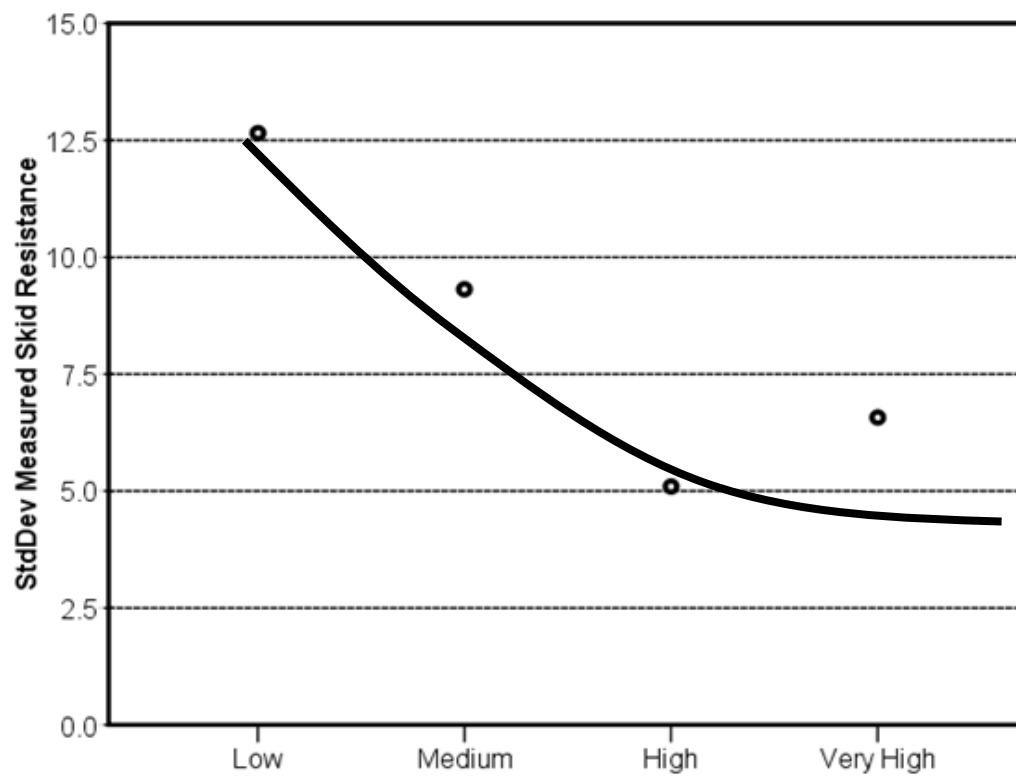


FIGURE 95 Standard deviation of measured SN values versus traffic level.

Mix Design

FIGURE 96 shows the measured SN values for different mix designs and clearly reveals that the results of skid measurements are highly variable and depend on the mix type. A plot of median values, as shown in FIGURE 97, gives a better understanding of the behavior of different mixes. These results confirm the findings from the laboratory phase of this study, which found that PFC mixes had higher skid resistance than Type C mixes.

FIGURE 98 shows the standard deviation of the measured skid number for different mixes; the standard deviation for PFC mixes is less than five in all cases. This result demonstrates the low variability and consistency in frictional performance of PFC mixes. Type C mixes have more variability than PFC mixes. Surface-treatment mixes have more variation than Type C and PFC mixes.

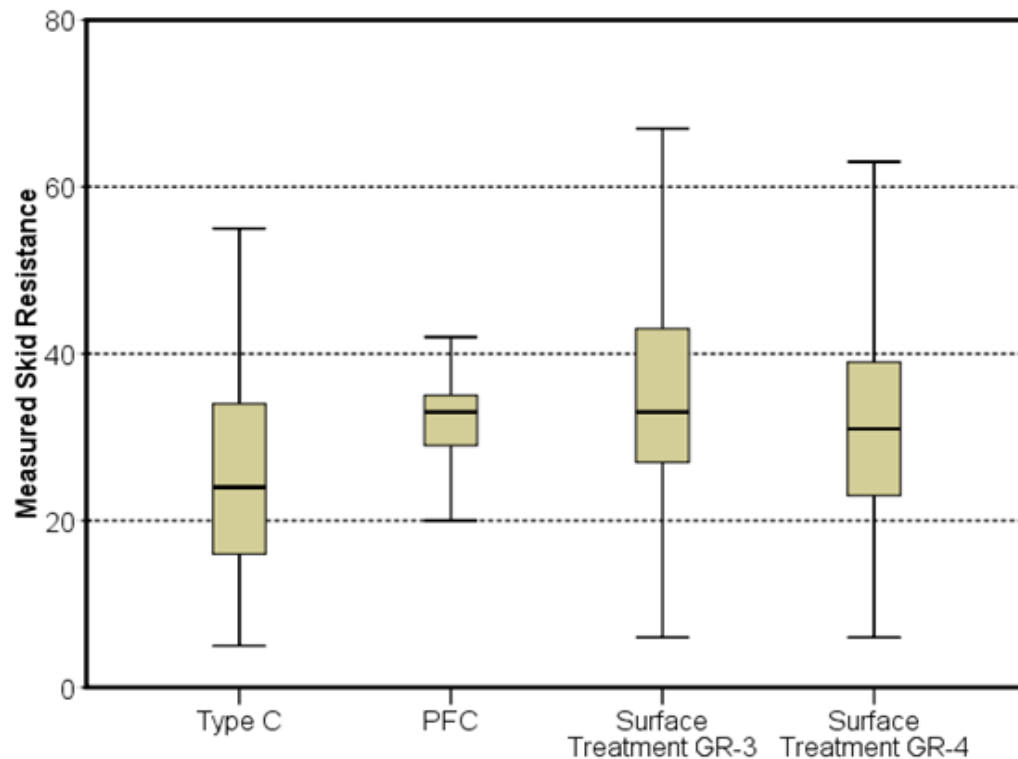


FIGURE 96 Measured SN values for different mix types.

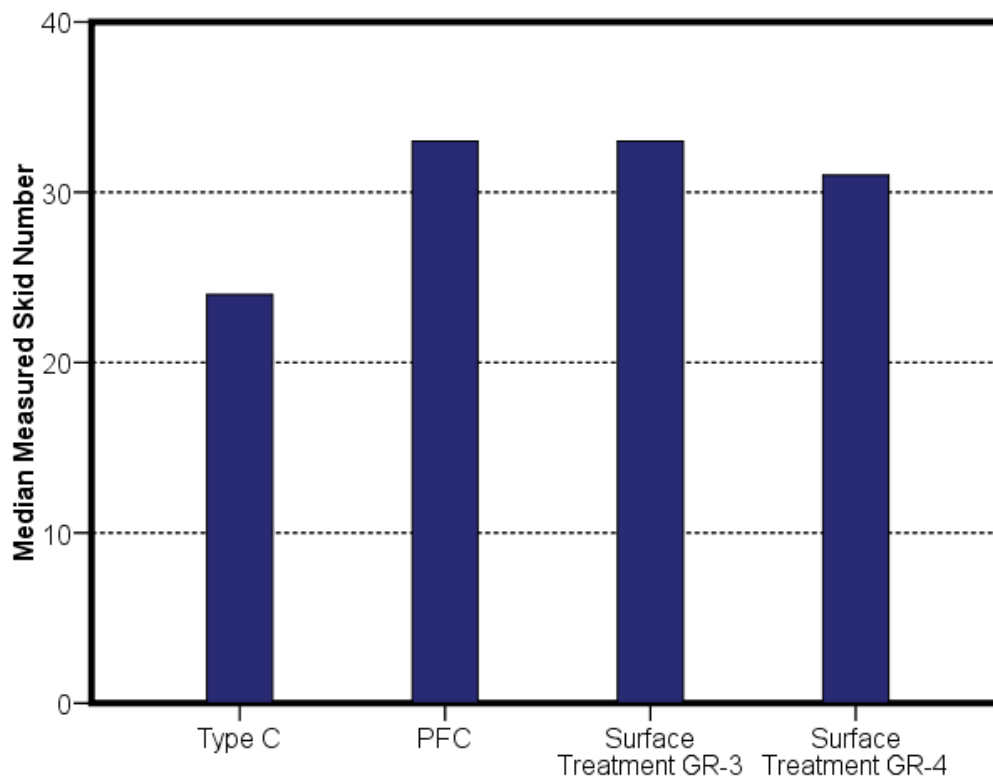


FIGURE 97 Median of measured SN values for different mix types.

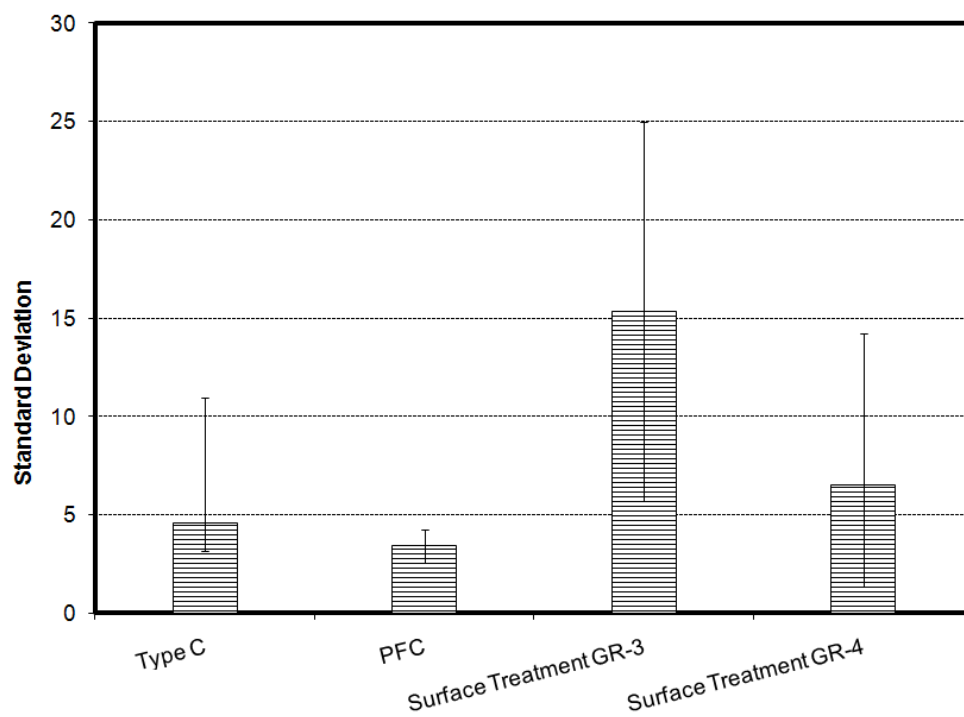


FIGURE 98 Standard deviation of measured SN values for different mixes.

Figures 99 and 100 show the variability of measured SN values for different mixes in low and medium/high traffic-level categories, respectively. The variability of skid resistance decreased significantly from low traffic levels to high traffic levels. Moreover, the variability of skid measurement for surface treatments is high, and the variability for PFC mixes is the lowest among all mixes. The variability of Type C mixes is generally higher than PFC mixes. These results confirm that the PFC mix is the most consistent and has the lowest variability among all mixes. One reason for this might be the requirement for using aggregate SAC A or SAC B in preparing the PFC mixes.

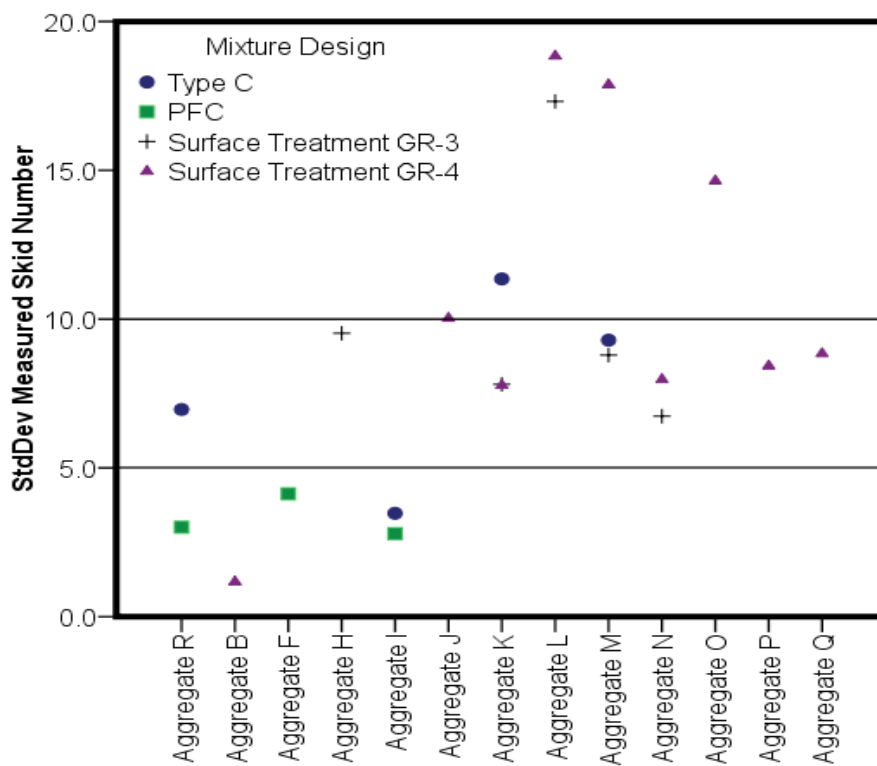


FIGURE 99 Standard deviation of the measured SN values for low TMF level.

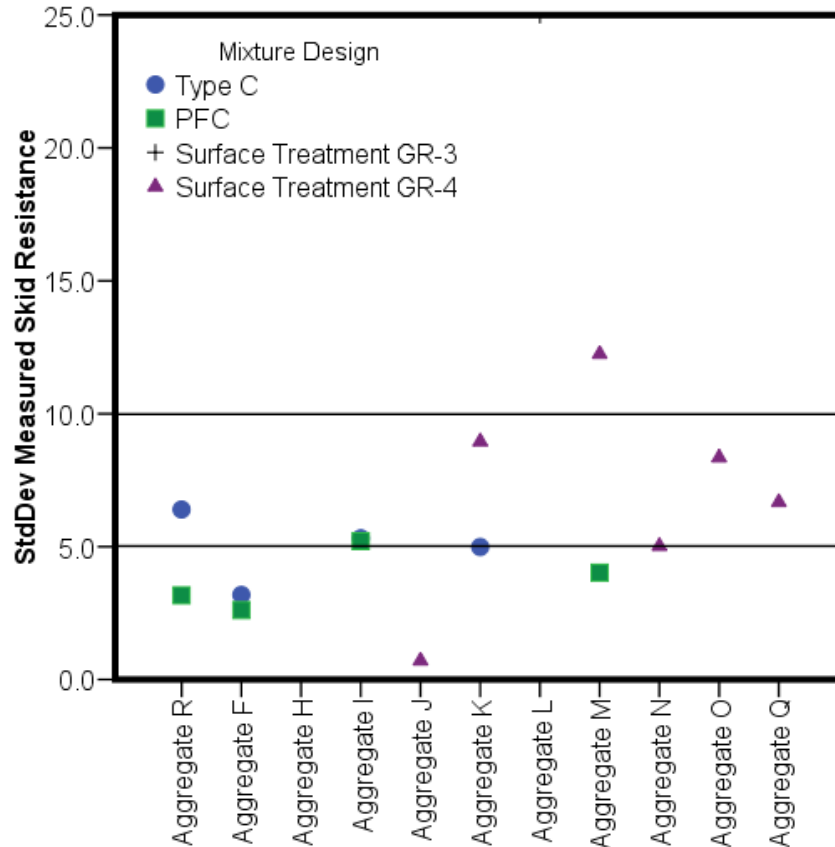


FIGURE 100 Standard deviation of the measured SN values for medium and high TMF level.

Aggregate Type

FIGURE 101 shows the values of measured SN for different aggregate types. The influence of aggregate type on skid resistance cannot be studied in isolation from the effect of mix design and traffic level. Therefore, a detailed analysis of the measured skid values for different mix types and traffic level was performed.

FIGURE 102 shows that in almost all aggregate types, surface treatments grade 3 have the highest SN value, and among dense-graded mixes, PFC mixes have the highest skid number.

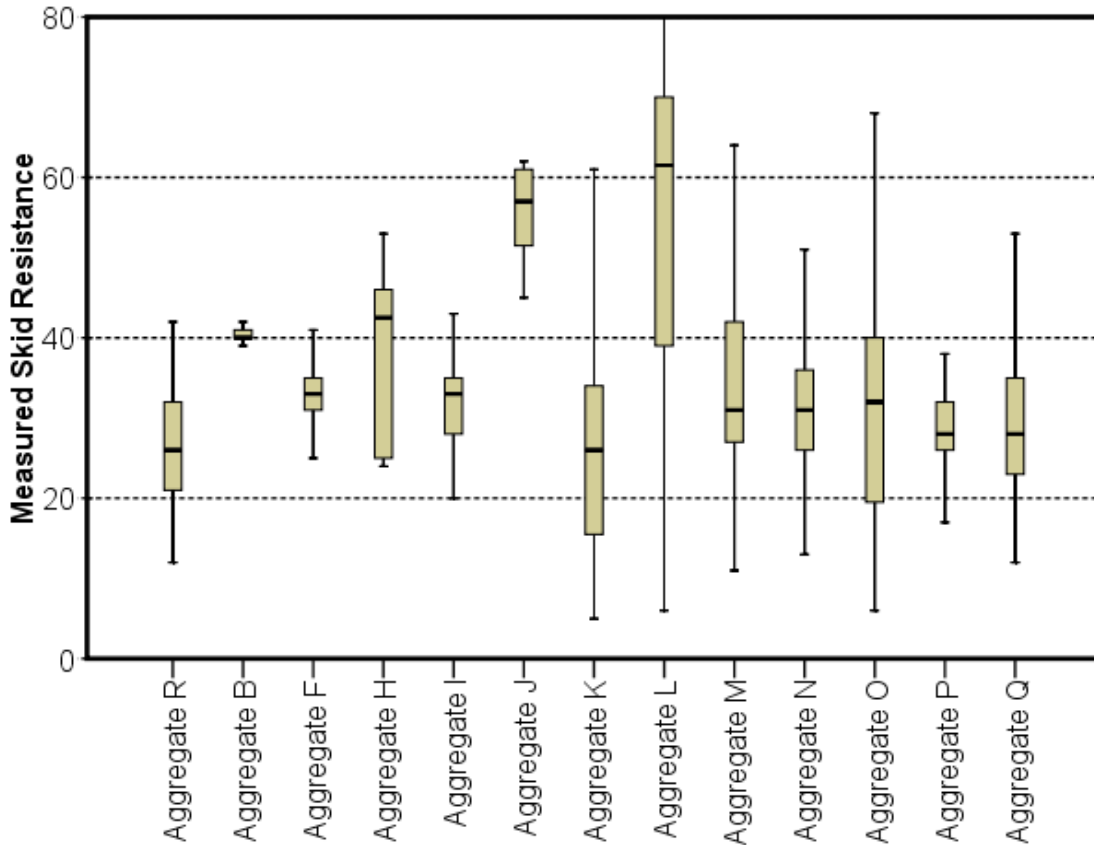
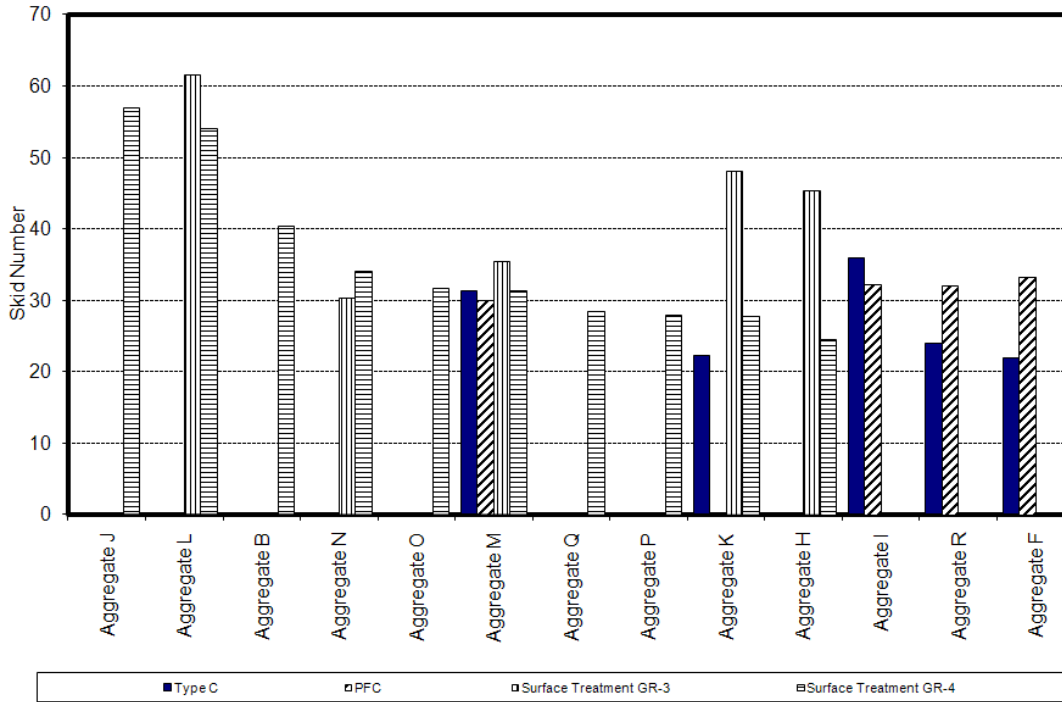
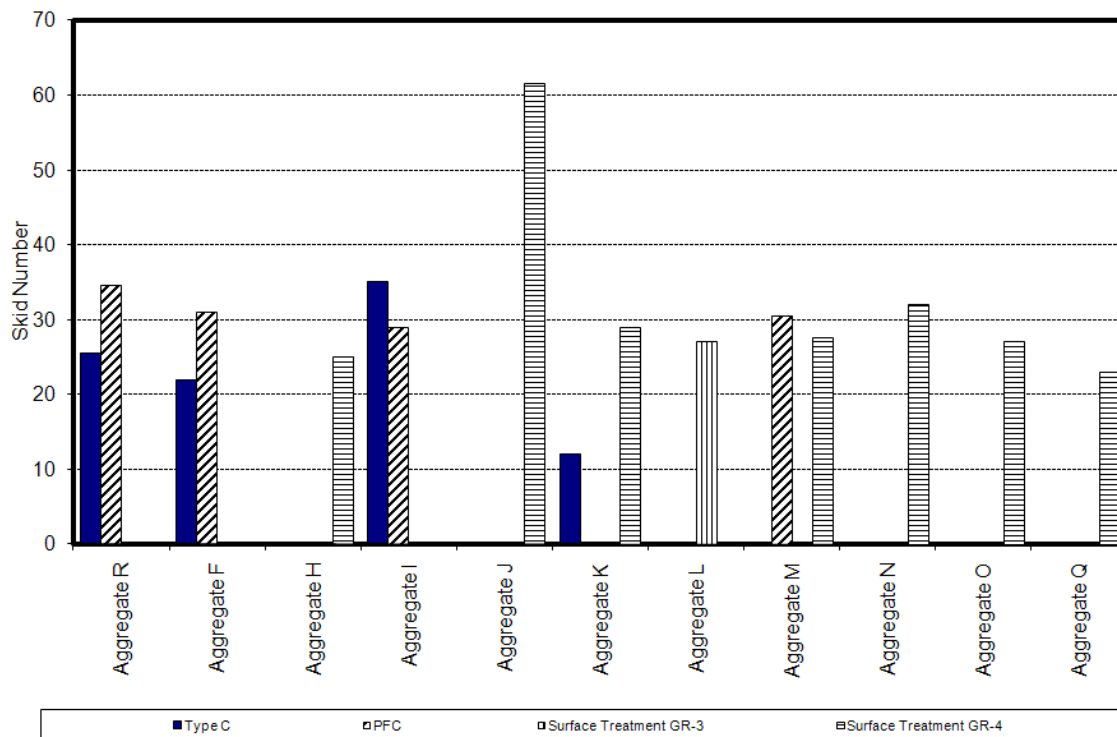


FIGURE 101 Values of measured SN for different aggregate types.

TABLE 42 shows the median value for measured skid resistance and aggregate ranking for surface treatments grade 3. In this mix design, aggregate L has the highest skid value. Furthermore, aggregate K (classified as SAC B in the TxDOT classification system) shows satisfactory skid characteristics and lies in second place. Aggregate H, which is classified as SAC A in the TxDOT classification system, has the third rank in this group, and both M and N aggregate types, classified as SAC B, are ranked in the fourth and fifth places, respectively.

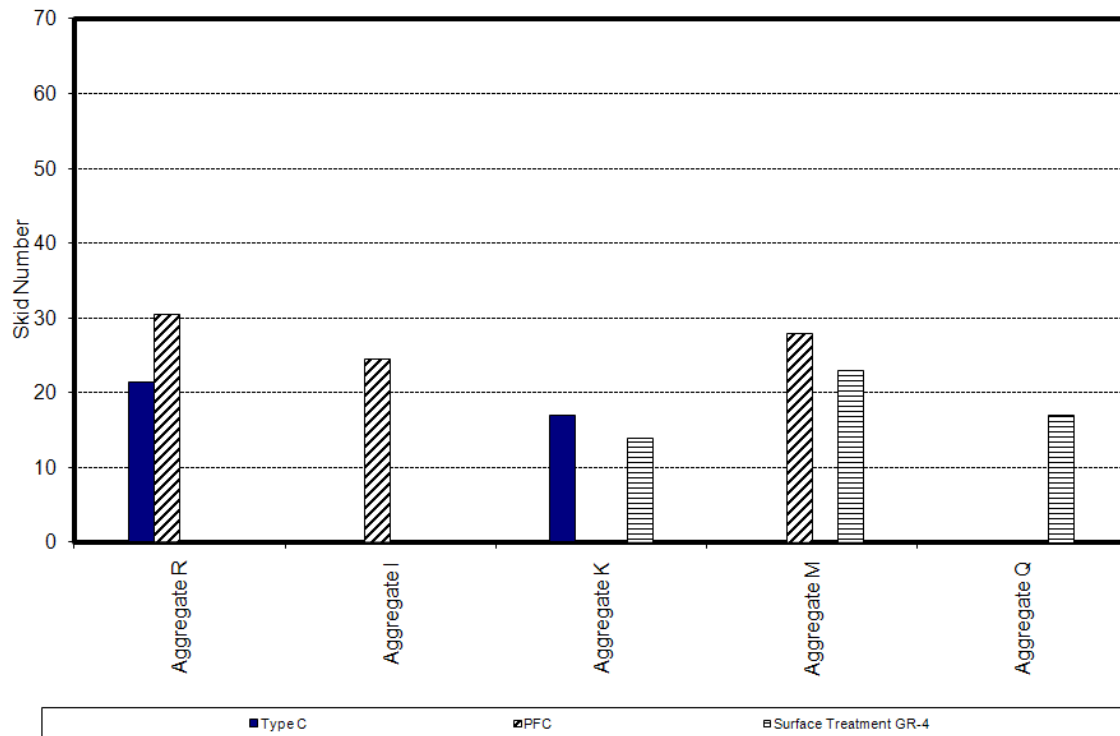


(a) Low TMF level.



(b) Medium TMF level.

FIGURE 102 Median of measured SN values for different aggregate and mix types.



(c) High TMF level.

FIGURE 102 Continued.

TABLE 42 Aggregate Ranking Based on Measured Skid Resistance for Surface Treatment Grade 3 in Low Traffic Level

Aggregate Type	Skid Number Median	Rank	TxDOT Classification
Aggregate L	62	1	SAC A
Aggregate K	48	2	SAC B
Aggregate H	45	3	SAC A
Aggregate M	36	4	SAC B
Aggregate N	30	5	SAC B

The results of skid number values measured for surface treatment grade 4 are tabulated in TABLE 43. The results indicate that both aggregate L and aggregate J have satisfactory skid properties and are ranked the first and second place, respectively.

TABLE 44 shows the median skid resistance values and aggregate ranking for the Type C mixture. In this mixture type, aggregate I provides the highest friction level. The results of the analysis of field data confirmed the findings from the laboratory phase of this project, which showed aggregate R to have superior skid properties compared with aggregates K and M individually. Furthermore, data in Table 8 show that mixtures containing aggregate K lose the initial texture faster than other aggregate types. The skid number of mixtures containing aggregate K dropped below 20 at higher traffic levels. TABLE 45 illustrates the results for PFC mixes. It appears that aggregate R has the highest skid value. Again, this finding is in accordance with the results of the laboratory phase of this study. Aggregates F and I function well, and their skid values are close to or above 30.

TABLE 43 Aggregate Ranking Based on Measured Skid Resistance for Surface Treatment Grade 4 in Medium and Low Traffic Levels

Cluster Number of Case	Producer Name	Measured Skid Resistance	Rank	TxDOT Classification
Low (0-5500)	Aggregate L	54	1	SAC A
	Aggregate J	54	2	SAC B
	Aggregate B	40	3	SAC B
	Aggregate N	35	4	SAC B
	Aggregate O	33	5	SAC A
	Aggregate M	33	6	SAC B
	Aggregate Q	30	7	SAC B
	Aggregate K	29	8	SAC B
	Aggregate P	28	9	SAC A
	Aggregate H	25	10	SAC A
Medium (5500-13,500)	Aggregate J	62	1	SAC B
	Aggregate N	32	2	SAC B
	Aggregate K	29	3	SAC B
	Aggregate M	28	4	SAC B
	Aggregate O	27	5	SAC A
	Aggregate H	25	6	SAC A
	Aggregate Q	23	7	SAC B

TABLE 44 Aggregate Ranking Based on Measured Skid Resistance for Type C Mixture in High, Medium, and Low Traffic Levels

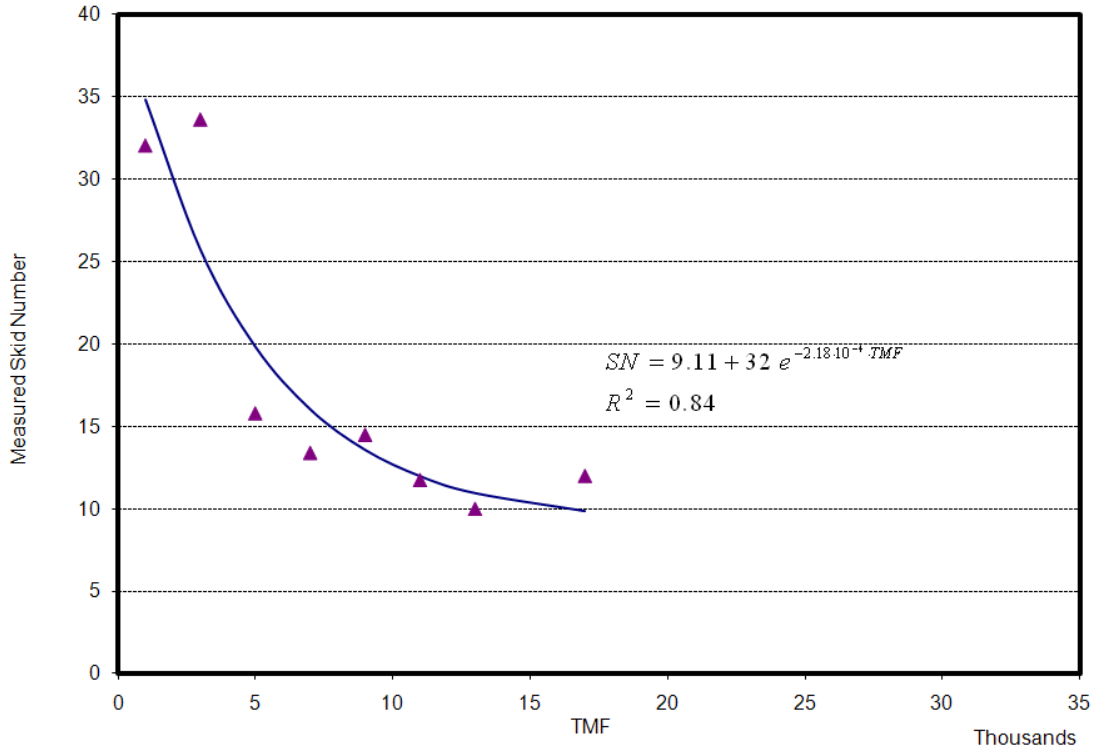
Cluster Number of Case	Producer Name	Measured Skid Resistance	Rank	TxDOT Classification
Low (0-5499)	Aggregate I	38	1	SAC A
	Aggregate R	32	2	SAC B
	Aggregate K	31	3	SAC B
	Aggregate M	31	4	SAC B
Medium (5500-13,499)	Aggregate I	35	1	SAC A
	Aggregate R	26	2	SAC B
	Aggregate F	22	3	SAC B
	Aggregate K	12	4	SAC B
High (13,500-24,999)	Aggregate R	22	1	SAC B
	Aggregate K	17	2	SAC B

TABLE 45 Aggregate Ranking Based on Measured Skid Resistance for PFC Mixture in High, Medium, and Low Traffic Levels

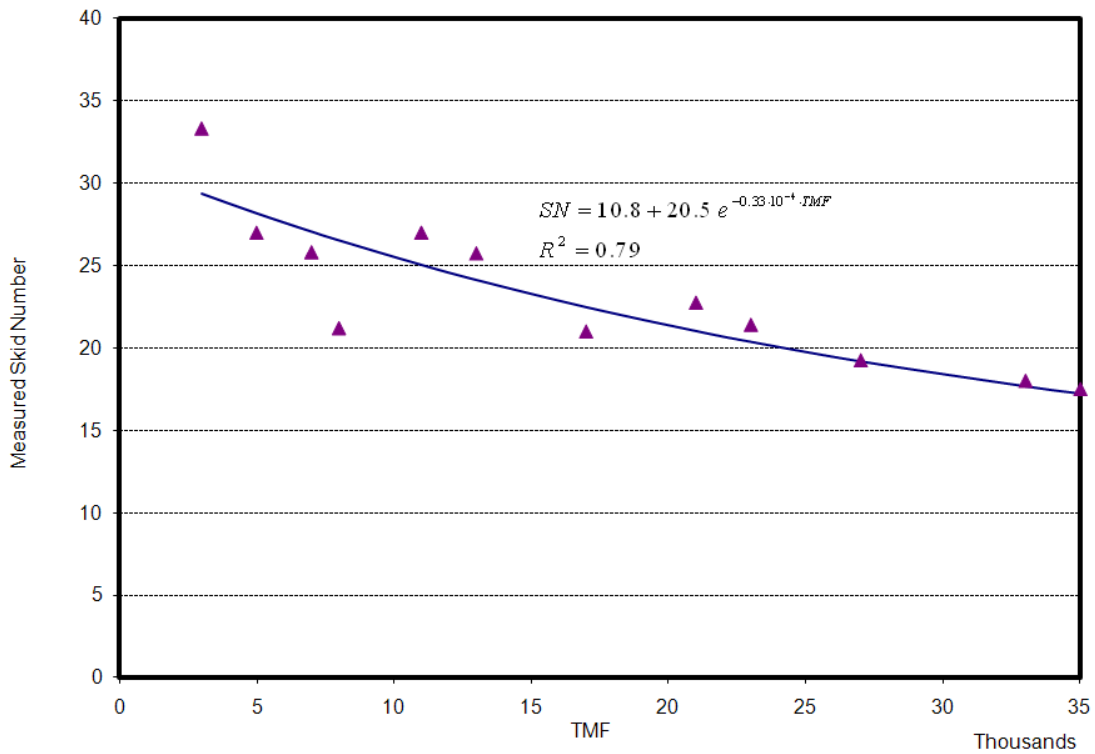
Cluster Number of Case	Producer Name	Measured Skid Resistance	Rank	TxDOT Classification
Low (0-5499)	Aggregate R	37	1	SAC B
	Aggregate F	34	2	SAC B
	Aggregate I	34	3	SAC A
Medium (5500-13,499)	Aggregate R	35	1	SAC B
	Aggregate F	31	2	SAC B
	Aggregate M	31	3	SAC B
	Aggregate I	30	4	SAC A
High (13,500-24,999)	Aggregate R	31	1	SAC B
	Aggregate M	28	2	SAC B
	Aggregate I	25	3	SAC A

FIGURE 99, presented previously, shows the standard deviation of the measured values of skid number for different aggregate types at low traffic levels. Aggregates used in surface treatments grade 3 and grade 4, such as aggregates L, O, and M, have high variability (a standard deviation higher than 20). Conversely, aggregates used in PFC mixes, such as aggregates M, F, and I, have a standard deviation less than 5.

Because the majority of the collected data lie in low and medium traffic categories, a new classification was used to capture the variation of each aggregate source against TMF level. FIGURE 103 shows the median of measured SN values for the Type C mix design and clearly shows that aggregate K was polished rapidly and loses its frictional characteristics in the early stages of its service life. The terminal SN value for this aggregate (about 9) seems to be less than that for other aggregates. This observation confirms the laboratory findings regarding the rapid polishing of this aggregate type. Aggregate R seems to modify the skid characteristics compared with aggregate K alone because this combination has a terminal value of about 11. These graphs show that an exponential equation with the form presented in Equation 1 in Chapter II can fit the data. Moreover, the rate of change in aggregate R is lower than that of aggregate K. Aggregate I has the highest skid number in this mix and can maintain its initial texture. The collected data for aggregate M do not extend over a number of years to allow for a conclusion. This aggregate, however, shows a high rate of decrease in friction compared to other aggregate sources.

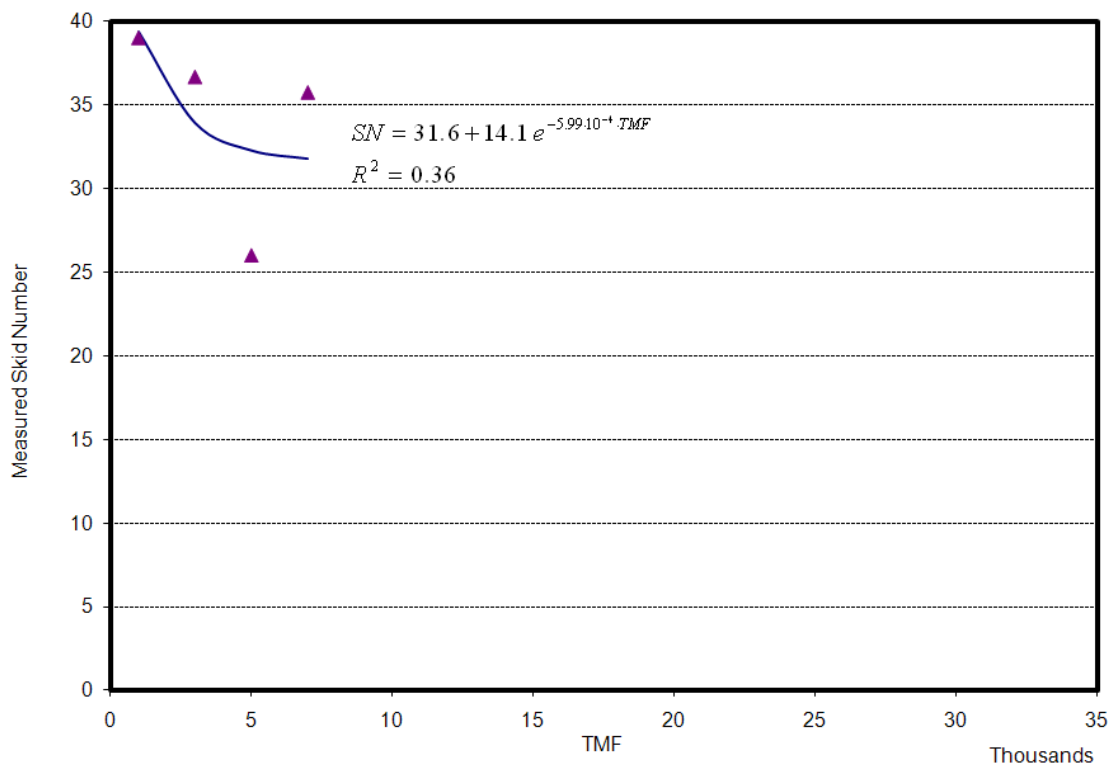


(a) Aggregate K (SAC B)

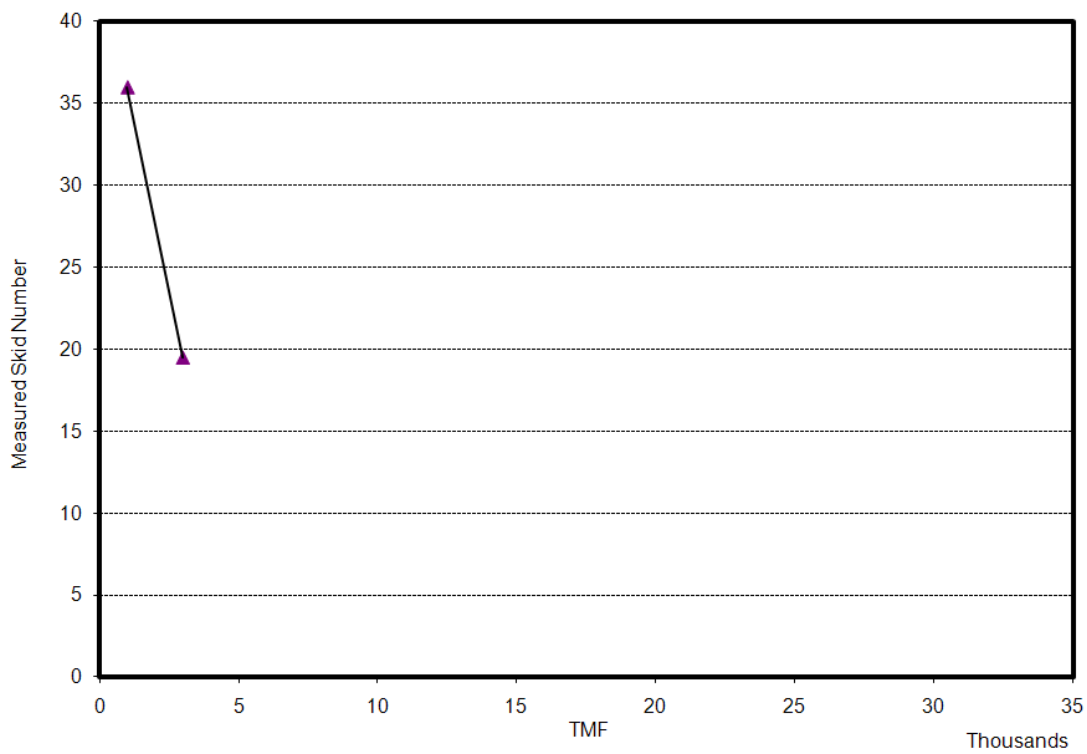


(b) Aggregate R (SAC B)

FIGURE 103 Median of measured SN values for Type C mix design.



(c) Aggregate I (SAC A)



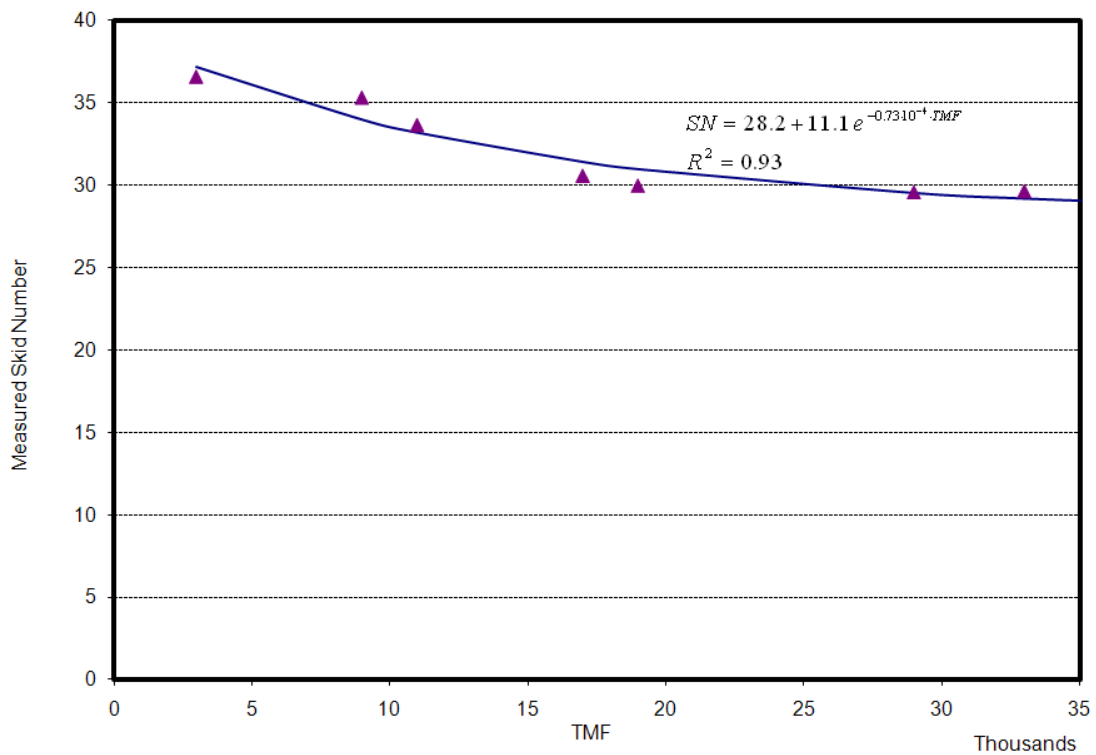
(d) Aggregate M (SAC B)

FIGURE 103 Continued.

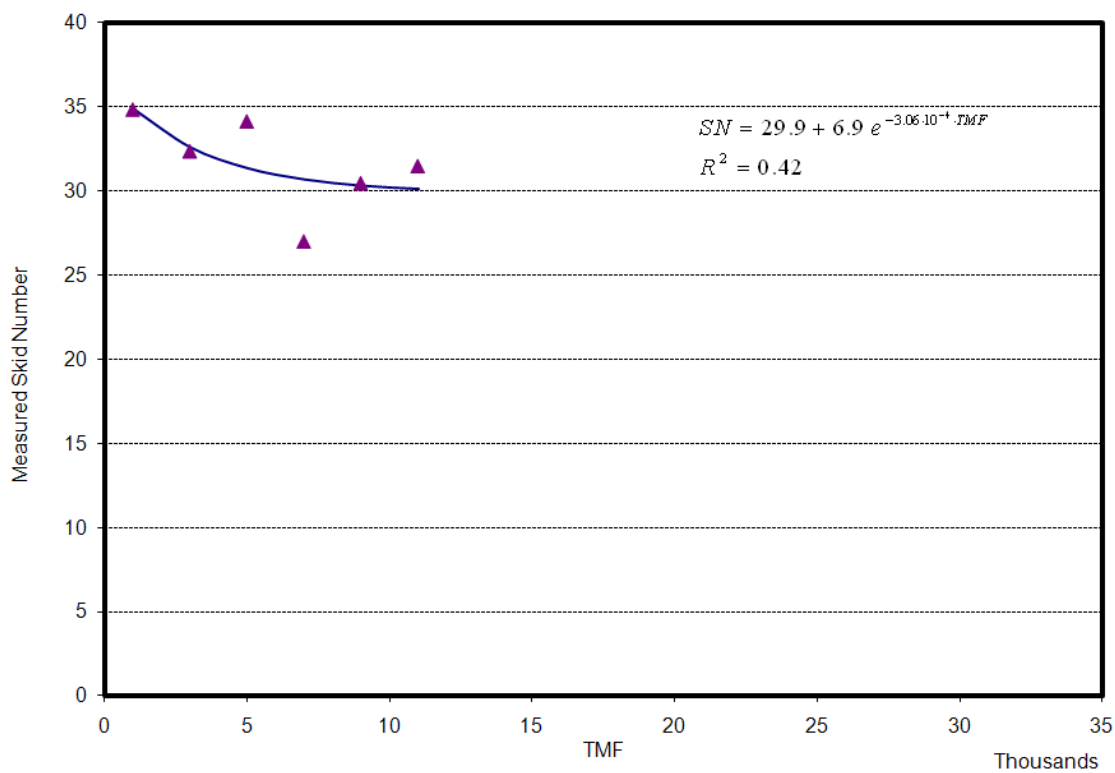
FIGURE 104 shows the median of measured SN values for the PFC mix design. Equation 1 can fit the data reasonably well. FIGURE 104 illustrates that aggregates I and R have low polishing rates compared to aggregates F and N. The terminal values of aggregates I and M are less than 30. Aggregates R and F can maintain their initial texture over 30. The duration of collected skid data for aggregate M is not long enough to make a conclusive statement, but it seems this aggregate loses its initial texture rapidly and falls below 30 in its initial stages of service life. This observation confirms the finding of the laboratory phase of this study.

FIGURE 105 shows the median of measured SN values for surface treatments grade 3. The collected data displayed in FIGURE 105 do not cover the complete range of traffic levels but show that aggregate L provides high initial skid resistance. A longer traffic range is needed to estimate the frictional performance of this aggregate in the field. Moreover, aggregates M and N have the lowest skid values in this mixture type. Aggregate K provides a fairly high level of friction ($SN > 40$), although in other mix types, it does not provide acceptable friction levels. Surface treatments grade 3 have an almost uniform skid number value throughout the range of TMF levels, and all aggregates are able to provide acceptable friction levels. These results suggest that the skid values for this mix are affected by gradation more than aggregate type.

FIGURE 106 illustrates the median of measured SN values for surface treatments grade 4. Aggregate J provides considerably high skid resistance over 40. Aggregate K has the lowest terminal skid value at around 10. There is no significant difference between the median values of skid values for other aggregates. Similar to the performance in Type C mixes, aggregate K has the lowest terminal skid values. Aggregates M, O, and N have a fair terminal skid number between 25 and 30. Aggregate Q shows a decreasing rate of polishing, but a wider range of traffic data is needed to analyze the characteristics of this aggregate.

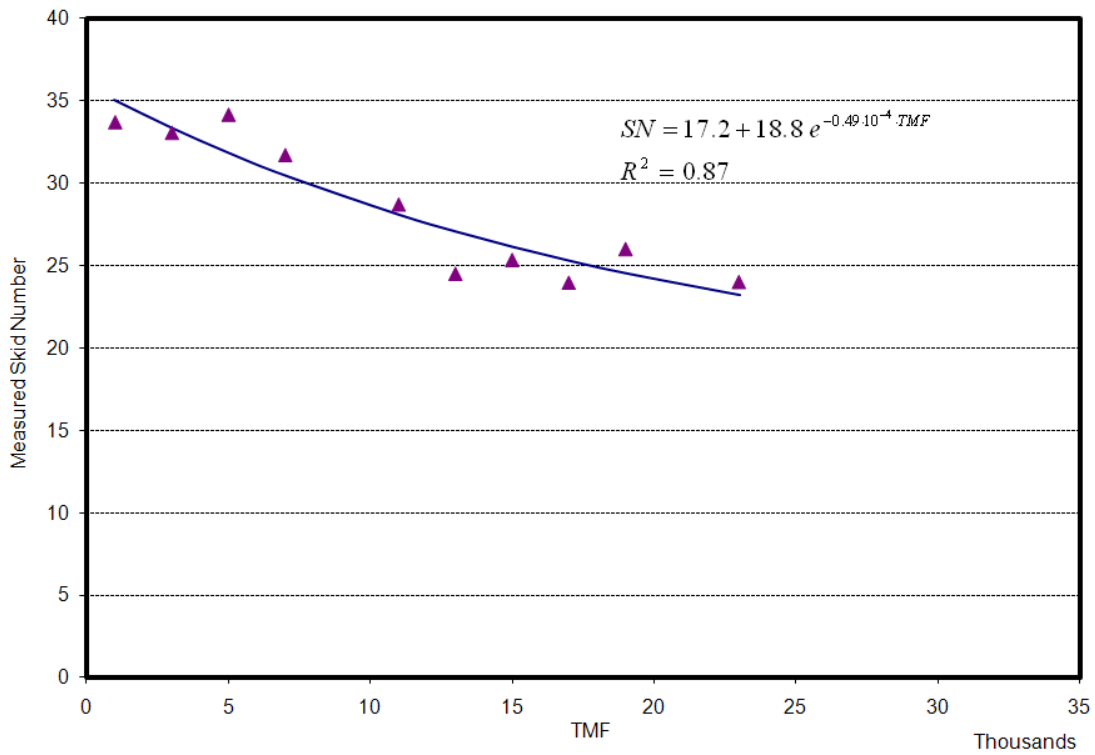


• Aggregate R (SAC B)

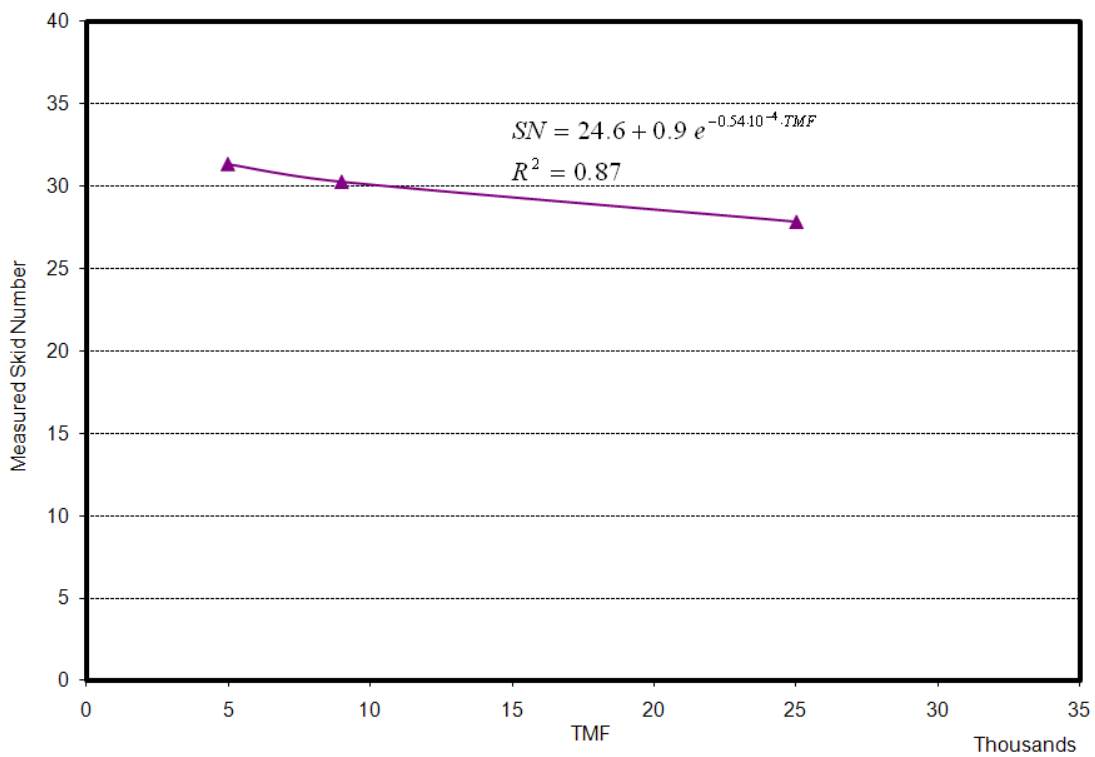


• Aggregate F (SAC B)

FIGURE 104 Median of measured SN values for PFC mix design.



• Aggregate I (SAC A)



• Aggregate M (SAC B)

FIGURE 104 Continued.

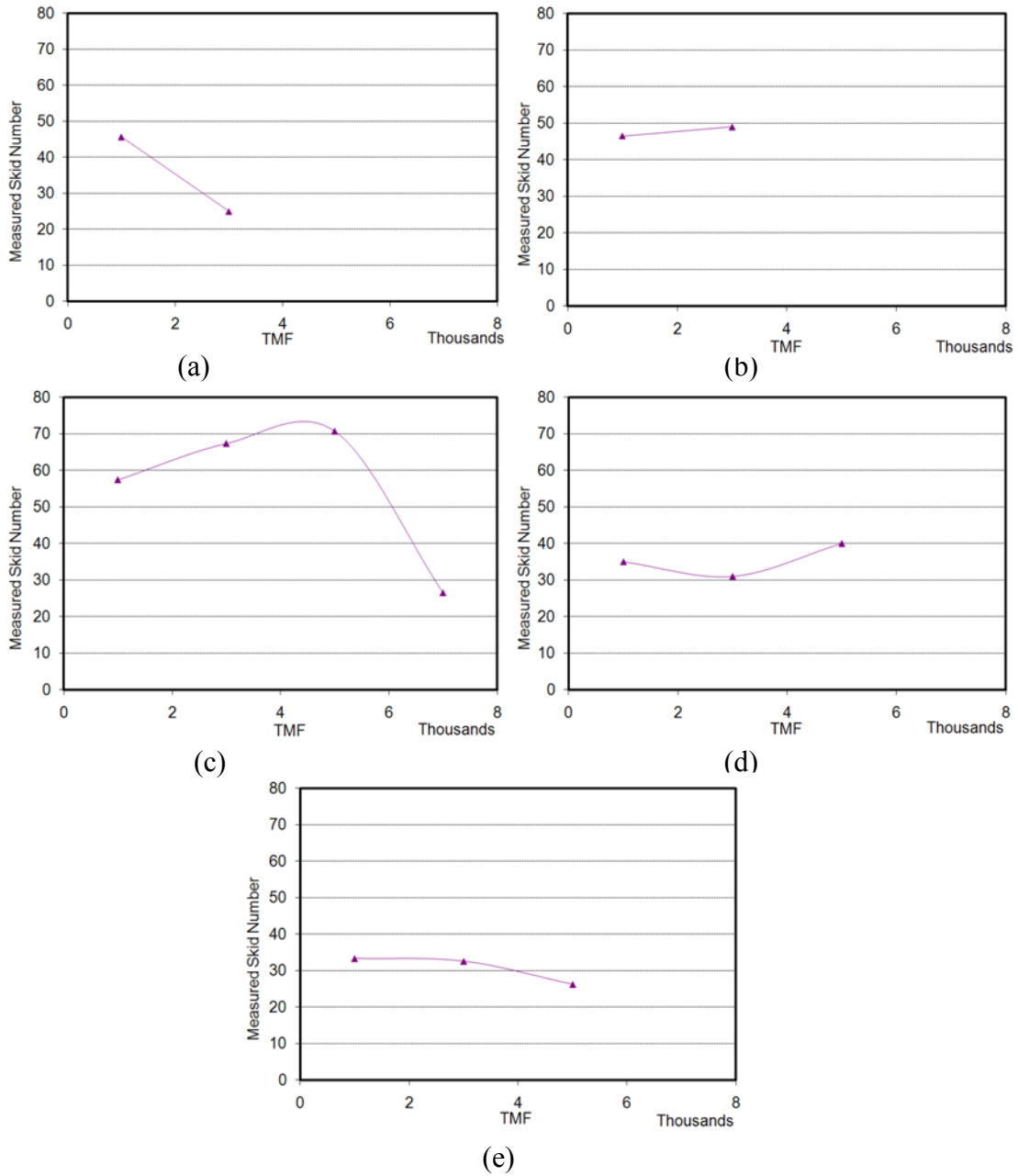


FIGURE 105 Median of measured SN values for surface treatments grade 3: (a) aggregate H (SAC A); (b) aggregate K (SAC B); (c) aggregate L (SAC A); (d) aggregate M (SAC B); (e) aggregate N (SAC B).

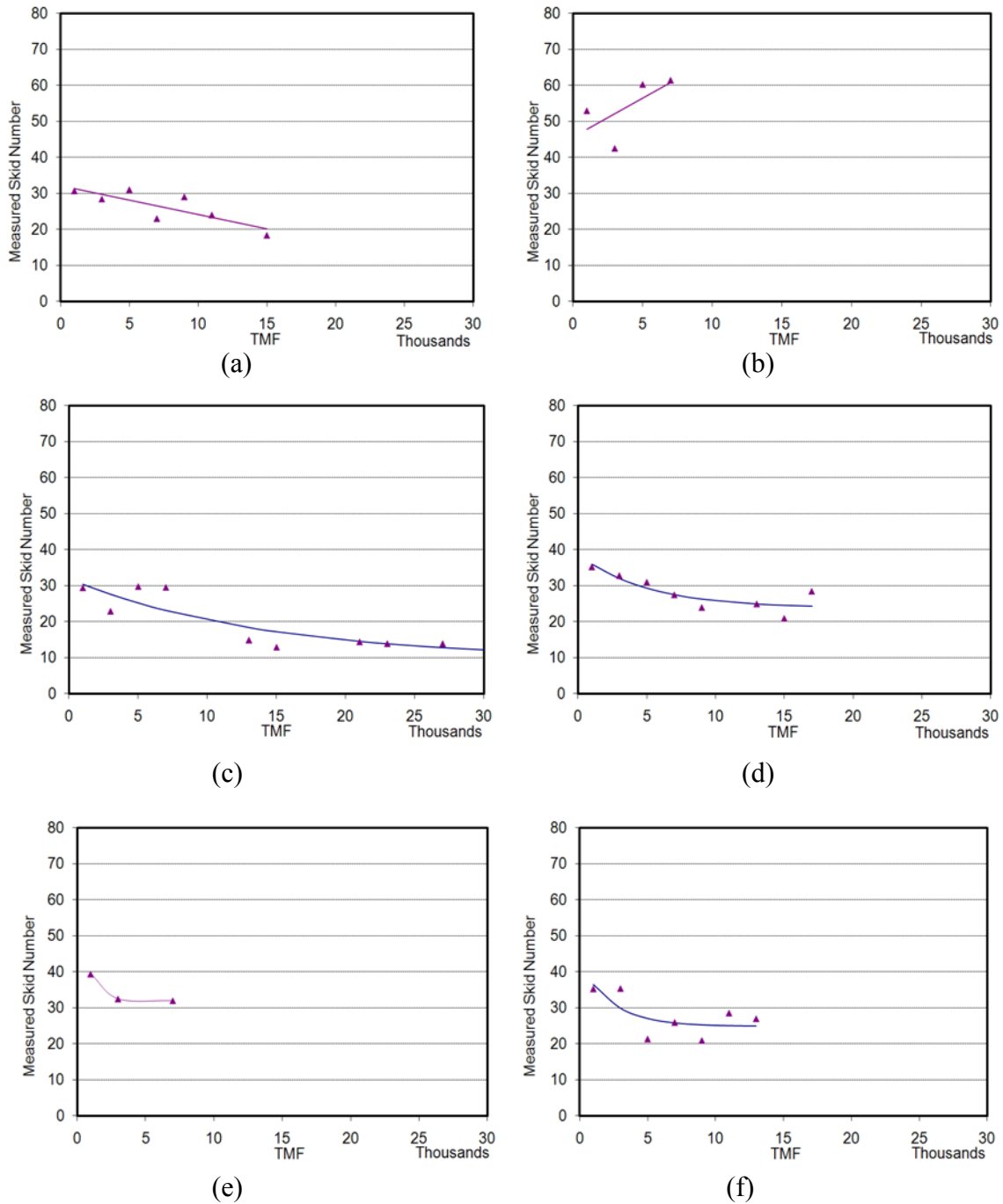


FIGURE 106 Median of measured SN values for surface treatments grade 4: (a) aggregate Q (SAC B); (b) aggregate J (SAC B); (c) aggregate K (SAC B); (d) aggregate M (SAC B); (e) aggregate N (SAC B); (f) aggregate O (SAC A).

SUMMARY

The field experiments involved many sections that incorporated several mixtures and aggregate sources. These sections had experienced different traffic loading levels. In order to facilitate comparing different pavement sections, a single factor denoted TMF was defined. This factor was the multiplication of AADT in the design lane and years in service divided by 1000, and it considered both traffic level and years of operation.

As expected, the results of the data analysis showed the measured skid number decreased as TMF increased. The measured skid numbers had less variation at higher TMF levels. This phenomenon could be attributed to mixtures reaching close to a terminal skid condition, which is associated with aggregates approaching their equilibrium (or terminal) state of texture after a high number of polishing or loading cycles.

Four mix types (surface treatment grade 3, surface treatment grade 4, PFC, and Type C) were included in the field measurements. The results showed that surface treatments generally had higher skid numbers than Type C mixes, which are conventional dense-graded mixes. Additionally, PFC mixes exhibited better skid resistance than Type C mixes and surface-treatment mixes. The results further revealed that the PFC mixes had the lowest variation in skid number, while surface-treatment mixes had the highest variability.

The effect of aggregate type was studied, and the results illustrated that there was a high level of interaction between aggregate performance, mix type in which aggregate was used, and traffic level. In general, it is hard to classify aggregates without specifying mixture type and traffic levels.

Overall, the results of the field-data analysis are in agreement with the findings of the laboratory phase. The same equation form (i.e., Equation 1) that was used to describe the aggregate rate of polishing can be used to describe skid number versus TMF values in the field and to describe skid number versus polishing cycles in the laboratory.

The next chapter explains the results of the analysis performed on the measured values of dynamic friction and macrotexture using DFT and CTMeter on selected pavement sections.

CHAPTER VII

ANALYSIS OF FRICTION AND TEXTURE OF ASPHALT PAVEMENT SECTIONS

INTRODUCTION

This chapter presents the analysis and results of field measurements using the DFT and CTMeter, as well as the development of a theoretical relationship between laboratory and field data. During the field testing, efforts were made to test the same part of the pavement section that was already tested by the TxDOT towed friction trailer.

Friction and macrotexture tests using the DFT and CTMeter, respectively, were conducted in the selected sections in such a way that the total number of tests was distributed uniformly within the length of the tested section (section length was about 0.5 mi for the highway).

SELECTION OF THE FIELD SECTIONS

In this study, 64 pavement sections were chosen for friction and macrotexture evaluation. The sections were selected to cover a wide range of material type and traffic levels and to represent different road types (i.e., interstates, state highways, U.S. highways, and farm-to-market roads); in addition, selection was based on the availability of a complete record of the construction and skid measurement in the TxDOT database. The pavement age of these sections was between 2 and 11 years. These sections were distributed in different TxDOT districts. TABLE 46 shows a list of the sections.

TABLE 46 Field Sections Used in Measuring Friction and Texture

District	County	Highway	Des.	Mix Design	TRM	Dir.
Abilene	Nolan	IH20	L	CRM	247+0.1	WB
	Taylor	IH20	L	PFC	272+0.1	WB
				Superpave 1/2"	280+0.8	WB
				PFC	284-0.55	WB
				US83	L	PFC
Atlanta	Harrison	IH20	R	SMA-C	634+320'	EB
Austin	Bastrop	US290	K	PFC	628+0.53	EB
	Travis	SH71	L	Type C	582-0.61	WB
Beaumont	Hardin	FM421	K	Type C	747+0.7	EB
		US69	K	SMA-D	489+0.1	SB
	Jefferson	SH73	L	PFC	772+0.1	WB
		US69	L	PFC	538-0.05	NB
	Tyler	SH146	K	Type C	422+0.7	NB
Brownwood	Brown	FM2376	K	Type D	460+1.6	NB
		FM2524	K	Type D	340+ 0.4	SB
		FM3064	K	Type D	458+0.9	WB
		SH153	K	Type D	372+0.7	WB
		US67	K	Type D	570+0.4	WB
	Eastland	IH20	L	Type D	362+0.6	WB
		SH36	K	Type C	346+1.6	WB
	McCullough	US87	R	Type D	458+0.2	SB
Bryan	Limestone	US84	K	Type C	736+150'	EB
Chorus Christi	Nueces	IH37	R	PFC	15+0.73	NB
	San Patricio	IH37	R	PFC	17+0.64	NB
Fort Worth	Johnson	IH35	WL	Type D	29-100'	SB
Houston	Brazoria	SH288	R	PFC	496+1.35	SB
	Conroe	IH45	L	PFC	93+0.1	SB
	Fort Bend	SH6	K	PFC	682+0.75	SB
	Waller	SH6	L	PFC	628+1	NB
Lubbock	Crosby	US 62	L	CMHB-C	352+1.7	WB
	Floyd	US 62	R	CMHB-C	386+0.1	EB
	Garza	SH207	K	CMHB-F	254+1.7	SB
		US84	L	CMHB-C	352+1.7	NB
	Lynn	FM1317	K	CMHB-F	296 +80'	EB
		US380	K	CMHB-C	320+1.7	EB
		US87	L	CMHB-C	306+1-400'	NB
Terry	US62	L	Novachip	296+0.5+100'	WB	
Odessa	Ector	IH20	R	CMHB-F	117+0.7	EB
	Midland	IH20	R	PFC	147+0.5+400'	EB

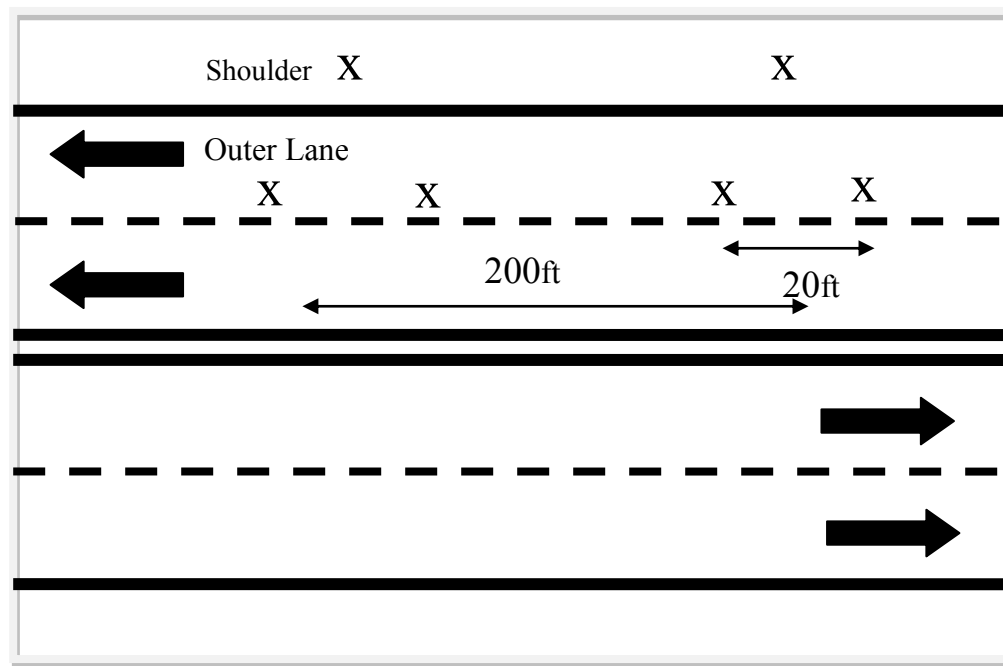
TABLE 46 Continued

District	County	Highway	Des.	Mix Design	TRM	Dir.
Paris	Hopkins	IH30	L	PFC	134-.035	WB
		SH154	K	Type D	674-0.74	NB
San Antonio	Bexar	IH35	R	PFC	168+0.8	NB
		SH16	R	Type C	614	SB
		US90	R	Type C	560+1.75	EB
	Wilson	US181	R	Novachip	518	SB
Tyler	Anderson	US287	K	Type D	604+0.1	NB
	Greg	IH20	L	Type D	580+0.7	WB
				Type C	591-200'	WB
	Smith	IH20	L	Type C	550-500'	WB
				Type C	557-500'	WB
	Van Zandt	IH20	L	Type C	518-200'	WB
Waco	Hill	IH35	L	SMA-D	358-200'	SB
	McLennan	SH6	L	PFC	502-0.1	WB
Wichita Falls	Clay	US287	K	PFC	532+0.5	NB
		US287	L	PFC	368 + 1.8	WB
	Wichita	SH240	L	PFC	470-0.85	NB
		SL473	K	PFC	192-0.35	SB
Yoakum	Gonzales	IH10	L	PFC	636+0.2	WB
	Victoria	US59	L	Type C	632+60'	NB
		US59	R	PFC	632+0.5	SB
				PFC	634+120'	SB
	Wharton	US59	L	Type C	562-550'	NB
		US59	R	PFC	560+1+260'	SB
Austin	SH36	K	Type D	612+1.5+200'	SB	

Measurements were conducted in the outer lane, as the skid trailer measurements are typically performed on this lane in the case of multiple lanes. The outer lane experiences the most polishing because most truck traffic uses this lane. Measurements were done on the travel lane and shoulder. Because the shoulders are subjected to little or no traffic, skid resistance measurements were assumed to represent the initial skid measurements of travel lane.

The DFT and CTMeter devices were positioned in the left wheel-path in all test sections because the skid number is measured by the trailer by locking the left wheel. Six locations were tested in each section. Two locations were at the shoulder and four locations were in the outer lane. Two DFT and six CTMeter readings were performed at

each location. The DFT and CTMeter measurements were conducted at the same exact locations following ASTM E 2157 and ASTM E 1911 procedures, respectively. FIGURE 107 shows the layout of the measurement locations. During the testing, the research team avoided extreme cold ambient temperature or rain. Information about construction, traffic, and skid trailer measurement data was also collected. These sections did not include any surface treatments. Appendix D shows some examples of pavement texture measured by CTMeter and DFT during filed measurements.



(a)



(b)



(c)

FIGURE 107 Layout of the measurement section: (a) schematic of measurement plan; (b) CTMeter measurement; (c) DFT measurement.

Based on the AADT traffic information, the TMF on the test section was calculated. The following assumptions were made in calculating the TMF:

- The number of vehicles is the same in both directions (AADT was divided by two).
- The TxDOT-recommended traffic lane distribution factors, shown in TABLE 47, are applicable for calculating the percent of traffic in the outer lane.
- All vehicle types have the same polishing effect on the pavement surface. This assumption was employed because there is no published information available on the difference in polishing effects between trucks and passenger cars.

TABLE 47 Lane Distribution Factor

Total Number of Lanes in Both Directions	Lane Distribution Factor
Less than or equal to 4	1
6	0.7
Greater than or equal to 8	0.6

ANALYSIS OF FIELD MEASUREMENTS

This section presents the DFT and CTMeter results and a comparison between the frictional characteristics of field sections and the laboratory slabs that were tested in the laboratory phase of this study. The PIARC model was developed to express IFI as a function of DFT results obtained according to ASTM E 1911 (Equation 13) and skid number obtained by a skid trailer with a smooth tire according to ASTM E 274 (Equation 14) (167). The S_p value in these two equations is a function of MPD (see Equation 15), which is obtained using the CTMeter device:

$$IFI = 0.081 + 0.732DFT_{20} e^{\frac{-40}{S_p}} \quad (13)$$

$$IFI = 0.045 + 0.925 \times 0.01 \times SN(50) e^{\frac{20}{S_p}} \quad (14)$$

$$S_p = 14.2 + 89.7MPD \quad (15)$$

The measured range of the MPD values using the CTMeter for selected pavement sections was quite wide (from 0.32 mm to 2.65 mm). FIGURE 108 shows the mean MPD values measured at the shoulder for the different mixes, with the PFC mixes having higher MPD values compared with Type C and Type D mixes. Type D mixes had the lowest MPD values because the gradation used in this mix is finer than the other mixes. Higher macrotexture mixes allow water to drain quickly from the tire-pavement interface and increases the skid resistance at higher speeds. The porous nature of PFC surface also expedites the drainage of water from the surface.

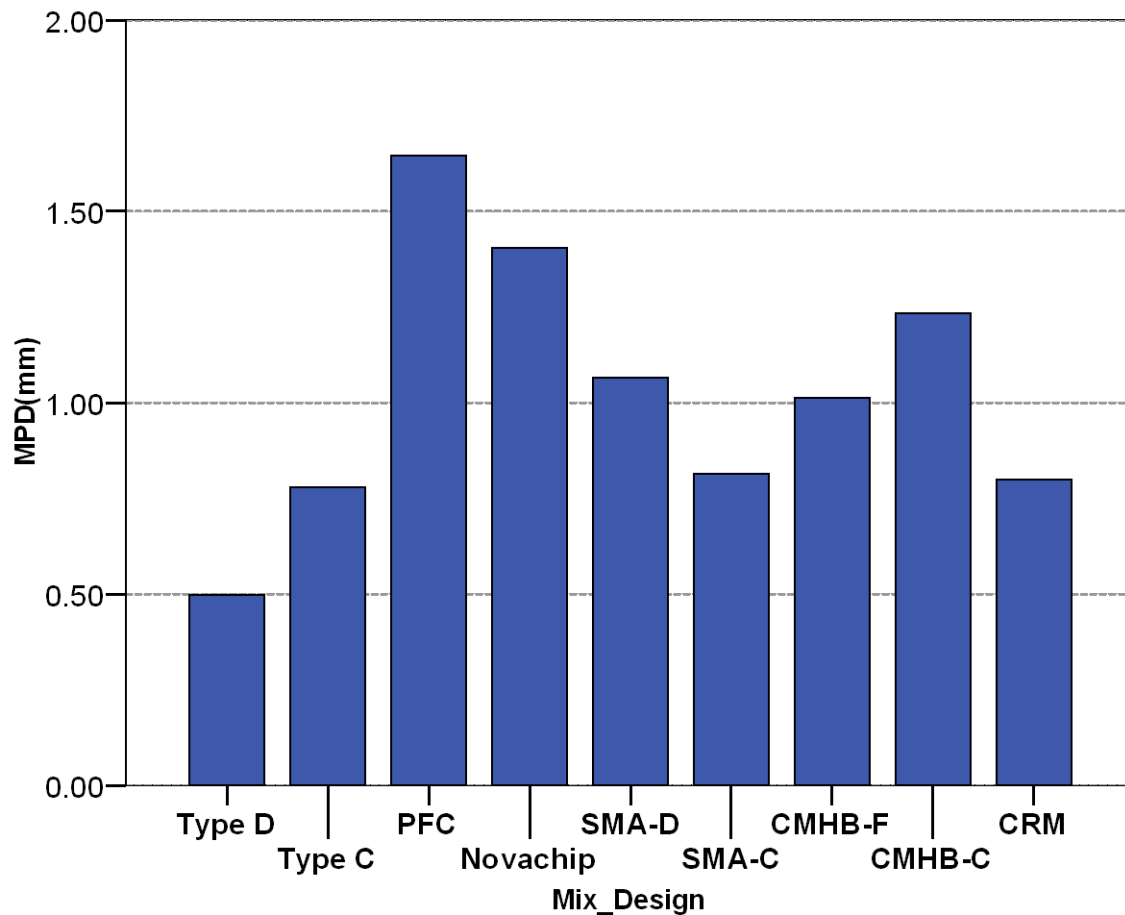


FIGURE 108 Measured MPD values for different mix types.

FIGURE 109 shows very high scatter in the relationship between measured skid number and MPD. The results indicate that there is no direct relationship between MPD and measured skid number.

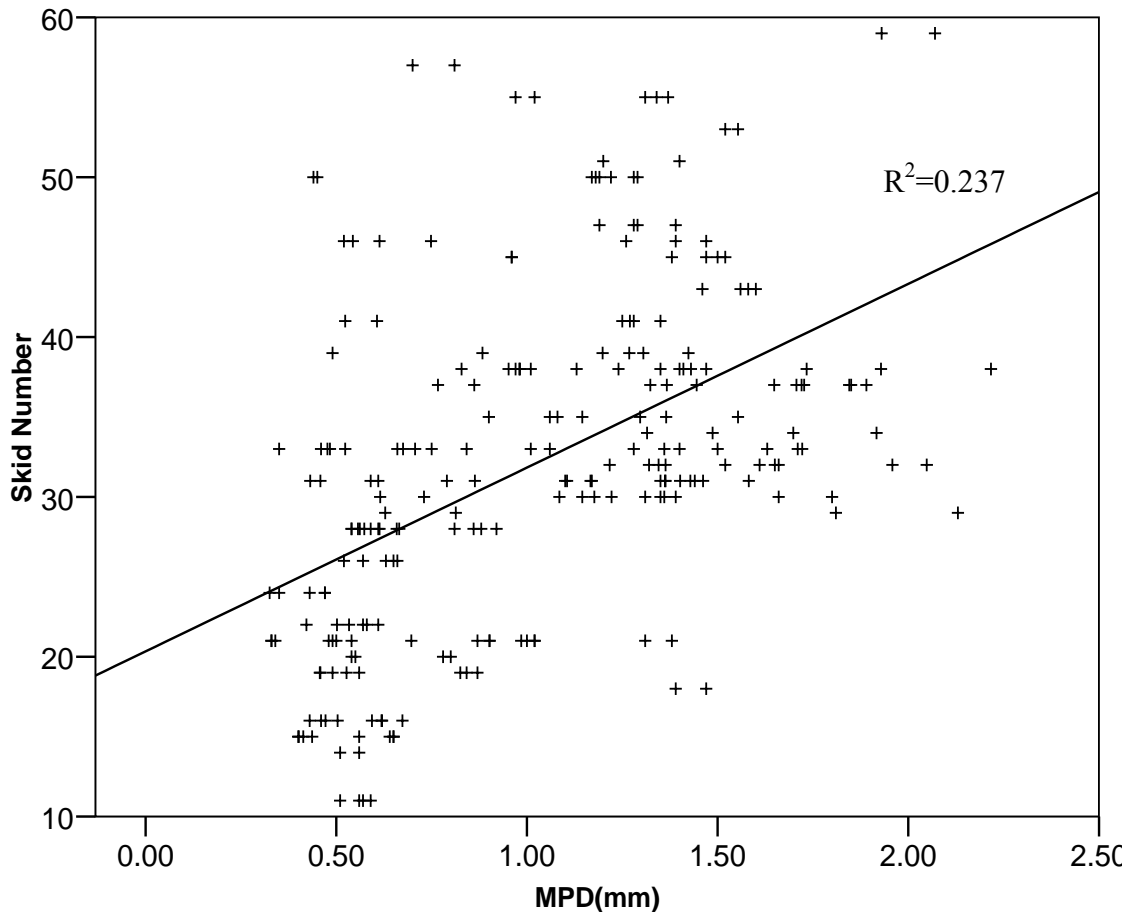


FIGURE 109 Mean profile depth vs. measured skid number.

FIGURE 110 shows the mean DFT_{20} for the different aggregate types used in constructing pavement sections. Dynamic friction measured at 20 km/h measured by DFT is a measure of microtexture. FIGURE 110 illustrates that the initial microtexture level depends on aggregate type. Moreover, sandstone has a very high microtexture compared to other aggregate types. The microtexture of limestone aggregate is generally low. Because of the diversity of constituents included in the limestone aggregates used in this study, the variability of measured microtexture for this aggregate is high. FIGURE 110

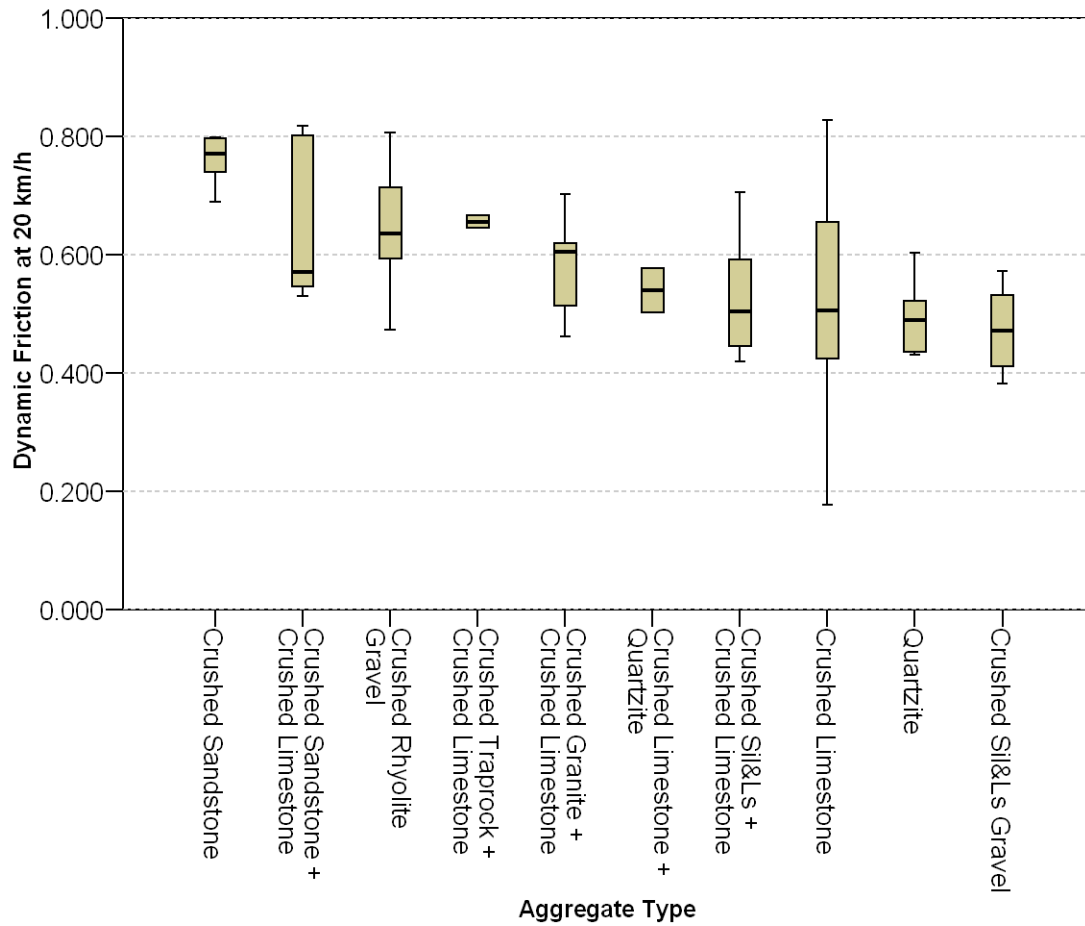


FIGURE 110 Mean dynamic friction at 20 km/h for different aggregates.

also shows that the combination of limestone with other aggregate types such as quartzite or traprock results in a higher microtexture.

FIGURE 111 demonstrates the measured DFT_{20} values at different traffic levels for different aggregate types. Limestone aggregate rapidly loses its initial texture under the polishing effect of traffic. Other aggregate types such as sandstone, quartzite, and granite are able to maintain their initial texture. Moreover, mixing limestone with other aggregate types such as quartzite and granite can help this aggregate in maintaining the initial texture.

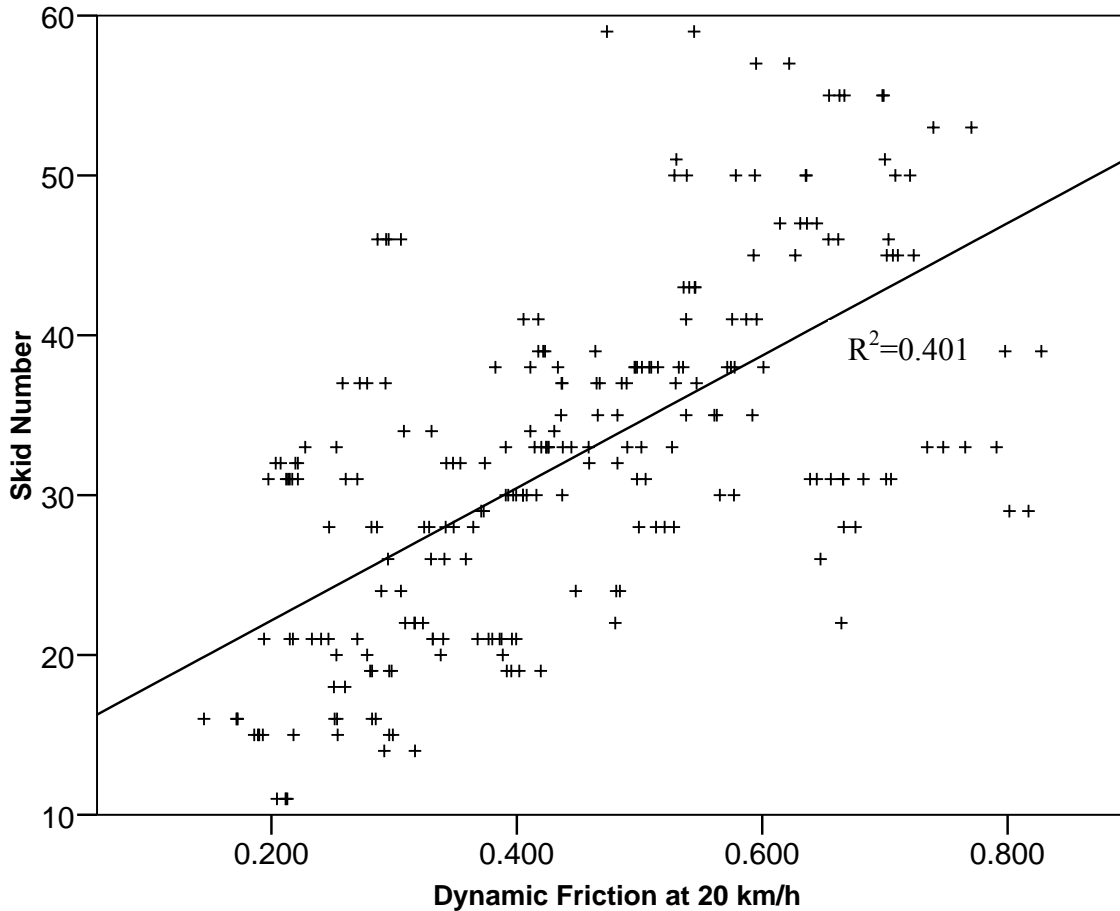


FIGURE 112 Dynamic friction at 20 km/h vs. measured skid number for different mix types.

SUMMARY

This chapter presented the results of measuring pavement friction and texture analysis of 64 field sections using the DFT and CTMeter, respectively. The sections were selected such that they cover a wide range of material types and traffic conditions and, more importantly, included some of the mixtures that were tested in the laboratory.

The results of the macrotexture measurements by CTMeter showed that the PFC mixes had higher MPD values compared with other mixes. Type D had the lowest MPD values due to its finer gradation.

The DF_{20} value, which is an indication of microtexture, revealed that the initial pavement microtexture depended on aggregate type. Mixes containing sandstone aggregate had higher initial microtexture compared to other aggregate types such as limestone. The rate of polishing was also found to be a function of aggregate type. For example, limestone aggregate had a high rate of polishing, but sandstone and granite could maintain their initial texture over time. Aggregate combinations were found to help with maintaining the overall pavement friction. For example, a combination of sandstone and limestone functions considerably better than limestone alone.

The results illustrated that there was no correlation between the MPD values and measured skid number. The results also indicated that there was a fair correlation between DF_{20} and measured skid number for all mixes. The next chapter describes the method to combine the result of the laboratory measurements and field measurements to develop a model for asphalt pavement skid number.

CHAPTER VIII
A MODEL FOR PREDICTING SKID NUMBER
OF ASPHALT PAVEMENTS

INTRODUCTION

The results of laboratory and field measurements of this study have shown that the influence of a certain aggregate type on mixture skid resistance depends on the mixture design. Therefore, a method is presented in this chapter to predict the skid number of asphalt pavements as a function of traffic based on aggregate characteristics and mix design. This system will be very valuable for selecting the optimum combination of aggregate type and mixture design in order to achieve the desired level of skid resistance. Some of the equations presented previously in this dissertation are also included in this chapter in order to present a complete procedure for predicting the field skid number without having to refer to equations presented in other chapters.

DEVELOPMENT OF THE SYSTEM FOR PREDICTING SKID NUMBER

As discussed in Chapter V of this dissertation, a method was developed during the laboratory phase for predicting IFI as a function of number of loading cycles (N) using the NCAT polishing device. As shown in Equations 16 to 20, the parameters of the relationship of IFI versus N are dependent on aggregate texture measurements from AIMS before and after polishing in the Micro-Deval and aggregate gradation.

$$IFI(N) = a_{mix} + b_{mix} \cdot \exp(-c_{mix} \cdot N) \quad (16)$$

$$F(x; \kappa, \lambda) = 1 - \exp[-(x/\lambda)^\kappa] \quad (17)$$

$$a_{mix} = \frac{18.422 + \lambda}{118.936 - 0.0013 \times (AMD)^2} \quad (18)$$

$$a_{mix} + b_{mix} = 0.4984 \ln(5.656 \times 10^{-4} (a_{agg} + b_{agg}) + 5.846 \times 10^{-2} \lambda - 4.985 \times 10^{-2} \kappa) + 0.8619 \quad (19)$$

$$c_{mix} = 0.765 \cdot e^{\left(\frac{-7.29710^{-2}}{c_{agg}}\right)} \quad (20)$$

where:

a_{mix} = terminal IFI value for the mix;

$a_{mix} + b_{mix}$ = initial IFI value for the mix;

c_{mix} = rate of change in IFI for the mix;

AMD = aggregate texture after Micro-Deval;

$a_{agg} + b_{agg}$ = aggregate initial texture using texture model;

c_{agg} = aggregate texture rate of change using texture model;

k-value = shape factor of Weibull distribution used to describe aggregate gradation; and

λ -value = scale factor of Weibull distribution used to describe aggregate gradation.

The $a_{agg} + b_{agg}$ and c_{agg} are obtained from measuring aggregate texture after 105- and 180-min time intervals of polishing in the Micro-Deval. It would be desirable to predict these values from only two texture measurements of aggregates using AIMS before Micro-Deval (BMD) and after Micro-Deval (AMD) polishing for 105 min, which is the standard time currently used by TxDOT. For this purpose, nonlinear regression analysis was used to examine the possibility of predicting a_{agg} , b_{agg} , and c_{agg} from AMD and BMD texture. A total of nine aggregate samples were used in this regression analysis. Moreover, these samples were part of a database of AIMS measurements of aggregates in the laboratory phase combined with three other aggregate sources. Equations 21 through 23 can be used to determine the texture model coefficients:

$$a_{agg} + b_{agg} = 0.983BMD + 5.258 \quad R^2 = 0.98 \quad (21)$$

$$a_{agg} = 0.811AMD + 4.258 \quad R^2 = 0.94 \quad (22)$$

$$c_{agg} = \frac{A + TL}{B + C \times ARI} \quad R^2 = 0.74 \quad (23)$$

where BMD and AMD are the AIMS texture indices measured before and after Micro-Deval polishing of aggregates, respectively. A, B, and C are regression constants and

have the value of -0.357 , 20.18 , and -23.676 , respectively. TL and ARI are texture loss and aggregate roughness index, respectively, and are defined as:

$$TL = \frac{BMD - AMD}{AMD} \quad (23a)$$

$$ARI = \frac{AMD/BMD}{\sqrt{1 - (AMD/BMD)^2}} \quad (23b)$$

The polishing rate (c_{mix}) and the terminal friction value (a_{mix}) of an asphalt mixture can be determined using Equations 21 to 23 along with Equations 18 and 20. Because the scale and shape parameter (λ and κ) of the Weibull cumulative distribution function are also required in Equations 18 and 20, a nonlinear regression analysis can be used. Eight Texas mix designs were included in this analysis, as shown in TABLE 48. The gradation boundaries for these mix designs were extracted from the TxDOT specification manual, and the scale and shape parameter (λ and κ) of the cumulative Weibull distribution was calculated using the SOLVER function of Microsoft[®] Excel. For most cases, the coefficient of determination of the regression was more than 0.95.

TABLE 48 Calculated Scale and Shape Factors for Different Mixes

Mix Design	Scale Parameter λ	Shape Parameter κ
Type C	5.605	0.830
Type D	4.052	0.864
PFC	10.054	3.954
SMA_D	9.201	1.494
Crack Attenuating Mixture (CAM)	3.168	1.000
SMA_C	9.431	1.276
CMHB_C	8.578	1.077
CMHB_F	5.574	1.415

Next, the results of the laboratory measurements and field measurements were used to develop a relationship between laboratory polishing and field polishing in terms of the number of polishing cycles in the laboratory (N) and TMF. Equation 16 was

developed for predicting the IFI values in a mixture as a function of N (number of the cycles in terms of thousands of cycles in the NCAT polishing device). Based on the measured DF_{20} values and macrotexture measurements by the CTMeter, the IFI values were determined for each section using Equations 13 and 15 for each pavement section.

Then, Equation 16 was used to determine the N value that would give the same IFI that is calculated using Equation 13. The coefficients a_{mix} , b_{mix} , and c_{mix} that were substituted in Equation 16 were for the same mixtures that were tested in the field. A statistical analysis was performed to determine the outliers that were removed from the analysis. A non-linear regression analysis was performed to find the relationship between TMF and number of polishing cycles (N), as in Equation 24 and Figure 29.

$$N = TMF \times 10^{\frac{1}{A+B \times c_{mix} + \frac{C}{c_{mix}}}} \quad R^2 = 0.74 \quad (24)$$

where A, B, and C are regression coefficients and have the values of -0.452 , -58.95 , and 5.834×10^{-6} , respectively. The relationship between N and TMF is not only a function of traffic but also a function of mixture polishing characteristics denoted as the rate of change in IFI (c_{mix}) in Equation 24. FIGURE 113 shows the relationship between the measured and calculated number of polishing cycles. The proposed equation has a high R-squared value and can be used to estimate the variation of IFI in the field in terms of TMF.

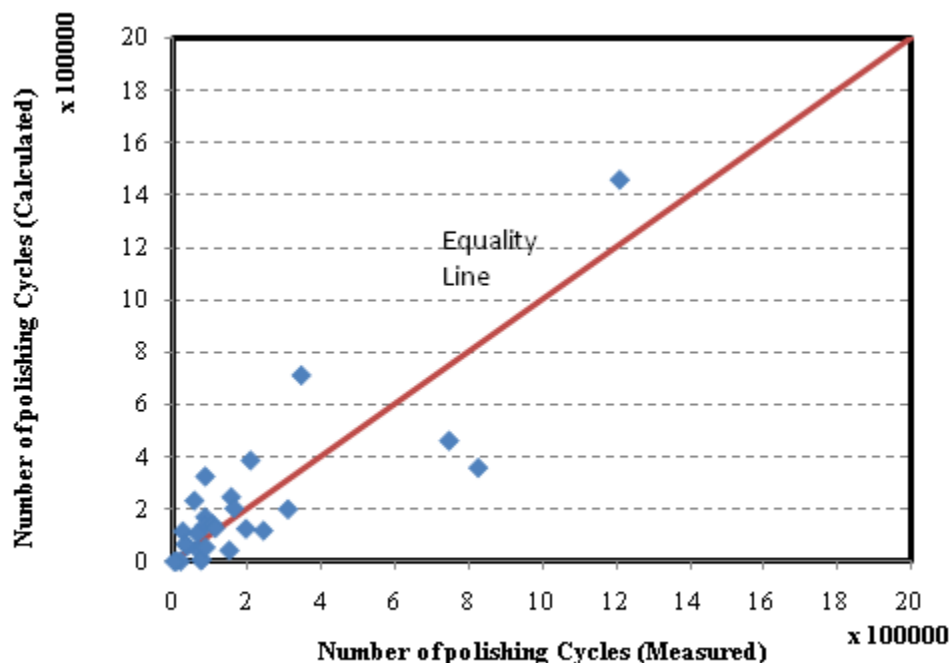


FIGURE 113 TMF vs. number of polishing cycles.

The last step in the analysis was to predict the SN value given the IFI. In order to obtain the relationship between measured skid resistance by the skid trailer and DFT/CTMeter combination, the PIARC procedure for finding the IFI value was used and the IFI values were calculated via DFT, CTMeter, and skid number using Equations 13 to 15.

In principle, Equations 13 and 14 should give the same value for the IFI. Therefore, IFI calculated from Equation 13 can be substituted in Equation 14 to find the SN(50). As illustrated in FIGURE 114, the measured value of SN by the skid trailer is greater than the calculated value using the PIARC equation (167). The R-squared value for the relation is 0.76 and is relatively high. There are two main factors that could explain this difference between SN(50) obtained from Equation 14 and measured values. The first is the propagation of errors. Error is present in the PIARC regression equation and is propagated during the mathematical manipulation required to back-calculate the SN. The second factor is experimental error. Each friction measuring device will generate some experimental error due to the equipment design and human factors and different

simplifying assumptions made in this research. The presence of these errors could account for the differences between the measured and calculated SN.

Based on the relationship between measured and calculated SN values, Equation 14 was modified to account for the difference between calculated and measured skid numbers. Equation 25 shows the modified form of Equation 14 to predict the field skid number:

$$SN(50) = 1.41 + 143.19(IFI - 0.045)e^{\frac{-20}{S_r}} \quad (25)$$

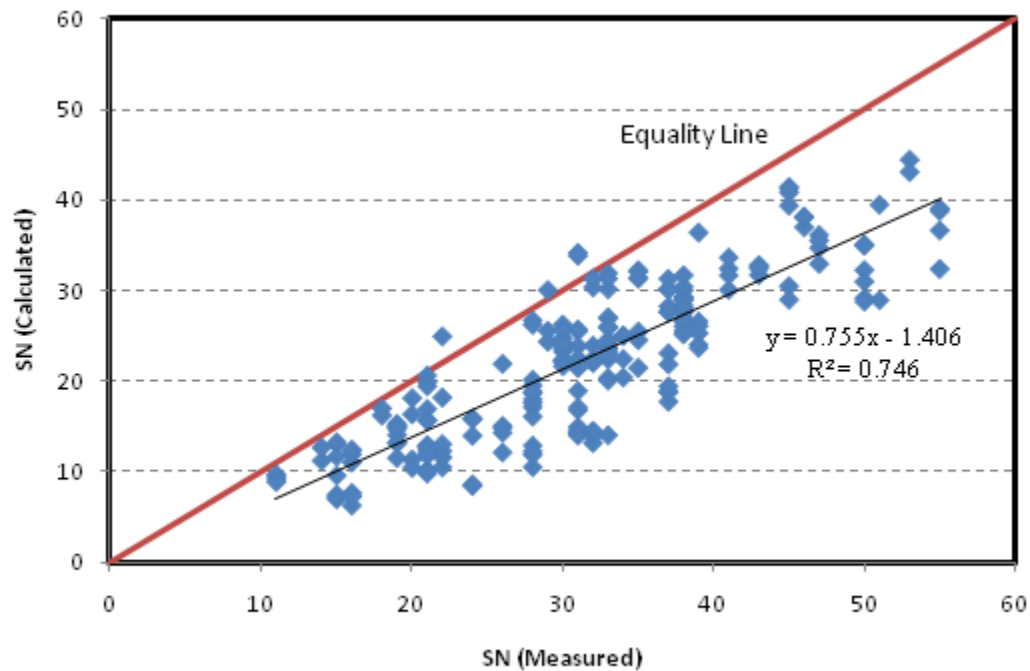


FIGURE 114 Measured skid number vs. calculated skid number using PIARC equation.

FIGURE 115 shows the measured and calculated skid number values using the modified PIARC equation (Equation 25). The calculated and measured values are relatively close, and the modified equation can be used to predict the measured skid number.

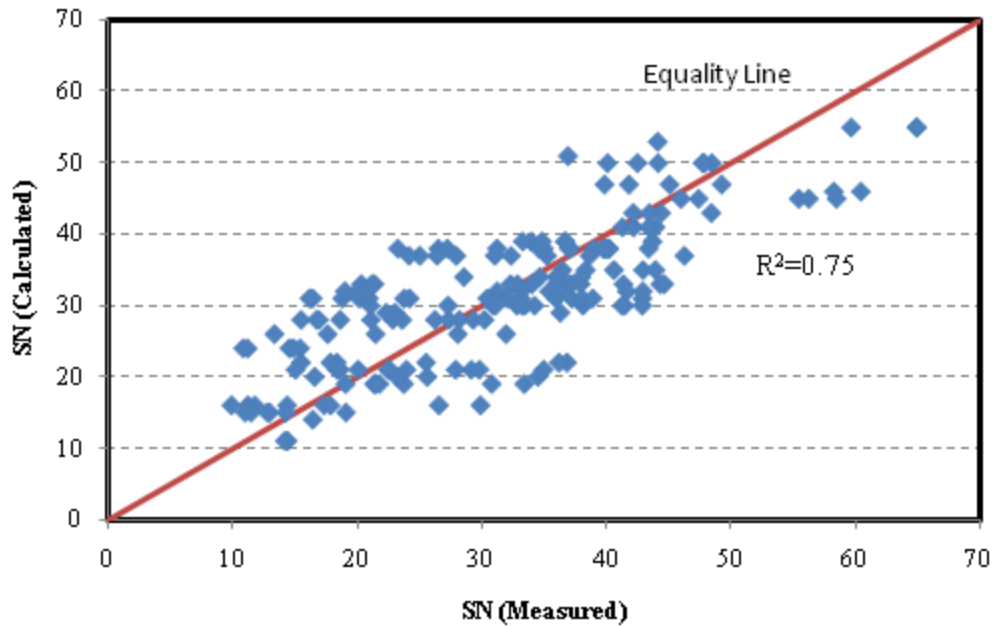


FIGURE 115 Measured skid number vs. calculated skid number using modified PIARC equation.

Equation 25 includes the S_p value, which is a function of MPD. Macrotexture, which is represented by MPD, is a function primarily of mixture gradation. Therefore, a nonlinear regression analysis was conducted to determine MPD as a function of the gradation parameters λ and κ . The best correction found between measured MPD and Equation 26 shows these gradation parameters. FIGURE 116 shows the relationship between measured and calculated MPD values.

$$MPD_0 = 0.139\lambda + 0.086\kappa - \frac{0.041}{\kappa^4} \quad R^2 = 0.79 \quad (26)$$

where λ and κ are Weibull distribution function coefficients.

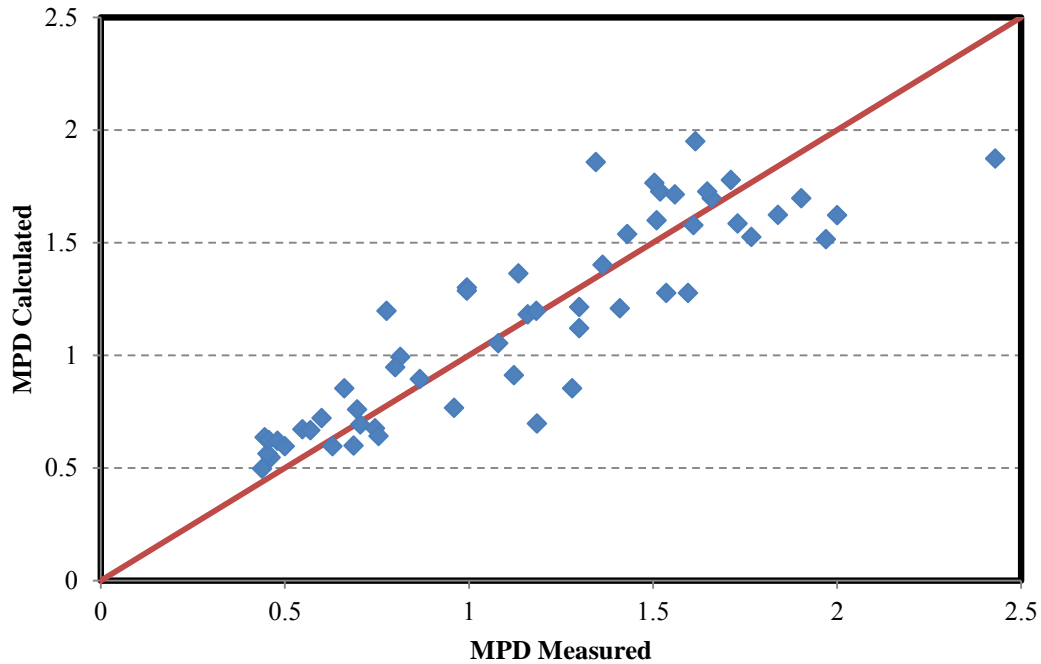


FIGURE 116 Relationship between measured and calculated MPD values.

SENSITIVITY ANALYSIS OF PREDICTION SYSTEM

The sensitivity analysis was conducted using several aggregate types and mixture designs. Aggregates were selected to represent a wide spectrum of texture values corresponding with the minimum, maximum, first quartile, second quartile, and third quartile of terminal texture (a_{agg}) and polishing rate (c_{agg}), as shown in Tables 49 and 50, respectively.

TABLE 49 Selected Aggregates Based on Terminal Texture

Sample	Quartile	Terminal Texture a_{mix}	Polish Rate	Material Type	Material Group
1	Minimum	26.67	0.0233	Crushed Limestone	3. LS-Dolomites
2	1st	56.34	0.0094	Crushed Limestone	3. LS-Dolomites
3	Median	72.46	0.0145	Crushed Limestone	3. LS-Dolomites
4	3rd	92.43	0.0049	Crushed Sandstone	2. Sandstone
5	Maximum	216.34	0.0298	Crushed LS Rock Asphalt	6. Miscellaneous

TABLE 50 Selected Aggregates Based on Polishing Rate

Sample	Quartile	Polish Rate c_{mix}	Terminal Texture a_{mix}	Aggregate Type	TxDOT Aggregate Group
6	Minimum	0.0001	84.55	Crushed Sil. & LS Gravel	4. Gravels
7	1 st Quarter	0.0182	216.34	Crushed LS Rock Asphalt	6. Miscellaneous
8	Median	0.0227	109.58	Crushed Limestone	3. LS-Dolomites
9	3 rd Quarter	0.0253	69.17	Crushed Limestone	3. LS-Dolomites
10	Maximum	0.0364	279.45	Crushed LS Rock Asphalt	6. Miscellaneous

Using Equations 18 and 20, the terminal friction value and polish rate of change were calculated. FIGURE 117 shows the terminal friction values for different aggregates and mix designs.

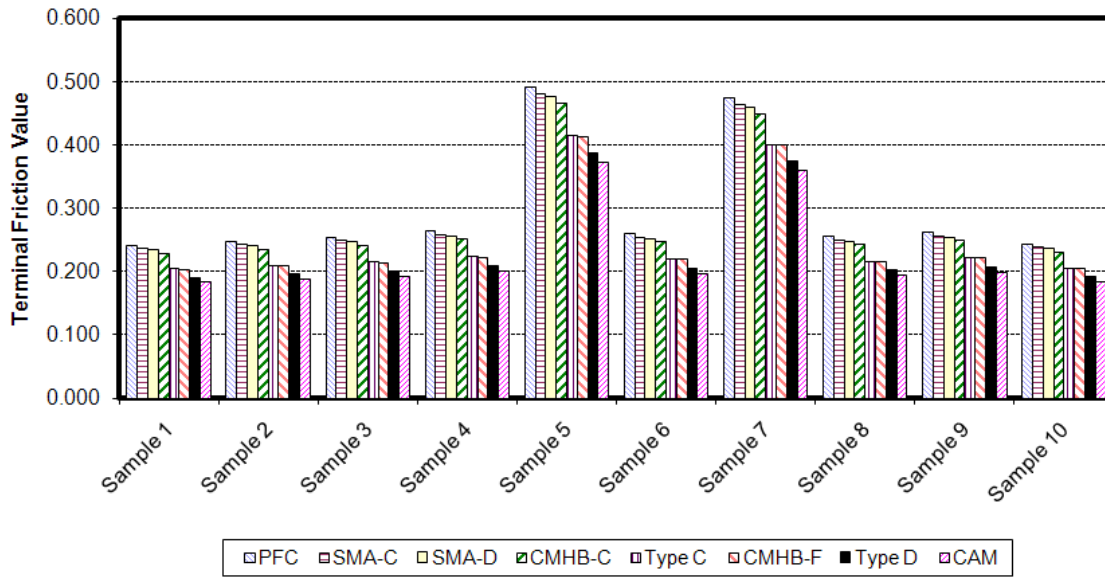


FIGURE 117 Terminal friction values for different aggregates and mix designs.

The PFC mixes have the highest terminal friction values. Stone mastic asphalt (SMA-C and SMA-D) and a coarse matrix high binder (CMHB-C) are the next mixes in the list. The terminal polish values of the Type C and CHMB-F mixes are almost the same. Type D mixes and crack attenuating mix (CAM) have the lowest terminal friction among all mixes. Among the aggregates, sample 10 and sample 5 have the highest terminal friction values. These values can be attributed to the high texture index after Micro-Deval. The difference among other aggregates is not significant. FIGURE 118 shows the polishing rate for different aggregates.

Given polishing rate and initial and terminal friction values, IFI can be calculated using Equations 16 and 24 as a function of TMF. For instance, Figures 119 and 120 illustrate the IFI and SN values for sample 1. The SN values were calculated using Equation 23 as a function of TMF and are plotted in FIGURE 120. Figures 119 and 120 indicate the use of the model to predict the variation of skid number as a function of traffic.

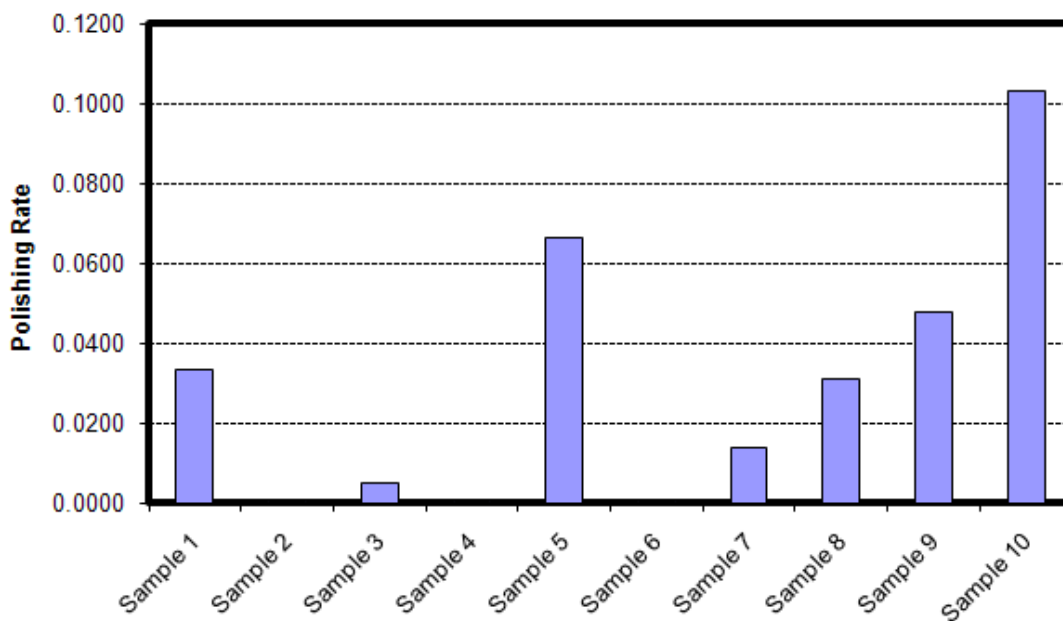


FIGURE 118 Polishing rate for different aggregates.

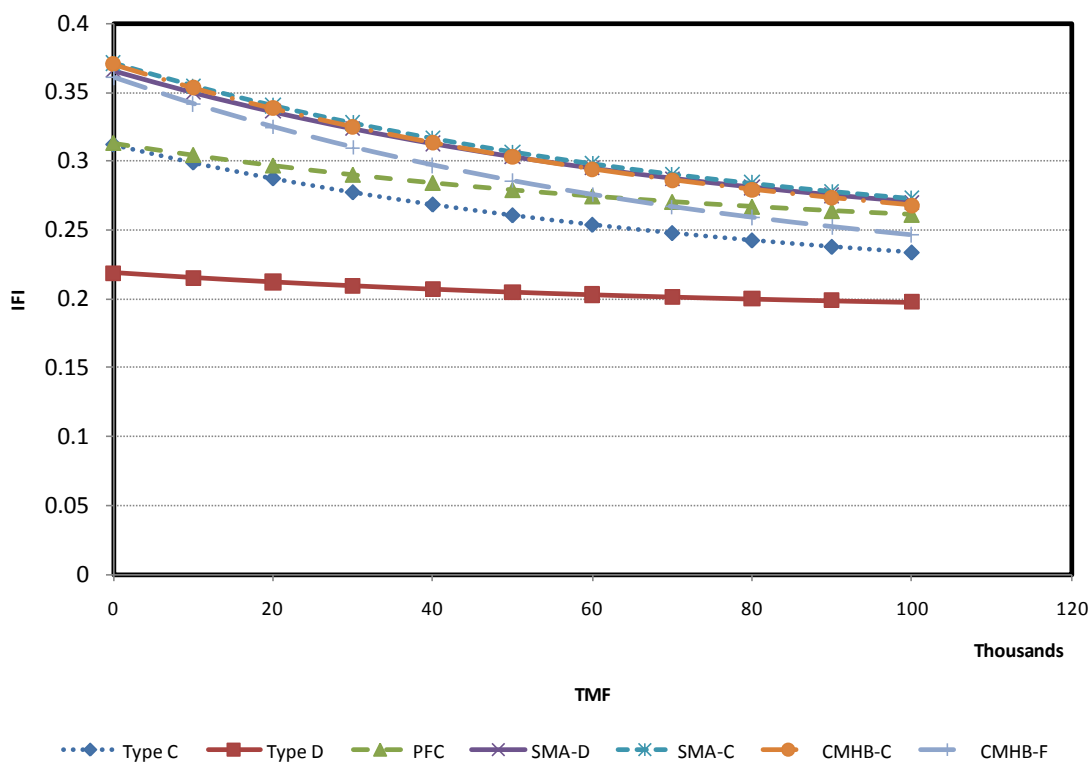


FIGURE 119 IFI values as a function of TMF for sample 1.

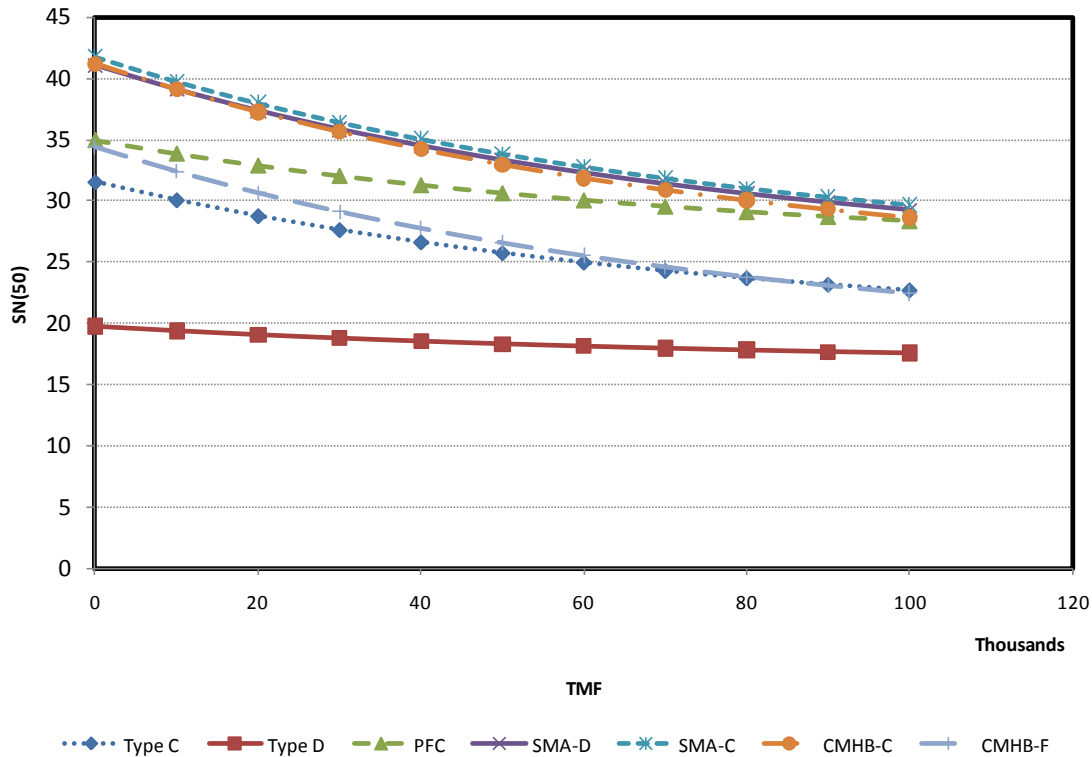


FIGURE 120 SN values as a function of TMF for sample 1.

RECOMMENDED SYSTEM FOR PREDICTING SKID NUMBER

This chapter presented a system for predicting the skid number of asphalt mixtures. This system consists of the following steps:

1. Measure aggregate texture using AIMS before Micro-Deval (Appendix C).
2. Measure aggregate texture using AIMS after Micro-Deval (Appendix C).
3. Calculate $a_{agg} + b_{agg}$ using Equation 21.
4. Calculate a_{agg} Equation 22.
5. Calculate TL using Equation 23a.
6. Calculate ARI using Equation 23b.
7. Calculate c_{agg} using Equation 23.
8. Determine the gradation parameters (λ and κ) from TABLE 48 or by fitting the cumulative Weibull function (Equation 17) to the gradation curve.
9. Calculate a_{mix} using Equation 18.

10. Calculate $a_{mix} + b_{mix}$ using Equation 19.
11. Calculate c_{mix} using Equation 20.
12. Calculate MPD using Equation 26.
13. Calculate S_p using Equation 15.
14. Calculate IFI as a function of N using Equation 11.
15. Calculate TMF in terms of N using Equation 24.
16. Calculate SN using Equation 25.

ILLUSTRATION OF AN AGGREGATE CLASSIFICATION SYSTEM BASED ON PROPOSED MODEL

In this section, the model is used to illustrate the influence of aggregate characteristics and aggregate gradation on skid resistance. In addition, the results presented herein demonstrate how this model can be used to select the optimum aggregate characteristics and gradation such that the required skid resistance level is achieved given a certain traffic level.

The analysis involved the use of four AADT/lane levels representing interstate, U.S. highway, state highway, and farm-to-market sections from the state of Texas. Four different mix types commonly used in the state of Texas were selected, and scale and shape parameters of the corresponding Weibull function were determined. The analysis utilized the texture characteristics of aggregates K, H, and M, as listed in TABLE 38. In order to facilitate the comparison between the various sections, the SN(50) values in TABLE 51 were used to classify the pavement sections after 5 years of service.

TABLE 51 Skid Number Threshold Values after 5 Years of Service

Aggregate Class	SN Threshold Value
High	$SN(50) > 30$
Medium	$21 < SN(50) < 29$
Low	$SN(50) < 20$

Table 8 shows the classification of the various pavement sections. All types of mixtures with aggregate H achieved high skid resistance (level H after 5 years) for all mixtures and all traffic levels. However, the performance of mixtures incorporating aggregates K and M was dependent on the mixture type and traffic level. Another observation is that PFC and SMA mixes with aggregate K maintained level H of skid resistance irrespective of the traffic level, while mixture M with the same aggregate experienced a reduction in skid resistance from H to M when the AADT/lane reached 5800. These results clearly demonstrate how the proposed model provides flexibility for engineers to select an aggregate source and a mixture design that achieves the required skid number after a certain traffic level.

TABLE 52 Aggregate Classification for Different Roads

AADT/Lane	Mix Type			
	Type C	Type D	PFC	SMA
Aggregate K				
550	H	L	H	H
5800	M	L	H	H
16800	M	L	H	H
34000	M	L	H	H
Aggregate H				
550	H	H	H	H
5800	H	H	H	H
16800	H	H	H	H
34000	H	H	H	H
Aggregate M				
550	H	M	H	H
5800	M	L	H	H
16800	M	L	H	H
34000	M	L	M	M

SKID ANALYSIS OF ASPHALT PAVEMENTS (SAAP)

A computer program was developed using Visual Basic programming language to execute the steps needed to calculate the skid resistance of asphalt pavements as a

function of traffic. This section describes the program and the steps needed to be taken in order to calculate the pavement skid resistance.

First window (see FIGURE 121) shows the software credentials. In the second step (see FIGURE 122), the mixture gradation is input in the software. The user can either enter the gradation or select one of the standard mixture gradations used in the Texas. If the user chooses to manually enter gradation by clicking on the <input gradation> button, a window pops up (see FIGURE 123) where the amount of percent passing for selected sieves is entered. The user can select any number of sieves and enter the percent passing values for each selected sieve.

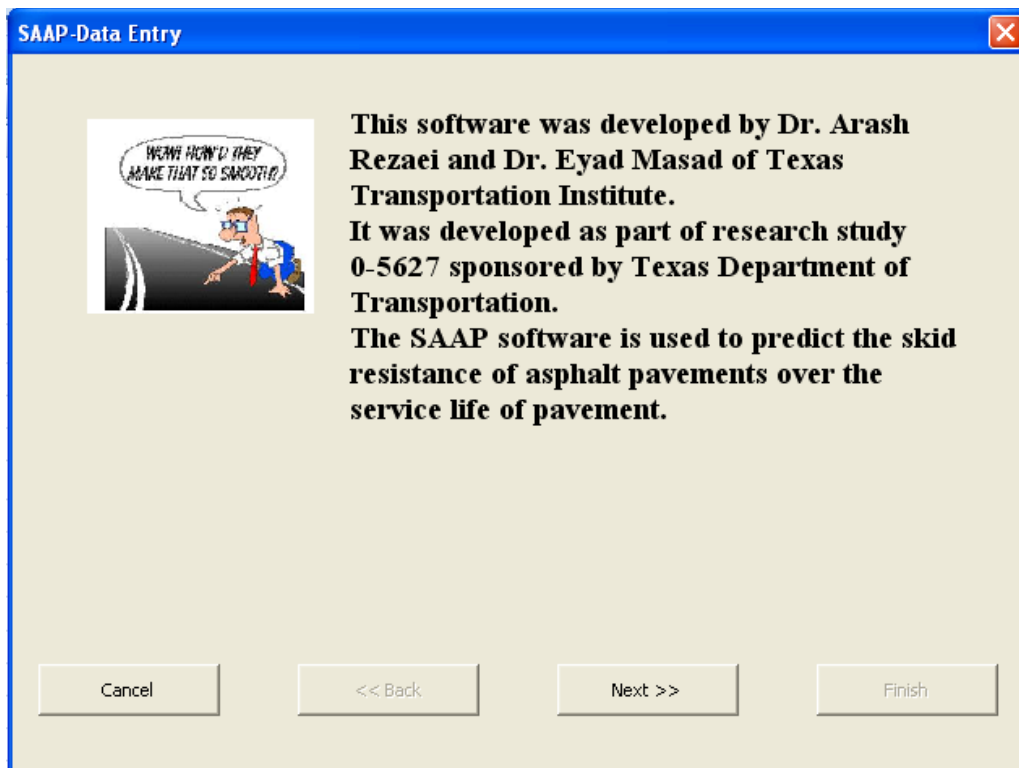


FIGURE 121 Initial window of the program.

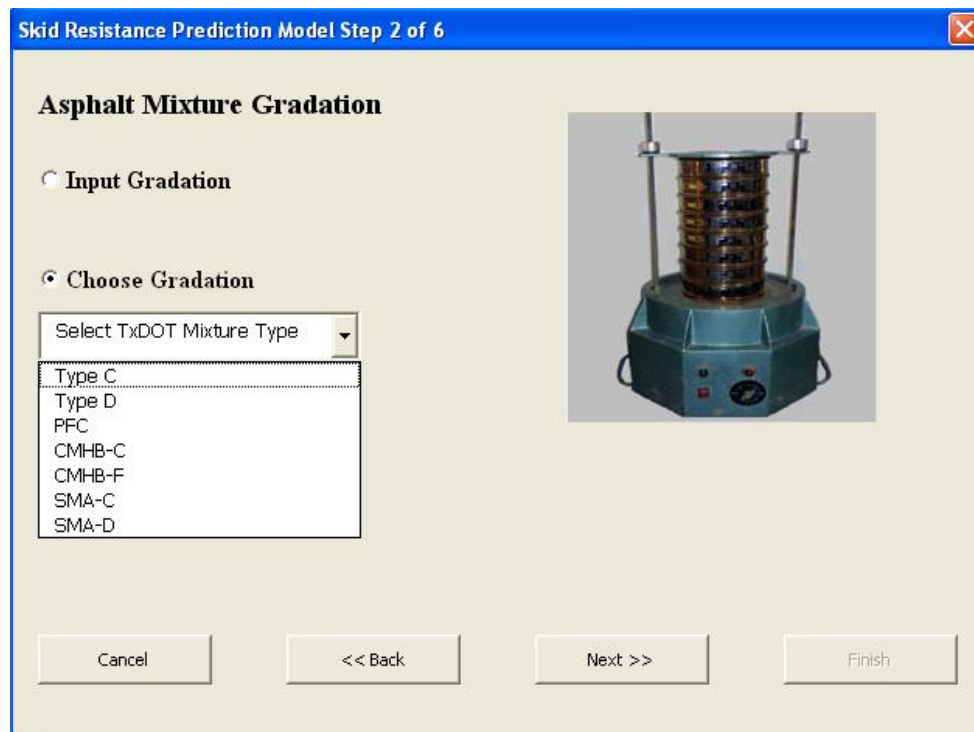


FIGURE 122 Aggregate gradation input window.

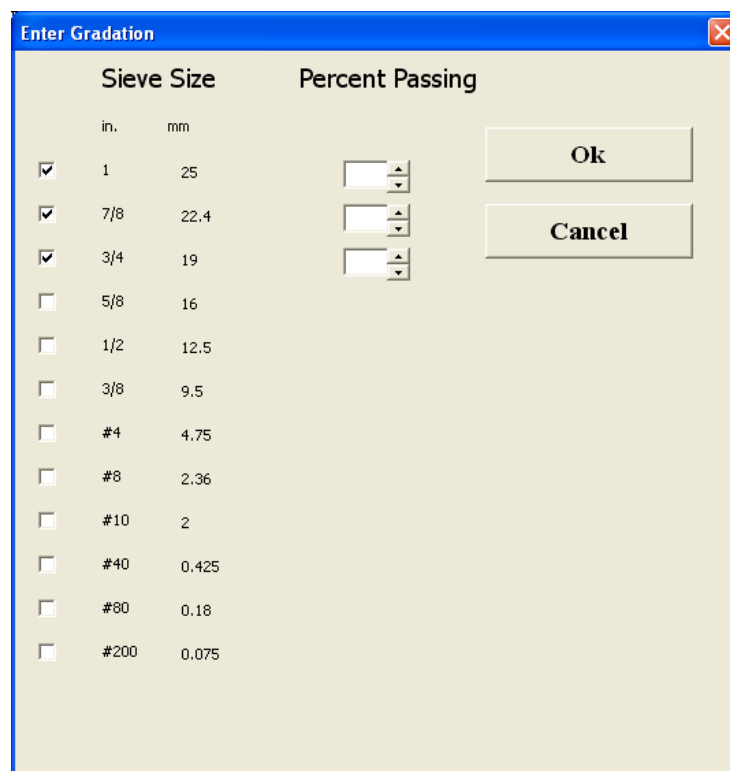


FIGURE 123 Manual aggregate gradation window.

In the next step, the aggregate texture values measured using AIMS are entered (see FIGURE 124). Here, the user has the option to input either the texture measured at two points (before and after polishing for 105 min in the Micro-Deval) or the texture measured at three points (before polishing, after polishing for 105 min and 180 min in the Micro-Deval; see FIGURE 125). The use of three data points provides more accurate estimation of aggregate resistance to polishing. This step as shown in Figures 126 and 127 will be followed by windows to enter the texture data of aggregates from one or more sources. The user can select up to three aggregate sources used in the mixture. As shown in Figures 22 and 23, users can input the texture value of component aggregate sources.

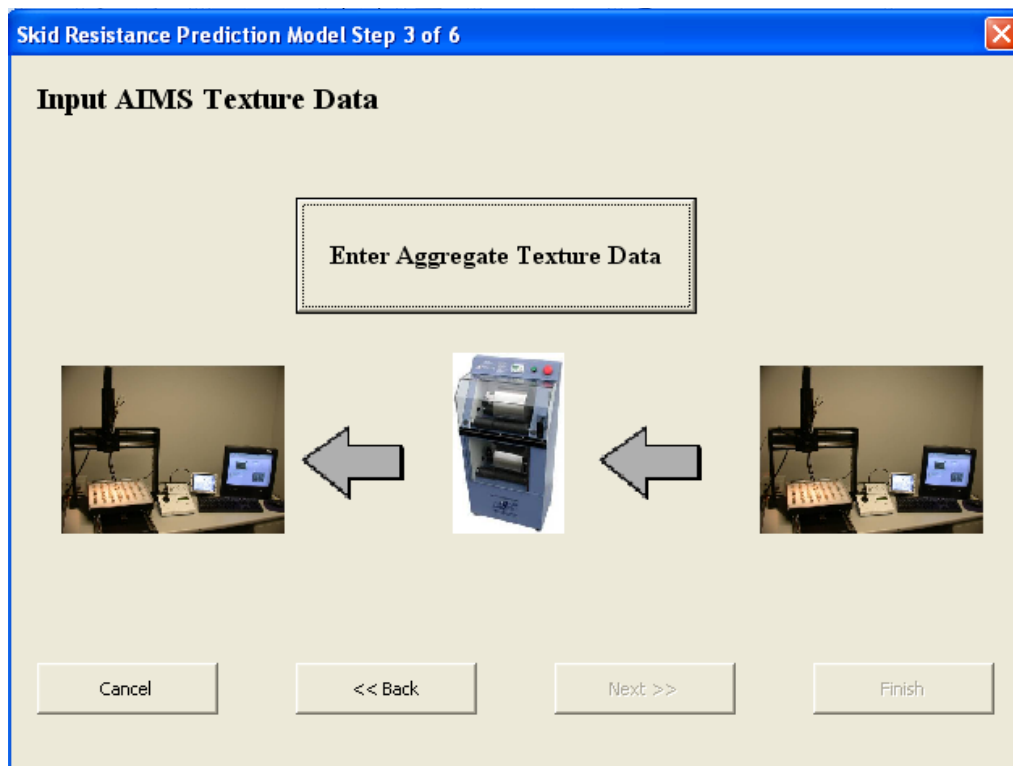


FIGURE 124 AIMS texture data input window.

Skid Resistance Prediction Model Step 3 of 6

Input AIMS Texture Data

Select Number of Data Points

Two Data Points (Before Micro-Deval, After 105 Minutes in Micro-Deval)

Three Data Points (Before Micro-Deval, After 105 Minutes in Micro-Deval, After 180 Minutes in Micro-Deval)

Cancel << Back Next >> Finish

FIGURE 125 Texture data points selection window.

Enter Texture Data

Enter Number of Aggregate Sources: 3

Enter Name of Aggregate Source 1:

Enter Name of Aggregate Source 2:

Enter Name of Aggregate Source 3:

Ok Cancel

Source1	Source2	Source3
Proportion of Aggregate in the Mix (Percentage): <input type="text"/>	Proportion of Aggregate in the Mix(Percentage): <input type="text"/>	Proportion of Aggregate in the Mix(percentage): <input type="text"/>
Percent Passing #4: <input type="text"/>	Percent Passing #4: <input type="text"/>	Percent Passing #4: <input type="text"/>
Texture Before Micro-Deval: <input type="text"/>	Texture Before Micro-Deval: <input type="text"/>	Texture Before Micro-Deval: <input type="text"/>
Texture After 105 minutes Micro-Deval: <input type="text"/>	Texture After 105 minutes Micro-Deval: <input type="text"/>	Texture After 105 minutes Micro-Deval: <input type="text"/>

FIGURE 126 Two-point texture measurement input window.

The screenshot shows a software dialog box titled "Enter Texture Data". At the top, there is a numeric input field for "Enter Number of Aggregate Sources" containing the number "3". Below this are three text input fields for "Enter Name of Aggregate Source 1", "Enter Name of Aggregate Source 2", and "Enter Name of Aggregate Source 3". To the right of these fields are "Ok" and "Cancel" buttons. The main body of the dialog is organized into three columns, each representing a source: "Source1", "Source2", and "Source3". Each column contains five rows of input fields: "Proportion of Aggregate in the Mix(Percentage)", "Percent Passing #4", "Texture Before Micro-Deval", "Texture After 105 minute Micro-Deval", and "Texture After 180 minute Micro-Deval".

FIGURE 127 Three-point texture measurement input window.

By clicking on the <Next > button, the MPD value is entered or calculated (see FIGURE 128). The MPD value can be either entered by the user if the user has measured the MPD value for that particular mix or estimated by the software based on gradation. The following step is when the user inputs the traffic data. In this step, users enter the information about the highway type, total number of through traffic lanes, total AADT for both directions, and percent truck traffic (see FIGURE 129).

Skid Resistance Prediction Model Step 4 of 6

Input Pavement Texture Data

Measured Mean Profile Depth (MPD) in mm

Use SAAP Estimation of Mean Profile Depth (MPD) in mm Based on Mixture Gradation




FIGURE 128 MPD value input window.

Skid Resistance Prediction Model Step 5 of 6

Input Traffic data:

Highway Type

 Divided
 Undivided

Total Number of Through Traffic Lanes

 Two Lanes
 Four Lanes
 Six Lanes
 Eight Lanes or More

Average Annual Daily Traffic (AADT) for Both Directions

Percent Truck Traffic

FIGURE 129 Traffic data input window.

The next step in the software provides the options on how the user wants to see the output. One option is to obtain a prediction of skid resistance as a function of years in service; the other option is to get a classification of the pavement section based on its skid resistance after a specified number of years (see FIGURE 130).

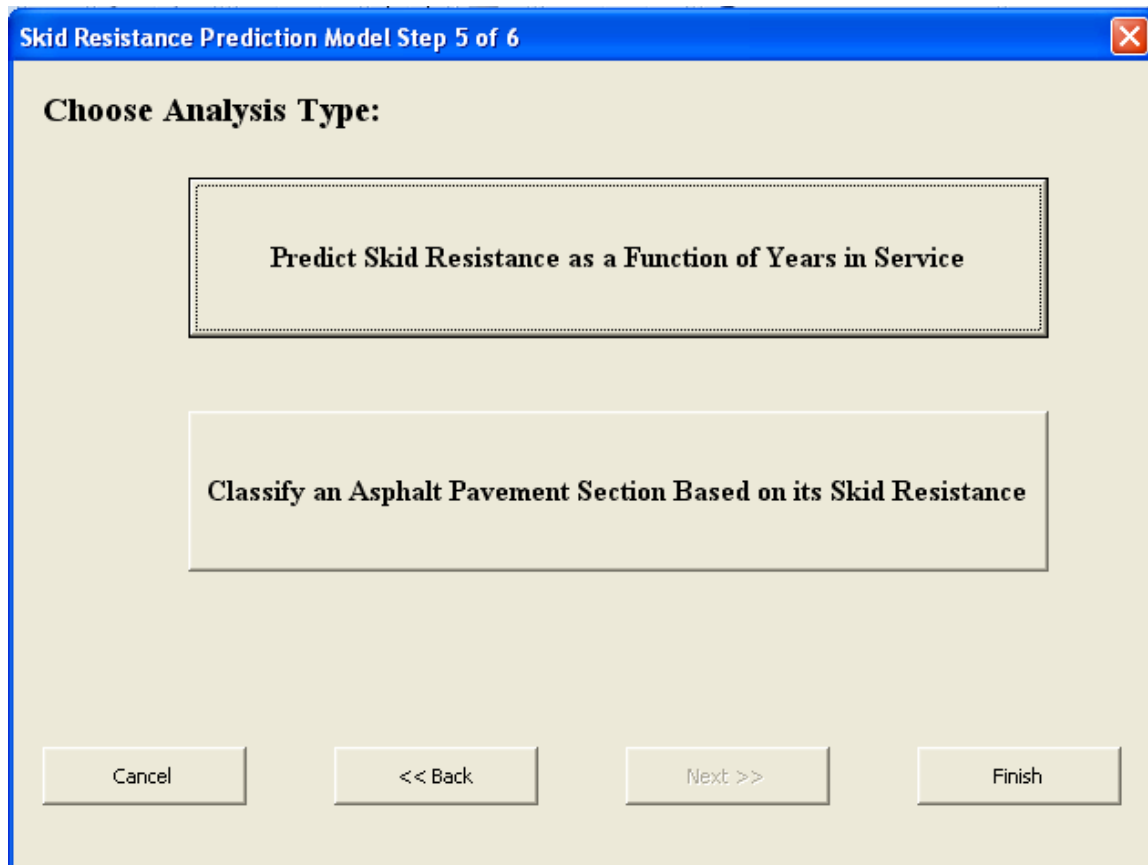


FIGURE 130 Analysis type window.

If the user chooses <Skid Resistance Prediction Model>, the software will provide a plot of skid number over the service life (see FIGURE 131). If the user selects the <Aggregate Classification>, a window pops up in which the user needs to input some additional information used for pavement classification (see FIGURE 132). These input parameters are the number of years in service based on which pavement section is classified, and the skid resistance thresholds based on which pavement section will be classified (see FIGURE 132). The first threshold value is the acceptable skid number above which the designer is not concerned. The second threshold value is the skid number above which (but below the acceptable value) one should monitor the surface

condition more frequently and below which one should take corrective measures to restore surface friction.

After clicking on the <Set> button, a window with the pavement classification will be presented (see FIGURE 133). Depending on the predicted skid number at the end of service life and designer selected threshold values, the pavement is classified as high, medium, or low. By clicking on the <Finish> button, the program will be terminated and Microsoft® Excel will be closed.

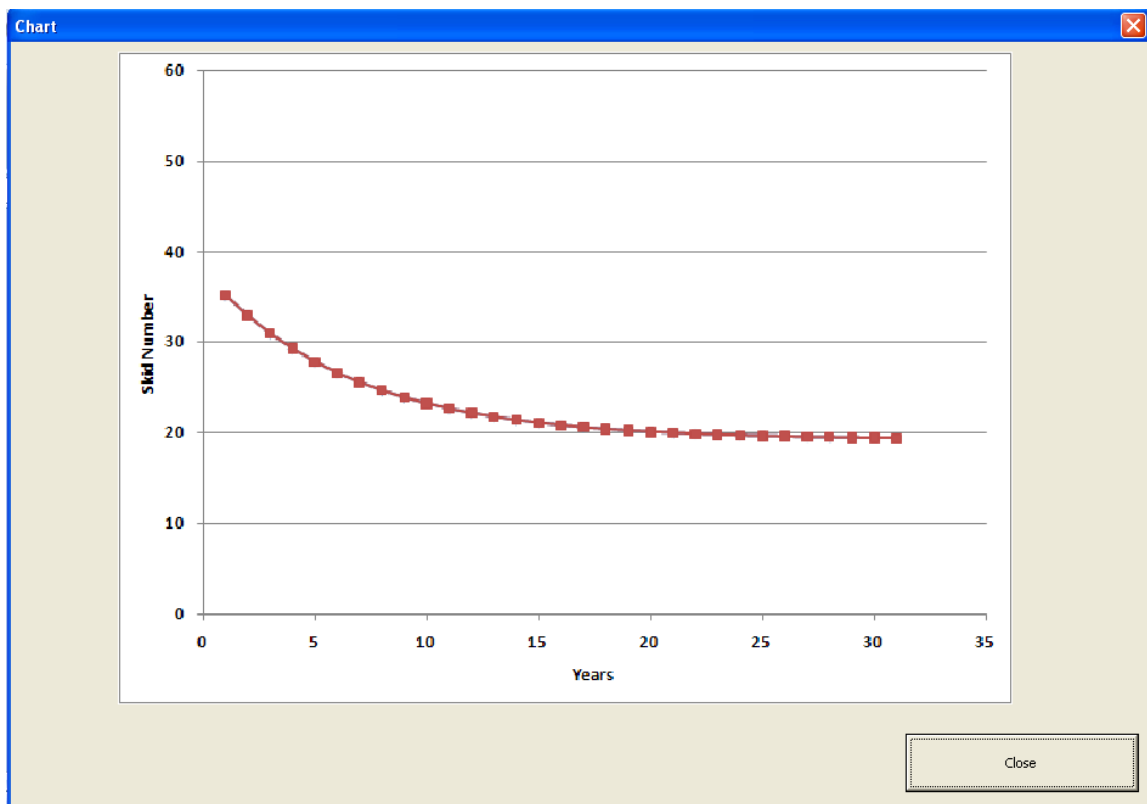


FIGURE 131 A sample plot of skid number over the service years.

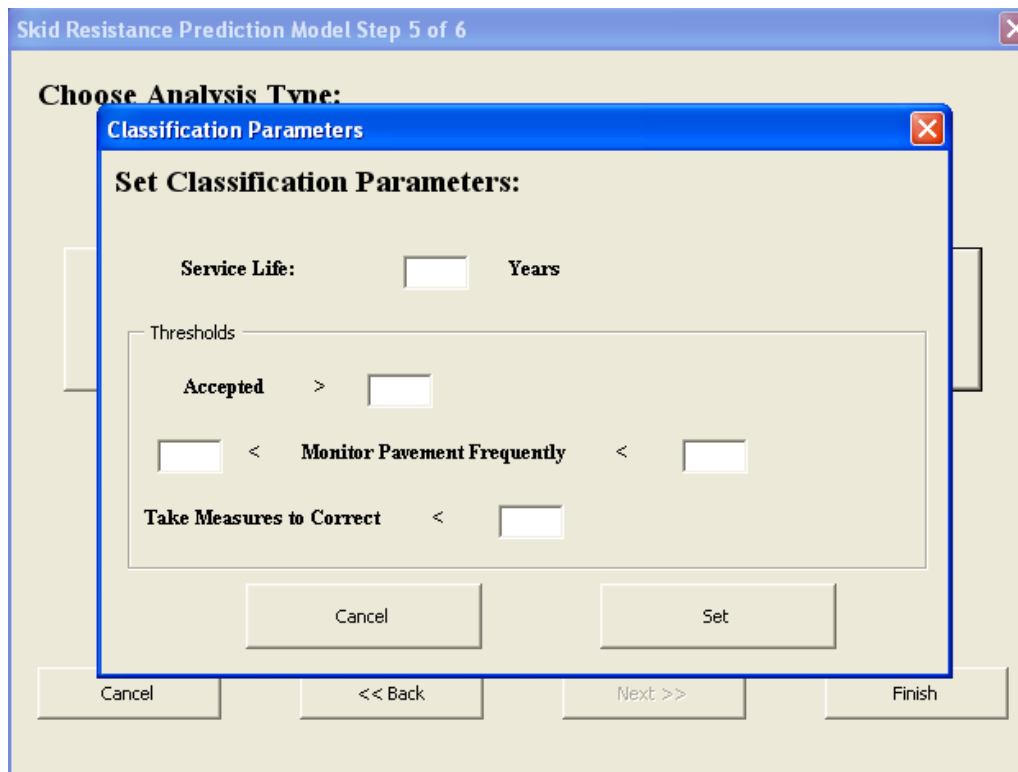


FIGURE 132 Classification value setting window.

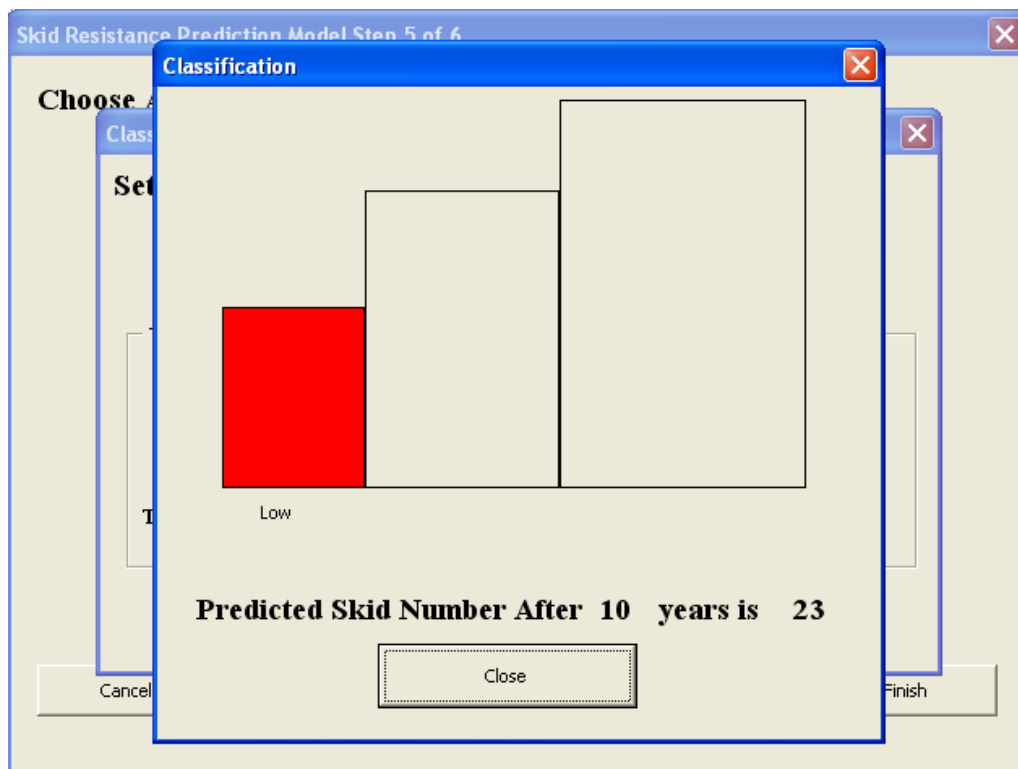


FIGURE 133 Classification sample.

SUMMARY

This chapter explained the details of the development of a model for predicting pavement skid resistance. The laboratory results led to development of a pavement prediction model as a function of polishing cycles caused by the NCAT polishing machine. The results of the field measurements confirmed the laboratory findings in which the aggregate texture characteristics and mix type were proved to be significant factors in pavement friction. Statistical analysis was performed and the relationship between traffic and the NCAT polishing machine was established. It was found that the correlation between the NCAT polishing cycles and traffic depends on mix type as well.

Based on the findings of the laboratory and field measurements, a simple procedure for obtaining components of the pavement friction prediction model was presented. This procedure involves measuring the aggregate texture before and after Micro-Deval by AIMS, calculating the coefficients of the Weibull cumulative distribution function from gradation data, and calculating the pavement macrotexture using the mix gradation parameters.

The prediction model was used to classify aggregates based on their frictional performance. Furthermore, a design service life was considered and the pavement skid resistance in terms of skid number was predicted. Based on the predicted skid number and some threshold values, the performance of the aggregate was rated.

In order to facilitate analyzing the data, a user-friendly software was developed in this study. In this software, the user is able to input aggregate and gradation data and obtain the prediction curve and aggregate classification. The user can input aggregate gradation or select some conventional mixes from a list or input different aggregate combinations and study the effect of combinations on predicted skid resistance.

CHAPTER IX

CONCLUSIONS AND RECOMMENDATIONS

CONCLUSIONS

The main outcome of this study was the development of a model to predict the skid number of asphalt mixtures as a function of traffic level. This model requires input parameters that can be easily obtained. These input parameters are aggregate texture measured using AIMS before Micro-Deval polishing, aggregate texture measured using AIMS after Micro-Deval polishing, and aggregate gradation.

A computer program was developed using Visual Basic programming language to execute the steps needed to calculate the skid resistance of asphalt pavements as a function of traffic. This software can be used to estimate the skid number of a pavement section over the service years. Different combination of aggregates and mix types can be evaluated to obtain the optimum mix design that meets the safety requirements of the pavement surface. This software can also be used to plan the maintenance and rehabilitation measures to keep the pavement friction above an acceptable limit.

In addition to this main contribution of the dissertation, the following are some specific findings from the laboratory experimental measurements:

- Statistical analysis of the laboratory Sand Patch test results did not show any significant differences between Mean Texture Depth (MTD) values before and after polishing. Hence, it was concluded that the sand patch test was not able to detect changes in macrotexture due to polishing with the selected polishing device.
- The British Pendulum (BP) values obtained in the laboratory decreased with an increase in polishing cycles for all mixtures except those containing Brownlee aggregate. For Brownlee aggregate, the BP values remained almost constant. The BP values of PFC mixes were generally higher than those for Type C mixes. In addition, the frictional characteristics of some aggregates varied depending on the mix in which the aggregate was used. For example, the PFC and Type C mixes

- with Brownwood aggregate had similar BP values at a low number of polishing cycles. However, the PFC mixes with Brownwood aggregate had higher BP values than corresponding Type C mixes at a high number of polishing cycles.
- Statistical analysis showed that the British Pendulum test was not able to detect the difference between frictional performances of mixtures incorporating aggregates with known differences in frictional characteristics.
 - The results of dynamic friction measurements at 20 km/h (DF_{20}) showed that DF_{20} decreased as polishing cycles increased. The DF_{20} curves leveled off and reached a terminal value after a certain number of polishing cycles. Analysis of the measured DF_{20} values showed that there was a significant difference in the measured friction at different numbers of polishing cycles for Type C mixes. In contrast, the magnitude of dynamic friction in PFC mixes did not have a significant difference between polishing cycles. The results also revealed that the PFC mix has a higher friction value than the Type C mix.
 - Comparing the rate of change and terminal values of F60 for mixtures with different aggregates revealed that in all cases the Brownlee aggregate had the highest terminal values and lowest rate of change in both Type C and PFC mixes. In contrast, mixes containing Beckman and Brownwood aggregates had the lowest terminal values and highest rates of change.

The following are some specific findings from the field measurements:

- In order to account for the influence of traffic on the skid resistance of pavement sections, a single factor denoted as Traffic Multiplication factor (TMF) was defined. This factor is the multiplication of AADT in the design lane and years in service divided by 1000. As such, TMF considers both traffic level and years of operation. The results of the field data analysis showed that the measured skid number decreased as TMF increased. The measured skid numbers had less variation at higher TMF levels. This phenomenon could be attributed to mixtures reaching close to a terminal skid condition that is associated with aggregates approaching their equilibrium (or terminal) state of texture after a high number of polishing or loading cycles.

- The field measurements showed that surface treatments generally had higher skid numbers than Type C mixes, which is a conventional dense graded mix. Additionally, PFC mixes exhibited better skid resistance than Type C mixes and surface treatment mixes. The results showed the PFC mixes had the lowest variation in skid number, while surface treatment mixes had the highest variability.
- It is very difficult to classify aggregates without specifying mixture type in which they are used. Some aggregate types performed poorly in certain mixtures, while their performance was acceptable in other mixtures.
- There was no correlation between the Mean Profile Depth (MPD) values obtained from CTMeter and measured skid number. However, the results also indicated that there was a fair correlation between friction and measured skid number for all mixes

RECOMMENDATIONS

The system that was developed in this study is very promising and has been verified using the data collected in this study. Although extensive field testing on HMA surfaces was conducted, the evaluation of surface treatment skid resistance was limited to the analyses of corresponding data from the PMIS database. There is a need for further testing so that the HMA asphalt prediction model can be tailored to the skid prediction model of surface treatments. There is also a need for validation of the skid prediction model to a wide variety of conditions and for more asphalt mixtures types.

The developed model uses a simple parameter to account for the influence of traffic on the skid resistance. This parameter describes only the number of traffic loading in the outer lane of the pavement without making a distinction between different traffic categories. An analysis is needed to evaluate the influence of traffic distribution on skid number and subsequent assessment of developing a new method for including the influence of traffic and its distribution on skid resistance.

This study primarily focused on developing skid prediction of HMA surface mixes. The prediction model should be modified so that it can also be applied for surface treatments. Using the data from testing on surface treatments, the necessary adjustments in the model and the software can be made to accommodate the method to be used for surface treatments.

It is recommended that a rational method for setting the acceptable values of skid resistance based on climatic data and pavement geometry be developed. This can be achieved by studying the relationship between accident data, skid resistance, climatic data, and pavement and highway geometry.

REFERENCES

1. Noyce, D. A., H. U. Bahia, J. M. Yambó, and G. Kim. *Incorporating Road Safety into Pavement Management: Maximizing Asphalt Pavement Surface Friction for Road Safety Improvements*. Midwest Regional University Transportation Center Traffic Operations and Safety (TOPS) Laboratory, Madison, WI, 2005.
2. Smith, H. Pavement Contributions to Wet-Weather Skidding Accident Reduction. In *Transportation Research Record: Journal of the Transportation Research Board*, No. 622, Transportation Research Board of the National Academies, Washington, D.C., 1976, pp. 51-59.
3. Davis, R. M., G. W. Flintsch, I. L. K. Al-Qadi, and K. McGhee. Effect of Wearing Surface Characteristics on Measured Pavement Skid Resistance and Texture. Presented at the 81st Transportation Research Board Annual Meeting, CD-ROM. Transportation Research Board of the National Academies, Washington, D.C., 2002.
4. *Nationwide Personal Transportation Survey*. Publication FHWA-PL-94-010. FHWA, U.S. Department of Transportation, Washington, D.C., 1990.
5. Chelliah, T., P. Stephanos, M. G. Shah, and T. Smith. Developing a Design Policy to Improve Pavement Surface Characteristics. Presented at the Transportation Research Board 82nd Annual Meeting, CD-ROM. Transportation Research Board of the National Academies, Washington, D.C., 2003.
6. Kuemmel, D. A., R. C. Sontag, J. Crovetti, A. Y. Becker, J. R. Jaeckel, and A. Satanovsky. *Noise and Texture on PCC Pavements*. Publication WI/SPR-08-99. Wisconsin Department of Transportation, Madison, WI, 2000.

7. Rizenbergs, R. L., J. L. Burchett, and C. T. Napier. *Skid Resistance of Pavements*. Publication KYHPR-64-24, Part II. Kentucky Department of Highways, Lexington, KY, 1972.
8. Giles, C. G., B. E. Sabey, and K. H. F. Cardew. Development and Performance of the Portable Skid Resistance Tester. *Road Research Technical Paper 66*. Road Research Laboratory, Department of Scientific and Industrial Research, HMSO, London, United Kingdom, 1964.
9. McCullough, B. V., and K. D. Hankins. Skid Resistance Guidelines for Surface Improvements on Texas Highways. In *Transportation Research Record: Journal of the Transportation Research Board*, No. 131, Transportation Research Board of the National Academies, Washington, D.C., 1966, pp. 204-217.
10. Wallman, C. G., and H. Astron. *Friction Measurement Methods and the Correlation between Road Friction and Traffic Safety*. Swedish National Road and Transport Research Institute, Linköping, Sweden, 2001.
11. Gandhi, P. M., B. Colucci, and S. P. Gandhi. Polishing of Aggregates and Wet Weather Accident Rate for Flexible Pavements. In *Transportation Research Record: Journal of Transportation Research Board*, No. 1300, Transportation Research Board of National Academies, Washington, D.C., 1991.
12. Flintsch, G. W., Y., Luo, and I. L. Al-Qadi. Analysis of the Effect of Pavement Temperature on the Frictional Properties of Flexible Pavement Surfaces. Presented at the 84th Transportation Research Board Annual Meeting, CD-ROM. Transportation Research Board of the National Academies, Washington, D.C., 2005.
13. Jayawickrama, P. W. and B. Thomas. Correction of Field Skid Measurements for Seasonal Variations in Texas. In *Transportation Research Record: Journal of*

- Transportation Research Board*, No.1639, Transportation Research Board of National Academies, Washington, D.C., 1998, pp. 147-154.
14. Agrawal S. K. and J. J. Henry. Technique for Evaluating Hydroplaning Potential of Pavements. In *Transportation Research Record: Journal of Transportation Research Board*, No.633, Transportation Research Board of National Academies, Washington, D.C., 1979, pp. 1-7.
 15. Hall, J. W., L. T. Glover, K. L. Smith, L. D. Evans, J. C. Wambold, T. J. Yager, and Z. Rado. *Guide for Pavement Friction*. Project No. 1-43, Final Guide, National Cooperative Highway Research Program, Transportation Research Board, National Research Council, Washington, D.C., 2006.
 16. Miller, M. M. and H. D. Johnson. *Effects of Resistance to Skidding on Accidents: Surface Dressing on an Elevated Section of the M4 Motorway*, Report No. LR 542, Transport and Road Research Laboratory, Berkshire, United Kingdom, 1973.
 17. Kamel, N. and T. Gartshore. *Ontario's Wet Pavement Accident Reduction Program*. ASTM Special Technical Publication No.763, American Society of Testing and Materials (ASTM), Philadelphia, PA., 1982.
 18. *Road Surface Characteristics – Their Interaction and Their Optimization*. OECD Scientific Expert Group, Road Transport Research, Organization for Economic Cooperation and Development (OECD), Paris, France, 1984.
 19. Roe, P. G., D. C. Webster, and G. West. The Relation between Surface Texture of Roads and Accidents. In *Transport and Road Research Laboratory, Research Report*, No.296, TRRL, Berkshire, United Kingdom, 1991.

20. Wambold, J. C., J. J. Henry, and R. R. Hegmon. *Skid Resistance of Wet-Weather Accident Sites*. ASTM Special Technical Publication, No.929, American Society of Testing and Materials (ASTM), Philadelphia, PA., 1986.
21. Gothie, M. Relationship between Surface Characteristics and Accidents. *Proceedings of 3rd International Symposium on Pavement Surface Characteristics*, Christchurch, New Zealand, 1996.
22. Bray, J. The Role of Crash Surveillance and Program Evaluation: NYSDOT's Skid Accident Reduction Program (SKARP). Presented at the 28th International Forum on Traffic Records and Highway Information System, Orlando, FL., 2002.
23. McLean, J. The Relationship between Pavement Condition and Road Safety. Presented at the Load-Pavement Interaction Workshop, Newcastle, United Kingdom, 1995.
24. Larson, R. M. *Consideration of Tire/Pavement Friction/Texture Effects on Pavement Structural Design and Material Mix Design*. Federal Highway Administration (FHWA), Office of Pavement Technology, Washington, D.C., 1999.
25. Schulze, K. H., A. Gerbaldi, and J. Chavet. Skidding Accidents, Friction Numbers, and the Legal Aspects Involved. In *Transportation Research Record: Journal of Transportation Research Board*, No.623, Transportation Research Board of National Academies, Washington, D.C., 1976.
26. Henry J. J. Overview of the International PIARC Experiment to Compare and Harmonize Texture and Skid Resistance Measurements: The International Friction Index. *Proceedings of the 3rd International Symposium on Pavement Surface Characteristics*, Christchurch, New Zealand, September, 1996.

27. Wambold, J. C., C. E. Antle, J. J. Henry, and Z. Rado. *International PIARC Experiment to Compare and Harmonize Texture and Skid Resistance Measurement*, PIARC (Permanent International Association of Road Congress) Report, C-1 PIARC Technical Committee on Surface Characteristics, France, 1995.
28. Fulop, I. A., I. Bogardi, A. Gulyas, and M. Csicsely-Tarpay. Use of Friction and Texture in Pavement Performance Modeling. *ASCE Journal of Transportation Engineering*, Vol. 126, No. 3, 2000, pp. 243-248.
29. Hanson, D. I. and B. D. Prowell. *Evaluation of Circular Texture Meter for Measuring Surface Texture of Pavements*. NCAT Report 04-05, National Center for Asphalt Technology, Auburn, AL., 2004.
30. Kowalski, K. J. *Influence of Mixture Composition on the Noise and Frictional Characteristics of Flexible Pavements*. Ph.D. Dissertation, Purdue University, West Lafayette, IN., 2007.
31. West, T. R., J. C. Choi, D. W. Bruner, H. J. Park, and K. H. Cho. Evaluation of Dolomite and Related Aggregates Used in Bituminous Overlays for Indiana Pavements. In *Transportation Research Record: Journal of Transportation Research Board*, No.1757, Transportation Research Board of National Academies, Washington, D.C., 2001, pp. 137-147.
32. Goodman, S. N., Y. Hassan, and A. O. Abd El Halim. Preliminary Estimation of Asphalt Pavement Frictional Properties from Superpave Gyrotory Specimen and Mix Parameters. In *Transportation Research Record: Journal of Transportation Research Board*, No.1949, Transportation Research Board of National Academies, Washington, D.C., 2006, pp. 173-180.
33. *Skid Accident Reduction Program*. Technical Advisory T5040.17, Federal Highway Administration, U.S. Department of Transportation, Washington, D.C., 1980.

34. Li, S., K. Zhu, S. Noureldin, and D. Harris. Identifying Friction Variations with the Standard Smooth Tire for Network Pavement Inventory Friction Testing. Presented at the Transportation Research Board 84th Annual Meeting, CD-ROM. Transportation Research Board of the National Academies, Washington, D.C., 2005.
35. Lee, Y. P. K., T. F. Fwa, and Y. S. Choo. Effect of Pavement Surface Texture on British Pendulum Test. *Journal of the Eastern Asia Society for Transportation Studies*, Vol. 6, 2005, pp. 1247-1257.
36. Dewey, G. R., A. C. Robords, B. T. Armour, and R. Muethel. Aggregate Wear and Pavement Friction. Presented at the 80th Transportation Research Board Annual Meeting, CD-ROM. Transportation Research Board of the National Academies, Washington, D.C., 2001.
37. Wilson, D. J. and R. C. M. Dunn. Analyzing Road Pavement Skid Resistance. Institute of Transportation Engineers ITE, *Proceedings of 2005 Annual Meeting*, Australia, 2005.
38. Moore, D. F. *The Friction and Lubrication of Elastomers*. Pergamon Press LTD., Oxford, Great Britain, 1972.
39. Choubane, B., C. R. Holzschuher, and S. Gokhale. Precision of Locked-Wheel Testers for Measurement of Roadway Surface Friction Characteristics. In *Transportation Research Record: Journal of Transportation Research Board*, No.1869, Transportation Research Board of National Academies, Washington, D.C., 2004, pp.145-151.
40. Person, B. N. J. *Sliding Friction: Physical Principles and Applications*. Springer, Berlin, Germany, 1998.

41. Zimmer, R. A., B. Choubane, and C. R. Holzschuher. Friction Testing Method for Open-Grated Steel Bridge Decks. In *Transportation Research Record: Journal of Transportation Research Board*, No.1860, Transportation Research Board of National Academies, Washington, D.C., 2003, pp. 137-143.
42. Hogervorst, D. Some Properties of Crushed Stone for Road Surfaces. *Bulletin of the International Association of Engineering Geology*, Vol. 10, No.1, Springer, 1974.
43. Linder, M., M. Kröger, K. Popp, and H. Blume. Experimental and Analytical Investigation of Rubber Friction. *XXI International Congress of Theoretical and Applied Mechanics*, Warsaw, Poland, 2004.
44. Yandell, W. O. A New Theory of Hysteretic Sliding Friction. *Wear*, Vol. 17, 1971.
45. Yandell, W. O. and S. Sawyer. Prediction of Tire-Road Friction from Texture Measurements. In *Transportation Research Record: Journal of Transportation Research Board*, No.1435, Transportation Research Board of National Academies, Washington, D.C., 1994, pp. 86-91.
46. Do, M. T., H. Zahouani, and R. Vargiolu. Angular Parameter for Characterizing Road Surface Microtexture. In *Transportation Research Record: Journal of Transportation Research Board*, No.1723, Transportation Research Board of National Academies, Washington, D.C., 2000, pp. 66-72.
47. Forster, S. W. Pavement Microtexture and its Relation to Skid Resistance. In *Transportation Research Record: Journal of Transportation Research Board*, No.1215, Transportation Research Board of National Academies Washington D.C., 1989, pp. 151-164.
48. Roberts, A. D. Rubber Adhesion at High Rolling Speeds. *Journal of Natural Rubber Research*, Vol. 3, No. 4, 1988, pp. 239-260.

49. Kummer, H. W. and W. E. Meyer. Penn State Road Surface Friction Tester as Adapted to Routine Measurement of Pavement Skid Resistance. Presented at the Road Surface Properties, 42nd Annual Meeting, January, 1963.
50. Bond, R., I. E. D. Katekhda, G. Lees, and A. R. Williams. Tire/Road Surface Interaction. *Journal of the Institution of Highway Engineers*, Vol. 23, No.11, November, 1976, pp. 11-19.
51. Johnsen, W.A. *Advances in the Design of Pavement Surfaces*. Ph.D. Dissertation, Worcester Polytechnic Institute, 1997.
52. Leu, M. C. and J. J. Henry. Prediction of Skid Resistance as a Function of Speed from Pavement Texture. In *Transportation Research Record: Journal of Transportation Research Board*, No.666, Transportation Research Board of National Academies Washington D.C., 1978, pp. 7-13.
53. Horne, W. B. and F. A. Buhmann. *Frictional Interaction of Tire and Pavement: A Method for Rating the Skid Resistance and Micro/Macrotexture Characteristics of Wet Pavements.*, ASTM Special Technical Publication 793, American Society of Testing and Materials (ASTM), Philadelphia, PA., 1983.
54. *Hot Mix Asphalt Materials, Mixture Design, and Construction*. National Asphalt Pavement Association, NAPA Education Foundation, Lanham, MD., 1996.
55. Jayawickrama, P. W., R. Prasanna, and S. P. Senadheera. Survey of State Practices to Control Skid Resistance on Hot-Mix Asphalt Concrete Pavements. In *Transportation Research Record: Journal of Transportation Research Board*, No.1536, Transportation Research Board of National Academies, Washington, D.C., 1996, pp. 52-58.

56. Moore, D. F. *The Friction of Pneumatic Tires*. Elsevier Scientific Publishing Company, Amsterdam, Netherland, 1975.
57. Taneerananon, P. and W. O. Yandell. Microtexture Roughness Effect on Predicted Road/Tire Friction in Wet Conditions. *Wear*, Vol. 69, 1981, pp. 321-337.
58. Kokkalis, A. G. and O. K. Panagouli. Fractal Evaluation of Pavement Skid Resistance Variations Surface Wear. *Chaos, Solutions and Fractals*, Vol. 9, No. 11, 1999, pp. 1875-1890.
59. *Annual Book of ASTM Standards*, Vol. 04.03, American Society for Testing and Materials, West Conshohocken, PA., 2007.
60. Ergun, M., Iyınam, S., and Iyınam, A.F. Prediction of Road Surface Friction Coefficient Using Only Macrottexture and Microtexture Measurements. *Journal of Transportation Engineering*, Vol. 131, No. 4, 2005, pp. 311-319.
61. Bloem, D. L. Skid-Resistance: The Role of Aggregates and Other Factors. *National Sand and Gravel Association Circular 109*, Silver Spring, MD., 1971.
62. Balmer, G. G. Pavement Texture: Its Significance and Development. In *Transportation Research Record: Journal of Transportation Research Board*, No.666, Transportation Research Board of National Academies, Washington, D.C., 1978, pp. 1-6.
63. Gardiner, S., J. Studdard, and C. Wagner. Evaluation of Hot Mix Asphalt Macrottexture and Microtexture. *Journal of Testing and Evaluation*, January 2004, Vol. 32, No.1, 2004, pp. 1-10.
64. Rhode, S. M. On the Effect of Pavement Microtexture and Thin Film. *Traction, International Journal of Mechanic Sciences*, Vol. 18, 1976, pp 95-101.

65. Savkoor, A. R. Tribology of Tire Traction on Dry and Wet Roads. *Proceedings of the 17th Leeds-Lyon Symposium on Tribology*, September 4-7, 1990.
66. Horne, W. B. Status of Runway Slipperiness Research. In *Transportation Research Record: Journal of Transportation Research Board*, No.624, Transportation Research Board of National Academies, Washington, D.C., 1977, pp. 95-121.
67. Ong, G. P., T. F. Fwa, and J. Guo. Modeling Hydroplaning and Effects of Pavement Microtexture. In *Transportation Research Record: Journal of Transportation Research Board*, No., 1905, Transportation Research Board of National Academies, Washington, D.C., 2005, pp. 166-176.
68. Pelloli, R. Road Surface Characteristics and Hydroplaning. In *Transportation Research Record: Journal of Transportation Research Board*, No.624, Transportation Research Board of National Academies, Washington, D.C., 1972, pp. 27-32.
69. Rose, J. G. and B. M. Gallaway. Macrotexture Measurement and Related Skid Resistance at Speeds from 20 to 60 Miles per Hour. In *Highway Research Record: Journal of Highway Research Board*, No.341, Transportation Research Board of National Academies, Washington, D.C., 1970, pp. 33-45.
70. Gallaway, B. M., J. G. Rose, and R. E. Schiller. The Relative Effect of Several Factors Affecting Rainwater Depths on Pavement Surface. In *Highway Research Record: Journal of Highway Research Board*, No.396, Transportation Research Board of National Academies, Washington, D.C., 1972.
71. Cairney, P. *Skid Resistance and Crashes – A Review of the Literature*. Research Report No. 311, ARRB Transport Research Ltd., Vermont South Victoria, Australia, 1997.

72. Kokot, D. Evaluating Skidding Resistance in Slovenia. Slovenian National Building and Civil Engineering Institute, 2005,
www.ectri.org/liens/yrs05/Session%205bis/Kokot.pdf. Access date: 11/27/2006.
73. *International PIARC Experiment to Compare and Harmonize Texture and Skid Resistance Measurements*, PIARC Technical Committee on Surface Characteristics (C1), Paris, France, 1995.
74. Roe, P. G., A. R. Parry, and H. E. Viner. *High and Low Speed Skidding Resistance: The Influence of Texture Depth*. Transport and Road Research Laboratory Report 367, TRRL, Berkshire, U.K., 1998.
75. Lee, S. W., Y. H. Cho, H. J. Lee, N. C. Kim, and S. J. Chun. Rate of Skid Resistance Loss for Tinned Concrete Pavements. Presented at the Transportation Research Board 84th Annual Meeting, CD-ROM. Transportation Research Board of the National Academies, Washington, D.C., 2005.
76. Saito, K., T. Horiguchi, A. Kasahara, H. Abe, and J. J. Henry. Development of Portable Tester for Measuring Skid Resistance and Its Speed Dependency on Pavement Surfaces. In *Transportation Research Record: Journal of Transportation Research Board*, No.1536, Transportation Research Board of National Academies, Washington D.C., 1996, pp. 45-51.
77. Giles, C. G., B. E. Sabey, and Cardew, K.H.F. *Development and Performance of the Portable Skid Resistance Tester*. ASTM Special Technical Publication, No.326, American Society of Testing and Materials (ASTM), Philadelphia, PA., 1962.
78. Fwa, T. F., Y. S. Choo, and Y. R. Liu. Effect of Aggregate Spacing on Skid Resistance of Asphalt Pavement. *Journal of Transportation Engineering*, Vol. 129, No. 4, American Society of Civil Engineering, ASCE, 2003, pp. 420-426.

79. Liu, Y., T. F. Fwa, and Y. S. Choo. Effect of Surface Macrotexture on Skid Resistance Measurements by the British Pendulum Test. *Journal of Testing and Evaluation*, Vol. 32, No. 4, American Society of Civil Engineering, ASCE, 2004, pp. 304-309.
80. Forde, M. C., R. M. Birse, and D. M. Fraser. An Assessment of British Pendulum Based Methods of Skid Resistance Evaluation Using Schonfield's Photo-Interpretation Method. *Proceedings of 8th ARRB Conference*, 8(4), Session 17, 1976.
81. Salt, G. F. Research on Skid Resistance at the Transport and Road Research Laboratory (1927-1977). In *Transportation Research Record: Journal of Transportation Research Board*, No.622, Transportation Research Board of National Academies, Washington, D.C., 1977, pp. 26-38.
82. Purushothaman, N., B. S. Heaton, and I. D. Moore. Experimental Verification of a Finite Element Contact Analysis. *Journal of Testing and Evaluation*, Vol. 16, No, 1988, pp. 497-507.
83. Won, M. C. and C. N. Fu. Evaluation of Laboratory Procedures for Aggregate Polish Test. In *Transportation Research Record: Journal of Transportation Research Board*, No.1547, Transportation Research Board of National Academies, Washington, D.C., 1996, pp. 23-28.
84. Abe, H., J. J. Henry, A. Tamai, and J. C. Wambold. Measurement of Pavement Macrotexture Using the CTMeter. In *Transportation Research Record: Journal of Transportation Research Board*, No.1764, Transportation Research Board of National Academies Washington, D.C., 2000, pp. 201-209.

85. Henry, J. J. *Evaluation of Pavement Friction Characteristics*. NCHRP Synthesis: Topic 30-11, National Cooperative Highway Research Program, Washington, D.C., 2000.
86. Yandell, W. O., P. Taneerananon, and V. Zankin. *Frictional Interaction of Tire and Pavement : Prediction of Tire-Road Friction from Surface Texture and Tread Rubber Properties*, ASTM Special Technical Publication 793, W.E Meyer and J.D. Walter, Ed., American Society of Civil Engineering, Washington, D.C., 1983.
87. Leland, T. J. W., T. J. Yager, and U. T. Joyner. *Effects of Pavement Texture on Wet-Runway Braking Performance*. NASA Technical Note TN D-432, National Aeronautics and Space Administration, 1968.
88. Henry, J. J. and R. R. Hegmon. *Pavement Texture Measurement and Evaluation*. ASTM Special Technical Publication 583, American Society for Testing and Materials, Philadelphia, PA., 1975.
89. Moore, D. F. Prediction of Skid Resistance Gradient and Drainage Characteristics for Pavements. In *Highway Research Record: Journal of Highway Research Board*, No.131, Transportation Research Board of National Academies, Washington, D.C., 1966, pp. 181-203.
90. Walker, R. S. and L. D. Payne. *Use of Selcom Laser for Pavement Texture and Skid Resistance Measurement*. Technical Memorandum, Research Project 1290. Transportation Instrumentation Laboratory, University of Texas, Arlington, TX, undated.
91. Her, I., J. J. Henry, and J. C. Wambold. Development of a Data Acquisition Method for Non-contact Pavement Macrotecture Measurement. In *Transportation Research Record: Journal of Transportation Research Board*, No.1000, Transportation Research Board of National Academies, Washington, D.C., 1984, pp. 8-14.

92. Henry, J. J., H. Abe, S. Kameyama, A. Tamai, A. Kasahara, and K. Saito. Determination of the International Friction Index Using the Circular Track Meter and the Dynamic Friction Tester. *Proceedings of SURF 2000*, the World Road Association. Paris, France, 2000.
93. Schonfeld, R. Photo-Interpretation of Pavement Skid Resistance in Practice. In *Transportation Research Record: Journal of Transportation Research Board*, No.523, Transportation Research Board of National Academies, Washington, D.C., 1974, pp. 11-25.
94. Leu, M. C., J. J. Henry. Prediction of Skid Resistance as a Function of Speed from Pavement Texture. In *Transportation Research Record: Journal of Transportation Research Board*, No.666, Transportation Research Board of National Academies, Washington, D.C., 1978, pp. 7-13.
95. Williams, A.R. and G. Lees. Topographical and Petrographical Variation of Road Aggregates and the Wet Skidding Resistance of Tires. *Journal of Engineering Geology*, Vol. 2, 1970, pp. 217-236.
96. Tourenq, C. and D. Fourmaintraux. Road Surface Roughness and the Properties of Aggregates (in French). *Bulletin de Liaison des Laboratoires des Ponts et Chaussées*, No. 51, 1971, pp. 61-69.
97. Do, M. T. and P. Marsac. Assessment of the Polishing of the Aggregate Microtexture by Means of Geometric Parameters. Presented at the 81st Transportation Research Board Annual Meeting, CD-ROM. Transportation Research Board of the National Academies, Washington, D.C., 2002.
98. Samuels, S. E. *The Feasibility of Measuring Road Surface Microtexture by Means of Laser Techniques*. Research Report No. TF 52-03, Road User and Vehicle Division, VTI, Linköping, Sweden, 1986.

99. McDaniel, R. S. and B. J. Coree. *Identification of Laboratory Techniques to Optimize Superpave HMA Surface Friction Characterization*. Phase I: Final Report SQDH 2003–6, North Central Superpave Center, Purdue University, West Lafayette, IN., 2003.
100. Masad, E., T. Al-Rousan, J. Button, D. Little, and E. Tutumluer. *Test Methods for Characterizing Aggregate Shape, Texture, and Angularity*. NCHRP Project 4-30A Final Report, National Cooperative Highway Research Program, Washington, D.C., 2005.
101. Perry, M., R. Woodside, and W. Woodward. Observations on Aspects of Skid Resistance of Greywacke Aggregate. *Quarterly Journal of Engineering Geology and Hydrology*, No. 24, 2001, pp. 347-352.
102. Kennedy, C.K., A. E. Young, and I. C. Buttler. *Measurement of Skidding Resistance and Surface Texture and the Use of Results in the United Kingdom*. Symposium: Surface Characteristics of Roadways. American Society of Testing and Materials (ASTM), Philadelphia, PA., 1990.
103. Harald, A. *Skid Resistance and Road Surface Texture*. Symposium: Surface Characteristics of Roadways, American Society of Testing and Materials (ASTM), Philadelphia, PA., 1990.
104. Kulakowski, B. T. and W. E. Meyer. Skid Resistance of Adjacent Tangent and Nontangent Sections of the Roads. In *Transportation Research Record: Journal of Transportation Research Board*, No.1215, Transportation Research Board of National Academies, Washington, D.C., 1990, pp. 132-136.
105. Kokkalis, A. G., G. H. Tsohos, and O. K. Panagouli. Consideration of Fractals in Pavement Skid Resistance Evaluation. *Journal of Transportation Engineering*, Vol. 128, No. 6, American Society of Civil Engineering, 2002, pp 591-595.

106. Colony, D. C. *Skid Resistance of Bituminous surfaces in Ohio*. Final Report of ODOT Project No. 3775, Ohio Department of Transportation, 1984.
107. Lay, C. and B. Judith. Friction and Surface Texture Characterization of 14 Pavement Test Sections in Greenville, North Carolina. In *Transportation Research Record: Journal of Transportation Research Board*, No.1639, Transportation Research Board of National Academies, Washington, D.C., 1998, pp. 156-161.
108. Burnett, W. C., J. L. Gibson, and E, J. Kearney. Skid Resistance of Bituminous Surfaces. In *Highway Research Record: Journal of Highway Research Board*, No.236, Transportation Research Board of National Academies, Washington, D.C., 1968, pp. 49-60.
109. Skerritt, W. H. Aggregate Type and Traffic Volume as Controlling Factors in Bituminous Pavement Friction. In *Transportation Research Record: Journal of Transportation Research Board*, No.1418, Transportation Research Board of National Academies, Washington, D.C., 1993, pp. 22-29.
110. Hill, B. J. and J. J. Henry. Short-Term Weather Related Skid Resistance Variations. In *Transportation Research Record: Journal of Transportation Research Board*, No.1215, Transportation Research Board of National Academies, Washington, D.C., 1981, pp. 76-81.
111. Cenek, P. D., R. B. Davies, M. W. McLarin, and N. J. Griffith-Jones. Road Environment and Traffic Crashes. In *Transfund Research Report*, No. 79, Transfund New Zealand, Wellington, New Zealand, 1997.
112. *Specification for Skid Resistance Deficiency Investigation and Treatment Selection*. TNZ T/10 Transit New Zealand, Wellington, New Zealand, 2002.

113. West, N. W. and T. F. Ross. Polishing of the Road Surfaces in New South Wales. *Proceedings of the Australian Road Research Board*, Vol. 1, 1962.
114. Anderson, D. A., W. E. Meyer, and J. L. Rosenberger. Development of a Procedure for Correcting Skid-Resistance Measurements to a Standard End-of-Season Value. In *Transportation Research Record: Journal of Transportation Research Board*, No.1084, Transportation Research Board of National Academies, Washington, D.C., 1986, pp. 40-48.
115. Subhi, M. B. and R. Farhad. Changes in Asphalt Pavement Friction Components and Adjustment of Skid Number for Temperature. *Journal of Transportation Engineering*, Vol. 131, No. 6, 2005, pp. 470-476.
116. Whitehurst, E. A. and W. A. Goodwin. Pavement Slipperiness in Tennessee. *Proceedings Highway Research Board*, Vol. 34, Highway Research Board, National Research Council, Washington, D.C., 1955, pp. 194-209.
117. Nichols, F. P., Jr., J. H. Dillard, and R. L. Orwood. *Skid Resistant Pavement in Virginia*. Virginia Council of Highway Investigation and Research. Reprint No. 18, 1957.
118. Gray, J. E. and F. A. Renninger. The Skid Resistant Properties of Carbonate Aggregates. In *Highway Research Record: Journal of Highway Research Board*, No.120, Transportation Research Board of National Academies, Washington, D.C., 1966, pp. 18-34.
119. Balmer, G. G. and B. E. Colley. Laboratory Studies of the Skid Resistance of Concrete. American Society for Testing and Materials, *Journal of Materials*, Vol. 1, No. 3, 1966, pp. 536-559.

120. Csathy, T. I., W. C. Burnett, and M. D. Armstrong. State-of-the-Art of Skid Resistance Research. *Highway Research Board Special Report 95*, Highway Research Board, National Research Council, Washington, D.C., 1968.
121. Moore, D. F. *Recommendations for an International Minimum Skid-Resistance Standard for Pavements*. Highway Research Board Special Report 101, Highway Research Board, National Research Council, Washington, D.C., 1969.
122. Shupe, J. W. *Pavement Slipperiness*. Section 20 of the Highway Engineering Handbook by K.B. Woods, McGraw-Hill Book Co., Inc., New York, NY, 1960.
123. Prasanna R., B. Nageswaran, and P. W. Jayawickrama. Use of Relation Database Management Systems Principles in Reliable Prediction of Pavement Skid Resistance. In *Transportation Research Record: Journal of Transportation Research Board*, No.1655, Transportation Research Board of National Academies, Washington D.C., 1999, pp. 192-199.
124. Roberts, F. L., P. S. Kandhal, E. R. Brown, D. Y. Lee, and T. W. Kennedy. *HMA Materials, Mixture Design, and Construction*. Second Edition, NAPA, Research and Education Foundation, 1996.
125. Wasilewska, M. and W. Gardziejczyk. Polishing Resistance of Road Aggregates Applied in Wearing Course. *Proceedings of the 3rd International Conference of Modern Technologies in Highway Engineering*, Poznan, Poland, September 8-9, 2005.
126. Liang, R. Y. and L. L. Chyi. *Polishing and Friction Characteristics of Aggregates Produced in Ohio*. FHWA Report FHWA/OH-2000/001, Federal Highway Administration, Columbus, OH, 2000.

127. Shupe, J. W. and R. W. Lounsbury. Polishing Characteristics of Mineral Aggregates. *Proceedings First International Skid Prevention Conference*, University of Virginia, Charlottesville, VA., 1958.
128. Mills, J. A. Control of Pavement Slipperiness: *A Skid Resistance Study in Four Western States*. Highway Research Board Special Report 101, Highway Research Board, National Research Council, Washington, D.C., 1969, pp. 3-17.
129. Stutzenberger, W. J. *A Study of the Polishing Characteristics of Limestone and Sandstone Aggregates in Regard to Pavement Slipperiness*. Highway Research Board Bulletin 186, Highway Research Board, National Research Council, Washington, D.C., 1958, pp. 58-81.
130. Knill, D. C. Petrographical Aspects of the Polishing of Natural Roadstone. *Journal of Applied Chemistry*, Vol. 10, 1960, pp 28-35.
131. Abdul-Malak, M. A. U., A. H. Meyer, and D. W. Fowler. Research Program for Predicting the Frictional Characteristics of Seal-Coat Pavement Surface. In *Transportation Research Record: Journal of Transportation Research Board*, No.1217, Transportation Research Board of National Academies, Washington, D.C., 1990, pp. 53-84
132. Luce, A. D. *Analysis of Aggregate Imaging System (AIMS) Measurements and Their Relationship to Asphalt Pavement Skid Resistance*. M.S.C.E Thesis, Texas A&M University, College Station, TX, 2006.
133. Dahir, S. A Review of Aggregate Selection Criteria for Improved Wear Resistance and Skid Resistance of Bituminous Surfaces. *Journal of Testing and Evaluation*, Vol. 7, 1979, pp. 245-253.

134. Henry, J. J. and S. Dahir. Effects of Textures and the Aggregates that Produce them on the Performance of Bituminous Surfaces. In *Transportation Research Record: Journal of Transportation Research Board*, No.712, Transportation Research Board of National Academies, Washington, D.C., 1979, pp. 44-50.
135. Crouch, L. K., G. Shirley, G. Head, and W. A. Goodwin. Aggregate Polishing Resistance Pre-Evaluation. In *Transportation Research Record: Journal of Transportation Research Board*, No.1530, Transportation Research Board of National Academies, Washington, D.C., 1996, pp. 103-110.
136. Prowell, B. D., J. Zhang, and E. R. Brown. *Aggregate Properties and the Performance of Superpave-Designed Hot Mix Asphalt*. National Cooperative Highway Research Program, NCHRP Report 539, Transportation Research Board, National Research Council, Washington, D.C., 2005.
137. Mahmoud, E., and E. Masad. Experimental Methods for the Evaluation of Aggregate Resistance to Polishing, Abrasion and Breakage. *Journal of Materials in Civil Engineering*, ASCE, Vol.19, No.11, 2007, pp. 977–985.
138. Dames, J. *The Influence of Polishing Resistance of Sand on Skid Resistance of Asphalt Concrete*. *Surface Characteristics of Roadways: International Research and Technologies*, ASTM Special Technical Publication 1031, W.E. Meyer, and J. Reichert, Eds., American Society for Testing and Materials, Philadelphia, PA., 1990.
139. Vollar, T. W. and D. I. Hanson. *Development of Laboratory Procedure for Measuring Friction of HMA Mixtures-Phase 1*. NCAT Report 06-06, National Center of Asphalt Technology, Auburn University, AL., 2006.
140. Stephens, J. E. and W. H. Goetz. Designing Fine Bituminous Mixtures for High Skid Resistance. *Highway Research Board Proceedings*, Vol. 39, Highway Research Board, National Research Council, Washington, D.C, 1960, pp. 173-190.

141. Dahir, S. H., W. E. Meyer, and R. R. Hegmon. Laboratory and Field Investigation of Bituminous Pavement and Aggregate Polishing. In *Transportation Research Record: Journal of Transportation Research Board*, No.584, Transportation Research Board of National Academies, Washington, D.C., 1976, pp. 1-14.
142. Kamel, N., and G. R. Musgrove. Design and Performance of Bituminous Mixes in Ontario. *RTAC Forum*, Vol. 5, Issue 3, 1981, pp53-64.
143. Mullen, W. G., S. H. M. Dahir, and N. F. El Madani. Laboratory Evaluation of Aggregates, Aggregate Blends, and Bituminous Mixes for Polish Resistance. In *Transportation Research Record: Journal of Transportation Research Board*, No.523, Transportation Research Board of National Academies, Washington, D.C., 1974, pp. 56-64.
144. Emery, J. J. *Slag Utilization in Pavement Construction. Extending Aggregate Resources*. ASTM Special Technical Publication 774, American Society for Testing and Materials (ASTM), 1982.
145. Stroup-Gardiner, M., J. Studdard, and C. Wagner. Evaluation of Hot Mix Asphalt Macrotexture and Microtexture. *Journal of Testing and Evaluation*, Vol. 32, No.1, 2004.
146. Ahammed A. M. and S. L. Tighe. Evaluation of Concrete Pavement's Surface Friction Using LTPP Data: Preliminary Analysis and Texture Performance Models. Presented at the 86th Transportation Research Board Annual Meeting, CD-ROM. Transportation Research Board of the National Academies, Washington, D.C., January, 2007.
147. Yeaman, J. Are We Afraid on the IFI? *Proceedings of the International Conference on Surface Friction*, Christchurch, New Zealand, May, 2005.

148. Wambold, J. C., C. E. Antle. International PIARC Experiment to Compare and Harmonize Texture and skid Resistance Measurements. Paris, France, Permanent International Association of Road Congresses PIARC, 1995.
149. Ivey, D. L., L. I. Griffin, J. R. Lock, and D. L. Bullard. *Texas Skid Initiated Accident Reduction Program*. Texas Transportation Institute, Research Report 910-1F, College Station, TX, 1992.
150. Masad, E., A. Luce, and E. Mahmoud. *Implementation of AIMS in Measuring Aggregate Resistance to Polishing Abrasion and Breakage*. Texas Transportation Institute, Research Report 5-1707-03-1, Texas A&M University, College Station, TX, 2006.
151. Bituminous Rated Sources Quality Catalogue (BRSQC). Texas Department of Transportation, 2008. <ftp://ftp.dot.state.tx.us/pub/txdot-info/cmd/mpl/brsq.pdf>. Access date: 6/29/08.
152. Scholle, P. A. Carbonate Rock Constituents, Texture, Cements, and Porosities. *American Association of Petroleum Geologists Memoir 27*, Tulsa, OK, 1978.
153. Meininger, R. Micro-Deval vs. LA Abrasion. 2004, http://Rockproducts.com/mag/rock_microdeval_abrasion/. Access date: 22/2/2008.
154. Cooley, L., Jr. and R. James. Micro-Deval Testing of Aggregates in the Southeast. In *Transportation Research Record: Journal of Transportation Research Board*, No.1837, Transportation Research Board of National Academies, Washington, D.C., 2003, pp. 73-79.
155. Rogers, C. Laboratory Tests for Predicting Coarse Aggregate Performance in Ontario. *Advances in Aggregate and Armourstone Evaluation 13*, 1991.

156. Jayawickrama, P. W., S. Hossain, and F. Phillips. Evaluation of Aggregate Durability Using Micro-Deval Test. Presented at the Transportation Research Board 85th Annual Meeting, CD-ROM. Transportation Research Board of the National Academies, Washington, D.C., 2006.
157. Masad, E., T. Al-Rousan, J. Button, D. Little, and E. Tutumluer. *Test methods for characterizing aggregate shape, texture and angularity*. NCHRP 4-30A Final Report, No. 555, National Cooperative Highway Research Program, National Research Council, Washington, D.C., 2007.
158. Al-Rousan, T. M. *Characterization of Aggregate Shape Properties Using a Computer Automated System*. Ph.D. Dissertation, Texas A&M University, College Station, TX, 2004.
159. Pavement Selection for City Streets. <http://www.txhotmix.org>. Access date: 02/18/08.
160. Hot Mix Asphalt Property and Performance Testing Equipment., 2008, http://www.umassd.edu/engineering/cen/materials/equipment/performance_testing.cfm. Access date: 2/22/08.
161. Smit, A. de F., F. Hugo, and Y. Yeldirim. A Discussion of MMLS3 Performance Testing of Laboratory Prepared HMA Slabs and Briquettes Compared with Hamburg and APA Wheel Tracking Tests. CD-ROM, *Proceedings Second International APT Conference*, Seattle, WA, U.S., 2004.
162. Hugo, F. *MMLS3 An APT Tool for Pavement Performance Prediction and Material Evaluation*. *APT Meeting*, Accelerated Pavement Testing, 2005, http://www.gautrans-hvs.co.za/popup/APT%20Steering%20Committee%20Documents/15May07/fred_Hugo.pdf. Access date: 9/5/2008.

163. Pendulum, <http://www.wessextestequipment.co.uk/products/pendulum.aspx> Access date: 2/23/08.
164. *DFT Manual*, <http://www.nippou.com/en/products/dft.html>. Access date: 02/23/08.
165. *CTMeter Manual*, <http://www.tics.hu/CTMeter.htm>. Access date: 02/23/08.
166. Alvarado, C., E. Mahmoud, I. Abdullah, E. Masad, S. Nazarian, J. Tandon, and J. Button. *Feasibility of Quantifying the Role of Coarse Aggregate Strength on Resistance to Load in HMA*. Research Report 0-5268-2, Center for Transportation Infrastructure Systems, University of Texas at El Paso, October, 2006.
167. Report of the Committee on Surface Characteristics. World Road Association (PIARC), *Proceedings of 18th World Road Congress*, Brussels, Belgium, 1987.

APPENDIX A

TABLE 53 Mix Design for Brownwood Aggregate and Type C Mixture

Aggregate Source	Vulcan								Total Cumulative Pass %	TxDOT Specs.		
	Brownwood		Brownwood		Brownwood		Brownwood					
	C-Rock		DF		M-Sand		Field Sand					
Sieve Size	Bin #1	Total	Bin #2	Total	Bin #3	Total	Bin #4	Total				
	26.0	%	32.0	%	32.0	%	10.0	%				
1"	100.0	26.0	100.0	32.0	100.0	32.0	100.0	10.0	100.0			
7/8"	100.0	26.0	100.0	32.0	100.0	32.0	100.0	10.0	100.0	98	100	
5/8"	95.0	24.7	100.0	32.0	100.0	32.0	100.0	10.0	98.7	95	100	
3/8"	15.5	4.0	98.5	31.5	100.0	32.0	100.0	10.0	77.5	70	85	
#4	0.8	0.2	40.0	12.8	99.0	31.7	100.0	10.0	54.7	43	63	
#10	0.4	0.1	5.0	1.6	79.5	25.4	100.0	10.0	37.1	30	40	
#40	0.3	0.1	0.8	0.3	23.2	7.4	96.0	9.6	17.4	10	25	
#80	0.3	0.1	0.4	0.1	6.6	2.1	35.0	3.5	5.8	3	13	
#200	0.1	0.0	0.3	0.1	1.8	0.6	8.8	0.9	1.6	1	6	
Pan												
Optimum Asphalt Content			5.20%									
Asphalt Source & Grade			Koch Pav Solutions 76-22									

TABLE 54 Mix Design for Beckman Aggregate and Type C Mixture

Aggregate Source	Beckman												Total Cumulative Pass %	TxDOT Specs.	
	3/4"-5/8"		5/8"-1/2"		3/8"-1/4"		Grade 10		Mfg Sand		W. Poteet Sand				
	Bin #1	Total	Bin #2	Total	Bin #3	Total	Bin #4	Total	Bin #5	Total	Bin #6	Total			
Sieve Size	20.0	%	19.0	%	13.0	%	10.0	%	28.0	%	10.0	%	100.0%		
1"	100.0	20.0	100.0	19.0	100.0	13.0	100.0	10.0	100.0	28.0	100.0	10.0	100.0	100	100
3/4"	94.6	18.9	100.0	19.0	100.0	13.0	100.0	10.0	100.0	28.0	100.0	10.0	98.9	95	100
3/8"	3.8	0.8	58.1	11.0	100.0	13.0	100.0	10.0	100.0	28.0	100.0	10.0	72.8	70	85
# 4	1.1	0.2	3.6	0.7	26.0	3.4	84.0	8.4	99.9	28.0	100.0	10.0	50.7	43	63
# 8	1.1	0.2	2.8	0.5	14.7	1.9	2.0	0.2	85.6	24.0	99.8	10.0	36.8	32	44
# 30	1.0	0.2	1.7	0.3	2.8	0.4	2.0	0.2	32.9	9.2	88.0	8.8	19.1	14	28
# 50	1.0	0.2	1.5	0.3	2.0	0.3	1.7	0.2	18.6	5.2	52.2	5.2	11.3	7	21
# 200	0.7	0.1	1.3	0.2	1.6	0.2	1.5	0.2	8.6	2.4	1.6	0.2	3.3	1	6
Pan		0.0		0.0		0.0		0.0		0.0		0.0	0.0		
Optimum Asphalt Content			4.5%												
Asphalt Source & Grade			Valero PG 76-22												

TABLE 55 Mix Design for 50 Percent Brownlee + 50 Percent Beckman Aggregate and Type C Mixture

Aggregate Source	Delta Materials				Beckman								Total Cumulative Pass %	TxDOT Specs.	
	Type C		Type D		3/4"-5/8"		3/8"-1/4"		Mfg Sand		Washed Poteet Sand				
Sieve Size	Bin #1	Total	Bin #2	Total	Bin #3	Total	Bin #4	Total	Bin #5	Total	Bin #6	Total	100.0%	98	100
	9.0	%	19.0	%	8.0	%	22.0	%	27.0	%	15.0	%			
7/8"	100.0	9.0	100.0	19.0	100.0	8.0	100.0	22.0	100.0	27.0	100.0	15.0	100.0	98	100
5/8"	96.6	8.7	100.0	19.0	89.2	7.1	100.0	22.0	100.0	27.0	100.0	15.0	98.8	95	100
3/8"	3.8	0.3	70.9	13.5	3.8	0.3	100.0	22.0	100.0	27.0	100.0	15.0	78.1	70	85
# 4	1.5	0.1	16.3	3.1	1.1	0.1	26.0	5.7	99.9	27.0	100.0	15.0	51.0	43	63
# 10	1.0	0.1	4.0	0.8	1.0	0.1	3.4	0.7	70.9	19.1	99.6	14.9	35.7	30	40
# 40	0.7	0.1	2.3	0.4	1.0	0.1	2.1	0.5	25.0	6.8	69.2	10.4	18.3	10	25
# 80	0.6	0.1	1.8	0.3	0.9	0.1	1.9	0.4	13.1	3.5	14.4	2.2	6.6	3	13
# 200	0.4	0.0	1.1	0.2	0.7	0.1	1.6	0.4	8.6	2.3	1.6	0.2	3.2	1	6
Pan		0.0		0.0		0.0		0.0		0.0		0.0	0.0		
Optimum Asphalt Content					4.7%										
Asphalt Source & Grade					Valero PG 76-22										

TABLE 56 Mix Design for Brownlee Aggregate and Type C Mixture

Aggregate Source	Delta Materials				Capitol-GT		RTI-N				TXI		Total Cumulative Pass %	TxDOT Specs.	
	Delta C		D-Rock		F-Rock		Dry Screenings		Washed Screening		Field Sand				
	Bin #1	Total	Bin #2	Total	Bin #3	Total	Bin #4	Total	Bin #5	Total	Bin #6	Total			
	24.0	%	27.0	%	5.0	%	9.0	%	23.0	%	12.0	%	100.0%		
7/8"	100.0	24.0	100.0	27.0	100.0	5.0	100.0	9.0	100.0	23.0	100.0	12.0	100.0	98	100
5/8"	95.6	22.9	100.0	27.0	100.0	5.0	100.0	9.0	100.0	23.0	100.0	12.0	98.9	95	100
3/8"	3.8	0.9	88.4	23.9	100.0	5.0	100.0	9.0	100.0	23.0	100.0	12.0	73.8	70	85
#4	3.7	0.9	37.6	10.2	73.2	3.7	99.8	9.0	98.7	22.7	100.0	12.0	58.4	43	63
#10	3.6	0.9	4.4	1.2	10.2	0.5	80.7	7.3	46.6	10.7	100.0	12.0	32.5	30	40
#40	3.5	0.8	0.7	0.2	2.2	0.1	49.6	4.5	17.4	4.0	87.2	10.5	20.1	10	25
#80	3.4	0.8	0.6	0.2	1.7	0.1	36.4	3.3	11.0	2.5	28.7	3.4	10.3	3	13
#200	3.3	0.8	0.4	0.1	1.1	0.1	27.6	2.5	4.7	1.1	6.0	0.7	5.2	1	6
Pan		0.0		0.0		0.0		0.0		0.0		0.0	0.0		
Optimum Asphalt Content		4.50%													
Asphalt Source & Grade		Fina or Valero PG 76-22													

TABLE 57 Mix Design for Fordyce Aggregate and Type C Mixture

Aggregate Source	Fordyce C		Fordyce D/F		Fordyce Man Sand		Cl Mt Limestone Screening		Austin White		Total Cumulative Pass %	TxDOT Specs.		
	1323505		1323505		1323505		1504605		Lime					
Sieve Size	Bin #1	Total	Bin #2	Total	Bin #3	Total	Bin #4	Total	Bin #5	Total				
	18.0	%	57.0	%	10.0	%	14.0	%	1.0	%				
1"	100.0	18.0	100.0	57.0	100.0	10.0	100.0	14.0	100.0	1.0	100.0			
3/4"	100.0	18.0	100.0	57.0	100.0	10.0	100.0	14.0	100.0	1.0	100.0	98	100	
1/2"	70.0	12.6	100.0	57.0	100.0	10.0	100.0	14.0	100.0	1.0	94.6	90	100	
3/8"	10.0	1.8	95.0	54.2	100.0	10.0	100.0	14.0	100.0	1.0	81.0	70	95	
# 4	5.0	0.9	50.0	28.5	100.0	10.0	100.0	14.0	100.0	1.0	54.4	43	63	
# 8	3.0	0.5	15.0	8.6	99.0	9.9	92.0	12.9	100.0	1.0	32.9	32	44	
# 30	2.0	0.4	4.0	2.3	49.0	4.9	54.0	7.6	100.0	1.0	16.2	14	28	
# 50	1.5	0.3	3.0	1.7	23.0	2.3	41.0	5.7	100.0	1.0	11.0	7	21	
# 200	0.5	0.1	1.0	0.6	3.0	0.3	25.0	3.5	100.0	1.0	5.5	1	6	
Pan														
Optimum Asphalt Content			4.50%											
Asphalt Source & Grade			Eagle PG 76-22											

TABLE 58 Mix Design for El Paso Aggregate Type C and PFC Mixtures

Property		Mixture Type	
		Superpave-C	PFC
Binder Grade		PG 76-22	
Binder Content, %		4.8	6.6
Sieve Size, inch	(Sieve No.)		
1	1"	100	100
0.75	3/4"	99	100
0.492	1/2"	95	90
0.375	3/8"	92.5	47.5
0.187	# 4	77.5	10.5
0.0929	# 8	43	5.5
0.0469	# 16	30	5
0.0234	# 30	-	4.5
0.0117	# 50	-	3.5
0.0029	# 200	6	2.5

TABLE 59 Mix Design for Brownlee Aggregate and PFC Mixture

Aggregate Source	Delta				Capitol		Austin White		Total Cumulative Pass %	TxDOT Specs.		
	C-Rock		GR. 4		F-Rock		Lime					
Sieve Size	Bin #1	Total	Bin #2	Total	Bin #3	Total	Bin #4	Total				
3/4"	100.0	21.0	100.0	68.0	100.0	10.0	100.0	1.0	100.0		100	
1/2"	58.2	12.2	98.7	67.1	100.0	10.0	100.0	1.0	90.3	90	100	
3/8"	19.1	4.0	65.4	44.5	100.0	10.0	100.0	1.0	59.5	35	60	
# 4	2.0	0.4	2.2	1.5	84.5	8.5	100.0	1.0	11.4	10	25	
# 8	1.5	0.3	1.8	1.2	29.1	2.9	100.0	1.0	5.4	5	10	
# 200	0.5	0.1	1.3	0.9	2.3	0.2	100.0	1.0	2.2	1	4	
Pan												
Optimum Asphalt Content			6.0%									
Asphalt Source & Grade			Marlin PG 76-22S									

TABLE 60 Mix Design for Beckman Aggregate and PFC Mixture

Aggregate Source	Beckman				Austin White		Hi-tech Fibers		Total Cumulative Pass %	TxDOT Specs.	
	C-Rock		D-Rock		Lime						
Sieve	Bin #1	Total	Bin #2	Total	Bin #3	Total	Bin #4	Total			
Size	32.7	%	66.0	%	1.0	%	0.3	%	100.0%		
3/4"	100.0	32.7	100.0	66.0	100.0	1.0	100.0	0.3	100.0	100	100
1/2"	54.1	17.7	99.3	65.5	100.0	1.0	100.0	0.3	84.5	80	100
3/8"	4.0	1.3	76.0	50.2	100.0	1.0	100.0	0.3	52.8	35	60
# 4	1.1	0.4	7.5	5.0	100.0	1.0	100.0	0.3	6.6	1	20
# 8	1.0	0.3	3.9	2.6	100.0	1.0	100.0	0.3	4.2	1	10
# 200	0.4	0.1	1.4	0.9	100.0	1.0	100.0	0.3	2.4	1	4
Pan		0.0		0.0		0.0		0.0	0.0		
Optimum Asphalt Content			6.0%								
Asphalt Source & Grade			Marlin PG 76-22S								

TABLE 61 Mix Design for Brownwood Aggregate and PFC Mixture

Aggregate Source	Vulcan BWD		Total Cumulative Pass %	TxDOT Specs.	
	Grade 4				
Sieve	Bin#1	Total			
Size	100.0	Percent	100.0%		
3/4"	100.0	100.0	100.0	100	100
1/2"	99.2	99.2	99.2	95	100
3/8"	69.7	69.7	69.7	50	80
# 4	2.0	2.0	2.0	0	8
# 8	0.7	0.7	0.7	0	4
# 200	0.1	0.1	0.1	0	4
Optimum Asphalt Content			6.40%		
Asphalt Source & Grade			Valero 76-22		

TABLE 62 Mix Design for Beckman Aggregate and Type D Mixture

Aggregate Source	Beckman										Total Cumulative Pass %	TxDOT Specs.	
	1/2"-3/8"		3/8"-1/4"		Grade 10		Mfg Sand/LSF		W. Poteet Sand				
Sieve Size	Bin #1	Total	Bin #2	Total	Bin #3	Total	Bin #4	Total	Bin #5	Total	100%		
	9	%	34	%	20	%	22	%	15	%	100%		
3/4"	100	9	100	34	100	20	100	22	100	15	100	100	100
1/2"	100	9	100	34	100	20	100	22	100	15	100	98	100
3/8"	66	5.94	100	34	100	20	100	22	100	15	96.94	85	100
# 4	4.7	0.423	26	8.84	84	16.8	99.9	21.978	100	15	63.041	50	70
# 8	3.8	0.342	14.7	4.998	2	0.4	85.6	18.832	99.8	14.97	39.542	35	46
# 30	2.7	0.243	2.8	0.952	2	0.4	32.9	7.238	88	13.2	22.033	15	29
# 50	2.4	0.216	2	0.68	1.7	0.34	18.6	4.092	52.2	7.83	13.158	7	20
# 200	2.1	0.189	1.6	0.544	1.5	0.3	8.6	1.892	1.6	0.24	3.165	2	7
Pan		0		0		0		0		0	0		
Optimum Asphalt Content			4.7										
Asphalt Source & Grade			Valero PG 64-22										

TABLE 63 Mix Design for Brownlee Aggregate and Type D Mixture

Aggregate Source	Delta		Capitol-GT		Brownlee		RTI-N				TXI		Total Cumulative Pass %	TxDOT Specs.	
	D-Rock		F-Rock		Grade #4		Dry Screenings		Washed Screening		Field Sand				
Sieve Size	Bin #1	Total	Bin #2	Total	Bin #3	Total	Bin #4	Total	Bin #5	Total	Bin #6	Total	100.0	100	100
	50.0	%	10.0	%	7.0	%	0.0	%	21.0	%	12.0	%			
7/8"	100.0	50.0	100.0	10.0	100.0	7.0	100.0	0.0	100.0	21.0	100.0	12.0	100.0	100	100
5/8"	100.0	50.0	100.0	10.0	100.0	7.0	100.0	0.0	100.0	21.0	100.0	12.0	100.0	98	100
3/8"	79.9	40.0	100.0	10.0	60.0	4.2	100.0	0.0	100.0	21.0	100.0	12.0	87.2	85	100
# 4	40.3	20.1	77.9	7.8	10.4	0.7	97.5	0.0	99.6	20.9	100.0	12.0	61.6	50	70
# 10	14.7	7.3	10.2	1.0	0.7	0.1	74.5	0.0	84.0	17.6	99.3	11.9	38.0	35	46
# 40	9.4	4.7	2.7	0.3	0.6	0.0	41.9	0.0	32.0	6.7	84.4	10.1	21.8	15	29
# 80	8.5	4.2	2.0	0.2	0.5	0.0	34.6	0.0	11.4	2.4	15.9	1.9	8.8	7	20
# 200	6.9	3.4	1.5	0.2	0.5	0.0	26.7	0.0	3.1	0.7	0.7	0.1	4.4	2	7
Optimum Asphalt Content			5.3%												
Asphalt Source & Grade			Valero PG 76-22												

TABLE 64 Mix Design for 50 Percent Beckman and 50 Percent Brownlee and Type D Mixture

Aggregate Source	Delta Materials		Beckman				Beckman				Total Cumulative Pass %	TxDOT Specs.	
	Brownlee Type D		3/8"-1/4"		Mfg Sand		W. Poteet Sand		Sieved Mfg Sand				
Sieve Size	Bin #1	Total	Bin #2	Total	Bin #3	Total	Bin #4	Total	Bin #5	Total	100%	100	100
	20.0	%	31.0	%	31.0	%	11.0	%	7.0	%			
7/8"	100.0	20.0	100.0	31.0	100.0	31.0	100.0	11.0	100.0	7.0	100.0	100	100
5/8"	100.0	20.0	100.0	31.0	100.0	31.0	100.0	11.0	100.0	7.0	100.0	98	100
3/8"	70.9	14.2	100.0	31.0	100.0	31.0	100.0	11.0	100.0	7.0	94.2	85	100
No. 4	16.3	3.3	26.0	8.1	99.9	31.0	100.0	11.0	100.0	7.0	60.3	50	70
No. 10	4.0	0.8	3.4	1.1	70.9	22.0	99.6	11.0	100.0	7.0	41.8	35	46
No. 40	2.3	0.5	2.1	0.7	25.0	7.8	69.2	7.6	100.0	7.0	23.5	15	29
No. 80	1.8	0.4	1.9	0.6	13.1	4.1	14.4	1.6	100.0	7.0	13.6	7	20
No. 200	1.1	0.2	1.6	0.5	8.6	2.7	1.6	0.2	0.0	0.0	3.6	2	7
Optimum Asphalt Content			5.3%										
Asphalt Source & Grade			Valero PG 76-22										

APPENDIX B

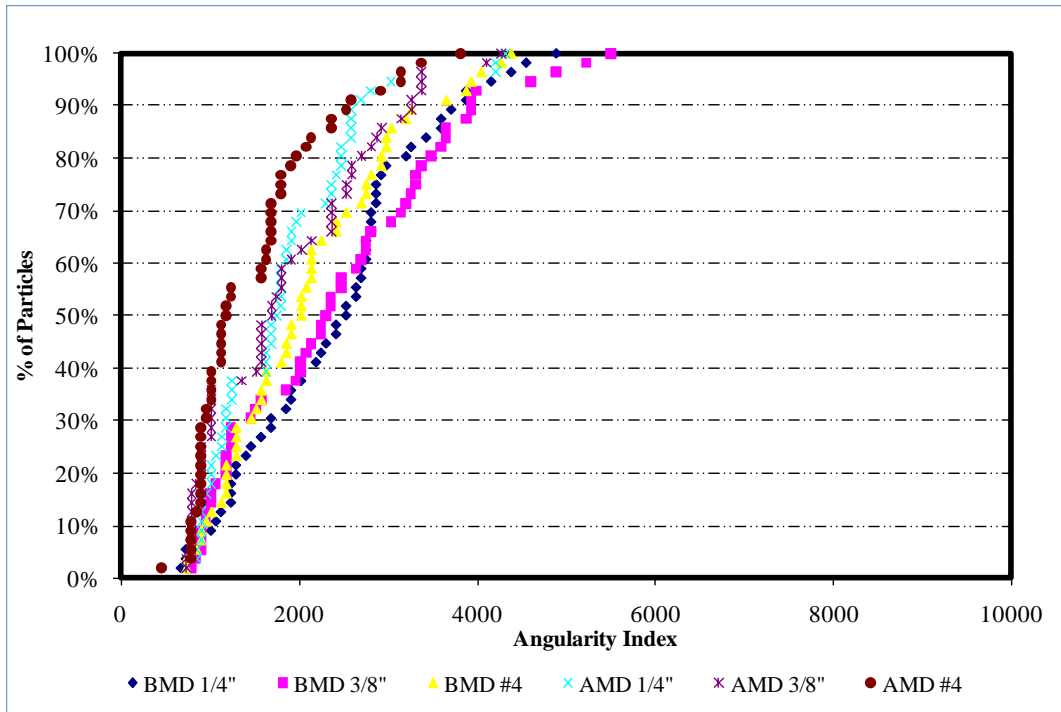


FIGURE 134 Results of angularity measurements by AIMS for Brownwood aggregate.

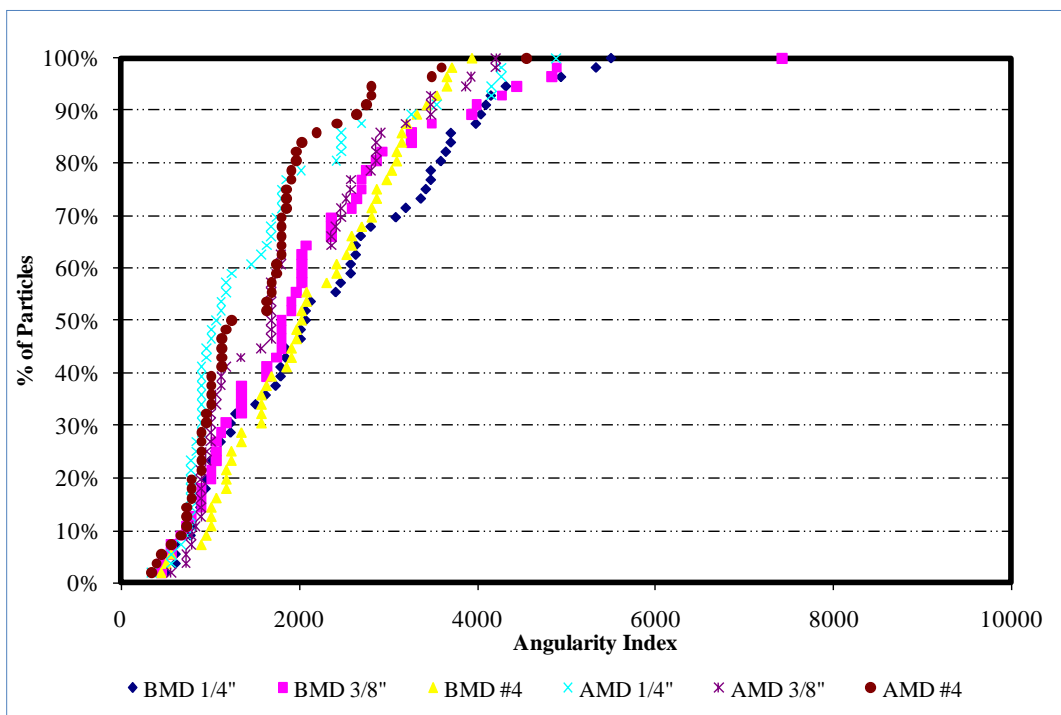


FIGURE 135 Results of angularity measurements by AIMS for Beckman aggregate.

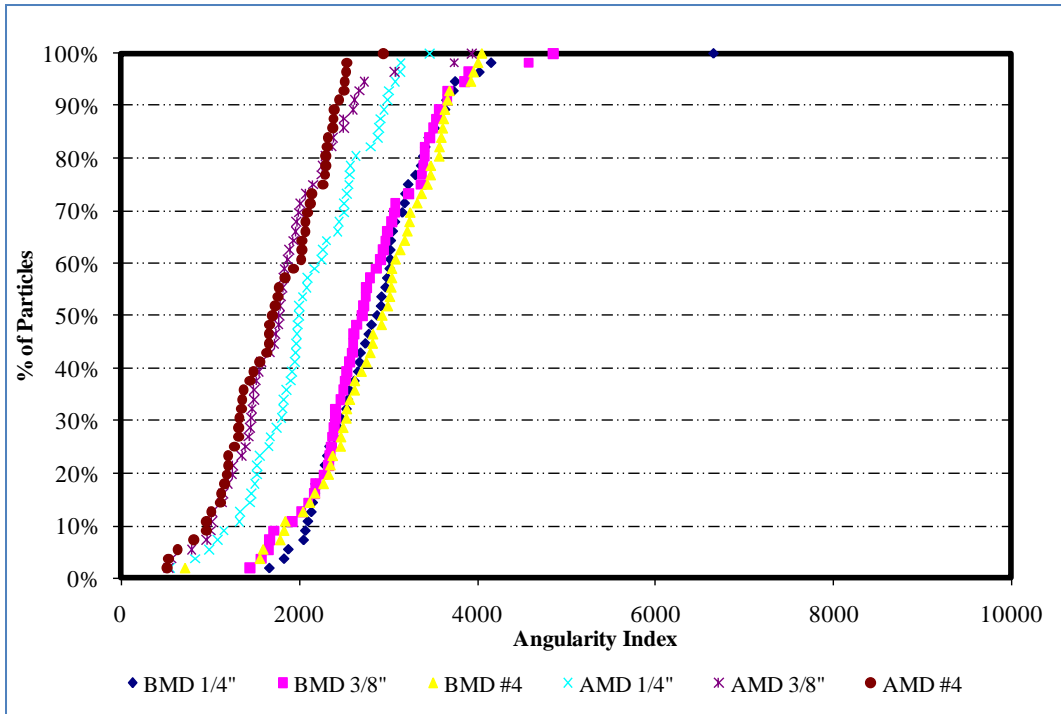


FIGURE 136 Results of angularity measurements by AIMS for Brownlee aggregate.

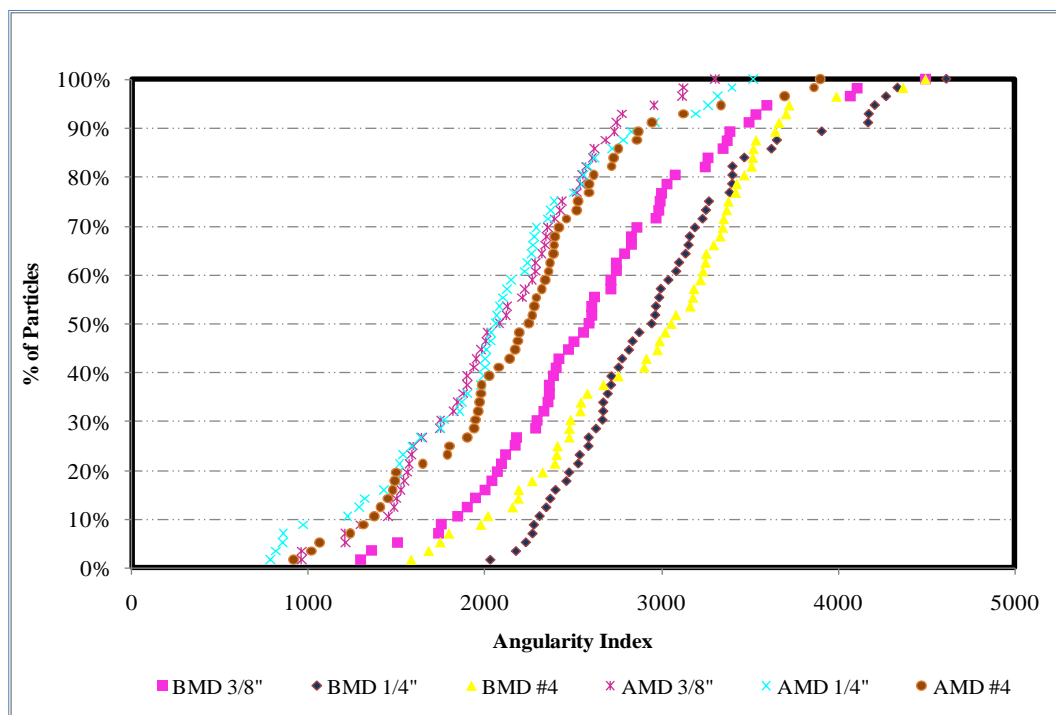


FIGURE 137 Results of angularity measurements by AIMS for El Paso aggregate.

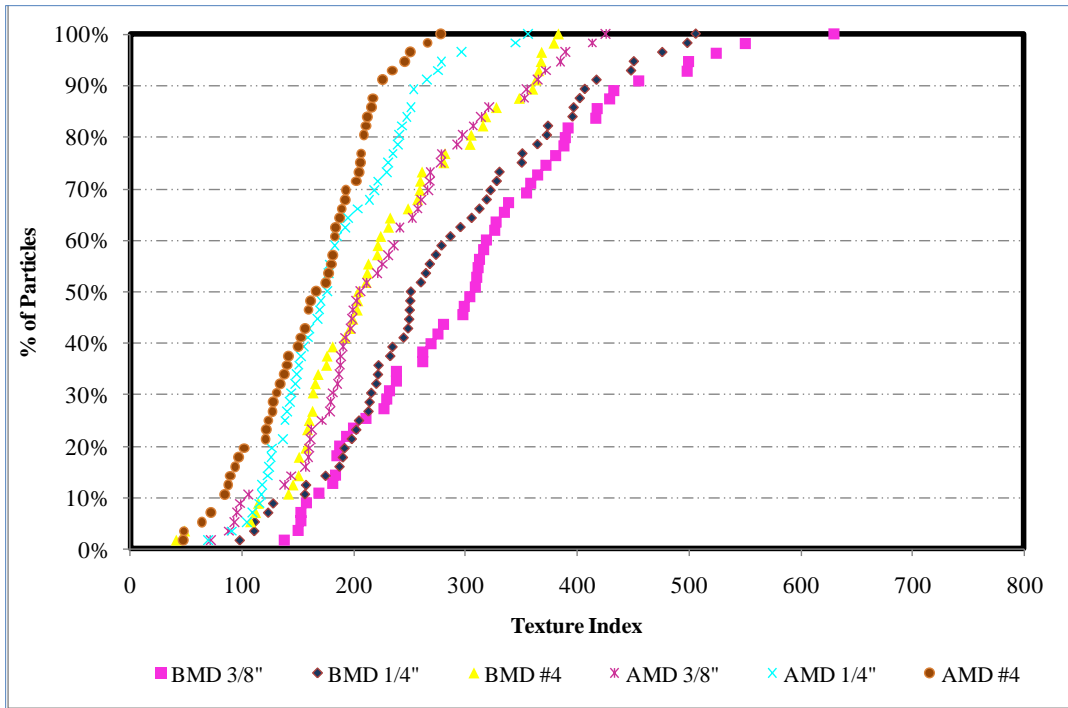


FIGURE 138 Results of texture measurements by AIMS for El Paso aggregate.

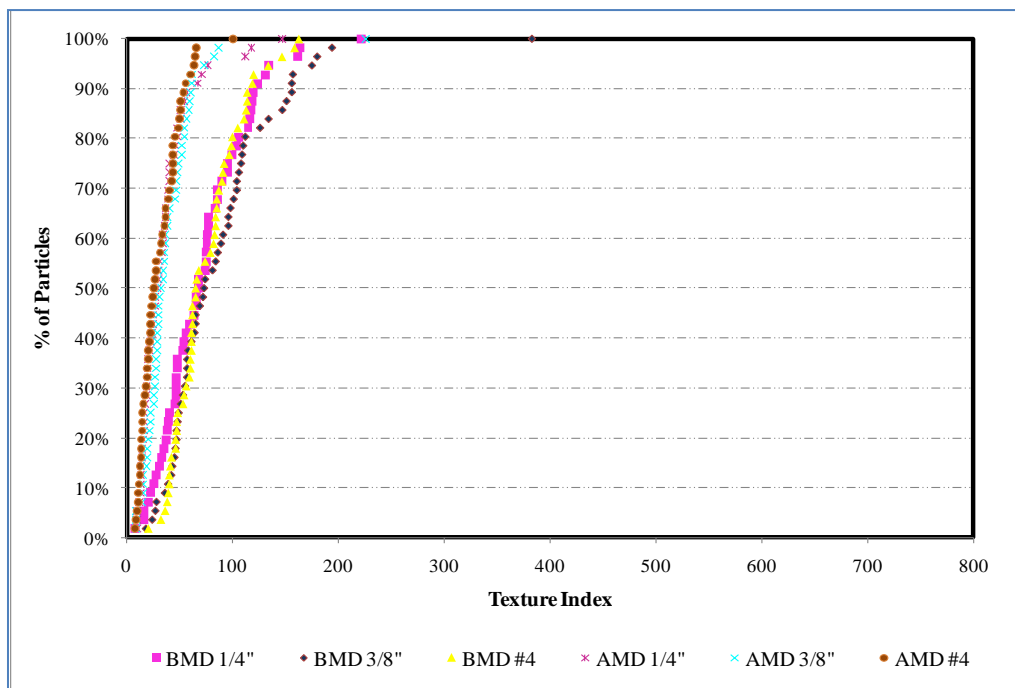


FIGURE 139 Results of texture measurements by AIMS for Beckman aggregate.

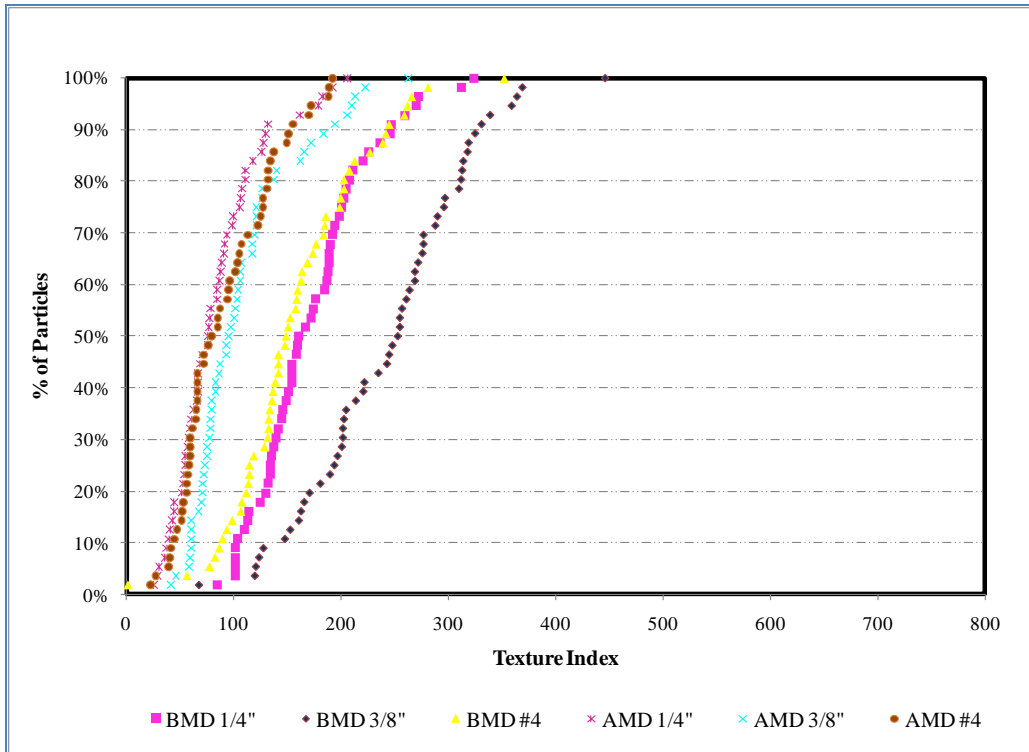


FIGURE 140 Results of texture measurements by AIMS for Brownwood aggregate.

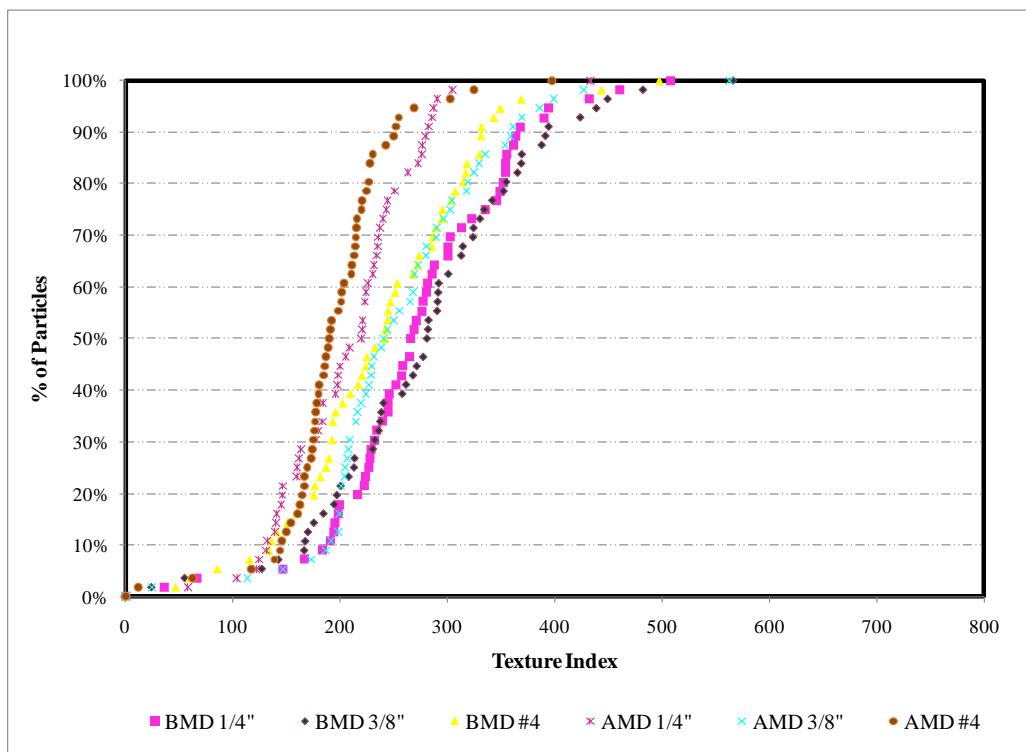


FIGURE 141 Results of texture measurements by AIMS for Brownlee aggregate

APPENDIX C

TEX-461-A, DEGRADATION OF COARSE AGGREGATE BY MICRO-DEVAL ABRASION

Section 1

Overview

Use this test method to test coarse aggregate for resistance to abrasion and weathering using the Micro-Deval apparatus.

Units of Measurement

The values given in parentheses (if provided) are not standard and may not be exact mathematical conversions. Use each system of units separately. Combining values from the two systems may result in nonconformance with the standard.

Section 2

Definitions

The following term is referenced in this test procedure.

◆ **Constant weight.** Constant weight is defined as aggregates other than limestone rock asphalt are dried at a temperature of $230 \pm 9^{\circ}\text{F}$ ($110 \pm 5^{\circ}\text{C}$) to a condition such that they will not lose more than 0.1% moisture after 2 hr of drying. Limestone rock asphalt samples will be dried at a temperature of $140 \pm 5^{\circ}\text{F}$ ($60 \pm 3^{\circ}\text{C}$) to a condition such that they will not lose more than 0.1% moisture after 2 hr of drying. Such a condition of dryness can be verified by weighing the sample before and after successive 2-hr drying periods. In lieu of such determination, samples may be considered to have reached constant weight when they have dried at a temperature of $230 \pm 9^{\circ}\text{F}$ ($110 \pm 5^{\circ}\text{C}$) for an equal or longer period than that previously found adequate for producing the desired constant condition under equal or heavier loading conditions of the oven.

Section 3

Apparatus

Use the following apparatus:

- ◆ Micro-Deval Abrasion machine and accessories that meet department specification No. 845-49-40.
- ◆ Standard U.S. sieves and pans, meeting the requirements of “Tex-907-K, Verifying the Accuracy of Wire Cloth Sieves,” including:
 - 3/4 in. (19.0 mm).
 - 1/2 in. (12.5 mm).
 - 3/8 in. (9.5 mm).
 - 1/4 in. (6.3 mm).
 - No. 4 (4.75 mm).
- ◆ Oven, capable of maintaining a temperature of $230 \pm 9^{\circ}\text{F}$ ($110 \pm 5^{\circ}\text{C}$)
- ◆ Balance, accurate and readable to 0.1 g or 0.1% of the mass of the test sample, whichever is greater.

Section 4

Preparing Sample

Wash and dry the test sample to constant weight. Separate the sample into individual size fractions according to “Tex 401-A, Sieve Analysis of Fine and Coarse Aggregate” and recombine to meet the grading as shown. Dry limestone rock asphalt to constant weight at $140 \pm 9^{\circ}\text{F}$ ($60 \pm 5^{\circ}\text{C}$).

- ◆ For bituminous aggregate, use the following standard gradation:

Bituminous Aggregate		
Passing	Retained	Wt. (g)
1/2 in. (12.5 mm)	3/8 in. (9.5 mm)	750 ±5
3/8 in. (9.5 mm)	1/4 in. (6.3 mm)	375 ±5
1/4 in. (6.3 mm)	No. 4 (4.75 mm)	375 ±5

- ◆ For concrete aggregate, use the following standard gradation:

Concrete Aggregate		
Passing	Retained	Wt. (g)
3/4 in. (19.0 mm)	1/2 in. (12.5 mm)	660 ±5
1/2 in. (12.5 mm)	3/8 in. (9.5 mm)	330 ±5
3/8 in. (9.5 mm)	1/4 in. (6.3 mm)	330 ±5
1/4 in. (6.3 mm)	No. 4 (4.75 mm)	180 ±5

SECTION 5

Procedure

The following table outlines the procedure for testing coarse aggregate for resistance to abrasion and weathering using the Micro-Deval apparatus.

Testing Coarse Aggregate	
Step	Action
1	<ul style="list-style-type: none"> ◆ Prepare a representative 1500 ±5 g sample according to the applicable standard grading. A maximum of 10% of an adjacent size material from the standard grading may be substituted if the sample does not contain appropriate weights. Crush parent material to obtain sizes if necessary. ◆ Record the weight to the nearest 1.0 g, as 'A' under "Calculations."
2	Saturate the sample in 0.5 gal (2000 ±500 mL) of tap water (temperature 68 ±9°F [20 ±5°C]) for a minimum of 1 hr either in the Micro-Deval container or in another suitable container.
3	<ul style="list-style-type: none"> ◆ Place the sample, water, and 5000 ±5 g of stainless steel balls in the Micro-Deval container. ◆ Place the Micro-Deval container on the machine.
4	<ul style="list-style-type: none"> ◆ Set the timer and start the machine. <ul style="list-style-type: none"> ◆ Test concrete aggregate samples at 100 ±5 rpm for 120 ±1 min. ◆ Test bituminous aggregate samples at 100 ±5 rpm for 105 ±1 min. ◆ Record the rpms registered by the tachometer at the end of the test period.
5	<ul style="list-style-type: none"> ◆ Stack a No. 4 (4.75 mm) and a No. 16 (1.18 mm) sieve together and carefully decant the sample over them. Take care to remove the entire sample from the stainless steel jar. ◆ Wash the retained material with water until the wash water is clear and all materials smaller than No. 16 (1.18 mm) pass the sieve.
6	<ul style="list-style-type: none"> ◆ Remove the stainless steel balls using a magnet or other suitable means. ◆ Discard material passing the No. 16 (1.18 mm) sieve.
7	<ul style="list-style-type: none"> ◆ Oven-dry the sample to constant weight at 230 ±9°F (110 ±5°C). ◆ Oven-dry limestone rock asphalt to constant weight at 140 ±9°F (60 ±5°C).
8	<ul style="list-style-type: none"> ◆ Weigh the sample to the nearest 1.0 g. ◆ Record the oven-dry weight as 'B' under "Calculations."

Section 6

Calculations

Calculate the Micro-Deval abrasion loss as follows:

$$\text{Percent loss} = (A - B) / A \times 100$$

Record the nearest whole percentage point.

DETERMINING AGGREGATE SHAPE PROPERTIES BY MEANS OF DIGITAL IMAGE ANALYSIS

SCOPE

This standard covers the measurement of aggregate shape properties using the digital image analysis techniques.

This standard may involve hazardous materials, operations, and equipment. This standard does not purport to address all of the safety problems associated with its use. It is the responsibility of the user of this standard to establish appropriate safety and health practices and determine the applicability of regulatory limitations prior to use.

REFERENCED DOCUMENTS

AASHTO Standards:

- M 92 Standard Specification for Wire-Cloth Sieves for Testing Purposes
- T 2 Sampling of Aggregates
- T 11 Amount of Material Finer Than 75 μ m in Aggregate
- T 27 Standard Method of Test for Sieve Analysis of Fine and Coarse Aggregates
- T 84 Standard Method of Test for Specific Gravity and Absorption of Fine Aggregate
- T 85 Standard Method of Test for Specific Gravity and Absorption of Coarse Aggregate
- T 248 Standard Method of Test for Reducing Samples of Aggregate to Testing Size

Other References:

- ASTM C 802, "Standard Practice for Conducting an Interlaboratory Test Program to Determine the Precision of Test Methods for Construction Materials."
- ASTM C 670 "Standard Practice for Preparing Precision and Bias Statements for Test Methods for Construction Materials."

TERMINOLOGY

Aggregate Size—sieve size in which material is retained after passing the next larger sieve.

Fine Aggregate—Aggregate material passing 4.75mm (#4) sieve.

Sieve sizes: 2.36mm (#8), 1.18mm (#16), 0.60mm (#30), 0.30mm (#50), 0.15mm (#100), 0.075mm (#200).

Coarse Aggregate—Aggregate material retained on 4.75mm (#4) sieve.

Sieve sizes: 25.0mm (1”), 19.0mm (3/4”), 12.5mm (1/2”), 9.5mm (3/8”), 4.75mm (#4)

Shape Properties for each Retained Sieve (X).

Gradient Angularity (GA)—Applies to both fine and coarse aggregate sizes and is related to the sharpness of the corners of 2-dimensional images of aggregate particles. The gradient angularity quantifies changes along a particle boundary with higher gradient values indicating a more angular shape. Gradient angularity has a relative scale of 0 to 10000 with a perfect circle having a value of 0.

$$\text{Gradient Angularity: } GA = \frac{1}{\frac{n}{3} - 1} \sum_{i=1}^{n-3} |\theta_i - \theta_{i+3}| \quad (1)$$

where: θ angle of orientation of the edge points

n is the total number of points

subscript i denoting the i^{th} point on the edge of the particle

Texture or Micro-Texture (TX)—Applies to coarse aggregate sizes only describing relative smoothness or roughness of surface features less than roughly 0.5 mm in size which are too small to affect the overall shape. Texture has a relative scale of 0 to 1000 with a smooth polished surface approaching a value of 0.

$$TX = \frac{1}{3N} \sum_{i=1}^3 \sum_{j=1}^N (D_{i,j}(x, y))^2 \quad (2)$$

where:

D = decomposition function

n = decomposition level

N = total number of coefficients in an image

$i = 1, 2, \text{ or } 3$ for detailed images

j = wavelet index

x, y = location of the coefficients in transformed domain

Sphericity (SP)—Applies to coarse aggregate sizes only and describes the overall three dimensional shape of a particle. Sphericity has a relative scale of 0 to 1. A sphericity value of one indicates a particle has equal dimensions (cubical).

$$SP = \sqrt[3]{\frac{d_s * d_l}{d_L^2}} \quad (3)$$

where: d_s = particle shortest dimension

d_l = particle intermediate dimension

d_L = particle longest dimension

Form 2D—Applies to fine aggregate sizes only and is used to quantify the relative form from 2-dimensional images of aggregate particles. Form2D has a relative scale of 0 to 20. A perfect circle has a Form 2D value of zero.

$$Form2D = \sum_{\theta=0}^{\theta=360-\Delta\theta} \left[\frac{R_{\theta+\Delta\theta} - R_{\theta}}{R_{\theta}} \right] \quad (4)$$

where: R_{θ} is the radius of the particle at an angle of θ

$\Delta\theta$ is the incremental difference in the angle

Flat and Elongated—those particles having a ratio of longest dimension to shortest dimension greater than a specified value.

Aggregate particle dimensions in an x, y, z coordinate system

d_s = particle shortest dimension

d_l = particle intermediate

d_L = particle longest dimension

$$\text{Flatness Ratio (S/L): } \text{Flatness} = \frac{d_s}{d_l} \quad (5)$$

$$\text{Elongation Ratio (I/L): } \text{Elongation} = \frac{d_l}{d_L} \quad (6)$$

$$\text{Flat and Elongated Value (F\&E): } L/S = \frac{d_L}{d_s} \quad (7)$$

Flat or Elongated—those particles having a ratio of intermediate dimension to shortest dimension or longest dimension to intermediate dimension greater than a specified value.

$$\text{Flat or Elongated Value (ForE): } \frac{d_l}{d_s} \text{ or } \frac{d_L}{d_l} > \text{Ratio (i.e.: 1, 2, 3...)} \quad (8)$$

SIGNIFICANCE AND USE

Shape, angularity, and surface texture of aggregates have been shown to directly affect the engineering properties of highway construction materials such as hot mix asphalt concrete, Portland cement concrete, and unbound aggregate layers. This standard provides direct measurement of aggregate shape, angularity, and texture. For coarse aggregates, the shape properties include: gradient angularity, sphericity, texture, and flat and elongated value. For fine aggregates the shape properties include: gradient angularity and form-2d.

Note 1—The National Cooperative Highway Research Program Report 555 provides background information relevant to characterizing aggregate shape, texture, and angularity.

This test method may be used to characterize and monitor the shape properties of aggregate material samples sizes 0.075 mm (#200) through 25.0mm (1"). This method may be used to characterize a single size within a material source or all sizes within the source.

APPARATUS

Digital image acquisition and analysis system—a computer controlled electro-mechanical instrument for capturing digital images at variable magnification and software for image analysis. Instrumentation and analysis software shall include algorithms for gradient angularity, form 2d, flat and elongated, sphericity, and texture.

A camera and optic system capable of providing the required resolutions over the range of particles being analyzed.

A system for positioning the particle for imaging. This can be a movable camera, a movable support tray, or a combination thereof.

A system for auto-focusing the image.

A system for determining particle three-dimensional measurements x, y, z in millimeters.

A system for detecting and removing touching particles from the analysis.

A system for presenting the particles for imaging consisting of trays or other support surface for aggregate sizes from 0.075 mm (#200) through 25.0mm (1"). The particles shall be presented for imaging on a flat surface. A small recess for aligning particles is acceptable.

A variable lighting system for backlighting and/or top lighting the material sample.

Note 2—The Aggregate Image Measurement System and the associated AIMS SOFTWARE algorithms for image analysis computations have proven to be an acceptable system for this analysis.

Balance—a balance meeting the requirements of m 231, class g 5, for determining the mass of aggregates.

Oven—an oven of appropriate size capable of maintaining a uniform temperature of $110\pm 5^{\circ}\text{C}$ ($290\pm 9^{\circ}\text{F}$)

Miscellaneous— equipment to perform sample preparation methods AASHTO t 2, t 11, t 27, t 248.

HAZARDS

Use standard safety precautions and protective clothing when handling materials and preparing material samples.

STANDARDIZATION

Confirm the image acquisition system has been standardized. Frequency and method of standardization shall follow manufacturer's instructions.

PREPARATION OF APPARATUS

Confirm the system has been standardized by verifying the standardization date.

Confirm the machine operation settings are correct for the analysis to be performed.

SAMPLE PREPARATION

Sample the aggregate according to procedures in AASHTO T2.

Note 3—Material samples obtained for AASHTO T84 and T85 specific gravity determinations have proven to be acceptable.

Thoroughly mix the sample and reduce it to the approximate quantity needed using the applicable procedures in AASHTO T248.

Determine the amount of material finer than 0.075 mm (#200) by AASHTO T11.

Oven dry the sample at $110\pm 5^{\circ}\text{C}$ ($230\pm 9^{\circ}\text{F}$) to substantially constant mass.

Determine the sample grading on the washed, dry sample in accordance with AASHTO T27. Calculate the percentage of material in each size fraction. Maintain sample material as separate retained sieve sizes.

Obtain the required aggregate of each size from the sample using the procedures described in AASHTO T248.

Maintain the necessary size fractions obtained in a dry condition in separate containers for each size.

The following list provides suggested sample mass to achieve the required minimum particle count for each size fraction:

<u>Size</u>	<u>Approx. Mass</u>	<u>Minimum Number of Particles</u>
0.075 mm (#200)	200 g	150
0.15 mm (#100)	200 g	150
0.3 mm (#50)	200 g	150
0.6 mm (#30)	200 g	150
1.18 mm (#16)	200 g	150
2.36 mm (#8)	200 g	150
4.75 mm (#4)	2 kg	50
9.5 mm (3/8 inch)	2 kg	50
12.5 mm (1/2 inch)	2 kg	50
19.0 mm (3/4 inch)	2 kg	50
25.0 mm (1 inch)	5 kg	50

PROCEDURE FOR COARSE AGGREGATE

Position the coarse aggregate sample for image acquisition by size fraction. Each size fraction of retained material may be run separately.

Distribute the coarse aggregate sample over the support surface in a manner that provides separation of at least 1.0 mm between particles. Particle orientation shall be determined by permitting them to come to rest randomly.

Initiate the image acquisition sequence and analysis algorithms. This process is typically automated. The operator inputs the material size and the system automatically captures the required images and calculates the shape properties for each particle.

Each characterization requires the minimum number of particles for each size fraction listed in section 0 to be analyzed. If the required particle count is not achieved in one sequence, repeat the sequence with additional particles until the required number of images is acquired.

For sizes that contain inadequate percent retained mass to achieve minimum particle count use the shape value obtained from the next larger or the next smaller size, whichever is present.

PROCEDURE FOR FINE AGGREGATE

Position the fine aggregate sample for image acquisition by size fraction. Each size fraction of retained material may be run separately.

Note 4—Most fine aggregate materials are analyzed using backlighting. However, some translucent materials may require a dark background and top lighting to achieve the appropriate image contrast. If the system fails to capture usable images with backlighting, use a dark background and top lighting. A dark background is typically required for 0.30mm (#50) and smaller sizes.

Distribute the fine aggregate sample over the support surface in a manner that provides separation between particles. Typically only a very light coating is needed. Particles orientation shall be determined by permitting them to come to rest randomly.

Initiate the image acquisition sequence and run the analysis routines. This process is typically automated. The operator selects the material size and the system automatically captures the required images and calculates the shape properties for each particle.

Each characterization requires the minimum number of particles for each size fraction listed in section 0 to be analyzed. If the required particle count is not achieved in one sequence, repeat the sequence until the required number of images is acquired.

For sizes that contain inadequate percent retained mass to achieve minimum particle count use the shape value obtained from the next larger or the next smaller size, whichever is present.

CALCULATIONS

Calculate gradient angularity value for each fine and coarse aggregate particle.

Calculate the gradient angularity mean and standard deviation for each size fraction.

Calculate the texture (TX) value for each coarse particle.

Calculate the texture mean and standard deviation for each coarse size fraction.

Calculate the sphericity (Sp) for each coarse aggregate particle.

Calculate the sphericity mean and standard deviation for each coarse size fraction.

Calculate the form 2d value for each fine particle.

Calculate the form2d mean and standard deviation for each fine size fraction.

Calculate the percent distribution of flat and elongated at the following ratios:

$\geq 1:1, >2:1, >3:1, >4:1, >5:1$

$\%L/S(\geq 1)_x = \% \text{ of Particles with } d_L/d_S \geq 1$

$\%L/S(>2)_x = \% \text{ of Particles with } d_L/d_S > 2$

$\%L/S(>3)_x = \% \text{ of Particles with } d_L/d_S > 3$

$\%L/S(>4)_x = \% \text{ of Particles with } d_L/d_S > 4$

$\%L/S(>5)_x = \% \text{ of Particles with } d_L/d_S > 5$

where: x designates the retained sieve size

Calculate the percent distribution of flat or elongated at the following ratios:

$\geq 1:1, >2:1, >3:1, >4:1, >5:1$

$\%F_{orE}(\geq 1)_x = \% \text{ of Particles with } d_I/d_S \text{ or } d_L/d_I \geq 1$

$\%F_{orE}(>2)_x = \% \text{ of Particles with } d_I/d_S \text{ or } d_L/d_I > 2$

$\%F_{orE}(>3)_x = \% \text{ of Particles with } d_I/d_S \text{ or } d_L/d_I \leq 3$

$\%F_{orE}(>4)_x = \% \text{ of Particles with } d_I/d_S \text{ or } d_L/d_I > 4$

$\%F_{orE}(>5)_x = \% \text{ of Particles with } d_I/d_S \text{ or } d_L/d_I > 5$

where: x designates the retained sieve size

REPORT

Report the following information:

Procedure used.

Date of the analysis.

Material sample identification: type, source, and size.

Number of particles analyzed.

Material shape property mean and standard deviation. Graphical representations of the property distributions may be included.

PRECISION AND BIAS

Precision—an inter-laboratory study (ILS) was conducted in 2009 in accordance with ASTM C802, “standard practice for conducting an inter-laboratory test program to

determine the precision of test methods for construction materials.” The ILS results were used to develop a precision statement for the test method using ASTM C670, “standard practice for preparing precision and bias statements for test methods for construction materials.” The ILS featured eight systems, 32 laboratories, and three material sources.

Precision for Sizes (mm) 25, 19, 12.5, 9.5, 4.75, 2.36, 1.18, 0.60, 0.30, and 0.15.

Aggregate Shape Characteristic	Within Laboratory		Between Laboratory	
	Coefficient of Variation (% of mean)	Acceptable Range of Two Results (% of mean)	Coefficient of Variation (% of mean)	Acceptable Range of Two Results (% of mean)
Angularity	2.9%	8.2%	4.3%	12.1%
Texture	4.5%	12.7%	7.1%	19.8%
Sphericity	1.2%	3.4%	2.6%	7.2%
Flat or Elongated	2.1%	5.9%	3.4%	9.6%
2D Form	2.8%	7.7%	3.5%	9.9%

Bias—since there is no accepted reference device suitable for determining the bias in this method, no statement of bias is made.

KEYWORDS

Aggregate; angularity; consensus property, shape, texture, form, elongated.

DETERMINING AGGREGATE SOURCE SHAPE VALUES FROM DIGITAL IMAGE ANALYSIS SHAPE PROPERTIES

SCOPE

This standard covers the determination of aggregate source and source blend shape characteristics using gradation analysis and shape properties determined by means of digital image analysis.

This standard may involve hazardous materials, operations, and equipment. This standard does not purport to address all of the safety problems associated with its use. It is the responsibility of the user of this standard to establish appropriate safety and health practices and determine the applicability of regulatory limitations prior to use.

REFERENCED DOCUMENTS

AASHTO Standards:

- T 11 Amount of Material Finer than 75 μ m in Aggregate
- T 27 Standard Method of Test for Sieve Analysis of Fine and Coarse Aggregates
- T 84 Standard Method of Test for Specific Gravity and Absorption of Fine Aggregate
- T 85 Standard Method of Test for Specific Gravity and Absorption of Coarse Aggregate
- TP XX Standard Method of Test for Determining Aggregate Shape Properties by Means of Digital Image Analysis

TERMINOLOGY

Aggregate Size—material retained on a given sieve size after passing the next larger sieve.

Fine Aggregate—Aggregate material passing 4.75mm (#4) sieve.

Sieve Sizes: 2.36mm (#8), 1.18mm (#16), 0.60mm (#30), 0.30mm (#50), 0.15mm (#100), 0.075mm (#200).

Coarse Aggregate—Aggregate material retained on 4.75mm (#4) sieve.

Sieve Sizes: 25.0mm (1"), 19.0mm (3/4"), 12.5mm (1/2"), 9.5mm (3/8"), 4.75mm (#4).

Shape Properties For Each Retained Sieve (X).

Gradient Angularity (GA)—Applies to both fine and coarse aggregate sizes and is related to the sharpness of the corners of 2-dimensional images of aggregate particles. The gradient angularity quantifies changes along a particle boundary with higher gradient values indicating a more angular shape. Gradient angularity has a relative range of 0 to 10,000 with a perfect circle having a value of 0.

$$\text{Gradient Angularity: } GA = \frac{1}{\frac{n}{3} - 1} \sum_{i=1}^{n-3} |\theta_i - \theta_{i+3}| \quad (1)$$

where: θ angle of orientation of the edge points

n is the total number of points

subscript i denoting the i^{th} point on the edge of the particle

Texture (or Micro-Texture) (TX)—Applies to coarse aggregate sizes only and describes the relative smoothness or roughness of surface features less than roughly 0.5 mm in size that are too small to affect the overall shape. Texture has a relative scale of 0 to 1000 with a smooth polished surface approaching a value of 0.

$$TX = \frac{1}{3N} \sum_{i=1}^3 \sum_{j=1}^N (D_{i,j}(x, y))^2 \quad (2)$$

where:

D = decomposition function

n = decomposition level

N = total number of coefficients in an image

$i = 1, 2, \text{ or } 3$ for detailed images

j = wavelet index

x, y = location of the coefficients in transformed domain

Sphericity (SP)—Applies to coarse aggregate sizes only and describes the overall three dimensional shape of a particle. Sphericity has a relative scale of 0 to 1. A sphericity value of one indicates a particle has equal dimensions (cubical).

$$SP = \sqrt[3]{\frac{d_s * d_l}{d_L^2}} \quad (3)$$

where: d_s = particle shortest dimension

d_l = particle intermediate dimension

d_L = particle longest dimension

Form 2D—Applies to fine aggregate sizes only and is used to quantify the relative form from 2-dimensional images of aggregate particles. Form2D has a relative scale of 0 to 20. A perfect circle has a Form 2D value of zero.

$$Form2D = \sum_{\theta=0}^{\theta=360-\Delta\theta} \left[\frac{R_{\theta+\Delta\theta} - R_{\theta}}{R_{\theta}} \right] \quad (4)$$

where: R_{θ} is the radius of the particle at an angle of θ

$\Delta\theta$ is the incremental difference in the angle

Flat and Elongated—those particles having a ratio of longest dimension to shortest dimension greater than a specified value.

Aggregate particle dimensions in an x, y, z coordinate system

d_s = particle shortest dimension

d_l = particle intermediate

d_L = particle longest dimension

$$Flatness Ratio (S/L): Flatness = \frac{d_s}{d_l} \quad (5)$$

$$\text{Elongation Ratio (I/L): } \text{Elongation} = \frac{d_I}{d_L} \quad (6)$$

$$\text{Flat and Elongated Value (F\&E): } L/S = \frac{d_L}{d_s} \quad (7)$$

Flat or Elongated—those particles having a ratio of intermediate dimension to shortest dimension or longest dimension to intermediate dimension greater than a specified value.

$$\text{Flat or Elongated (ForE): } \frac{d_I}{d_s} \text{ or } \frac{d_L}{d_I} > \text{Ratio (i.e.: 1, 2, 3...)} \quad (8)$$

%Pass_x = % passing sieve x

%R_x = % retained on sieve x (passing sieve x+1)

SIGNIFICANCE AND USE

Shape, angularity, and surface texture of aggregates have been shown to directly affect the engineering properties of highway construction materials such as hot mix asphalt concrete, Portland cement concrete, and unbound aggregate layers. This standard is used to characterize the combined shape values for an aggregate source from the individual particle shape properties determined by digital image analysis from AASHTO test method xx-xx. The aggregate shape characterization includes gradient angularity, form 2d, sphericity, texture, and flat and elongated value.

Note 1—The National Cooperative Highway Research Program Report 555 provides background information relevant to characterizing aggregate shape, texture, and angularity.

This practice may be used to characterize the shape characteristics of single source aggregate materials and multiple source aggregate material blends.

PROCEDURE

Determine the aggregate sample grading according to AASHTO T27 and the amount finer than 75 μ m according to AASHTO T11.

Determine the aggregate sample specific gravities according to AASHTO T84 and T85. Determine the material sample shape values for form 2d, gradient angularity, sphericity, form ratios (F&E, F or E), and texture according to AASHTO TP xx.

CALCULATIONS – SINGLE SOURCE

The material sample is typically characterized by individual evaluation of material retained on each sieve size, passing the next larger sieve. For the purpose of calculating the combined shape values, consider any sizes that contain inadequate percent retained mass to achieve minimum particle count to have the same shape value as the average of the next larger or the next smaller size, whichever is present.

Calculate the percent retained for the aggregate sample on each sieve using the AASHTO T27 results.:

Sieve Sizes (x):

Coarse: 25.0mm(1”), 19.0mm(3/4”), 12.5mm(1/2”), 9.5mm(3/8”), 4.75mm(#4)

Fine: 2.36mm(#8), 1.18mm(#16), 0.60mm(#30), 0.30mm(#50), 0.15mm(#100), 0.075mm(#200)

Percent Passing: $\%Pass_x = \% \text{ passing sieve } x$

Percent Retained: $\%R_x = \% \text{ retained on sieve } x$

$$\%R_x = \%Pass_{x+1} - \%Pass_x \quad (9)$$

Calculate average particle size, volume, and surface area for each sieve size x for unit mass.

For the purposes of shape characterization, volume and surface area of an average particle is estimated by using a cubical shape with side dimensions estimated by the average of the retained sieve and next larger sieve dimension.

$$\text{Average Particle Size: } D_x = \frac{(\text{Sieve}_x + \text{Sieve}_{x+1})}{2} \text{ (mm)} \quad (10)$$

$$\text{Average Particle Surface Area (cubical): } PSA_x = 6 * D_x^2 \text{ (mm}^2\text{)} \quad (11)$$

$$\text{Average Particle Volume (cubical): } V_x = D_x^3 \text{ (mm}^3\text{)} \quad (12)$$

Calculate number of particles per sample unit mass for each sieve size from the size distribution of AASHTO T27 and the respective specific gravities from AASHTO T84 and T85.

$$\text{Number of particles per sieve size: } \#P_x = \frac{\%R_x * 1000}{G_{sb} * V_x} \quad (13)$$

Note 2—A mass of 1 is assumed in Eq 13. This calculation determines the weighting factor applied to each sieve size for a material sample, therefore, actual mass is not required.

Calculate total particle surface area for each sieve size per sample unit mass.

$$\text{Particle Surface Area (each sieve } x\text{) (mm}^2\text{): } SSA_x = PSA_x * \#P_x \quad (14)$$

Calculate sample surface area (per unit mass):

$$\text{Total Surface Area (mm}^2\text{): } TSA = \sum_{x=0.075}^{25.0} SSA_x \quad (15)$$

$$\text{Coarse Surface Area (mm}^2\text{): } CSA = \sum_{x=4.75}^{25.0} SSA_x \quad (16)$$

$$\text{Fine Surface Area (mm}^2\text{): } FSA = \sum_{x=0.075}^{2.36} SSA_x \quad (17)$$

Calculate sample particles count (per unit mass):

$$\text{Total Particles: } \#TP = \sum_{x=0.075}^{25.0} \#P_x \quad (18)$$

$$\text{\# Coarse Particles: } \#CP = \sum_{x=4.75}^{25.0} \#P_x \quad (19)$$

$$\text{\# Fine Particles: } \#FP = \sum_{x=0.075}^{2.36} \#P_x \quad (20)$$

Calculate sample gradient angularity (weighted by surface area):

$$\text{Fine Gradient Angularity: } FGA = \frac{1}{FSA} \sum_{x=0.075}^{2.36} [SSA_x * GA_x] \quad (21)$$

$$\text{Coarse Gradient Angularity: } CGA = \frac{1}{CSA} \sum_{x=4.75}^{25.0} [SSA_x * GA_x] \quad (22)$$

$$\text{Overall Gradient Angularity: } GA = \frac{1}{TSA} \sum_{x=0.075}^{25.0} [SSA_x * GA_x] \quad (23)$$

Calculate sample fine aggregate form 2D (weighted by surface area):

$$Form2D = \frac{1}{FSA} \sum_{x=0.075}^{2.36} [SSA_x * 2D_x] \quad (24)$$

Calculate sample coarse aggregate texture (weighted by surface area):

$$TX = \frac{1}{CSA} \sum_{x=4.75}^{25.0} [SSA_x * TX_x] \quad (25)$$

Calculate sample coarse aggregate sphericity (weighted by particle count):

$$SP = \frac{1}{\#CP} \sum_{x=4.75}^{25.0} [\#P_x * SP_x] \quad (26)$$

Calculate sample sphericity range distribution (weighted by particle count):

% of Particles with Sphericity ≤ 0.3 :

$$SP(0.3) = \frac{1}{\#CP} \sum_{x=4.75}^{25.0} [\#P_x * SP(0.3)_x] \quad (27)$$

% of Particles with Sphericity $0.3 < SP \leq 0.7$:

$$SP(0.7) = \frac{1}{\#CP} \sum_{x=4.75}^{25.0} [\#P_x * SP(0.7)_x] \quad (28)$$

% of Particles with Sphericity $0.7 < SP \leq 1.0$:

$$SP(1.0) = \frac{1}{\#CP} \sum_{x=4.75}^{25.0} [\#P_x * SP(1.0)_x] \quad (29)$$

Calculate sample weighted percentages of coarse aggregate flat and elongated values (weighted by mass fraction) at the following ratios: $\geq 1:1$, $>2:1$, $>3:1$, $>4:1$, $>5:1$

$$\% d_L/d_S \geq 1 : \% L/S(\geq 1) = \sum_{x=4.75}^{25.0} \left[\frac{\% R_x * \% L/S(\geq 1)_x}{100} \right] \quad (30)$$

$$\% d_L/d_S > 2 : \% L/S(> 2) = \sum_{x=4.75}^{25.0} \left[\frac{\% R_x * \% L/S(> 2)_x}{100} \right] \quad (31)$$

$$\% d_L/d_S > 3 : \% L/S(> 3) = \sum_{x=4.75}^{25.0} \left[\frac{\% R_x * \% L/S(> 3)_x}{100} \right] \quad (32)$$

$$\% d_L/d_S > 4 : \% L/S(> 4) = \sum_{x=4.75}^{25.0} \left[\frac{\% R_x * \% L/S(> 4)_x}{100} \right] \quad (33)$$

$$\% d_L/d_S > 5 : \% L/S(> 5) = \sum_{x=4.75}^{25.0} \left[\frac{\% R_x * \% L/S(> 5)_x}{100} \right] \quad (34)$$

Calculate the sample weighted percentages of Coarse Aggregate Flat or Elongated (weighted by mass fraction) at the following ratios: $\geq 1:1$, $>2:1$, $>3:1$, $>4:1$, $>5:1$

$$\% d_I/d_S \text{ or } d_I/d_I \geq 1 : \% ForE(\geq 1) = \sum_{x=4.75}^{25.0} \left[\frac{\% R_x * \% ForE(\geq 1)_x}{100} \right] \quad (35)$$

$$\% d_I/d_S \text{ or } d_I/d_I > 2 : \% ForE(> 2) = \sum_{x=4.75}^{25.0} \left[\frac{\% R_x * \% ForE(> 2)_x}{100} \right] \quad (36)$$

$$\% d_I/d_S \text{ or } d_I/d_I > 3 : \% ForE(> 3) = \sum_{x=4.75}^{25.0} \left[\frac{\% R_x * \% ForE(> 3)_x}{100} \right] \quad (37)$$

$$\% d_I/d_S \text{ or } d_I/d_I > 4 : \% ForE(> 4) = \sum_{x=4.75}^{25.0} \left[\frac{\% R_x * \% ForE(> 4)_x}{100} \right] \quad (38)$$

$$\% d_I/d_S \text{ or } d_I/d_I > 5 : \% ForE(> 5) = \sum_{x=4.75}^{25.0} \left[\frac{\% R_x * \% ForE(> 5)_x}{100} \right] \quad (39)$$

CALCULATIONS – MULTIPLE SOURCE BLEND

Use the calculations in this section to estimate the shape characteristics of multiple material source blends. Each source must be sampled and characterized according to section 0 calculations.

Determine blend composition percentages

%AS_n = Percent Aggregate Source n

$$\sum_{i=1}^n \% AS_i = 100 \quad (40)$$

where: n = # of aggregate sources

Calculate blend surface area

Blend Total Surface Area (each sieve):

()

$$SSA_{Blend_x} = \sum_{i=1}^n \sum_{x=0.075}^{37.5} \left[\frac{\% AS_i * SSA_{ix}}{100} \right]$$

where: x= 0.075 to 25.0 mm

n= # of aggregate sources

Total Surface Area Blend (all sieves x = 0.075 to 25.0 mm)

$$TSA_{Blend} = \sum_{x=0.075}^{25.0} SSA_{Blend_x} \quad (41)$$

Coarse Surface Area Blend (sieve x = 4.75 to 25.0):

$$CSA_{Blend} = \sum_{x=4.75}^{25.0} SSA_{Blend_x} \quad (42)$$

Fine Surface Area Blend (sieve x =0.075 to 2.36):

$$FSA_{Blend} = \sum_{x=0.075}^{2.36} SSA_{Blend_x} \quad (43)$$

Calculate number of particles per blend unit mass for each sieve size:

$$\# P_{Blend_x} = \sum_{i=1}^n \sum_{x=0.075}^{25.0} \left[\frac{\% AS_i * \# P_{ix}}{100} \right] \quad (44)$$

Calculate number of particles per blend unit mass

Total Particle Count Blend:

$$\#TP_{Blend} = \sum_{x=0.075}^{25.0} \#P_{Blend_x} \quad (45)$$

Coarse Particles Blend:

$$\#CP_{Blend} = \sum_{x=4.75}^{25.0} \#P_{Blend_x} \quad (46)$$

Fine Particles Blend:

$$\#FP_{Blend} = \sum_{x=0.075}^{2.36} \#P_{Blend_x} \quad (47)$$

Calculate blend gradient angularity for each size $x = 0.075$ to 25.0 mm and combined (weighted by surface area):

$$GA_{Blend_x} = \frac{1}{SSA_{Blend_x}} \left[\sum_{i=1}^i \left[\frac{\%AS_i * SSA_{ix} * GA_{ix}}{100} \right] \right] \quad (48)$$

Blend Fine Gradient Angularity:

$$FGA_{Blend} = \frac{1}{FSA_{Blend}} \left[\sum_{x=0.075}^{2.36} [SSA_{Blend_x} * GA_{Blend_x}] \right] \quad (49)$$

Blend Coarse Gradient Angularity:

$$CGA_{Blend} = \frac{1}{CSA_{Blend}} \left[\sum_{x=4.75}^{25.0} [SSA_{Blend_x} * GA_{Blend_x}] \right] \quad (50)$$

Blend Overall Gradient Angularity:

$$GA_{Blend} = \frac{1}{TSA_{Blend}} \left[\sum_{x=0.075}^{25.0} [SSA_{Blend_x} * GA_{Blend_x}] \right] \quad (51)$$

Calculate blend fine aggregate form 2D for each size $x = 0.075$ to 2.36 mm and combined (weighted by surface area):

$$Form2D_{Blend_x} = \frac{1}{SSA_{Blend_x}} \left[\sum_{i=1}^n \left[\frac{\% AS_i * SSA_{ix} * 2D_{ix}}{100} \right] \right] \quad (52)$$

Blend Form 2D:

$$Form2D_{Blend} = \frac{1}{FSA_{Blend}} \left[\sum_{x=0.075}^{2.36} [SSA_{Blend_x} * 2D_{Blend_x}] \right] \quad (53)$$

Calculate blend texture for each size $x = 4.75$ to 25.0 mm and combined (weighted by coarse aggregate surface area):

$$TX_{Blend_x} = \frac{1}{SSA_{Blend_x}} \left[\sum_{i=1}^n \left[\frac{\% AS_i * SSA_{ix} * TX_{ix}}{100} \right] \right] \quad (54)$$

Blend Texture:

$$TX_{Blend} = \frac{1}{CSA_{Blend}} \left[\sum_{x=4.75}^{25.0} [SSA_{Blend_x} * TX_{Blend_x}] \right] \quad (55)$$

Calculate average blend sphericity for each size 4.75 to 25.0 and blend (weighted by coarse particle count):

$$SP_{Blend_x} = \frac{1}{\# P_{Blend_x}} \left[\sum_{i=1}^n \left[\frac{\% AS_i * \# P_{ix} * SP_{ix}}{100} \right] \right] \quad (56)$$

Blend Sphericity:

$$SP_{Blend} = \frac{1}{\# CP_{Blend}} \left[\sum_{x=4.75}^{25.0} [\# P_{Blend_x} * SP_{Blend_x}] \right] \quad (57)$$

Calculate blend sphericity distribution for each sieve 4.75 to 25.0 mm and blend (weighted by coarse particle count):

% of Particles with Sphericity ≤ 0.3 (Blend):

$$SP(0.3)_{Blend_x} = \frac{1}{\#P_{Blend_x}} \left[\sum_{i=1}^n \left[\frac{\%AS_i * \#P_{ix} * SP(0.3)_{ix}}{100} \right] \right] \quad (58)$$

$$SP(0.3)_{Blend} = \frac{1}{\#CP_{Blend}} \left[\sum_{x=4.75}^{25.0} [\#P_{Blend_x} * SP(0.3)_{Blend_x}] \right] \quad (59)$$

% of Particles with Sphericity $0.3 < SP \leq 0.7$ (Blend):

$$SP(0.7)_{Blend_x} = \frac{1}{\#P_{Blend_x}} \left[\sum_{i=1}^n \left[\frac{\%AS_i * \#P_{ix} * SP(0.7)_{ix}}{100} \right] \right] \quad (60)$$

$$SP(0.7)_{Blend} = \frac{1}{\#CP_{Blend}} \left[\sum_{x=4.75}^{25.0} [\#P_{Blend_x} * SP(0.7)_{Blend_x}] \right] \quad (61)$$

% of Particles with Sphericity $0.7 < SP \leq 1.0$ (Blend):

$$SP(1.0)_{Blend_x} = \frac{1}{\#P_{Blend_x}} \left[\sum_{i=1}^n \left[\frac{\%AS_i * \#P_{ix} * SP(1.0)_{ix}}{100} \right] \right] \quad (62)$$

$$SP(1.0)_{Blend} = \frac{1}{\#CP_{Blend}} \left[\sum_{x=4.75}^{25.0} [\#P_{Blend_x} * SP(1.0)_{Blend_x}] \right] \quad (63)$$

Calculate combined flat and elongated values for each sieve 4.75 to 25.0 mm and blend (weighted by mass fraction):

% $d_L/d_S \geq 1$ (Blend):

$$\%L/S(\geq 1)_{Blend_x} = \left[\sum_{i=1}^n \left[\frac{\%AS_i * \%R_{ix} * \%L/S(\geq 1)_{ix}}{100^2} \right] \right] \quad (64)$$

$$\%L/S(\geq 1)_{Blend} = \left[\sum_{x=4.75}^{25.0} [\%L/S(\geq 1)_{Blend_x}] \right] \quad (65)$$

% $d_L/d_S > 2$ (Blend):

$$\%L/S(> 2)_{Blend_x} = \left[\sum_{i=1}^n \left[\frac{\%AS_i * \%R_{ix} * \%L/S(> 2)_{ix}}{100^2} \right] \right] \quad (66)$$

$$\% L/S(> 2)_{Blend} = \left[\sum_{x=4.75}^{25.0} [\% L/S(> 2)_{Blend_x}] \right] \quad (67)$$

$\% d_L/d_S > 3$ (Blend):

$$\% L/S(> 3)_{Blend_x} = \left[\sum_{i=1}^n \left[\frac{\% AS_i * \% R_{ix} * \% L/S(> 3)_{ix}}{100^2} \right] \right] \quad (68)$$

$$\% L/S(> 3)_{Blend} = \left[\sum_{x=4.75}^{25.0} [\% L/S(> 3)_{Blend_x}] \right] \quad (69)$$

$\% d_L/d_S > 4$ (Blend):

$$\% L/S(> 4)_{Blend_x} = \left[\sum_{i=1}^n \left[\frac{\% AS_i * \% R_{ix} * \% L/S(> 4)_{ix}}{100^2} \right] \right] \quad (70)$$

$$\% L/S(> 4)_{Blend} = \left[\sum_{x=4.75}^{25.0} [\% L/S(> 4)_{Blend_x}] \right] \quad (71)$$

$\% d_L/d_S \leq 5$ (Blend):

$$\% L/S(> 5)_{Blend_x} = \left[\sum_{i=1}^n \left[\frac{\% AS_i * \% R_{ix} * \% L/S(> 5)_{ix}}{100^2} \right] \right] \quad (72)$$

$$\% L/S(> 5)_{Blend} = \left[\sum_{x=4.75}^{37.5} [\% L/S(> 5)_{Blend_x}] \right] \quad (73)$$

Calculate flat or elongated values for each sieve 4.75 to 25.0 mm and blend (weighted by mass fraction):

$\% d_L/d_S$ or $d_L/d_L \geq 1$: (Blend):

$$\% ForE(\geq 1)_{Blend_x} = \left[\sum_{i=1}^n \left[\frac{\% AS_i * \% R_{ix} * \% ForE(\geq 1)_{ix}}{100^2} \right] \right] \quad (74)$$

$$\% ForE(\geq 1)_{Blend} = \left[\sum_{x=4.75}^{25.0} [\% ForE(\geq 1)_{Blend_x}] \right] \quad (75)$$

$\% d_I/d_S$ or $d_I/d_I > 2$: (Blend):

$$\% ForE(> 2)_{Blend_x} = \left[\sum_{i=1}^n \left[\frac{\% AS_i * \% R_{ix} * \% ForE(> 2)_{ix}}{100^2} \right] \right] \quad (76)$$

$$\% ForE(> 2)_{Blend} = \left[\sum_{x=4.75}^{25.0} [\% ForE(> 2)_{Blend_x}] \right] \quad (77)$$

$\% d_I/d_S$ or $d_I/d_I > 3$: (Blend):

$$\% ForE(> 3)_{Blend_x} = \left[\sum_{i=1}^n \left[\frac{\% AS_i * \% R_{ix} * \% ForE(> 3)_{ix}}{100^2} \right] \right] \quad (78)$$

$$\% ForE(> 3)_{Blend} = \left[\sum_{x=4.75}^{25.0} [\% ForE(> 3)_{Blend_x}] \right] \quad (79)$$

$\% d_I/d_S$ or $d_I/d_I > 4$: (Blend):

$$\% ForE(> 4)_{Blend_x} = \left[\sum_{i=1}^i \left[\frac{\% AS_i * \% R_{ix} * \% ForE(> 4)_{ix}}{100^2} \right] \right] \quad (80)$$

$$\% ForE(> 4)_{Blend} = \left[\sum_{x=4.75}^{25.0} [\% ForE(> 4)_{Blend_x}] \right] \quad (81)$$

$\% d_I/d_S$ or $d_I/d_I > 5$: (Blend):

$$\% ForE(> 5)_{Blend_x} = \left[\sum_{i=1}^n \left[\frac{\% AS_i * \% R_{ix} * \% ForE(> 5)_{ix}}{100^2} \right] \right] \quad (82)$$

$$\% ForE(> 5)_{Blend} = \left[\sum_{x=4.75}^{25.0} [\% ForE(> 5)_{Blend_x}] \right] \quad (83)$$

REPORT

Report the following information:

Project name.

Date of the analysis.

Material sample identifications: type, source, size, gradation.

Number of particles analyzed for each size.

Material shape property mean and standard deviation. Graphical representations of the property distributions may be included.

PRECISION AND BIAS

Precision—this practice uses data generated from other testing methods to develop cumulative information, therefore the precision of the values generated in this practice are established by the precision of the standards used to collect the raw data.

Bias—since there is no accepted reference device suitable for determining the bias in this method, no statement of bias is made.

KEYWORDS

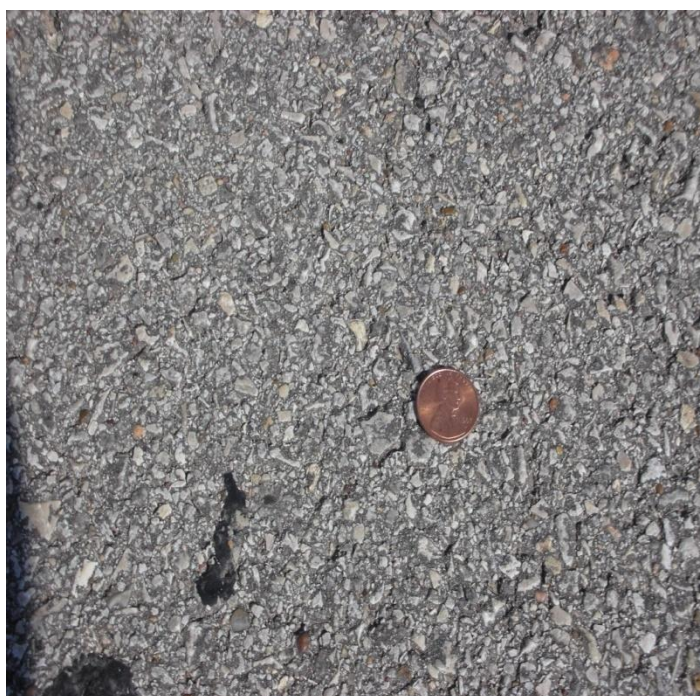
Aggregate; angularity; consensus property, shape, texture, form, elongation.

APPENDIX D



Mix: Type D
 Highway: SH 36
 District: Yoakum
 Age: 4 Years
 AADT: 4800
 MPD: 0.48 mm
 DFT 20: 0.331
 DFT 80: 0.307
 Aggregate:
 Colorado
 Materials
 Skid Number: 21

FIGURE 143 Type D mixture on wheelpath of SH 36 in Yoakum District.



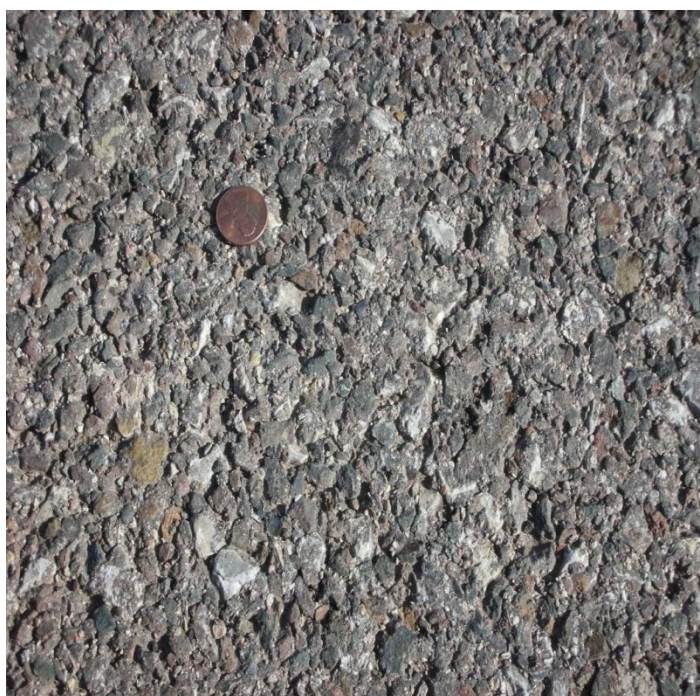
Mix: Type D
 Highway: SH 36
 District: Yoakum
 Age: 4 Years
 AADT: 4800
 MPD: 0.49 mm
 DFT 20: 0.643
 DFT 80: 0.535
 Aggregate:
 Colorado
 Materials
 Skid Number: N.A

FIGURE 144 Type D mixture on shoulder of SH 36 in Yoakum District.



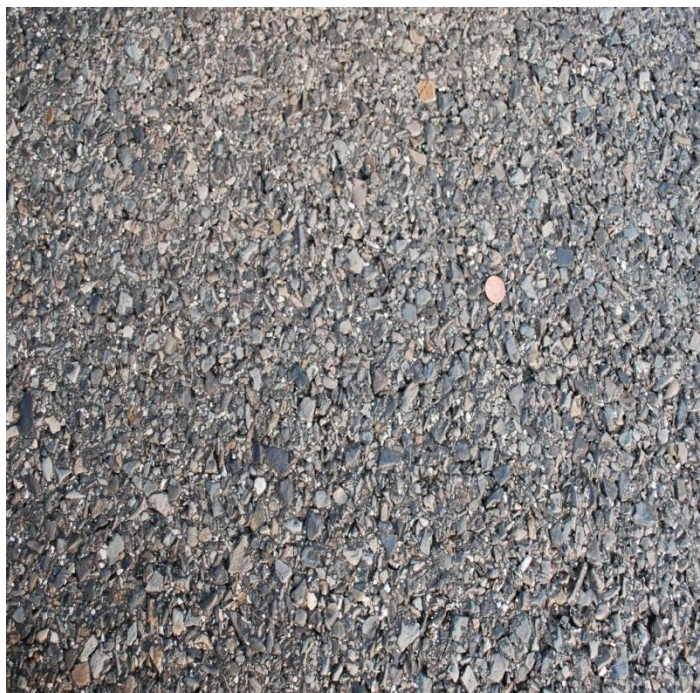
Mix: CMHB-C
 Highway: US 87
 District: Lubbock
 Age: 5 Years
 AADT: 2905
 MPD: 0.98mm
 DFT 20:0.498
 DFT 80:0.411
 Aggregate:
 Vulcan/Brownwood
 , Hanson/Davis
 Skid Number: 38

FIGURE 145 CMHB mixture on wheelpath of US 87 in Lubbock District.



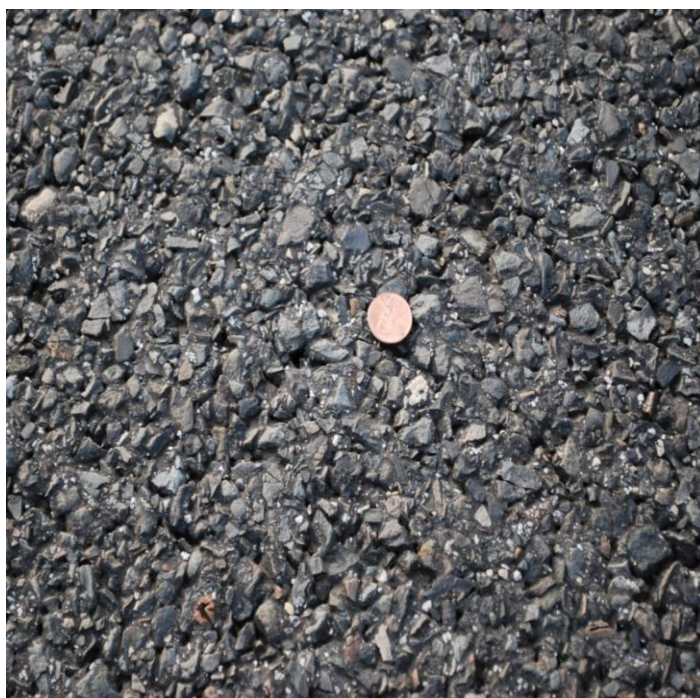
Mix: CMHB-C
 Highway: US 87
 District: Lubbock
 Age: 5 Years
 AADT: 2905
 MPD: 1.2mm
 DFT 20:0.502
 DFT 80:0.418
 Aggregate:
 Vulcan/Brownwood,
 Hanson/Davis
 Skid Number: 51

FIGURE 146 CMHB mixture on shoulder of US 87 in Lubbock District.



Mix: SMA-C
 Highway: IH 20
 District: Atlanta
 Age: 7 Years
 AADT: 15610
 MPD: 0.86mm
 DFT 20: 0.505
 DFT 80:0.423
 Aggregate: Martin
 Marietta/Jones Mill,
 Malvern Ark
 Skid Number: 31

FIGURE 147 SMA-C mixture on wheelpath of IH 20 in Atlanta District.



Mix: SMA-C
 Highway: IH 20
 District: Atlanta
 Age: 7 Years
 AADT: 15610
 MPD: 0.86mm
 DFT 20: 0.485
 DFT 80:0.402
 Aggregate: Martin
 Marietta/Jones Mill,
 Malvern Ark
 Skid Number: 37

FIGURE 148 SMA-C mixture on shoulder of IH 20 in Atlanta District.



Mix: Type C
 Highway: SH 16
 District: San Antonio
 Age: 6 Years
 AADT: 6400
 MPD: 0.61mm
 DFT 20:0.294
 DFT 80:0.282
 Aggregate: Martin Marietta/Beckman
 Skid Number: 13

FIGURE 149 Type C mixture on wheelpath of SH 16 in San Antonio District.



Mix: Type C
 Highway: SH 16
 District: San Antonio
 Age: 6 Years
 AADT: 6400
 MPD: 0.46mm
 DFT 20:0.424
 DFT 80:0.420
 Aggregate: Martin Marietta/Beckman
 Skid Number: 20

FIGURE 150 Type C mixture on shoulder of SH 16 in San Antonio District.



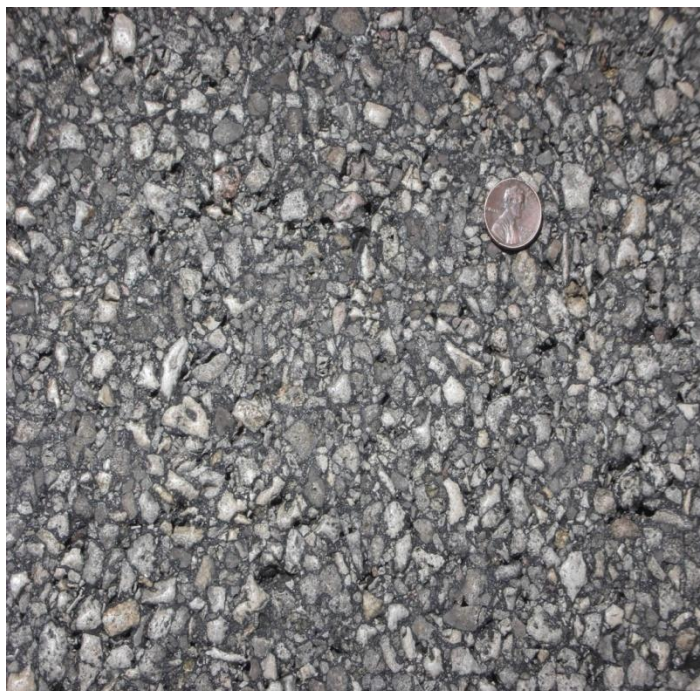
Mix: PFC
 Highway: IH 35
 District: San Antonio
 Age: 4 Years
 AADT: 107000
 MPD: 1.15mm
 DFT 20:0.437
 DFT 80:0.360
 Aggregate: Martin Marietta/Beckman, Delta/Brownlee
 Skid Number: 24

FIGURE 151 PFC mixture on wheelpath of IH 35 in San Antonio District.



Mix: PFC
 Highway: IH 35
 District: San Antonio
 Age: 4 Years
 AADT: 107000
 MPD: 1.37mm
 DFT 20:0.547
 DFT 80:0.468
 Aggregate: Martin Marietta/Beckman, Delta/Brownlee
 Skid Number: 31

FIGURE 152 PFC mixture on shoulder of IH 35 in San Antonio District.



Mix: Superpave
Highway: IH 20
District: Abilene
Age: 7 Years
AADT: 9535
MPD: 0.56mm
DFT 20:0.218
DFT 80:0.255
Aggregate:
Vulcan/Black Lease
Skid Number: 15

FIGURE 153 Superpave mixture on wheelpath of IH 20 in Abilene District.



Mix: Superpave
Highway: IH 20
District: Abilene
Age: 7 Years
AADT: 9535
MPD: 0.61mm
DFT 20:0.682
DFT 80:0.629
Aggregate:
Vulcan/Black Lease
Skid Number: 31

FIGURE 154 Superpave mixture on shoulder of IH 20 in Abilene District.

VITA

Arash Rezaei was born in Iran. He received his B.S. in civil engineering from Sharif University of Technology in September 1998 and his M.S. in civil engineering from Sharif University of Technology in December 2000. With an interest in construction materials, he came to Texas A&M University and received his Ph.D. degree in civil engineering/materials in December 2010. His research interests include microstructure characterization and modeling of asphalt mixtures, characterization of pavement surfaces, analysis and design of pavements, constitutive modeling of granular materials, and image analysis of granular materials. He can be reached at:

Texas Transportation Institute
3135 CE/TTI Bldg., Texas A&M University, Room 501g
College Station, TX 77843
Email: Arash.rezai@gmail.com